VIBRATION BASED ROBUST CONDITION MONITORING METHODS FOR ROLLING ELEMENT BEARING — A SIGNAL PROCESSING AND DATA BASED APPROACH

By

BUBATHI MURUGANANTHAM

Enrollment No. ENGG02200804025

Indira Gandhi Centre for Atomic Research, Kalpakkam

A thesis submitted to the

Board of Studies in Engineering Sciences

In partial fulfillment of requirements

For the Degree of

DOCTOR OF PHILOSOPHY

of

HOMI BHABHA NATIONAL INSTITUTE

November, 2013

HOMI BHABHA NATIONAL INSTITUTE

Recommendations of the Viva Voce Board

As members of the Viva Voce Board, we certify that we have read the dissertation prepared by **Bubathi Muruganantham** entitled "***Vibration based robust condition monitoring methods for rolling element bearing – a signal processing and data based approach***" and recommend that it may be accepted as fulfilling the dissertation requirement for the Degree of Doctor of Philosophy.

Chairman – **Prof. M. Sai Baba** Date:

28 Aug 2014

Guide/ Convener – **Prof. T. Jayakumar** Date:

25/8/2014

Member 1– **Prof. B. Purna Chandra Rao** Date:

25/8/2014

Member 2 – **Prof. B.K. Panigrahi** Date:

25/8/14

Technology Advisor (Invitee) – **Mr. S.A.V. Satya Murty** Date:

External Examiner – **Prof. C. Sujatha** Date:

25/8/14

Final approval and acceptance of this dissertation is contingent upon the candidate's submission of the final copies of the dissertation to HBNI.

I hereby certify that I have read this dissertation prepared under my direction and recommend that it may be accepted as fulfilling the dissertation requirement.

Date: 25 Aug. 2014

Place: Kalpakkam

25082014

Guide/ Convener

STATEMENT BY AUTHOR

This dissertation has been submitted in partial fulfillment of requirements for an advanced degree at Homi Bhabha National Institute (HBNI) and is deposited in the Library to be made available to borrowers under rules of the HBNI.

Brief quotations from this dissertation are allowable without special permission, provided that accurate acknowledgement of source is made. Requests for permission for extended quotation from or reproduction of this manuscript in whole or in part may be granted by the Competent Authority of HBNI when in his or her judgment the proposed use of the material is in the interests of scholarship. In all other instances, however, permission must be obtained from the author.

25/08/14

(Bubathi Muruganantham)

DECLARATION

I, hereby declare that the investigation presented in the thesis has been carried out by me. The work is original and has not been submitted earlier as a whole or in part for a degree/diploma at this or any other Institution/University.

25/08/14

(Bubathi Muruganantham)

List of Publications arising from the Thesis

Journal

a. Published

1. Bubathi Muruganatham, M.A. Sanjith, B. Krishna Kumar and S.A.V. Satya Murty, "*Roller element bearing fault diagnosis using singular spectrum Analysis*", **Mechanical Systems and Signal Processing**, Vol. 35, No. 1-2, pp. 150-166, (February 2013).
2. Bubathi Muruganatham and T. Jayakumar, "*Detection of faulty ball bearing using symbolic dynamics*", **International journal of Condition Monitoring**, Vol. 3, No.1, pp.23-34, (April 2013).
3. Bubathi Muruganatham, S.A.V. Satya Murty, and T. Jayakumar, "*Generalized Teager Kaiser Energy operator based bearing fault diagnosis under low SNR and comparison with teager kaiser energy operator*", **International Journal of COMADEM**, Vol. 16, No.3, pp.3-15, (July 2013).
4. Bubathi Muruganatham, S.A.V. Satya Murty, and T. Jayakumar, "*Identification of faulty ball bearings using singular value ratio: case study*", **International Journal of COMADEM**, Vol. 17, No.1, pp.33-42, (January 2014).

b. Communicated

1. Bubathi Muruganatham, S.A.V. Satya Murty, and T. Jayakumar, "*Rolling element bearing performance deterioration assessment method using support vector data description*" (to **International Journal of Prognostics and Health Management**).

Conference Proceedings

1. Bubathi Muruganatham, M.A. Sanjith, B. Krishna Kumar, S.A.V. Satya Murty, and P.Swaminathan, "Inner race bearing fault detection using singular spectrum analysis", ***IEEE International Conference on Communication Control and Computing Technologies*** ICCCCT '10, October 7-9, Ramanathapuram, India, (2010).

2. Bubathi Muruganatham, C. Sujatha, M.A. Sanjith, T. Jayakumar and B. Krishna Kumar, "Application of singular spectrum analysis for bearing fault diagnosis",

National Conference on Condition Monitoring of Engineering Systems & Structures NCCM-2012, June 15-16, Pune, India, (2012).

3. Bubathi Muruganatham, M.A. Sanjith, C. Sujatha and T. Jayakumar, "Symbolic dynamics based bearing fault detection", ***2012 IEEE Fifth India International Conference on Power Electronics*** IICPE 2012, December 6-8, New Delhi, India, (2012).

4. Bubathi Muruganatham, S.A.V. Satya Murty and T. Jayakumar, "Bearing fault diagnosis using generalized teager kaiser energy operator under low SNR", ***20^{th} International Congress on Sound and Vibration*** *ICSV20*, July 7-11, Bangkok, Thailand, (2013).

5. Bubathi Muruganatham, S.A.V. Satya Murty and T. Jayakumar, "A Method for Rolling Element Bearing Health Degradation Index", ***National Conference on Condition Monitoring*** NCCM 2013, October 4-5, Bangalore, India, (2013).

(Bubathi Muruganatham)

To my Mother, Mrs. M. Indirani

ACKNOWLEDGEMENTS

This research work could not have been realized without the support of many people. At the outset, I am very much indebted to Government of India and Department of Atomic Energy, India for providing the research fellowship to carry out the work at the Indira Gandhi Centre for Atomic Research (IGCAR), Kalpakkam, India in association with the Homi Bhabha National Institute (HBNI), Mumbai, India.

I express my gratitude towards Dr. Baldev Raj (former Director, IGCAR), Shri S.C. Chetal (former Director, IGCAR) and Dr. P.R.Vasudeva Rao (Director, IGCAR) for their support to the research scholars.

I express my sincere indebtedness to my guide Prof. T. Jayakumar, Director, Metallurgy and Materials Group for his guidance, valuable suggestions and encouragement during the research work.

I am grateful to my other doctoral committee members - Prof. M. Sai Baba (Chairman), Prof. P.Swaminathan (Ex-Technical Advisor and Ex-EIG Director), Mr. S.A.V. Satya Murty (Technical Advisor and EIRSG Director), Prof. B. Purna Chandra Rao (member), Head, NDED and Prof. B.K. Panigrahi (member), Head, IBCSS for their co-operation, valuable suggestions, reviewing the work progress and proof reading the synopsis.

Without the experimental data, my work would not have been completed. The research work uses several public and proprietary fault datasets. I am extremely thankful to Prof. Kenneth Loparo, Case Western Reserve University, Canada for making their data available freely. I sincerely thank Emeritus Prof. Robert Bond Randall, University of New South Wales, Australia for permitting to use their lab data (test data2) along with pictures and figures. I also thank him for the knowledge shared in the field of bearing condition monitoring and for providing comments on the synopsis. I thank the Society for Machinery Failure Prevention Technology [MFPT] and Dr. Eric Bechhoefer, President of Green Power Monitoring, Ex-chief engineer of NRG Systems who has prepared the data on behalf of MFPT. I thank Dr. Eric Bechhoefer for verifying the results and providing information related to his fault dataset. I appreciate the joint efforts of University of Cincinnati, Rexnord Technical Services and NASA for collecting the accelerated life data which is obtained from the NASA Ames Prognostics Data Repository.

Getting access to research articles are very important to remain updated in the field. I appreciate the efforts of Mr. K. Yuvaraj, Engineer at CREC, USA (during his MS at SUNY, Buffalo) and Mr. Balakrishna R, Scientist-C, RCI, DRDO for sending me the articles. I thank the article in-charge of IGCAR library and IIT-Madras for getting access to the various articles.

My profound thanks to Mr. M.A. Sanjith, EID, for always been there to help.

I am grateful to the teaching and non teaching staff of BARC Training School, IGCAR Campus for their efforts during my course work.

I am extremely thankful to many researchers for their timely help. I thank Dr. Tax for clearing some concepts related to SVDD and Dr. Gou Wei, City University of Hong for advice in writing the synopsis. I thank Mr. Paul Krot of Ukraine Iron and Steel plant for bearing fault data used for some analysis and Prof. Lorand Szabo of Technical University of Cluj for helping in the induction motor modeling. I thank Dr. Jianbo Yu for permitting to use the figures related to comparison of accelerated life test results. I thank FAG Bearing Corporation for permitting to use their content connected to bearing damage symptoms and their causes. I thank the Mobius Institute for the permission to use their information related to bearing fault development stages. I thank Prof. A.K. Jardine to allow the content linked to bearing condition monitoring philosophy used for the thesis.

I thank HBNI for providing the financial support to attend the 20th International Congress on Sound and Vibration (ICSV20), Bangkok, Thailand.

I extend my appreciation towards Mr. S. Ilanga Sambasivam (Ex-Head, EID), Mr. B. Krishna Kumar (Ex-Head, EID), Mr. B. Ramaswamy Pillai (Ex-Head, PES), Mr. D. Thirungana Murty (Head, EID), Mr. P.K. Palanisami (Head, PES), Shri. N. Murali (Associate Director, ICG), Shri Manimaran, Shri Kasinathan and every colleagues of ICG for their valuable support.

I appreciate the timely help of Mr. Logesh kumar, Mrs. E. Felicia, Mrs. Indira P. Logu and Mrs. N. Hemalatha.

I thank Dr. M. Sai Baba and his group members for providing us an excellent facility and environment for the accommodation at JRF Enclave. I thank him for providing me an opportunity to visit BARC, TAPS and NFC. I also thank Mrs. Devi and Mr. Suresh for their help at JRF Enclave.

I had the best of time with my batch mates - Naveen, Sharath, Ilayaraja, Srinivas, Mariyappa, Jagadeesh, Pradeep, Sudhanshu, Herojith, Balakrishna, Vasumalai, Vishnu, Laxmojit, Dr. Jammu Ravi, Vinod, Vijay, Balaji, Kishan, Yesu, Dr. Maneesha, Pravati and Dr. Priyada. I also thank other friends: Shashwat, Manas, Subrato, Dipika, Rajesh, Santhana, Aditya, Balachandran, Jayachandran, Manoj, Navtesh, Atul, Balbir, Srijan, Manan, Nimal, Uday, Balasubramanian, Alok, Kapil, Poonseeni, Bijender, Gaurav, Satender, Maji, Soumi, Vinita, Paawan, Arun babu, Ashutosh, Anil, Srinivasan, Raghavan, Anindya, Deepak, Dr. Hari Babu, Ashish, Shailesh, Karthick, Mahendren, Raghavendra, Gopi, Srinivasan, Dr. Subhra, Dr. Madhusmita, Sudipta, Madhusmita Sahoo. Special thanks to my sisters & sister-in-laws: Smiti Pati, Uma Swain, Banashree Ghosh, Niskruti Mohanty, Sreedevi.S for giving me a family environment. I thank all the other senior and junior friends for making my stay a wonderful.

I also thank my cricket teammates of department and enclave for the refreshing time.

I take this opportunity to extend my indebtness towards my Late Uncle Mr. Chandrabalan, AD, Tamil Nadu Highways, Chennai who helped and guided me during the B.E admission.

I would like to express my profound gratitude to Mrs. M. Indirani (mother), Mr. A. Muruganantham (father), Mr. M. Vasanth (brother), Mrs. S. Suganthi (sister), N. Sabapathy (Bro-in law), Kanishka (sister's daughter) for their love, care and encouragements. PhD would have been a dream, but for the parents' support and confidence in my decision to leave a job (for higher study).

It has been a great honour for me to work in IGCAR and to be surrounded with some of the brightest and loving people, I have met. To all, I say Thank you from the bottom of my heart.

November, 2013 *(Bubathi Muruganantham)*

“A Stitch in Time Saves Nine”

CONTENTS

SYNOPSIS

1. RESEARCH PROBLEM

Bearings are the most commonly used components in any mechanical equipment such as pumps, wind turbines, cranes and hoists. They bear much of the load component. This when combined with harsh operating conditions such as in high temperature, corrosive environment, dust increases the chances of bearing failures. Based on the survey reports on various faults occurring in rotating machines, it is observed that majority of the failures occur as bearings faults [1-3]. Condition monitoring refers to monitoring the current state of, e.g. rotating machine and predicting its further state while in operation. Currently, condition based maintenance is considered as the most efficient maintenance strategy for industries. A recent motor bearing failure case study in the thermal power plant of India [4], showed that the capital saved by condition monitoring was around 2.3 crores ($ 4,00,000). Condition monitoring of bearing is very much important for various reasons such as to increase equipment availability, safety, reliability, and preventing the capital loss due to its unavailability.

Generally, bearing is classified into two types- rolling element bearing and journal bearing. Rolling element bearings are used in more than 90% of the rotating machinery found in various applications [5]. They are prone to myriad of premature failures. A mere 10% of them reach their expected service life [5]. Hence, rolling element bearing (hereafter, bearing) condition monitoring is considered as the research problem.

Bearing condition monitoring is done using various methods [6] such as vibration analysis, chemical analysis, temperature measurement, acoustic emission and current monitoring. Of these, vibration based monitoring is widely used in industries and also available as a standard ISO 10816 [7]. Bearing condition monitoring is conducted in three phases namely fault detection, diagnosis and prognosis. Fault detection phase (Anything wrong?) determines whether the bearing is healthy or faulty. Once the fault is detected, the location of the fault is found in the diagnosis phase (Where it occurred?). Prognosis phase (How much is the level and when it occurred?) deals with fault degradation and remaining useful life of the bearing. It is the development and continuation of fault detection. In the prognosis study, only fault degradation assessment is considered.

In this thesis, monitoring methods for fault detection, fault diagnosis and fault degradation assessment are developed.

2. MOTIVATION AND SIGNIFICANCE

The main motivation of this research is to investigate the use of vibration analysis and to develop the state-of-art signal processing methods for the condition monitoring of bearings.

A vibration signal generated by a bearing fault is pseudo cyclo-stationary in nature [8], so it is essential to extract the fault features accurately from the collected vibration signal. These features are critical for determining the bearing condition (healthy or faulty) and would be used in the prognosis phase. Mostly time domain method is used for calculating the fault features. However, the results of these methods vary with sample size, load and noise. It is an area where research is still needed.

Spectrum analysis is the most commonly used method for fault diagnosis where the fault characteristic frequency components (FCF) are extracted from the vibration signal to localize the fault. FCFs are mainly amplitude modulated because of two reasons: first due to the transfer function of the transmission path between the bearing and the sensor and second, the load carried by the rolling elements. It is also frequency modulated due to the variation in the instantaneous shaft rotating frequency. Due to roller slippage [9], the repetition duration may vary slightly which causes smearing of the spectrum. The vibration measured from the equipment not only contains the fault characteristic frequencies, but also the vibrations generated by other mechanical components such as gear meshing, shaft imbalance or misalignment or bent /cracked shaft along with the background noise. All the above factors complicate the quality of diagnosis decisions to be taken when the faults occur in incipient stage. Thus, signal processing methods which can extract the incipient fault under the presence of masking sources and background noise are required to be developed. In addition to it, the method needs to be simple and efficient, from the practical implementation point of view.

Bearing fault degradation has strong fuzziness and the dynamic information is random. The main difficulty in its effective implementation is the highly stochastic nature of fault. The features (e.g. root mean square, kurtosis and crest factor) used for fault degradation assessment have stability problems with fault severity [10]. Hence, robust “fault” features are required to accurately trend the fault. Exploring new and effective indices should be carried out to develop an effective prognostic system.

The important significance of this research is the development of a simple online automated approach useful for a handheld vibration analyzer and development of some novel effective fault indices for fault detection and prognosis.

3. RESEARCH QUESTIONS

Based on the problem considered and the literature study carried out, the following questions would be investigated and solved in this thesis:

i. Is it possible to employ a simple online method for bearing fault detection?

ii. Whether an effective fault index to differentiate between healthy and faulty bearing could be developed?

iii. Whether a noise tolerant and an efficient bearing fault feature extraction and diagnosis method could be developed?

iv. How a bearing fault could be localized for a low signal-to-noise ratio (SNR) condition without using any de-noising technique or without the need of designing the band pass filter and nor applying a complex time–frequency method?

v. How to select some features which can evaluate comprehensive performance degradation severity?

vi. How an effective index for comprehensive performance degradation severity could be obtained after extracting the features?

4. OBJECTIVES

This research concentrates on the development of robust methods covering the three phases of bearing condition monitoring, namely fault detection, diagnosis and prognosis. The objectives behind each work are discussed below:

4.1 Fault Detection

At **detection** stage, the raw vibration signals are processed to extract the fault features. Most of the time domain and data based signal processing methods used are noise sensitive, sample size dependent, machine and load dependent or involving complex mathematical calculations or need of much training.

The main objective of the work in ‘Detection’ stage would be:

i. Development of an effective fault feature extraction algorithm, which could solve the above mentioned problems and is suitable for online bearing condition monitoring.

ii. Some novel fault indices would also be identified to detect the faulty bearing at its incipient fault stage.

4.2 Fault Diagnosis

Once the fault in bearing is identified at the detection stage, next (**diagnosis** stage) spectrum analysis is carried out to extract the fault characteristic frequency related to the location of the fault in bearing (inner race, outer race, rollers and cage). Considering that not much diagnostic information is obtained from the spectrum of the raw signal [8], the diagnostic method in this thesis is developed with an objective of:

i. An automated method which is simple in implementation and applicable to signals with low SNR. It should not require designing the band pass filter (conventional method) or de-noising, before processing for spectrum analysis.

ii. A time domain approach to be identified which is useful for diagnosis with advantages such as noise immunity and sample size variant.

4.3 Fault Prognosis

In the fault **prognosis** work, fault degradation assessment is considered. At this stage, information regarding the fault degradation in bearing performance should be accurate so that further decisions and actions could be planned. The method should provide information on the status of fault severity, its progression and time to failure. Many trending parameter have been developed which do not show consistent performance with fault severity. The work in this area focuses on :

i. Development of better fault trending features which show the different stages of bearing fault severity.

ii. Use of appropriate parameters to develop an accurate bearing performance indicator.

5 METHODS AND APPROACHES

The algorithms developed are mainly based on signal processing in time and frequency domain along with the application of various data mining techniques. To test and validate the algorithms, signals from various sources such as simulation, experimental and those from industries are considered. In order to address the various research questions, the methods and approaches explored are discussed in the following subsections.

5.1 Fault Detection

Two new fault detection methods are proposed. They are based on:

i. The concept of symbolic dynamics is used for the fault index.

ii. Singular spectrum analysis is used as a preprocessing method (time domain) for obtaining the fault feature.

5.2. Fault Diagnosis

Fault diagnosis is generally carried by using the spectrum analysis to detect the fault characteristic frequencies. An alternative approach based on time domain and data based technique is proposed in this stage. Overall, two algorithms are developed for bearing fault diagnosis: one is based on fault characteristic frequency detection and the other method is based on fault feature.

i. Generalized Teager Kaiser Energy Operator (GTKEO) is used extract the fault characteristic frequencies.

ii. Singular spectrum analysis is used as a fault feature extraction method and feed forward back propagation neural network is used for classifying the bearing into four classes namely healthy, inner race fault, outer race fault and ball fault.

5.3 Fault Prognosis

In the fault prognosis study, fault features developed in this thesis and the support vector data description method are used to obtain a condition degradation indicator.

6. STRUCTURE OF THESIS

Thesis layout : general

Part I The Background

Chapter 1 Introduction

Chapter 2 An Overview of Rolling element bearing faults and vibration based condition monitoring methods

Part II Fault Detection

Chapter 3 Detection of faulty bearing using symbolic dynamics

Chapter 4 Identification of faulty bearings using singular value ratio: case study

Part III Fault Diagnosis

Chapter 5 Bearing fault diagnosis using singular spectrum analysis

Chapter 6 Generalized Teager Kaiser Energy operator based bearing fault diagnosis

Part IV Fault Prognosis

Chapter 7 Performance Index development using support vector data description method

Part V Overview

Chapter 8 Summary, Contributions and Open questions/Further Scope

7. ANALYZED DATA's

The different types of bearing fault data used for verification and validation of the proposed methods of fault detection, fault diagnosis and fault degradation. Four sources of data are used: numerical simulation, with artificially seeded fault, bearing accelerated life test and real industrial case.

a) Experimental data with artificially seeded fault:

They are collected from two different test rigs. One test rig (**Test data1**) has a simple setup of induction motor with dynamometer. It is taken from Case Western Reserve University [11]. Point defects of different sizes (width 0.18 mm to 0.71 mm range, depth of 0.28 mm) are seeded on inner race, outer race and ball. SKF 6205 series deep grove ball bearing is used. The data are also collected for different combinations of load (no load to full load) and its corresponding speed. These are analyzed in fault detection (Chapter 3 and 4) and fault diagnosis (Chapter 5 and 6) approaches.

From second test rig (**Test data2**), signals are obtained in the presence of a spur gearbox. The data is obtained from University of New South Wales [12]. The setup consists of single stage gearbox driven primarily by a 3Φ motor and powered by a hydraulic motor-pump set. Koyo 1205, double row ball bearing is used. Point defects in inner race and outer race (width of 0.8 mm, depth of 0.3 mm), ball defect with both width and depth of 0.5 mm was made. These are used in fault detection (Chapter 3) and fault diagnosis (Chapter 5 and 6) approaches.

b) Numerical simulation signal: (Test data3)

It is used in fault detection method (Chapter 3). External interferences such as gearbox and noise are considered.

c) Bearing Accelerated life test data: (Test data4)

It is to evaluate the fault degradation method (Chapter 7). The data is taken from University of Cincinnati [13]. The test rig consists of AC motor coupled to the shaft via rubber belts. Rexnord ZA-2115 double row bearing are installed on a shaft and are oil force lubricated. The test is carried out until the amount of debris collected in the lubrication system exceeds a limit.

d) Industrial data: (Test data5)

The industrial data is obtained from the Society for Machinery failure Prevention Technology [14] which is used for validating the fault diagnosis based spectrum analysis method (Chapter 6). Three cases of data used: planet bearing (both ball and outer race defects); Intermediate shaft (ball defect) and Oil Pump (inner race defect) of a wind turbine.

8. CHAPTER DESCRIPTIONS

The thesis comprises of eight chapters. They are briefly discussed below:

CHAPTER 1 INTRODUCTION

Chapter 1 describes the research problem, motivation, significance of the work, the various research questions considered as the starting point of research. Also, the objectives and different approaches used for carrying out the work are discussed along with the structure of the thesis.

CHAPTER 2 AN OVERVIEW OF ROLLING ELEMENT BEARING FAULTS AND VIBRATION BASED CONDITION MONITORING METHODS

Chapter 2 expounds the various aspects related to bearing condition monitoring. It discusses the following concepts: rolling element bearing, its various types of defects and their causes, bearing fault signature and fault characteristic frequencies, different stages involved in bearing fault development (4 stages), condition monitoring philosophy (methods involving data acquisition, data processing and decision making) and some of the existing vibration based monitoring techniques used for fault detection, fault diagnosis and fault degradation studies.

CHAPTER 3 DETECTION OF FAULTY BEARING USING SYMBOLIC DYNAMICS

Chapter 3 discusses the method to detect the faulty bearing based on symbolic dynamics. Symbolic dynamic technique gives the behavioural description of nonlinear dynamical system. During the bearing fault occurrence, the vibration signal obtained is amplitude and frequency modulated which changes the statistics of the vibration signal and these changes are detected through symbolic dynamic method.

The time series data is converted into symbolic series. The symbolic series generation is done using maximum entropy based partitioning approach. The sequence of symbols represents the different states of the dynamical systems. The change of symbols represents the change from one state to another state. If system is normal, the statistics of the symbols would remain the same and the states would give a uniform probability distribution. An anomaly would change the probability distribution of the symbols. A measure of deviation, which is called as Common Signal Index (CSI), is the parameter which compares the fractional occurrence of the symbols for normal and anomaly conditions. Based on the CSI value, anomaly condition of bearing is detected.

In this method, two signals are used. One is a reference signal which is from healthy data. Other is a signal (test signal) whose condition is to be determined. A common signal index is calculated by using the fractional occurrences of the symbols in both the signals. Of the five CSI considered, two CSI (fault index) used are CSI1 and CSI3. Initially, testdata1 is used for testing the approach. For healthy bearing, CSI1 and CSI3 attain a value close to 0.5 and 0 respectively. For faulty conditions, CSI1 values are well below 0.5 and CSI3 values are farther above from 0. On the basis of the results obtained, bearing condition is classified using the rule: If CSI1 = 0.48 to 0.5 or CSI3 = 0 to 0.2, Bearing is in healthy else faulty.

The effect of noise and sample size on the fault index is also studied and the bearing fault detection was carried out successfully. In order to verify the results obtained from the test data1, the CSI values were computed for testdata2 and testdata3. For these test data also, the method was found to work well. Finally, a comparison of the proposed method with the other existing time domain and data based methods that used the same test data1 is carried out. The advantage of the developed symbolic dynamic method for bearing fault detection over the other methods is shown.

CHAPTER 4 IDENTIFICATION OF FAULTY BEARINGS USING SINGULAR VALUE RATIO: CASE STUDY

Chapter 4 investigates the possibility of using the ratio of singular value (SV) as a fault index for detection of faulty bearing. The fault index is calculated using singular spectrum analysis. Initially, a process known as embedding of the input vibration signal is carried out. In this step, the signal is mapped to L dimension vector matrix. To this matrix, singular value decomposition (SVD) is carried to calculate L singular values. SVD helps in decomposition of the input signal. Singular value is given by the square root of eigenvalue. Different L values are used to calculate the appropriate value (L=10). Singular Value Ratio (SVR) is the ratio of adjacent singular values. There are five SVRs considered.

The SVR should clearly differentiate the healthy and faulty conditions i.e. it should have different range of values in healthy and faulty conditions. Test data1 is used for the analysis. Two SVR are selected. The effect of load, noise, fault size and sample size is studied. The result shows that the faulty bearing is identified even under the variation of the above parameters.

CHAPTER 5 BEARING FAULT DIAGNOSIS USING SINGULAR SPECTRUM ANALYSIS

Chapter 5 reports the time series method for bearing fault feature extraction using Singular Spectrum Analysis (SSA)**.** SSA is used for the decomposition of the acquired signals into an additive set of principal components. A new approach for the selection of the principal components is also presented using the singular value plot. Two methods of feature extraction are implemented. In first method, the Singular Values of the selected principal components are adopted as the fault features, and in second method, the energy of the principal components corresponding to the selected SV numbers are used as features. A back propagation neural network (BPNN) is used for fault diagnosis.

Test data1 and Test data2 are used for the testing of the two approaches. The effect of sample size, fault size and load on the fault features is studied. The advantages of the proposed method over the exiting time series method are discussed. The experimental results demonstrate that this bearing fault diagnosis method is simple, noise tolerant, efficient even under masking sources and higher classification rate.

CHAPTER 6 GENERALIZED TEAGER KAISER ENERGY OPERATOR BASED BEARING FAULT DIAGNOSIS

Chapter 6 describes the demodulation method based on Generalized Teager Kaiser Energy operator (GTKEO) for detecting the FCF. Only one parameter is required to be known and method to choose it, is given. The concept of GTKEO in demodulating the bearing vibration signal is discussed in detail. The reason for the enhancement of faulty signal component in presence of other vibration interferences is provided.

The steps involved are: The input signal is transformed using Generalized Teager Kaiser Energy Operator; then, spectrum analysis of the transformed signal is performed to detect the presence of any fault characteristic frequency. Test data1 and Test data2 are used for verifying the method. The advantage of using Generalized Teager Kaiser Energy Operator with parameter free methods under a very low SNR is elucidated. Further, to validate the method, test data 5 is used. This approach could be used in a handheld vibration analyzer.

CHAPTER 7 PERFORMANCE INDEX DEVELOPMENT USING SUPPORT VECTOR DATA DESCRIPTION METHOD

Chapter 7 explains the proposed method to assess the bearing health using the combination of fault features and support vector data description (SVDD) classifier. The fault features (Singular Value Ratio and Common signal Index1, Common signal Index3) which are developed in this thesis are used. Test data 4 is used for the analysis. The fault features are compared with the existing fault features used for fault degradation studies. They are root mean square value, kurtosis value, crest factor, approximate entropy, spectral entropy and K-S statistic distance. To have a single parameter to trend the bearing condition, performance index is developed using SVDD classifier. The advantage of using SVDD is that it needs only healthy data during the training. The test data contains both healthy and faulty data. Performance index is formed based on the distance of the test data to the boundary of the training data. Gaussian kernel function is used in SVDD. Performance index is compared with another index known as H-statistic [15]. The developed performance index trends the bearing condition from healthy to fault initiation and until it fails.

CHAPTER 8 SUMMARY, CONTRIBUTIONS AND OPEN QUESTIONS/FURTHER SCOPE

Chapter 8 outlines the summary of the each work carried out along with the important contributions from the research work. Also, recommendations for further study are made.

OVERALL WORK

Condition Monitoring Stage	Methodology	Based on
Fault Detection	Symbolic dynamics (SD) Singular Spectrum Analysis (SSA)	Fault Index - Common Signal Index (CSI) Fault Feature - Singular Value Ratio (SVR)
Fault Diagnosis	SSA and Back Propagation Neural Network Generalized Teager Kaiser Energy Operator	Fault Feature - Singular Value, Energy Value Fault characteristic frequencies detection
Fault Prognosis (Degradation)	SSA, SD, Support Vector Data Description (SVDD)	Performance Index based on SVDD using CSI and SVR

9. CONTRIBUTIONS

The work presented in this thesis includes novel approaches and improved the state-of-art vibration based rolling element bearing condition monitoring. They are listed below:

- A first approach based on symbolic dynamics for detection of faulty bearing using vibration signal is implemented. It overcomes the shortcomings of existing time domain and data based methods.
- Noise immune and sample size invariant bearing fault detection methods based on new fault indices (Common Signal Index, Singular Value Ratio) are presented.

- ➔ A simple online fault diagnosis method based on Generalized Teager Kaiser Energy Operator is developed and effectively verified. It does not require the band pass filter (conventional approach) and works well even for a low SNR signals. It is a useful method for a handheld vibration analyzer.
- ➔ A method based on singular spectrum analysis is discussed for fault feature extraction and successfully diagnosed the faults of the tested bearings.
- ➔ A Performance Index (degradation condition indicator) for bearing fault prognosis is developed.

10. REFERENCES

1. Bell, R. N., McWilliams, D. W., O'DONNELL, P., Singh, C., & Wells, S. J. (1985). Report of large motor reliability survey of industrial and commercial installations. I.IEEE Transactions on Industry Applications, 21(4), 853-864.
2. Albrecht, P. F., Appiarius, J. C., Cornell, E. P., Houghtaling, D. W., McCoy, R. M., Owen, E. L., & Sharma, D. K. (1987). Assessment of the reliability of motors in utility applications. Energy Conversion, IEEE Transactions on, (3), 396-406.
3. Thorsen, O. V., & Dalva, M. (1995). A survey of faults on induction motors in offshore oil industry, petrochemical industry, gas terminals, and oil refineries. Industry Applications, IEEE Transactions on, 31(5), 1186-1196.
4. Bari, H. M., Deshpande, A. A., Jalkote, P. S., & Patil, S. S. (2012, May). Pump Coupling & Motor bearing damage detection using Condition Monitoring at DTPS. In Journal of Physics: Conference Series (Vol. 364, No. 1, p. 012022). IOP Publishing.
5. Graney, B.P., & Starry, K. (2012). Rolling Element Bearing Analysis. Materials Evaluation, 70(1), 78-85
6. Zhou, W., Habetler, T. G., & Harley, R. G. (2007, September). Bearing condition monitoring methods for electric machines: A general review. In Diagnostics for Electric Machines, Power Electronics and Drives, 2007. SDEMPED 2007. IEEE International Symposium on (pp. 3-6). IEEE.
7. ISO 10816 Series Mechanical vibration-Evaluation of machines vibration by measurements on non-rotating parts

8. R.B. Randall, Vibration based condition monitoring: industrial aerospace and automotive applications, Wiley, 2011.

9. Randall, R. B. (2004). Detection and diagnosis of incipient bearing failure in helicopter gearboxes. Engineering Failure Analysis, 11(2), 177-190.

10. Cong, F., Chen, J., & Pan, Y. (2011). Kolmogorov-Smirnov test for rolling bearing performance degradation assessment and prognosis. Journal of vibration and control, 17(9), 1337-1347.

11. Bearing data Centre, Case Western Reserve University Available : <http://csegroups.case.edu/bearingdatacenter/home>> [accessed May 2010]

12. Sawalhi, N., & Randall, R. B. (2008). Simulating gear and bearing interactions in the presence of faults: Part I. The combined gear bearing dynamic model and the simulation of localised bearing faults. Mechanical Systems and Signal Processing, 22(8), 1924-1951.

13. J. Lee, H. Qiu, G. Yu, J. Lin, and Rexnord Technical Services (2007). 'Bearing Data Set', IMS, University of Cincinnati. NASA Ames Prognostics Data Repository, [http://ti.arc.nasa.gov/project/prognostic-data-repository] [accessed: April 2013]

14. Society for Machinery failure Prevention Technology http://www.mfpt.org/FaultData/FaultData.htm [accessed : May 2013]

15. Yu, J. (2012). Local and nonlocal preserving projection for bearing defect classification and performance assessment. *Industrial Electronics, IEEE Transactions on*, *59*(5), 2363-2376.

LIST OF ABBREVIATIONS AND SYMBOLS

FCF	Fault Characteristic Frequency
SNR	Signal-to-Noise Ratio
d	Ball diameter
D	Pitch diameter
Z	Number of rolling elements
α	Contact angle
f_o	Outer race fault frequency
f_i	Inner race fault frequency
f_b	Ball fault frequency
f_c	Cage speed frequency
f_r	Rotational frequency
BPFO	Ball Pass Outer Race Frequency
BPFI	Ball Pass Inner Race Frequency
BSF	Ball Spin Frequency
FTF	Fundamental Train Frequency
L_{10}	Bearing service life or rating life
ANN	Artificial Neural Network
K-S	Kolmogorov-Smirnov
D	Statistic value of K-S test
SD	Symbolic dynamics
CSI	Common Signal Index
MEP	Maximum Entropy based Partitioning
ε	Threshold
K	Number of symbols
f_{xi}	Fractional occurrence
HP	Horse Power
H	Healthy
I	Point defect on inner race
O	Point defect on outer race
B	Point defect on ball

LIST OF ABBREVIATIONS AND SYMBOLS contd..

w_m	Word length
AR	Autoregressive
ARMA	Autoregressive Moving Average
SSA	Singular Spectrum Analysis
SVD	Singular Value Decomposition
SV	Singular Value
SS	Singular Spectrum
SVR	Singular Value Ratio
L	Window length
IF	Inner race Fault
OF	Outer race Fault
BF	Ball Fault
BPNN	Back Propogation Neural Network
PSD	Power Spectral density
C	Principal component
DH	Difference Histogram
ZC	Zero Crossing
HMM	Hidden Markov Model
GMM	Gaussian Mixture Model
SLLEP	Supervised Locally Linear Embedding Projection
SVM	Support Vector machine
RMS	root mean square
Kv	kurtosis
GTKEO	Generalized Teager Kaiser Energy Operator
M	Lag parameter
TKEO	Teager Kaiser Energy Operator
$\Psi[]$	TKEO mathematical notation
$\Psi_M[]$	GTKEO or M-TKEO mathematical notation
ER	Energy Ratio
f_n	Resonant frequency

LIST OF ABBREVIATIONS AND SYMBOLS contd..

β	Damping constant
Ψ_c	Cross energy term operator
WGN	White Gaussian Noise
SER	Signal Enhancement Ratio
SIR	Signal to Interference Ratio
IR	Improvement Ratio
RUL	Remaining Useful Life
SVDD	Support Vector Data Description
R1	Radius of hypersphere
R2	Distance of test data to centre
σ	Width of the gaussian function
PI	Performance Index
Crf	Crest factor
ApEn	Approximate Entropy
SpEn	Spectral Entropy
PMM	Power ratio of Maximal defective frequency to Mean
DLNPP	Dynamic Local And Nonlocal Preserving Projection
GUI	Graphical User Interface

LIST OF FIGURES

LIST OF FIGURES contd..

LIST OF FIGURES contd..

LIST OF FIGURES contd..

LIST OF FIGURES contd..

LIST OF FIGURES contd..

LIST OF TABLES

LIST OF TABLES contd..

PART I

THE BACKGROUND

MAIN CONTENTS:

CHAPTER 1

INTRODUCTION

MAIN CONTENTS:

- **Research Problem**
- **Motivation and Significance**
- **Research Questions**
- **Objectives**
- **Methods and Approaches**
- **Structure of Thesis**
- **Analyzed Data**
- **Organization of the Thesis**

1.1 RESEARCH PROBLEM

Bearings are the most commonly used components in any mechanical equipment such as pumps, wind turbines, cranes and hoists. They bear much of the load component. This when combined with harsh operating conditions such as in high temperature, corrosive environment, dust increases the chances of bearing failures. Based on the survey reports on various faults occurring in rotating machines, it is observed that majority of the faults occur as bearings faults [Bell et al. 1985; Albrecht et al. 1987; Thorsen et al. 1995]. Condition monitoring refers to monitoring the current state of a machine and predicting its future state while in the operation. Currently, condition based maintenance is considered as the most efficient maintenance strategy for industries. A recent motor bearing failure case study of a thermal power plant in India [Bari et al. 2012], showed that the capital saved by condition monitoring was around 2.3 crores rupees ($ 4,00,000). Condition monitoring of bearing is very much important for various reasons such as to increase equipment availability, safety, reliability, and preventing the capital loss due to its unavailability.

Generally, bearing is classified into two types- rolling element bearing and journal bearing. Rolling element bearings are used in more than 90% of the rotating machinery found in various applications [Graney & Starry, 2012]. They are prone to myriad of premature failures. A mere 10% of them reach their expected service life [Graney & Starry, 2012]. Hence, condition monitoring of rolling element bearing (hereafter, bearing) is considered for the research problem.

Bearing condition monitoring is done using various methods [Zhou et al., 2007] such as vibration analysis, chemical analysis, temperature measurement, acoustic emission and current monitoring. Of these, vibration based monitoring is widely used in industries and also available as the standard ISO 10816 [ISO 10816]. Bearing condition monitoring is conducted in three phases namely fault detection, diagnosis and prognosis. Fault detection phase (Anything wrong?) determines whether the bearing is healthy or faulty. Once the fault is detected, the location of the fault is found in the diagnosis phase (Where it occurred?). Prognosis phase (How much is the level and when it occurred?) deals with the fault degradation and remaining useful life of the bearing. It is the development and continuation of fault detection. In the prognosis study carried out, only the fault degradation assessment is considered.

For this thesis, monitoring methods for fault detection, fault diagnosis and fault degradation assessment are developed.

1.2 MOTIVATION AND SIGNIFICANCE

The main motivation of this research is to investigate the use of vibration analysis and to develop the state-of-art signal processing methods for the condition monitoring of bearings.

A vibration signal generated by a bearing fault is pseudo cyclo-stationary in nature [Randall, 2011], so it is essential to extract the fault features accurately from the collected vibration signal. These features are critical for determining the bearing condition (healthy or faulty) and would be useful in the prognosis phase. Mostly, time domain methods are used for calculating the fault features. However, the results of these methods are found to be vary with sample size, load and noise. It is an area where research is still needed.

Spectrum analysis is the most commonly used method for fault diagnosis where the fault characteristic frequency (FCF) components are extracted from a vibration signal to localize a fault. Fault on the each element of bearing produces a distinct FCF. FCFs are mainly amplitude modulated because of two reasons: First, due to the transfer function of the transmission path between the bearing and the sensor; Second, the load carried by the rolling elements. It is also frequency modulated due to the variation in the instantaneous shaft rotating frequency. Due to roller slippage [Randall, 2004], the repetition duration may vary slightly which causes the smearing of the spectrum. The vibration measured from a equipment not only contain the fault characteristic frequencies, but also the vibrations generated by other mechanical components (e.g. gear meshing), shaft imbalance or misalignment or bent /cracked shaft along with the background noise. All the above factors complicate the quality of diagnosis decisions to be taken when the fault is in the incipient stage. Thus, fault diagnosis methods which can extract the incipient fault under the presence of masking sources and background noise are required to be developed. In addition to it, the method needs to be simple and efficient, from the feasibility point of view.

Bearing fault degradation has strong fuzziness and the dynamic information is random. The main difficulty in its effective implementation is the highly stochastic nature of fault. The features (e.g. root mean square, kurtosis and crest factor) used for fault degradation assessment have stability problems with the fault severity [Cong et al., 2011]. Hence, robust "fault" features are required to accurately trend the fault. Exploration of new and effective indices has to be carried out to develop an effective prognostic system.

The important significance of this research is the development of a simple online automated approach useful for a handheld vibration analyzer and the development of some novel effective fault indices useful for fault detection and fault prognosis.

1.3 RESEARCH QUESTIONS

Based on the problem considered and the literature study carried out, the following questions would be investigated and solved in this thesis:

i. Is it possible to employ a simple online method for bearing fault detection?

ii. Whether an effective fault index to differentiate between the healthy and faulty bearing could be developed?

iii. Whether a noise tolerant and an efficient bearing fault feature extraction and diagnosis method could be developed?

iv. How a bearing fault could be localized for a low signal-to-noise ratio (SNR) condition without using any de-noising technique or without the need of designing a band pass filter and nor applying a complex time–frequency method?

v. How to select some features which can evaluate comprehensively the performance degradation severity?

vi. How an effective index for comprehensive performance degradation severity could be obtained after extracting the features?

1.4 OBJECTIVES

This research concentrates on the development of robust methods covering the three phases of bearing condition monitoring, namely fault detection, diagnosis and prognosis. The objectives behind each work are discussed below:

1.4.1 Fault Detection

At the fault **detection** stage, the raw vibration signals are processed to extract the fault features. Most of the time domain and data based signal processing methods used are noise sensitive, sample size dependent, machine and load dependent or involving complex mathematical calculations or need of much training.

The main objective of the work in ‘Detection’ stage would be:

i. Development of an effective fault feature extraction algorithm, which could solve the above mentioned problems and also suitable for online bearing condition monitoring.

ii. Some novel fault indices would also be identified to detect the faulty bearing at its incipient fault stage.

1.4.2 Fault Diagnosis

Once the fault in bearing is identified at the detection stage, next (**diagnosis** stage) spectrum analysis is carried out to extract the fault characteristic frequency related to the location of the fault in bearing (inner race, outer race, rollers and cage).

Considering that not many time, reliable diagnostic information may not be obtained from the spectrum of the raw signal [Randall, 2011], the diagnostic methods are developed in this thesis with an objective of:

i. An automated method which is simple in implementation and applicable to the signals with low SNR. It should not require designing the band pass filter (conventional method) or de-noising, before processing the raw signal for the spectrum analysis.

ii. A time domain approach to be identified which is useful for diagnosis with advantages such as noise immunity and sample size variant.

1.4.3 Fault Prognosis

In the fault **prognosis** work, fault degradation assessment is considered. At this stage, information regarding the degradation in the bearing performance should be accurate so that further decisions and actions could be planned. The method should provide various information's such as the status of fault severity, its progression and time to failure. Many trending parameter have been developed which do not show consistent performance with the fault severity. The work in this stage focuses on:

i. Development of better fault trending features which show the different stages of bearing fault severity with better accuracy.

ii. Use of appropriate parameters to develop an accurate bearing performance indicator.

1.5 METHODS AND APPROACHES

The algorithms developed are mainly based on the signal processing in time and frequency domains along with the application of various data mining techniques. To test and validate the algorithms, signals from various sources such as simulation, experimental and those from industries are considered. In order to address the various research questions, the methods and approaches explored are discussed in the following subsections.

1.5.1 Fault Detection

Two new fault detection methods are proposed. They are based on:

i. The concept of symbolic dynamics is used for the fault index.

ii. Singular spectrum analysis is used as a preprocessing method (time domain) for obtaining the fault feature.

1.5.2. Fault Diagnosis

Fault diagnosis is generally carried out by using the spectrum analysis to detect the fault characteristic frequencies. An alternative approach based on time domain and data based technique is proposed in this stage. Overall, two algorithms are developed for bearing fault diagnosis: first is based on fault characteristic frequency detection and the second method is based on the fault feature.

i. Generalized Teager Kaiser Energy Operator (GTKEO) is used to extract the fault characteristic frequencies.

ii. Singular spectrum analysis is used as a fault feature extraction method and feed forward back propagation neural network is used for classifying the condition of bearing into four classes: healthy, inner race fault, outer race fault and ball fault.

1.5.3 Fault Prognosis

In the fault prognosis study, fault features developed in this thesis and the support vector data description method are used to obtain a condition degradation indicator.

1.6. STRUCTURE OF THESIS

Thesis layout: general

Part I The Background

Chapter 1 Introduction

Chapter 2 An Overview of Rolling element bearing faults and vibration based condition monitoring methods

Part II Fault Detection

Chapter 3 Detection of faulty bearing using symbolic dynamics

Chapter 4 Identification of faulty bearing using singular value ratio: a case study

Part III Fault Diagnosis

Chapter 5 Bearing fault diagnosis using singular spectrum analysis

Chapter 6 Generalized Teager Kaiser Energy operator based bearing fault diagnosis

Part IV Fault Prognosis

Chapter 7 Performance Index development for fault degradation using the support vector data description method

Part V Highlights and Foresight

Chapter 8 Summary, Contributions and Further Scope/ Gap Areas

1.7. ANALYZED DATA's

Different types of bearing fault data's are used for the verification and validation of the proposed methods of fault detection, fault diagnosis and fault degradation. Four sources of data are used: numerical simulation, artificially seeded fault, bearing accelerated life test and real industrial case.

1.7.1 Experimental data with artificially seeded fault (Test data1 and 2)

They are collected from two different test rigs. First test rig (**Test data1**) has a simple setup of induction motor with dynamometer. It is taken from the Case Western Reserve University [Bearing data Centre]. Point defects of different sizes (width 0.18 mm to 0.71 mm range, depth of 0.28 mm) are seeded on inner race, outer race and ball. SKF 6205 series deep grove ball bearing is used. The data are also collected for different combinations of load (no load to full load) and its corresponding speed. These are analyzed in fault detection (Chapters 3 and 4) and fault diagnosis (Chapters 5 and 6) approaches.

From the second test rig (**Test data2**), signals are obtained in the presence of a spur gearbox. The data is obtained from the University of New South Wales [Sawalhi & Randall, 2008]. The setup consists of single stage gearbox driven primarily by a 3Φ motor and powered by a hydraulic motor-pump set. Koyo 1205 series of double row ball bearing is used. Point defects in inner race and outer race (width of 0.8 mm, depth of 0.3 mm), ball defect with both width and depth of 0.5 mm was made. These are used in fault detection (Chapter 3) and fault diagnosis (Chapters 5 and 6) approaches.

1.7.2 Simulation data (Test data3)

Bearing vibration signal is represented in simple mathematical form based on the single point defect model [McFadden & Smith, 1984a]. External vibration interferences such as gearbox and noise are considered. It is used in fault detection method (Chapter 3).

1.7.3 Industrial data (Test data4)

The industrial data is obtained from the Society for Machinery failure Prevention Technology [MFPT] which is used for validating the fault diagnosis based spectrum analysis method (Chapter 6). Three cases of data's are used: planet bearing (both ball and outer race defects); Intermediate shaft (ball defect) and oil pump (inner race defect) of a wind turbine.

1.7.4 Bearing Accelerated life test data (Test data5)

Bearing accelerated life test data is taken from University of Cincinnati [Lee et al., 2007]. It is to evaluate the fault degradation method (Chapter 7). The test rig consists of

AC motor coupled to the shaft via rubber belts. Rexnord ZA-2115 double row bearing are installed on a shaft and are oil force lubricated. The test is carried out until the amount of debris collected in the lubrication system exceeds a limit.

1.8 ORGANIZATION OF THE THESIS

The thesis is divided into **five parts** consisting of **eight chapters** including this chapter. Their contents are briefly described here.

Chapter 2 – Discussion of the general concepts related to bearing faults, their causes, condition monitoring philosophy and the various vibration signal analysis methods related to the each stage of bearing condition monitoring.

Chapter 3 – The method based on symbolic dynamics for classifying the bearing condition i.e. healthy or faulty is presented. Testing of the method is done using three sources of signals: simulation signal (Test data3) and two experimental test-rigs data (Test data1 and Test data2).

Chapter 4 – The method with the possibility of using the ratio of singular value for detection of a faulty bearing is described. Experimental test-rig data (Test data1) is used for testing.

Chapter 5 – Reports the application of singular spectrum analysis for bearing fault diagnosis. The analysis is carried on the Test data1 and Test data2 signals. The method is compared with the existing time domain and data based fault diagnosis methods.

Chapter 6 – Presents a simple approach for spectral analysis based on the application of Generalized Teager Kaiser Energy Operator. A comparison with the parameter-free fault diagnosis method (Teager Kaiser Energy Operator) is done. The method is tested with two experimental test-rig data’s (Test data1 and Test data2) and further validated using various the industrial signals (Test data4).

Chapter 7 – Description of the development of a Performance Index for bearing performance degradation assessment. The fault features developed for fault detection is used along with Support Vector Data Description for trend analysis. It is tested with the data obtained from an accelerated bearing life test bench (Test data5). The developed fault index is compared with the other reported one from the literature (H statistic).

Chapter 8 – Outlines the summary of the each work carried out along with their advantages and limitations. Important contributions from the research work are outlined. Finally, the recommendations for further study are made.

With this introduction to the research problem and thesis, the background of the research problem is further built in the next chapter (Chapter 2), where the general concepts related to bearing faults & its causes, condition monitoring philosophy and existing monitoring techniques are been discussed.

CHAPTER 2

AN OVERVIEW OF ROLLING ELEMENT BEARING FAULTS AND VIBRATION BASED CONDITION MONITORING METHODS

MAIN CONTENTS:

- **Introduction**
- **Rolling Element Bearing**
- **Bearing Faults and its Causes**
- **Bearing Fault Signature and its Frequencies**
- **Different Stages in Bearing Fault Development**
- **Bearing Condition Monitoring Philosophy**
- **Existing Vibration Signature Analysis Methods**
- **Need for newer methods and approaches**

2.1 INTRODUCTION

Chapter 2 provides the information regarding the basic concepts related to the rolling element bearing and its condition monitoring. It includes about the rolling element bearing in general, different types of defect found in bearings and its causes, bearing fault signature and the various fault characteristic frequencies, different stages of bearing fault development, basic bearing condition monitoring philosophy and the various techniques used in vibration based bearing condition monitoring.

The bearing condition monitoring philosophy discusses the steps involved namely, data acquisition, data processing and decision making. The methods used in each of these steps are briefly outlined. The existing methods of vibration based fault detection, fault diagnosis and fault prognosis (fault degradation) are presented. The concept described here does not include other techniques (oil, temperature, current, acoustic based), as vibration analysis is used in this thesis work.

2.2 ROLLING ELEMENT BEARING

Rolling element bearings are those bearings in which the load is transferred through the elements through rolling rather than sliding. The advantage in rolling over sliding is the reduction of friction between the moving objects. They are used in more than 90% of the rotating machines.

The structure of a typical bearing is shown in figure 2.1. It consists of outer race, inner race, rolling elements and cage. The rolling elements are of different shapes such as sphere and cylinder. The bearing dimensions are: d is the rolling element diameter, D is pitch diameter, Z is number of rolling elements and α represents the contact angle. α varies with the position of each rolling element in the bearing. It can be assumed to be fixed for calculation purpose. Defect or fault can occur in bearing in any of its structure. f_o, f_i, f_b, f_c and f_r represents the outer race fault frequency, inner race fault frequency, ball fault frequency, cage speed frequency and rotational frequency respectively. As the ratio of local radial to axial load changes, each element has a different effective rolling diameter and each rolls at a different speed. The cage ensures that the mean speed of all the rolling elements remains same.

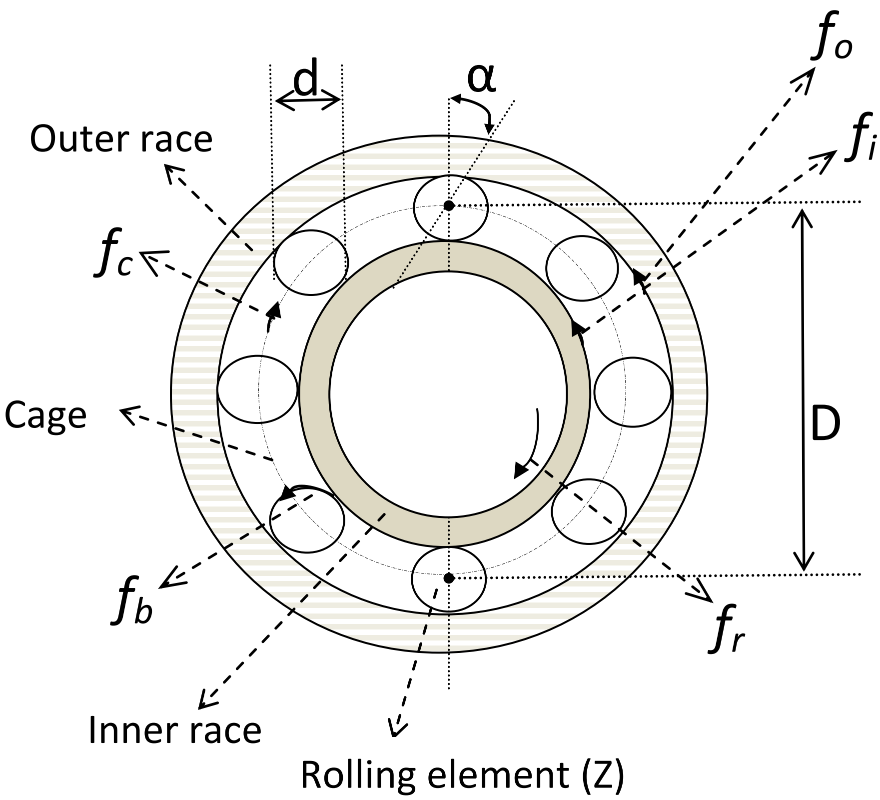

Figure 2.1 Typical bearing construction

Depending upon the load subjected (radial, thrust and both) different types of bearing are been used. Ball bearing has sphere as the rolling elements, where both the radial and thrust load are developed. However, it can sustain only small amount of load since the contact between the outer and inner race is a point contact (less area carrying the load). Roller bearing is used in application such as conveyor belts where radial load is formed. For cylindrical roller bearing, the rolling element is a cylinder which helps to increase the load bearing surface area and hence it used for larger load as compared to ball bearing. For ball and cylindrical roller bearing, α is 0°.There are ball thrust and roller thrust bearing designed to handle thrust loads. It's α value is 90°. Ball thrust bearings are found in barstools and roller thrust bearings are found in gearbox systems. The region of bearing supporting the load is known as load zone. For monitoring the bearing fault, vibration sensor has to be mounted in the direction of load zone.

Generally, bearing service life is given by the term L_{10} life. L_{10} life or Rating life is the total number of revolutions or hours at a given constant speed that 90% of similar bearings will complete before failure [Starns, 2002]. It is calculated as [ISO 281]:

$$L_{10} = \left(\frac{C}{P}\right)^p 10^6 \text{ revolutions} \quad \text{or} \quad L_{10} = \left(\frac{C}{P}\right)^p \frac{10^6}{60*RPM} \text{ hours} \tag{2.1}$$

where, C is rated capacity (kN), P is bearing load (kN), RPM is machine speed (rpm), exponent p = 3 for ball bearings and p = 10/3 for roller bearings.

The above equation (2.1) shows that for ball bearing, its service life is inversely proportional to load (P^3) and machine speed (RPM). On doubling the load, the service life reduces to 12.5 %. For doubling the speed, there is reduction in service life by 50%.

2.3 BEARING FAULTS AND ITS CAUSES

Bearing can fail in many ways and there are different reasons which occur at the different stages of its service life. Less than 1 percent of bearing do not attain their expected life [FAG bearing, 1979]. But when a bearing fails it can cause a huge consequential damage. When a bearing fails prematurely, it occurs due to an avoidable cause. The main causes considered are mounting issues, operational stress, lubrication problems and environmental effect. Figure 2.2 shows a survey of FAG corporation [FAG bearing, 1979] on the causes of bearing failure. A recent data on the different failure causes reported by Tranter [Tranter et al., 2013] is given in table 2.1.

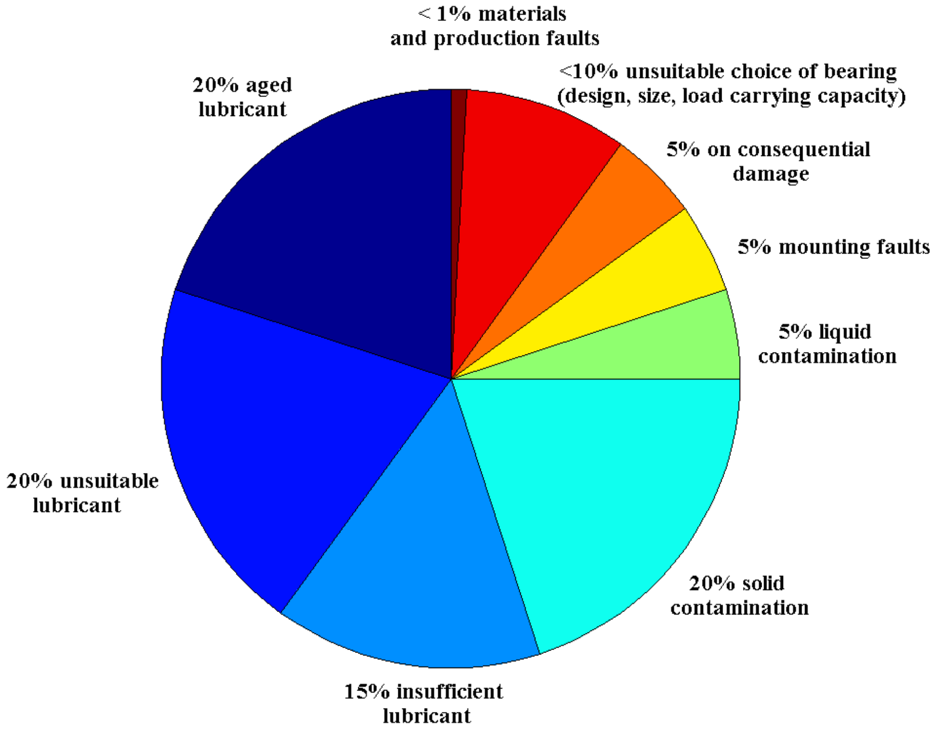

Figure 2.2 FAQ report on causes of failure of bearing [FAG bearing, 1979]

Table 2.1 Percentage of bearing failure cause [Tranter et al., 2013]

Failure Cause	% of occurrence
Over-lubrication	36
Fatigue Excessive loading (shaft misalignment and rotor imbalance)	34
Improper handling / installation	16
Lubricant contamination	14

By visually inspecting the defect appeared on the bearing part, there is a possibility to find the cause of a defect. In [FAG Bearings, 1997], the relationship between the defects appeared on the bearing parts and their causes are discussed which are given in table 2.2 and 2.3. Generally, bearing failures can occur as flaking, spalling, smearing, wear, speckles, rust, dents and fretting. Description of these failures with the illustrative figures is given in [Widner & Littmann, 1976].

2.4 BEARING FAULT SIGNATURE AND ITS FREQUENCIES

2.4.1 Bearing Fault Signature

Faults such as spalls or cracks on the inner race, outer race and ball elements causes failures in bearings. When these faults come in contact with the other surfaces, an impulsive force is generated. These impulses excite resonances in bearing, sensor, machine and the mechanical structure on which machine is erected. This high frequency resonance is damped out due to the structural damping of the system. Cyclic occurrence and damping out of resonance are observed due to the repetitive contact between the fault and other rolling surfaces. A series of impulse responses is generated which may be amplitude modulated by two factors [Randall & Antoni, 2011]: 1) Rate at which the fault is passing through the load zone. 2) The transfer function of the transmission path varies with respect to position of the transducer. The spectrum of such a signal would consist of harmonic series of characteristic fault frequency depending on the region of fault with the highest amplitude around the resonance frequency. Sidebands around the fault frequency are observed if there is an amplitude modulation [Ho & Randall, 2000]. By studying these sidebands, bearing fault can also be diagnosed. The roller slippage leads to the random deviation between the spacing of the impulses and causes the spectrum to smear.

Slippage occurs as the load angle on each rolling elements changes as rolling elements move in and out of the load zone. This means that some roll faster than others. However, the cage keeps them apart at a certain mean spacing and all the rolls rotate at an average cage speed [Ho & Randall, 2000]. Due to smearing and background noise, harmonics of fault characteristic frequency in the high frequency region may not be observed in the spectrum [Liang & Soltani, 2010]. The location of the vibration sensor is very much important in obtaining a clean fault signal [Fatima et al., 2013].

Table 2.2 Bearing damage symptoms and their causes: Part I [FAG Bearings, 1997]

Appearance found on bearing parts	**Typical causes of bearing damage**								
	Mounting						**Operational stress**		
	In-correct mounting procedure	Dirt	Fit too much	Loose fitting	Poor sup-port of rings	Misalign-ment or shaft deflection	Load too high or low	Vibrations	High speeds
Foreign particle indentation		●							
Fatigue	●	●	●		●	●	●		
Stationary Vibration marks								●	
Skidding				●			●		
rolling element indentation	●						●		
Seizing marks							●		●
Wear		●							
Over-heating damage			●						●
Fractures	●		●		●				
False brinelling				●	●			●	

Table 2.3 Bearing damage symptoms and their causes: Part II [FAG Bearings, 1997**]**

Appearance found on bearing parts	**Typical causes of bearing damage**						
	Lubricant			**Environmental influence**			
	Unsuitable lubricant	Insufficient lubricant	Excess lubricant	Dust, dirt	Aggressive media, water	External heat	Current passage
Foreign particle indentations				●			
Fatigue	●	●		●		●	
Molten dents & flutes						●	
Skidding		●					
Seizing marks	●	●					
Wear	●	●		●			
Corrosion	●				●		
Overheating damage	●	●	●			●	

Figure 2.3 shows a typical bearing fault vibration signals generated for a machine with rotating inner race [Randall, 2011]. In this figure, one could see that the vibration impact (pulses) pattern is different for the fault originating in different location.

It depends on how the fault moves with the load zone [McFadden & Smith, 1984a]. This is explained here: The pulse will have maximum value when fault is in load zone and minimum value when it is out of the load zone. A fault in the inner race moves in and out of the load zone at the rate of shaft speed (f_r), while a fault in the rolling element moves through the load zone at the cage speed (f_c). Hence, inner race fault frequency (f_i) is amplitude modulated by the shaft speed, while ball fault frequency (f_b)

amplitude modulated by the cage speed. A fault in a stationary race (outer) will be in the load zone (acted upon by the same impact force during each roll). Thus, all the pulses will be of equal magnitude and there is no modulation (no side bands) found in the outer fault pulse. Cage fault frequency (f_c) will not normally appear as the fundamental defect frequency but will appear as sideband of the ball fault frequency [Berry, 1991].

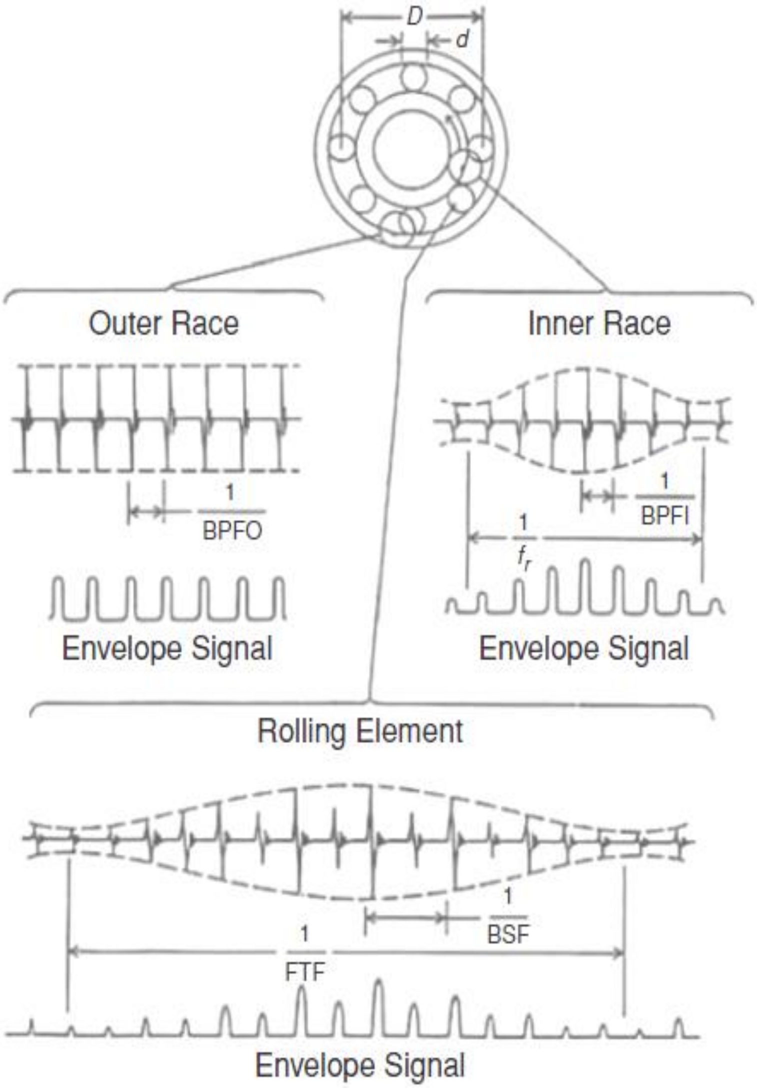

Figure 2.3 Typical bearing fault vibration signal and its envelope signal [Courtesy: Randall, 2011]. Note: BPFO is f_o ; BPFI is f_i ; 2*BSF is f_b and FTF is f_c .

In inner raceway, the defect propagates at a very faster rate than at outer raceway. The reasons are [Williams et al., 2001]: a) Fault characteristic frequency for inner race is greater than for an outer race. b) The impact force in inner race is concentrated on a smaller area due to small radius leading to high stress.

Inner race fault is less detected than outer race fault. It is because the defect in inner race moves through load zone once in every revolution and the impact vibration sensed by the sensor is attenuated largely through the various mediums (lubrication, outer race, bearing housing). If there is more than one type of fault, the vibration spectrum will contain all the respective fault characteristic frequencies. There will be a change in shape of the spectrum which depends on the relative position of the faults [Hansen, 2002].

2.4.2 Bearing fault characteristic frequencies

Defects in the different location of bearing generate additional vibrations at a particular frequency known as fault characteristic frequency which is used in the diagnosis of the bearing fault. Bearing fault characteristic frequencies are present in the vibration spectrum, but they are masked by the higher noise level and other vibration sources such as gearbox.

Theoretically, the fault characteristic frequencies for bearing with stationary outer race are calculated by the following formulas [Li et al., 2000]:

$$\left.\begin{aligned}
&\text{Inner race fault frequency, } f_i = \frac{Zf_r}{2}\left(1 + \frac{d}{D}\cos\alpha\right)\\
&\text{Outer race fault frequency, } f_o = \frac{Zf_r}{2}\left(1 - \frac{d}{D}\cos\alpha\right)\\
&\text{Rolling element fault frequency, } f_b = \frac{Df_r}{2d}\left(1 - \frac{d^2}{D^2}\cos\alpha\right)\\
&\text{Cage fault frequency, } f_c = \frac{f_r}{2}\left(1 - \frac{d}{D}\cos\alpha\right)
\end{aligned}\right\} \tag{2.2}$$

Where, Z is the number of rolling elements, d- rolling element diameter, D- Bearing pitch diameter, α- contact angle and f_r- shaft speed

Rolling element fault frequency is generally represented as double the ball spin frequency (BSF), where ball (rolling element) defect will impact both the outer and inner race during its rotation about its axis [Li et al., 2000; Ocak & Loparo, 2004].

When bearing geometry is unknown, the approximate fault characteristic frequencies are [Graney & Starry, 2012]: f_o = 0.4Zf_r, f_i = 0.6Zf_r, f_b =0.2Zf_r and f_c = 0.4f_r.

The fault characteristic frequencies in case of both the races rotating (for planetary bearing) are given in [Howard, 1994].

Theoretically calculated fault characteristic frequencies differ slightly (may be 1-2%) from the observed frequencies which depend on the type of bearing and operating conditions [Ho & Randall, 2000].

2.5 DIFFERENT STAGES IN BEARING FAULT DEVELOPMENT

For bearings even under normal operating conditions, fatigue failure begins with a small fissure [Eschmann et al., 1958]. These fissures are located between the surface of raceways and rolling elements. They propagate further to the surface level on further operation. The initiation of defect depends on the operating conditions, bearing design, installation and the environmental conditions. The occurrence of bearing failure is described generally in four stages as shown in Figure 2.4:

Stage 1 –In stage 1, the defect is minor (in the microscopic range) and predominantly sub-surface. The bearing has 10% to 20% of its L10 life [Mobius Institute]. The shock pulses will appear in the ultrasonic range (> 20 kHz). Hence, no change in the spectrum will be observed. Ultrasonic measuring equipment is required to detect this stage.

During this stage, the typically recommendation is to carry on with the monitoring at the scheduled period.

Stage 2 – When the fault progresses to stage 2, the sub-surface defects grows further and finally reach the surface in the form of cracks, flakes and spalls [Mobius Institute]. There will be a change in the vibration spectrum. The impact between the rolling elements and the races excites the bearing natural frequencies (850 to 1700 Hz) [Berry, 1991]. Bearing life would be 5% to 10% of its L10 life [Mobius Institute]. During the end of this stage, the natural frequency gets modulated with the motor rotational frequency. High frequency demodulated envelope analysis is required for detection. Time waveform may show some signs of defect.

At this stage, recommended action would be to check the lubrication and consider monitoring more frequently.

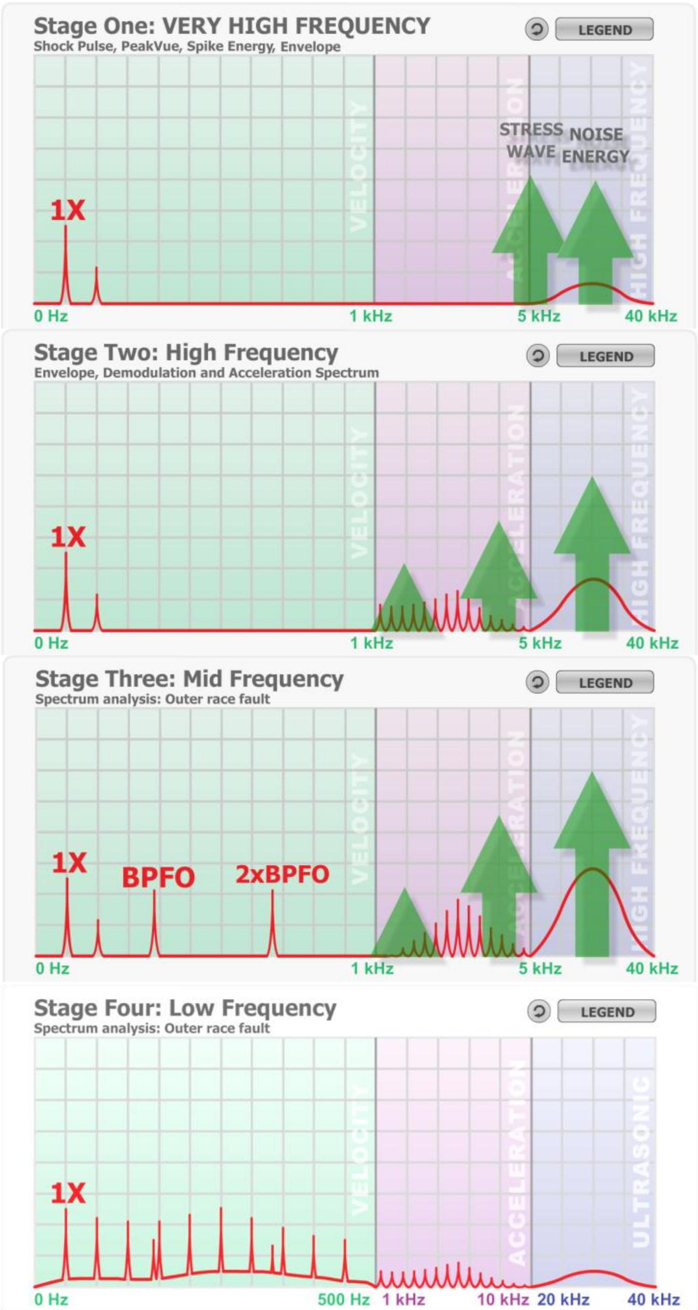

Figure 2.4 Typical vibration signatures during different stages of bearing defect progression [Courtesy of Mobius Institute]

Stage 3 – During the stage 3 of fault development, the defect grows more significantly and spreads to many locations. The bearing life is less than 5% of its L10 life [Mobius Institute].The bearing damage is clearly visible if removed. The fault characteristic frequency and its harmonics will increase in its magnitude. Time waveform will also show the presence of impacts.

At this stage, recommendation would be to replace the bearing unless the operation of machine is unavoidable with the knowledge of failure risk involved.

Stage 4 – At this stage of fault, the bearing is completely damaged. Due to complete wear, there are no huge impacts visible in vibration signal and there is a reduction in high frequency vibration. The distinct peaks at the fault characteristic frequencies may not be visible in the spectrum. Random peaks will develop and higher noise floor will be observed [Graney & Starry, 2012]. Due to loss of metal, large clearance in the bearing occur resulting into looseness. Hence, peaks at harmonics of fundamental rotating speed frequency will be observed.

During this stage, it will be recommended to schedule immediate change as the chance of catastrophic failure is very high.

In the above discussion of different stages of fault, it is assumed that all faults develop in the same pattern and there is a stage-wise degradation in the bearing condition. However, this assumption may not be valid in all the cases. Few of these cases are [Mobius Institute]:

i. In case of a machine operating for a longer period and false brinelling has occured, on further operation a catastrophic failure occurs. One may not see stage 1, 2 or even stage 3 vibration patterns; the bearing could go directly to the stage 4.

ii. During the formation of crack in a bearing, the metal pieces will be removed. At this moment, impacts will be visible in the vibration pattern. This shows that fault is of high severity. However, there are chances that during its further operation, the rolling element may smooth off the sharp edges and metal piece will flow along with the lubricant. Now, the vibration pattern may not show any impacts. It seems that bearing condition has improved which is actually not.

2.5.1 Estimation of the bearing defect stage

A general guideline for identification of the different stages of bearing defect was given by Woodward [Woodward, 1995]. It can be estimated by monitoring the highest fault characteristic frequency amplitude and maximum peak-to-peak value in time waveform. These values are compared with the values provided in the guideline for each stage for various rotational speeds [Woodward, 1995].

2.6 BEARING CONDITION MONITORING PHILOSOPHY

Condition monitoring deals with monitoring the present situation of a machine and predict its future condition during the operation. The general methodology [Jardine at al., 2006] involved is: data acquisition, data processing and decision making. The philosophy is been discussed below with respect to the bearing.

2.6.1 Data acquisition

Data acquisition deals with the process of collecting and obtaining the information regarding the machine condition. For bearing, the different parameters acquired are vibration, lubrication, temperature, ultrasound and current. Vibration analysis is used widely in industries and has been adopted as the standard ISO 10816 [ISO 10816-3, 1998]. For this thesis work, vibration signal is acquired for bearing condition monitoring using a accelerometer.

2.6.2 Data processing

Once the data is obtained, it is analyzed further to determine the condition. The data processing is done in two ways: based on scalar index or time series [Jardine at al., 2006].

2.6.2.1 Scalar index based

In scalar index based approach, fault information in the form of single value is obtained (For eg. vibration level). It includes both the raw data and the feature value extracted from the raw signal [Jardine at al., 2006]. Trend analysis is commonly used in this method. In [Sinha, 2002], polynomial regression and autoregressive moving average model was used to monitor the peak value of the raw vibration signal.

2.6.2.2 Time series based

The fault information is collected as a raw time series signal. It is processed using three approaches: Time domain analysis, frequency domain analysis and time-frequency domain analysis. These approaches with respect to bearing vibration analysis are described below.

2.6.2.2.1 Time domain analysis

Time domain analysis is carried out in many ways such as using visual analysis of history of time signal, time domain indices, probability density functions and statistical moments. The conventional time domain analysis involves calculation of the statistical features such as peak, peak-to-peak, standard deviation, root mean square, kurtosis, crest factor, skewness, clearance factor, impulse factor and shape factor [Dyer & Stewart, 1978; Alfredson & Mathew, 1985; Li & Pickering, 1992; Tandon, 1994; Sreejith et al., 2008]. The advanced methods deal with the application of time series models to the raw signals. The methods used are autoregressive (AR) model [Baillie & Mathew, 1996] and autoregressive moving average (ARMA) model [Ye et al., 2007]. The other methods also used are correlation dimension [Rolo-Naranjo & Montesino-Otero, 2005], principal component analysis [Malhi & Gao, 2004] and independent component analysis [Christian et al., 2007]. Methods have also been developed to separate the bearing fault signal from the masking vibration signals such gear mesh frequency. These methods are time synchronous averaging, linear prediction, Self adaptive noise cancellation technique, Discrete/random separation and new cepstral method. The review of these techniques is given in [Randall et al., 2011].

2.6.2.2.2 Frequency domain analysis

Frequency analysis helps in identification of the different vibration sources present in the vibration signal using spectrum analysis.

Spectrum comparisons are carried out to identify the faulty bearing using a reference healthy bearing spectrum. It has been suggested that an increase of 6-8 dB are to be seen as significant and changes of around 20 dB to be considered serious [Randall, 1985]. The fluctuation in the instantaneous speed causes a shift in position of the frequency peaks which leads to false warning. This problem was overcome by using a logarithmic frequency axis with constant percentage bandwidth [Bruel & Kjaer, 1990; Serridge, 1991]. Trending of the spectra has also been investigated using various spectral parameters such as matched filter root mean square and the RMS of the spectral difference [Mechefske, 1991].

Waterfall or Isoplot spectra are very useful in severe noisy conditions [Coffin & Jong, 1986; Howard, 1993]. A traditional water plot shows a three dimensional amplitude – time – frequency plot with a number of frequency spectra at a different time instant [Alfredson & Mathew, 1985b].

Spectrum analysis is also used to detect the fault characteristic frequencies [Su & Lin, 1992]. The conventional approach of spectrum analysis is by using Fast Fourier Transform (FFT) and power spectrum. The works related to the conventional approach is been discussed in [Randall, 1987]. The spectra are very much useful in determining the band of frequency where maximum change has occurred which could be further processed using the other techniques. The techniques used are cepstrum method [Bradshaw & Randall, 1983; Sujatha & Chandran, 2002] and envelope analyses by hilbert transform [Ho

& Randall, 2000]. High order spectrum [McCormick & Nand, 1999] such as bispectrum and trispectrum provides more diagnostic information than power spectrum. Also, parametric spectral based methods known as AR spectrum [Mechefske & Mathew, 1992a] and ARMA spectrum [Salami et al., 2001] have been used for estimating the power spectrum. Teager Kaiser Energy operator [Liang & Soltani, 2010] was used to demodulate the signals to obtain the fault characteristic frequency.

2.6.2.2.3 Time-Frequency domain analysis

Time-frequency (T-F) methods were introduced to overcome the limitation of frequency domain methods in analyzing the non-stationary signals. The traditional T-F domain methods are Short-time Fourier Transform (STFT) [Kaewkongka et al., 2003] and those based on distribution such as Wigner-Ville distribution (WVD) [Meng & Qu, 1991]. STFT has the limitation in time-frequency resolution. The distribution methods have the problem of introduction of interference terms during its operation. A method in which WVD is extended to higher order spectra known as Wigner higher order spectrum was used to analyze the outer race faults [Feng & Chu, 2008]. Wavelet transform [Abbasion et al., 2007] were developed to overcome the problem of STFT. It is a time-scale representation and decomposes the signal into a number of signals having different frequency band at different times. One of the main usage of wavelets is to de-noise the raw signals. There are many methods derived from Wavelet transforms such as redundant lifting scheme [Zhen, et al. 2008], anti-aliasing lifting scheme [Bao et al., 2009] and adaptive lifting scheme [Yang et al., 2012]. However, the result of wavelet transforms depends on the various factors such as selection of mother wavelet, the order of mother wavelet and the decomposition level. Empirical Mode Decomposition (EMD) [Rai & Mohanty, 2007] method was introduced to overcome the shortcomings of wavelet transform. EMD is applied for the decomposition as well as the de-noising of the signals. An improved form of EMD known as Ensemble Empirical Mode Decomposition (EEMD) method [Peng at al., 2005] was proposed to solve the problem of mode-mixing found in EMD. A new method similar to EMD known as local mean decomposition (LMD) [Cheng et al., 2012] has been used to diagnose bearing fault. EMD and LMD come under the category of adaptive non-parametric T-F methods. Adaptive parametric T-F methods such as matching pursuit [Liu et al., 2002] and basis pursuit [Yang et al., 2005] have also been used for diagnosis.

2.6.3 Decision making

The last step in condition monitoring involves the decision to be made related to the maintenance activity. Either the human expertise or a mathematical approach is used to ascertain the final condition. For fault detection, decision is taken based on the change in vibration level. The presence of fault characteristic frequencies denotes the location of fault and trending the fault feature is used for the fault degradation estimation. The automation of the condition monitoring is carried out using various mathematical techniques (for decision making) which are divided into three categories: distance metric methods, artificial intelligence techniques and model based approaches. The general methods used in these techniques are described below:

2.6.3.1 Distance metric methods

A conventional approach involves using some hypothesis test methods for fault detection. Methods such as Likelihood ratio test [Ma & Li, 1995] and Kolmogorov-Smirnov test [Cong et al., 2011] generate test statistic which accepts or rejects the hypothesis of bearing being faulty or not. The statistics are also used to study the fault progression [Cong et al., 2011]. Another approach uses a distance measure between the healthy data and test data. The commonly used distance measures are distance of the nearest neigbour [Mechefske & Mathew, 1992b], Euclidean distance [Hoffman & Van der Merwe, 2002] and Mahalanobis distance [Wong et al., 2006]. Nearest Neigbour Algorithm [Mechefske & Mathew, 1992b] is used to calculate the distance between two signals as the distance of the nearest neigbour. Support Vector Machines (SVM) [Abbasion et al., 2007] is used to optimize the boundary curve between the healthy and faulty signals. Other methods such as Hidden Markov Machine (HMM) [Nelwamond et al., 2006] and Gaussian Mixture Models [Nelwamond et al., 2006] are used to classify the unknown machine condition. However, SVM, HMM and GMM require to be trained with the existing data.

2.6.3.2 Artificial Intelligence techniques

Artificial Intelligence (AI) techniques are been used recently in condition monitoring. Mostly used AI techniques are artificial neural network (ANN) [Sreejith et al., 2008], Fuzzy logic [Da Silva Vicente et al., 2001], neuro-fuzzy [Zhao et al., 2009], Expert System [Ebersbach & Peng., 2008] and Evolutionary Algorithm [Samanta et al., 2003]. Different types of ANN [Yang et al., 2004] been used are feed forward neural network, self organizing maps and learning vector quantization. The classification performance of ANN depends on the training carried out using the observed inputs. Expert system uses the domain expert knowledge in the form of program to carry out the reasoning. Reasoning is carried out using the methods which are rule-based, case-based and model-based. Fuzzy logic is used generally in combination with ANN and Expert System. The most widely used evolutionary algorithm for condition monitoring is genetic algorithm [Samanta et al., 2003]. Using the fault index and AI methods, remaining useful life (RUL) of the machine could be estimated [Si et al., 2011].

2.6.3.3 Model based approaches

Model based approaches uses physics based models and mathematical models of the machine under consideration [Loparo et al., 2000]. Physics based models are based on studies such as the fatigue or creep phenomenon. Based on the mathematical models, residual (discrepancy between the predicted and actual values) is generated which are further evaluated to arrive at the decision. Commonly used method for residual generation is Kalman filter [Swanson, 2001].

2.7 EXISTING VIBRATION SIGNATURE ANALYSIS METHODS

Vibration based bearing condition monitoring is mostly used in the industries. Condition monitoring is carried in three phases: detection, diagnosis and prognosis. A lot of research work has been carried out in each of the above areas. Review of the various vibration based methods can be found in [McFadden & Smith, 1984b; Howard, 1994; Tandon & Choudhury, 1999; Yang et al., 2003; Jardine et al., 2006; Zhou et al., 2007; Patil et al., 2008; Immovilli et al., 2010; Randall & Antoni, 2011].

Some of the methods developed in each phase are discussed below:

2.7.1 Fault detection

Fault detection is carried out in time domain by studying the various time domain indices and in frequency domain using the spectrum comparisons.

With the occurrence of fault in bearing, the overall vibration level (energy) increases. This increase in level can be denoted using RMS value. RMS as a health indicator has been used with limited success [Miyachi & Seki, 1986]. In [Tandon & Nakra, 1993], the overall RMS acceleration level and the frequency spectrum of the healthy and faulty bearing are compared. It was observed that RMS level for faulty bearing was higher than the healthy bearing. Crest factor (ratio of peak to RMS) is shown as an alternative to RMS level for fault detection [Mathew & Alfredson, 1984]. Statistical parameters such as probability density functions [Bendat & Piersol, 1971] and moments of data [Martin et al., 1992] are generally used for time domain based fault detection approaches. In [Bendat & Piersol, 1971], it was reported that a healthy bearing has the probability density function of a inverted parabola which indicates the gaussian distribution. With the occurrence of fault, changes in the tail of the distribution occur and it further broadens. The change in probability at a particular amplitude level provides significant information for fault detection. The statistical moments based on beta distribution [Martin et al., 1992] were reported to show less sensitivity to noise than those based on gaussian distribution. In [Heng & Nor, 1998], different statistical moments were shown to indicate the shape of probability density function. The odd moments (order such as 1(mean), 3 (skewness)) gives the information of peak density with respect to the median value. Even moments (order such as 2 (standard deviation), 4 (kurtosis)) indicates the spread in the distribution. Kurtosis (normalized fourth order moment with respect to the square of standard deviation) indicates the impulsiveness in the signal. The use of kurtosis was first reported in [Dyer & Stewart, 1978] to detect a fault. It was observed that kurtosis varied with the initiation of defect and the extent of damage was also assessed based on the distribution of it in the selected frequency range. It was suggested to trend the kurtosis value at different frequencies to study the sensitivity of it with respect to the fault. In [Williams et al., 2001], it was observed that a healthy bearing has a kurtosis value of 3 (Gaussian distribution) and it increases further when defect increases. However, its value decreases when the bearing is close to failure condition. Other time domain parameters such as clearance factor, shape factor and impulse factor developed in [Li & Pickering, 1992], were useful in detecting the fatigue spalling. Among these three parameters, clearance factor was the most sensitive. Tandon [Tandon, 1994] compared the parameter such as RMS, peak, crest factor, power and cepstrum of faulty bearing with the healthy ones. The measurement results showed that defect detectability is higher for power followed by peak and RMS values.

A simple approach in frequency domain involves comparing the healthy and faulty spectrums. In [Alfredson & Mathew, 1985], number of discrimination features from the spectrum is considered to detect the changes in spectrum. Features such as matched filtered root mean square, arthimetic mean, geometric mean, and correlation mean have been used [McFadden & Smith, 1984b; Alfredson & Mathew, 1985] to quantify the difference in the healthy and faulty bearings.

Many methods have been used for enhancing the fault signals. It includes namely, adaptive noise cancellation [Chaturvedi, 1982; Antoni & Randall, 2004a; Antoni & Randall, 2004b; Ho & Randall, 2000; Randall, 2004], adaptive line enhancer [Shiroishi et al., 1997], autoregressive modeling technique [Baillie & Mathew, 1996], blind source separation [Bouguerriou et al., 2005; Antoni, 2005; Shen & Yang, 2006; Peter et al., 2006], blind equalization [Peter et al., 2006], blind deconvolution method [Mathew et al., 2001; Karimi, 2006] and schur filter [Makowski & Zimroz, 2013].

Adaptive noise cancellation technique was used as preprocessing method to remove the noise [Chaturvedi, 1982] and also been applied for minimizing the interference in the signals [Tse & Lai, 2003]. Adaptive line enhancer is used to separate the narrowband signals from the wideband noise. It was reported in [Shiroishi et al., 1997], the enhancing of the envelope signal by reducing the wideband noise of the demodulated signal.

The commonly used blind source separation algorithms are based on second order statistics, joint approximate diagonalization of eigenmatrices, fixed-point algorithm, natural gradient algorithm and higher order statistical algorithm. Performances of these methods are compared in [Peter et al., 2006]. In [Bouguerriou et al., 2005], cyclostationarity based blind source separation technique is developed using a new separation criterion. The criterion is based on the maximization of the cyclostationarity of the estimated signal. In [Boustany & Antoni, 2005], blind source separation algorithm using the subspace decomposition was proposed to overcome the failure of conventional blind source separation algorithms for signals with large unknown interfering sources. It was suggested in [Peter et al., 2006], to investigate the type of vibration interferences components before the use of blind source separation algorithms. Blind source separation method is used for separating the multiple vibration signals from multiple sensors, whereas blind equalization method is used to recover the vibration signals from only one sensor. In [Peter et al., 2006], blind equalization using generalized eigenvector algorithm is adopted for recovering the weak bearing fault vibration signal from the overall motor vibration. Blind equalization algorithm is constrained by the choice of filter length, sample number and iteration number. If the vibration signal involves time delay, then the suggested method of separation are blind equalization and blind deconvolution. Blind deconvolution refers to the process of learning the inverse of unknown path and applying it to the measured signal in order to recover the faulty signal. It performs better than blind source separation method where the transmission path of vibration dynamically changes or not known. A blind deconvolution method to separate the signals from the different sources which are convoluted and mixed is discussed in [Peled et al., 2005]. Mixing of the independent signals results in the gaussian distribution of signal. Kurtosis is non zero for non gaussian signals. Thus, maximizing the kurtosis was used as a separation approach. An eigenvector algorithm based blind deconvolution method [Tan et al., 2006] is developed to separate the noisy signals passing through transmission paths. An application of schur filter for enhancing the bearing fault signals is proposed in [Makowski & Zimroz, 2013]. In adaptive filter technique (Least Mean Square and Autoregressive) prediction error is used for fault analysis, while in schur filter, both prediction error and reflection coefficient along with its derivative is used for fault analysis.

Shock Pulse method (SPM) is an alternative approach of fault detection in time domain. It is based on the structural resonances which are excited by the impulsive loadings due to faults at a high frequency. It is been widely used in industries as it requires less skills for the interpretation. However, it is affected by the noise and vibration interferences [Tandon & Kumar, 2003]. The resonance frequency demodulated is that of the accelerometer, and thus it is fixed. An approach with variable demodulation band will provide better accuracy. In [Ray, 1980; Smith, 1982], it was reported that SPM could not detect fault efficiently at low speeds.

A better approach in time domain analysis is to apply the mathematical such as Autoregressive model (AR) and Autoregressive Moving Average model (ARMA). Baillie and Mathew [Baillie & Mathew, 1996] have presented a comparison of AR for fault detection. Jiang et al. [Jiang, et al., 2011] reported a fuzzy cluster analysis and AR model method for bearing health assessment. The AR coefficients are used as fault feature which are given as input to a neural network. In AR model, value of the residual squared error should approach zero for the model to be more accurate. It depends on the order selection of AR model which in turn depends on the number of measured points of signal. Ye et al. [Ye et al., 2007] described a method based on ARMA and higher order statistics. For AR and ARMA based method used along with Artificial Neural network (ANN) or fuzzy logic, if the order of model is large, then the inputs will increase correspondingly which would require more training time. If the order is small, then the residual squared error will be bigger. When AR or ARMA method is used for analysis, the noise is ignored and the model is fit from the noisy time series which is used for further processing, so fault classification could be less accurate. Wang et al. [Wang et al., 2010] showed that the method based on the difference values of AR coefficients (difference of AR coefficients of ideal signal for healthy condition and AR coefficient for faulty condition) with ANN is superior to the method using AR coefficients along with ANN.

In [Liao & Lee, 2009], instead of collecting the signals at constant load a new approach based on a fixed cycle test is carried out. It is done to identify the transient occurring at the different working loads. The data is collected for the various combinations of loads and operating conditions. Wavelet packet transform is used for the feature extraction followed by feature dimension reduction using principal component analysis. Gaussian mixture model is used to model the distribution. Confidence value (CV) is calculated based on the overlap between healthy and test signals. If CV is near to 1 (the two signals distribution overlap) which means bearing is healthy. If CV is near to zero, then abnormal condition arises. The advantage of using data at fixed cycle is shown using a case study. It was observed that when test is conducted at a full working load, abnormal condition is not detected. But, when tested at lower loads, the abnormal condition is detected. If CV is plotted with respect to time, it could be used to study the performance degradation.

In [Van Wyk, 2009], Difference Histogram is used to identify bearing as healthy or faulty using ANN. Histogram bin is used as a fault feature Sample size influences the classification and it has to be sufficient large (N=30,000) for high accuracy. Xiong et al. proposed [Xiong et al., 2010] multi scale entropy as a feature suitable for bearing fault detection. However, in noisy condition the classification accuracy comes down from 97.42% to 73.94%.

William and Hoffman [William et al., 2011] used zero crossing (ZC) of the signal for identification of faulty bearing. ZC count and ZC duration were used as fault features in combination with ANN. Their calculation depends on the signal length which requires the knowledge of accurate rotation frequency and longest expected time duration between successive zero crossing. Classification accuracy is affected by window length and varies from 91.5% to 97.1%. ANN when trained only with higher defect size and tested for other defect sizes gave good classification. It is also been used for fault diagnosis.

In [Boutros & Liang, 2011], bearing fault detection is based on comparison of the monitoring index with the reference vectors which are large in number along with Hidden Markov Model (HMM). The training time is more and not fixed as the random values are used to fix the model parameters which are calculated by Viterbi Algorithm. It is also been used for fault diagnosis.

A method based on comparing the closeness of the vibration signal with the healthy gaussian distribution signal [Obuchowski et al., 2013] has been proposed recently. The signal is decomposed using short time fourier transform and autocorrelation function is used to select the optimum sub-band. To compare the distributions, statistical test and visual test were used. In statistical test, the measures used were Kolmogorov-Smirnov statistic and Anderson-Darling statistic. The difference in the statistic value provides the evidence of faulty bearing. The visual test used was quantile-quantile plot which provided the goodness of fit. If the shape is straight, it means both the distributions are same.

Recently, an energy entropy value of the intrinsic mode function obtained using ensemble empirical mode decomposition and support vector machines was used to detect the faulty bearing [Zhang & Zhou, 2013]. The energy entropy values reduce with the fault [Yu & Junsheng, 2006].The energy value of the resonant frequency band is compared to detect the bearing fault.

2.7.2 Fault diagnosis

Fault diagnosis methods developed are based on two approaches. First, using fault features in combination with data mining techniques such as Artificial Neural Networks, Hidden Markov Models and Gaussian Markov Models. Secondly, spectrum analysis detection of the fault characteristic frequencies) based on a preprocessing method involving denoising or decomposition of the signal or demodulation.

A short history of bearing fault diagnosis is provided in [Randall & Antoni, 2011]. In 1969, Balderstan [Balderston, 1969] carried out one of the earliest work on bearing diagnosis. It was shown that the bearing fault signals were primarily observed near the high frequency resonant region.

Two common methods used in time series analysis are Autoregressive (AR) model [Baillie & Mathew, 1996; Junsheng et al., 2006; Wanga et al., 2010], Autoregressive Moving Average (ARMA) model [Ye et al., 2007]. AR analysis uses time variations and vibration amplitude to establish the mathematical model. AR models of different orders for each bearing defect type have been formed for analysis [Baillie & Mathew, 1996]. The AR coefficients are used as fault features which are given as an input to a classifier such as ANN. AR models of the same order for each bearing defect type were established in [Junsheng et al., 2006].

Statistical features [Sreejith et al., 2008] such as peak value, rms, kurtosis, crest factor, shape factor etc are calculated and used as an input to ANN for classification. However, noise affects the features which affect the accuracy.

Nelwamondo et al. [Nelwamondo et al., 2006] reported a method using multi scale entropy feature and classifiers such as Hidden Markov Models and Gaussian Mixture Model for bearing fault diagnosis, but it is affected by noise. Also, depending upon the number of samples, the classification accuracy varies from 81% to 100% at different bearing location.

Chaos theory and non linear dynamics are combined to obtain features such as fractal dimensions which are used to represent the non linear behavior of vibration signals. One of the fractal dimension known as correlation dimension was used for bearing fault diagnosis by logan and Mathew [Logan & Mathew, 1996a; Logan & Mathew, 1996b]. Other Fractal dimensions such as capacity dimension, information dimension along with correlation dimension are applied to classify various fault types using support vector machine [Yang et al., 2007]. The results showed that the classification performance for inputs using the three fractal dimensions along with time domain statistical features was higher than the case when trained with only time domain statistical features or three fractal dimensions.

In [Wang et al., 2009], reconstructive phase space (RPS) and GMM was used. RPS was used to bring out the non linear characteristic of the signal. A bayesian classifier was used to calculate the likelihood of the test signal with the learned GMM.

A fault diagnosis method based on walsh transform and rough sets theory is presented [Xiang et al., 2009]. The signal is first transformed using walsh matrix and then walsh spectrum is obtained. Frequency domain features from the spectrum are calculated which are used as input in rough set theory and fault diagnosis is carried out on the basis of diagnosis rule formed.

A feature extraction scheme based on generalized S transform is presented in [Li et al., 2011]. S transform combines the advantages of Short Time Fourier Transform and Wavelet transform which also provides the time frequency representation. A two dimensional non negative matrix factorization technique is used to extract the informative fault feature from the obtained time frequency representation. The fault classification is carried out using k nearest neighbor classifier, naïve bayes classifier and support vector machine.

Li [Li & Zhang, 2011] presented a non linear dimension reduction method known as Supervised Locally Linear Embedding Projection, which transforms the original signal assumed to be in higher dimension to a low dimension feature space. Its performance is very sensitive to the regularization parameter which represents the generalization capacity of algorithm. Also, its accuracy comes down in the presence of noise.

A fault feature extraction technique known as semi supervised kernel marginal fisher analysis which also extracts the low dimension feature from the higher dimension vibration signals is reported in [Jiang et al., 2013]. K- Nearest Neighbor classifier along with the extracted features is used for the classification of fault.

The second approach of fault diagnosis involves spectrum analysis to detect the fault characteristic frequencies. The High Frequency Resonance Technique (HFRT) or Envelope Analysis [McFadden & Smith, 1984b] is mostly used method in industry. Mechanical Technology Inc. developed the HFRT [Darlow et al., 1974]. Many methods were developed based on demodulation of the high frequency region. Patented techniques such as Shock Pulse Method (SPM®) of SKF Company and Spike Energy Method (Spike Energy™) of IRD Company were used for fault diagnosis where the demodulation frequency used was that of resonant frequency of transducer. Engja et al. [Engja et al., 1977] showed that there are chances of transducer resonant frequency been near to the external vibration interferences such as turbulence in pumps. It was recommended to use an appropriate resonant frequency with respect to the actual machine connected. In PeakVue® method developed by CSi (Emerson Process Management), instead of using the resonant frequency of the transducer, a high frequency of 102 kHz is used to capture the fault impulses.

McFadden and Smith [McFadden & Smith, 1984a; McFadden & Smith, 1985] put forwarded the vibration model to describe the vibration of bearing due to single point defects and multiple defects located at an arbitrary position and under varying load. The spectrum has peaks at defect frequency with harmonics with sidebands associated with loadings and transmission path. In [Su & Lin, 1992], the validity of the above analytical study is confirmed using extensive experimental analysis.

Order tracking is a widely used tool for the vibration analysis of machine with drive train components such as gearboxes, reciprocating engines. It refers to the frequency analysis of the RMS values of machine vibrations as a function of the rotational speed. The advantage of using order tracking is that the non stationary vibration signal in time domain gets converted to stationary signal in angular domain. In [McFadden & Toozhy, 2000], HFRT is combined with synchronous averaging method. The envelope signal is averaged synchronously with a trigger signal obtained from the rotation of shaft (using a tachometer signal). For increasing severity of defect, the fault spectrum distribution is clearly obtained using the synchronous averaging technique. Ho and Randall presented the technique of envelope analysis using Hilbert transform [Ho & Randall, 2000]. Also, it was suggested to use square of envelope instead of envelope for better results if Signal to Noise ratio (SNR) > 1. In [Siegel et al., 2012], a tachometer less synchronous averaging of envelope signal is performed to detect the defect frequency based on order spectrum. A representative of the tachometer signal is generated by band pass filtering the signal around the interested fault frequency region and then using the derivative of the Hilbert transform of the band pass filtered signal.

Generally, envelope involves band pass filtering, amplitude demodulation (AD) and spectral analysis. It gives correct diagnosis only when the centre frequency and bandwidth of the bandpass filter are known accurately [Bozchalooi & Liang, 2009]. If the band pass filter is designed properly then AD can be very effective in bringing out the fault characteristic frequencies.

Many efficient methods were proposed to select the parameters of band pass filter required for envelope analysis. Spectral Kurtosis, Kurtogram [Antoni & Randall, 2006; Sawalhi et al., 2007] and Fast Kurtogram [Antoni, 2007] were proposed initially to select the filter parameters.

In [Antoni & Randall, 2006], Short Time Fourier Transform based kurtosis was calculated. Different window lengths were used to calculate the spectral kurtosis and the band in which maximum value occurs is selected. A bandpass filter which maximizes the kurtosis of the envelope of the filtered signal is designed. The optimal centre frequency and bandwidth were selected such that maximum value of Kurtogram is obtained. Fast Kurtogram [Antoni, 2007] was developed to reduce the computational complexity of the Kurtogram using filter bands. In [Lei et al., 2011], wavelet packet transform is used instead of Short Time Fourier Transform to process the cyclo-stationary vibration signals which improved the obtained kurtogram. The wavelet packet nodes corresponding to higher kurtosis were used for the spectrum processing.

Minimal Shannon entropy was used by Qiu et al. [Qiu et al., 2006] to calculate the bandwidth and the periodicity detection method was used to find the centre frequency.

Autoregressive based minimum entropy deconvolution technique [Sawalhi et al., 2007] was introduced to remove the effects of transmission path along with the impulse responses between the vibration signal and the sensor. This is mostly found in high speed bearings [Randall & Antoni, 2011]. A limitation of the above method is the preference of the minimum entropy deconvolution algorithm to deconvolve only a single impulse or number of impulses, as opposed to the desired periodic fault impulses [McDonald, 2011].

A solution to the above limitation is proposed in [McDonald et al., 2012] where a technique known as maximum correlated kurtosis deconvolution is developed.

Bozchalooi and Liang [Bozchalooi & Liang, 2007] proposed a smoothness index guided method to find the scale and shape factors of Gabor wavelet corresponding to parameters of Gaussian filter. They also [Bozchalooi & Liang, 2008] have developed a method for online detection of resonant frequency which was further used as centre frequency for the wavelet based filtering approach.

Protrugram was proposed by Barszcz and Jablonski [Barszcz & Jablonski, 2011] to determine the optimum centre frequency with fixed band width for signal demodulation. Spectral Kurtosis was computed based on envelope spectrum using a fixed window length.

Wang and Liang [Wang & Liang, 2011; Wang & Liang, 2012] presented an adaptive spectral kurtosis method to find the adaptive bandwidth and the centre frequency. It showed better performance than Kurtogram and Protrugram. It was carried out by right-expanding a given window along the frequency axis through iteration to merge it with its subsequent neighboring windows to obtain a maximum value of spectral kurtosis. It represents an indirect implementation of wiener filter.

Chen et al. [Chen et al., 2012] proposed a hybrid method combining an Improved SK (ISK) and adaptive redundant multi-wavelet packet (ARMP) for fault diagnosis. SK was improved by including an index known as envelope spectrum entropy. ARMP was combined with ISK for various reasons such as to remove SK's filter limitations, for improving the spectral analysis resolution and to obtain the best fault feature.

Another method of improving the Kurtogram using the wavelet packet transform was developed [Wang et al., 2013]. The difference between this work and the enhanced Kurtogram [Lei et al., 2011] is that the kurtosis value is calculated based on the power spectrum of the envelope of the signals obtained from the wavelet packet node at different level instead of kurtosis value obtained directly from wavelet packet nodes. In contrast to Protrugram, fourier spectrum is replaced by the power spectrum to enhance the detection of fault characteristic frequencies.

A new concept known as sparsogram [Tse and Wang, 2013a] is proposed to calculate the resonant frequency band. It is constructed by measuring the sparsity of the power spectrum from envelope of the optimal wavelet packet coefficient. The sparsity values of the wavelet packet coefficient for all wavelet packet level are calculated and one with largest sparsity value is selected as the optimum coefficient. This wavelet packet coefficient is further demodulated for envelope analysis. In [Tse and Wang, 2013b] the authors of sparsogram discussed an automatic procedure to optimize the morlet filter based on genetic algorithm (to maximize the measured sparsity value). The wavelet coefficient optimized using the optimal wavelet filter is used to extract the envelope. The proposed optimization of wavelet filter is compared with various methods based on kurtosis, smoothness index and Shannon entropy.

Time–frequency domain based signal decomposition methods such as Wavelets [Bozchalooi & Liang, 2007; Al-Raheem et al., 2008], Empirical Mode Decomposition (EMD) [Yan & Gao, 2006], Ensemble Empirical Mode Decomposition (EEMD) [Ai et al., 2009] and S transform [Hou et al., 2010] have been used as preprocessor to the fault diagnosis algorithm.

An automatic frequency band selection of spectral kurtosis is developed using complex morlet wavelet and further envelope analysis is used to detect the fault characteristic frequencies [Li et al., 2013].

In [Hou et al., 2010], S transform was used to obtain the analytical band pass filtered envelope signal. The envelope signal was enhanced further by reconstruction based on singular value decomposition (SVD) method. Singular value ratio (SVR) spectrum which is the plot of ratio of first two singular values obtained using SVD and window length. The envelope is analyzed using the sweep frequency method based on examining the peak value of SVR spectrum to extract the periodic components.

EMD helps in decomposition of the signal into number of components called as intrinsic mode functions. In [Yan & Gao, 2006], bearing fault was diagnosed using the instantaneous frequency of intrinsic mode functions. Marginal spectrum of the intrinsic mode function was computed to detect different bearing faults [Li et al., 2009]. The intrinsic mode functions are better extracted using Ensemble Empirical Mode Decomposition (EEMD) than EMD. But there are few issues in EEMD [Lei et al., 2009] such as use of splines in interpolation procedure, calculation of mean value and signal end effects. The result of EEMD depends on the number of ensemble chosen and the amplitude of the added white noise to be set. A review of EMD and EEMD works related to bearing condition monitoring is discussed in [Lei et al., 2013].

EMD has also been used in combination with other techniques. Hilbert transform was used to decompose the signals into number of intrinsic mode functions and which were further processed using FFT to detect the fault characteristic frequencies [Rai & Mohanty, 2007]. Yu et al. [Yu et al., 2006] applied EMD technique for the decomposition of the vibration signal. Energy of the selected decomposed signal were calculated which was used as an input to back propagation neural network for fault classification. Junsheng et al. [Junsheng et al., 2007] applied EMD and Teager Kaiser Energy Operator to detect the fault characteristic frequencies. The amplitude and frequency demodulation was carried out separately. It was also shown that the energy operator demodulation approach is superior to Hilbert demodulation approach. The Hilbert transform based demodulation has drawback such as end effects; the transformed signal has some amount of modulation and it requires selection of centre frequency of filter [Junsheng et al., 2007]. This method was further extended by combining the order tracking to detect the fault using the order spectrum [Li et al., 2010].

Liang and Bozchalooi [Liang & Bozchalooi, 2010] proposed a parameter-free fault detection method to overcome the problems of HFRT. It is based on Teager Kaiser Energy Operator which incorporates both amplitude and frequency demodulation and has many advantages such as elimination of enveloping step, increased signal to interference ratio, simple and versatile due to parameter free. Also, high frequency noise amplification occurs due to Teager Kaiser Energy Operator [Liang & Bozchalooi, 2010].

Image processing methods have also been used for bearing fault diagnosis. Mathematical Morphology based approaches [Nikolaou & Antoniadis, 2003; Zhang et al., 2008; Hao & Chu, 2009; Wang et al., 2012; Li et al., 2011; Dong et al., 2011; Li et al., 2012; Li & Liang, 2012; Raj & Murali, 2013; Chen et al., 2013] have been used mainly for denoising the signal. There are different basic morphological operators such as dilation, erosion, opening, closing which are pre-processed to modify the shape of the signal. Gradient operator and Top Hat operator [Raj & Murali, 2013a] which are derived from the basic operators are used for denoising the signal whose results depends on the shape, type and length of structuring elements. It is similar to mother functions used in wavelets. A deconvolution algorithm known as Lucy-Richardson Algorithm [Raj & Murali, 2013b] is used as preprocessor for enhancing the bearing fault signal.

2.7.3 Fault prognosis (fault degradation)

Prognosis is carried out into two steps: trending the fault degradation and to predict the remaining useful life (RUL). Fault degradation assessment study provides a performance index to trend the actual condition of machine. This index is combined with some regression methods such as Artificial Neural Networks, Support Vector Machines etc. to calculate the RUL. A review of prognostic methods for rolling element bearing is reported in [Jammu & Kankar, 2011]. The methods involving assessment of fault degradation are discussed below:

A common approach found is trending the various time domain and frequency domain fault features such as root mean square (RMS), kurtosis, crest factor, shape factor, impulse factor, clearance factor, skewness, log-likelihood function and power ratio of maximum defective frequency to mean [Williams et al., 2001; Ocak et al., 2007; Yu, 2012]. These features have certain advantages and limitations. For e.g. an incipient defect is difficult to detect using RMS alone, but its value increases steadily with the defect degradation [Williams et al., 2001]. Kurtosis and crest factor increases with the onset of defect but their value reduces to healthy level as the fault severity increases. They also have some stability problem as the fault degradation level increases [Ocak et al., 2007]. In a case study [Lybeck et al., 2007] relating the spall length with the time domain features, it was observed that the features did not show consistency with the spall length. Effectiveness of kurtosis is limited by the spurious vibrations and noise level found in the signals [Tao et al., 2007].

Many works have been carried out exploring new effective indices. An alternative to kurtosis known as Honarvar third moment [Honarvar & Martin, 1997] was developed. It was found to be less responsive to changes in load and speed. Also, it is less sensitive to fault impulse during the onset of defect.

Different forms of entropy have also been used for assessing the performance of a bearing. A statistical moment based on Renyi entropy was developed [Tao et al., 2007]. It is tested using the mathematical model and artificially induced defect on bearing. It has performance similar to kurtosis and is less susceptible to spurious vibrations which are one of the short comings of higher statistical moments including kurtosis. The moment has better overall performance than kurtosis and Honarvar third moment. However, this entropy has to be verified for the complete life of bearing which was not carried out during its analysis. An index based on the complexity of signal such as approximate entropy [Yan & Gao, 2007] has been shown to increase with the defect size. Its value increases with increase in speed, while load has a negligible effect on it. Spectral Entropy [Pan et al., 2009] was presented as a complimentary index for the fault degradation assessment. With onset of defect it increases abruptly, then remains stable and finally decreases up to failure. It has advantage over RMS as it can more clearly detect an incipient defect. However, it has some disadvantages such as the change in value is not consistent enough with condition degradation and it is less sensitive to failure condition. A time–frequency approach known as Wigner–Ville spectrum based on cyclic spectral density [Dong & Chen, 2012] is used for feature extraction which is noisy resistive. Renyi information is obtained which is used as the degradation index. It is shown to be more sensitive than other indexes such as spectral entropy, squared envelope spectrum entropy, renyi information obtained from Wigner Ville Distribution (WVD) and pseudo WVD.

Qiu et al. [Qiu et al., 2003] proposed a minimum quantization error (MQE) as an index for evaluating the complete bearing life using an optimal wavelet filter and Self Organizing Map. Euclidean distance measure is used in the development of MQE. MQE denotes how far the input data is from the healthy data region.

In [Ocak et al., 2007], wavelet decomposition and Hidden Markov Model (HMM) was used and results showed that the probabilities of healthy bearing HMM decreases as the bearing defect severity increases.

Pan et.al [Pan et al., 2009b; Pan et al., 2010] developed heath indicator based on two methods: First, combination of improved wavelet packet decomposition and support vector data description method [Pan et al., 2009b.] and another using the lifting wavelet packet transform with fuzzy c-means approach [Pan et al., 2010].

A statistical test known as Kolmogorov-Smirnov (K-S) test is used for assessing the bearing degradation in combination with an autoregressive model in [Cong et al., 2011]. K-S test is used to compare the statistical similarity of the two vibration signals (reference and test signals) using the cumulative distribution function. Two indexes known as D-stat (the statistic value of K-S test) and its probability value (p(D)) is used for trending the bearing fault degradation. D-stat decreases while p(D) increases as the condition deviates from healthiness.

Based on feature extraction approach known as locality preserving projection (LPP) two indices were developed. First, Exponential Weighted Moving Average (EWMA) statistic [Yu, 2011a] was proposed combining LPP and multivariate statistical process control. LPP extracts low dimension information hidden in higher dimension better than the Principal Component Analysis (PCA). PCA approach extracts features globally, while LPP is locality based learning method. Second index known as Negative log-likelihood based EWMA [Yu, 2011b] developed using LPP and gaussian mixture model. The features which were used as an input to LPP were RMS, kurtosis, crest factor, skewness, peak to peak, impulse factor, margin factor, power ratio of maximum defective frequency to mean from FFT, power ratio of maximum defective frequency to mean from envelope and wavelet energy.

A different approach known as probability prognostic approach [Caesarendra et al., 2010; Widodo & Yang, 2011; Caesarendra et al., 2011] was used to study the health degradation. In [Caesarendra et al., 2010], it was based on the concept of probability, logistic regression and relevance vector machine (RVM) methods. Logistic regression is used to estimate the failure degradation of bearing. RVM is trained by outputs of logistic regression and it predicts the probability of failure. In [Caesarendra et al., 2011], kurtosis is used as the input to Support Vector Machine to build the prediction model. The bearing fault degradation is estimated using reliability theory.

A novel method based on Local and nonlocal preserving projection and multivariate statistic process control approach was presented in [Yu, 2012]. Local and nonlocal preserving projection is used for extracting the features from the set of features calculated in time domain, frequency domain and time-frequency domain. It extracts more useful information than Principal Component Analysis (only global information). Health Index known as H statistics is developed. Using Local and nonlocal preserving projection, first two eigenvector corresponding to the largest eigenvalues were considered for calculating the index. The threshold for the index limit is obtained using kernel density estimation method.

Coupled hidden markov model (CHMM) which has advantage over hidden markov model have also been used for prognosis studies [Liu et al., 2012; Liu et al., 2013]. Coupled Hidden Markov Model is a collection of several Hidden Markov Models which are connected using conditional probabilities across their time between the hidden states. In [Liu et al., 2012], Linear discriminant analysis (LDA) and CHMM are jointly used to develop a performance index to trend the bearing condition. The original features are calculated for three conditions: healthy, degradation and failure. LDA is used for reduction of the features and CHMM is used to develop the degradation model. Finally, a performance index is formed using log-likelihood and exponential weighted moving average method. In another work [Liu et al., 2013], zero crossing features was used along with CHMM to analyze the data from multiple channels to trend the bearing condition.

An integrated approach of recurrence quantification analysis (RQA) and auto-regression model is used for evaluating the bearing condition [Qian et al., 2013].

Recurrence plot entropy is used as fault feature which is obtained using RQA. The AR model using recurrence plot entropy predicts the bearing failure accurately.

2.8 NEED FOR NEWER METHODS AND APPROACHES

It is very much important to extract the appropriate features which indicate the presence of defect (or fault) and also to estimate it accurately. These features are critical in the fault detection and fault degradation stages. The features been developed have stability problems with the fault severity. Hence, robust features are required to accurately trend the fault. The results of the feature extraction methods developed vary with sample size, load and noise. Hence, novel methods to overcome these issues are required. Also, an effective approach for fault degradation is required. This concern is been addressed in this research.

The simplest method to diagnose the fault is to detect the fault characteristic frequencies. The method developed so far required either designing the band pass filter or denoising or decomposition of the signal. However, the methods are not simple in implementation. Also, the methods should perform efficiently under the presence of masking sources and background noise. Thus, a simple and efficient method to diagnose the fault is required to be developed.

With the ground work for the research work been discussed (Chapters 1 and 2), the chapters 3 to 7 deals with the research work been carried out. The novel methods developed in the area of fault detection, fault diagnosis and fault prognosis (fault degradation) stages are presented subsequently in detail.

PART II

FAULT DETECTION

CONTENTS:

CHAPTER 3

DETECTION OF FAULTY BEARING USING SYMBOLIC DYNAMICS

MAIN CONTENTS:

- **Introduction**
- **Symbolic Dynamic Technique**
- **Description of Test Data's: Test data1; Test data2; Test data3**
- **Algorithm for Bearing Fault detection based On Symbolic Dynamics**
- **Testing of the method**
    - Application to Test data1
    - Application to Test data2
    - Application to Test data3
- **Comparisons with other Time-Domain and Data Based Techniques**
- **Summary**

3.1 INTRODUCTION

Different approaches (section 2.7.1) have been developed so far in literature to detect a fault in the bearing. Most of these methods are based on complex signal processing concepts which require rigorous mathematical calculations. Moreover, they are noise affected, sample size, machine and load dependent. Though these methods are accurate, still a simple, efficient and process independent bearing fault detection algorithm is required. This chapter discusses a method which is a step in this direction. It is based on the concept of symbolic dynamics.

This chapter presents the symbolic dynamic based method for an online and simple bearing condition monitoring system. Symbolic dynamic technique gives the behavioural description of a nonlinear dynamical system such as the vibration of bearing during its operation. During the bearing fault occurrence, the vibration signal obtained is amplitude and frequency modulated which changes the statistics of the vibration signal and these changes are detected through the symbolic dynamic method.

The time series data is converted into a symbolic series. The sequence of symbols represents the different states of a dynamical system. The change of symbols represents the change from one state to another state. If system is healthy, the statistics of the symbols would remain the same and the states would give a uniform probability distribution. A defect (fault) would change the probability distribution of the symbols. One possible measure of deviation, called as Common Signal Index (CSI) (section 3.2.3), is a parameter which compares the occurrence of the symbols for the healthy and faulty conditions. Based on the value of CSI, bearing faulty condition is detected.

The block diagram of the symbolic dynamic based approach is given in figure 3.1.

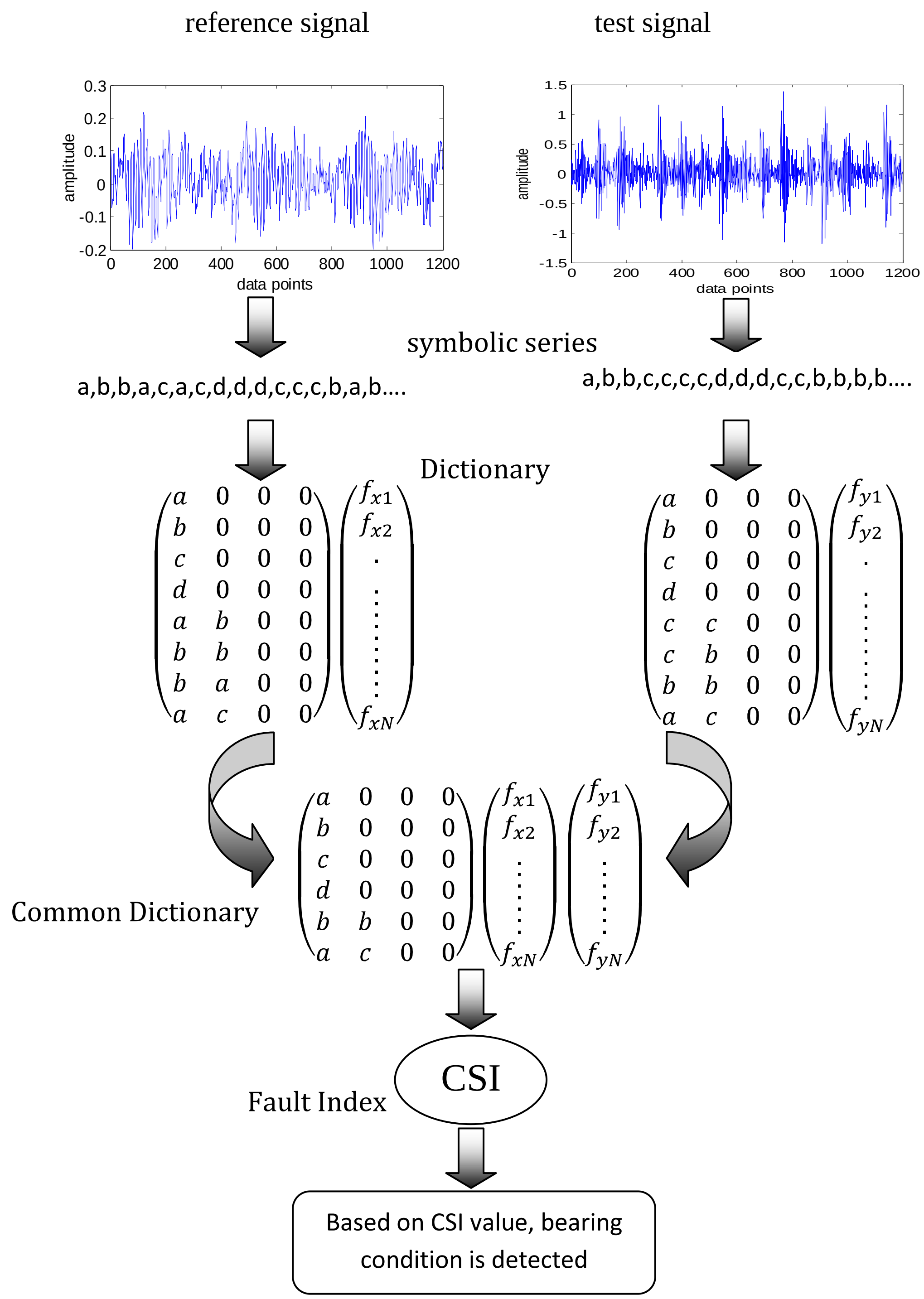

Figure 3.1 Block diagram of the symbolic dynamics based bearing fault detection approach

[Note: symbolic series → (section 3.2.1); Dictionary → (section 3.2.2); Common Dictionary and Fault Index → (section 3.2.3)]

3.2 SYMBOLIC DYNAMIC TECHNIQUE

Symbolic dynamic technique is based on the concept of representation for transitions from smooth dynamics to a discrete symbolic description [Remo & Antonio, 1997]. It is an information-theoretic method of feature extraction from a time series. In this method [Lind, 1995], the observed time series from a dynamical system are represented as a symbolic sequence.

The system behaviour is described at two-time scale level [Singh et al., 2009]: fast time and slow time. The concept of two time scales is illustrated in figure 3.2. The fast time scale is related to response time of the process dynamics. Over the span of a given time series data sequence, dynamic behaviour of the system is assumed to remain invariant, i.e., the process is quasi-stationary at the fast time scale. In other words, the variations in the behaviour of system dynamics are assumed to be negligible on the fast time scale. The slow-time scale, on the other hand, refers to the long-term behaviour of the system, where the patterns of the process dynamics might deviate from those under the nominal conditions. It is assumed that any observable non-stationary behaviour pattern is associated with changes occurring on the slow-time scale. In general, a long time span in the fast-time scale is a tiny (i.e. several orders of magnitude smaller) interval in the slow time scale [Singh et al., 2009]. In case of bearing fault, initiation of point defects in bearing occurs on the slow-time scale (may be in the order of months or years); bearing fault is essentially invariant on the fast-time scale (may be in the order of seconds or minutes). Time series data on the fast-time scale are collected at different slow time scale.

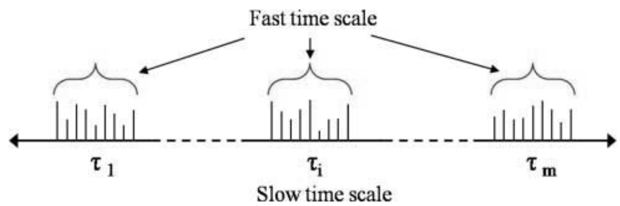

Figure 3.2 Pictorial view of the two time scales: slow time scale of anomaly evolution and fast time scale for data acquisition [Singh et al., 2009]

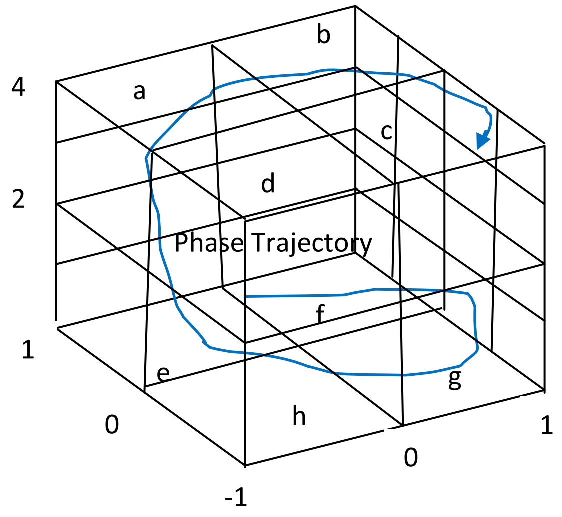

Figure 3.3 Phase trajectory [Gupta et al., 2009]

The system dynamics of a process is generally modelled using initial value problem, given by equation (3.1) [Gupta et al., 2009]

$$\frac{dx(t)}{dt} = f\big(x(t), \theta(\tau)\big); x(0) = x_0 \tag{3.1}$$

where $t \in [0\ \infty)$ represent the fast time scale; $x \in \mathbb{R}^n$ is the state vector in the phase space; and $\theta \in \mathbb{R}^l$ is the (possible anomalous) parameter vector varying in the slow time scale (τ). As the anomaly condition arises at τ, the θ parameter varies slowly which alters the system dynamics and thus changes the trajectory of the system [Gupta et al., 2009].

Figure 3.3 shows the phase trajectory of the system as governed by the equation (3.1). The phase trajectory is bounded within the region $\Omega \subset \mathbb{R}^n$. The region Ω is divided into the mutually exclusive and exhaustive number of cells denoted by each symbol (for example – symbols a to h are used to divide the region shown in figure 3.3). The time series data $x_0\, x_1\, x_2\, \ldots .\, x_n$ with n data points such that $x_i \in \Omega$ are partitioned. Depending on the cell in which the trajectory passes, the corresponding x_i is assigned by the corresponding symbol of the cell. Finally, a sequence of symbol is generated for the total trajectory of the system.

$$x_0\, x_1\, x_2 \ldots \ldots \Longrightarrow s_0\, s_1\, s_2 \ldots \tag{3.2}$$

where s_i , $i = 0, 1, 2 ...$ denotes the symbols used for the partitioning.

The mapping shown in equation (3.2) is called as symbolic dynamics as the dynamics of the system are represented by the symbols. Symbolic dynamics is subjected to loss of information due to improper partitioning [Remo & Antonio, 1997]. However, the loss of information could be minimized through better partitioning methods.

3.2.1 Symbolic series generation

The first and the crucial step in symbolic dynamic technique is partitioning of the time series for generating the symbolic sequence. Various partitioning techniques have been used for the symbolic series generation, which include hierarchical clustering based [Kakizawa et al., 1998], entropy-based [Chau & Wong, 1999] and variance-based [Veenman et al., 2002] methods. In addition to these methods, recently symbolic false nearest neighbors (SFNN) [Kennel & Buhl, 2003], wavelet space partitioning (WSP) [Rajagopalan & Ray, 2006], analytic signal space partitioning (ASSP) [Subbu & Ray, 2008] and simple partitioning (simpleP) [Subbu & Ray, 2008] have been used. Performance comparison of SFNN, WSP, ASSP and simpleP are reported in [Subbu & Ray, 2008].The execution time of simpleP was found to be less than the SFNN and ASSP, but more than WSP. WSP result depends on the identification of an appropriate mother wavelet and selection of appropriate scales. Hence, in this work simpleP is chosen for the symbolic series generation.

3.2.1.1 Maximum Entropy based Partitioning

In simpleP method, the signal phase space is directly partitioned into groups using the maximum entropy approach. A partition that maximizes the entropy of the generated symbol sequence is chosen as the suitable partition [Rajagopalan & Ray, 2006]. It induces a uniform distribution of symbols for the nominal pattern. The number of partitions K plays an important role in this approach. Entropy based approach [Rajagopalan & Ray, 2006] is selected to determine the K. With maximum entropy based partitioning, information rich region are represented by more symbols which gives a finer partition. Similarly, regions with less information are given fewer symbols leading to a coarser partition.

Let $H(K)$ denote the shannon entropy of a symbol sequence obtained by partitioning the time series with K symbols.

$$H(K) = -\sum_{i=1}^{i=K} p_i \, log_2 \, p_i \tag{3.3}$$

where, p_i represents the probability of occurrence of the symbol s_i

A quantity h(.) is defined to represent the change in entropy with respect to the number of symbols.

$$h(K) \ = \ H(K) - H(K-1) \tag{3.4}$$

where K ≥ 2, H(1)=0.

The algorithm [Rajagopalan & Ray, 2006] to select the number of partition is given below:

Step 1: Set $K = 2$. Choose a threshold ε, where $0 \ < \ \varepsilon \ \leq \ 1$.

Step 2: Arrange the time series (length N) in the ascending order.

Step 3: Every consecutive segment of length [N/K] in the sorted time series forms a distinct element of the partition.

Step 4: Convert the time series into a symbolic sequence with the partitions obtained in step (3). If the data point lies within or on the lower bound of a partition, it is coded with the symbol associated with that partition.

Step 5: Compute the symbol probabilities p_i; $i = 1,2, \dots K$. It is calculated as $p_i \ = \ \frac{\sum s_i}{total\ word}$, where s_i is the ith symbol.

Step 6: Compute $H(K) \ = \ -\sum_{i=1}^{i=K} \ p_i \ log_2 \, p_i$ and $h(K) \ = \ H(K) - H(K \ - \ 1)$.

Step 7: If $h(K) \ < \ \varepsilon$, then end: else increment K by 1 and go to Step 3.

A small value of threshold ε leads to a large size of the symbol partition, resulting in increased computation. Also, larger partitions will make the partitioning finer. This might increase the probability of false symbols being induced by noise. On the other hand, a large ε will lead to small partitions that may prove inadequate for condition identification. Hence, there is trade-off between accuracy and computational speed when ε is chosen. The variance of the noise process associated with the raw time series data may serve as a guideline for selection of ε [Rajagopalan et al., 2007]

Terminologies associated with symbolic dynamics are [Tiwari, 2002]: *word* is a combination of consecutive data; a *dictionary* is a collection of words formed from the time series; *frequency* (f) is the number of times a word appears in a dictionary; *fractional occurrence* (f_{xi} ; *i=1 to N*) is the ratio of frequency of a word to the number of words in that dictionary.

3.2.2 Dictionary formation

Dictionary (equation (3.5)) is a combination of two matrices. First is a word matrix, which has all the possible combination of word having one symbol at a time, then two consecutive symbols at a time and continuing till maximum word length is reached. All the non symbol space is filled with zero. Each row of this matrix is called word. Second is a column matrix consisting of fractional occurrence of each word occurring in the word matrix.

$$\text{Dictionary of signal X} = \begin{pmatrix} a & 0 & 0 & 0 \\ b & 0 & 0 & 0 \\ c & 0 & 0 & 0 \\ a & b & 0 & 0 \\ b & b & 0 & 0 \\ b & a & 0 & 0 \\ . & . & . & . \\ . & . & . & . \\ a & b & b & a \\ b & b & a & c \\ b & a & c & a \end{pmatrix} \begin{pmatrix} f_{x1} \\ f_{x2} \\ \vdots \\ \vdots \\ f_{xN} \end{pmatrix} \tag{3.5}$$

If there are N data points in a signal and maximum word length is w_m then total number of words W_t in a dictionary can be calculated as [Tiwari, 2002]

$$W_t = w_m \left[N - (w_m - 1)/2 \right] \tag{3.6}$$

3.2.3 Common Signal Index

Common Signal Index is a parameter which gives the distortion between two signals. A separate two-dimensional array (Common Dictionary) is formed by taking all the common words and their frequencies in both dictionaries of the two signals. From the common dictionary, a common signal index is defined by using the fractional occurrences of the words in both dictionaries. Based on the suitable CSI value between the reference signal and the test signal, the system state can be estimated.

The following CSIs [Tiwari, 2002] are considered:

$$CSI1 = \sum_{j=1}^{n} \frac{f_{xj} f_{yj}}{f_{xj} + f_{yj}} \tag{3.7}$$

$$CSI2 = \sum_{j=1}^{n} \frac{f_{xj} f_{yj}}{(1 + |f_{xj} - f_{yj}|)} \tag{3.8}$$

$$CSI3 = \sum_{j=1}^{n} \frac{|f_{xj} - f_{yj}|}{1 + f_{xj} + f_{yj}} \tag{3.9}$$

$$CSI4 = \sum_{j=1}^{n} \frac{f_{xj} f_{yj}}{1 + f_{xj} + f_{yj}} \tag{3.10}$$

$$CSI5 = \sum_{j=1}^{n} \frac{f_{xj} f_{yj}}{f_{xj} + f_{yj} + f_{xj} f_{yj}} \tag{3.11}$$

where, n is the total number of different words in the common dictionary; f_{xj}, f_{yj}, fractional occurrence of the j^{th} word in dictionary for reference signal X and test signal Y.

3.2.4 Illustration of the method

Figure 3.4 shows an example for the phase space partitioning. The phase space is divided into 8 partitions with symbols $(a, b, c, d, e, f, g \ and \ h)$. Generally, the number of symbols depends on the system condition and noise level. Thus, each data of the time series is replaced by the corresponding symbol under which it lies. For 1st cycle of the time series of figure 3.4, we get a symbolic series as 'aaaacghdachbbhagbgagagdaggaacghggg'.

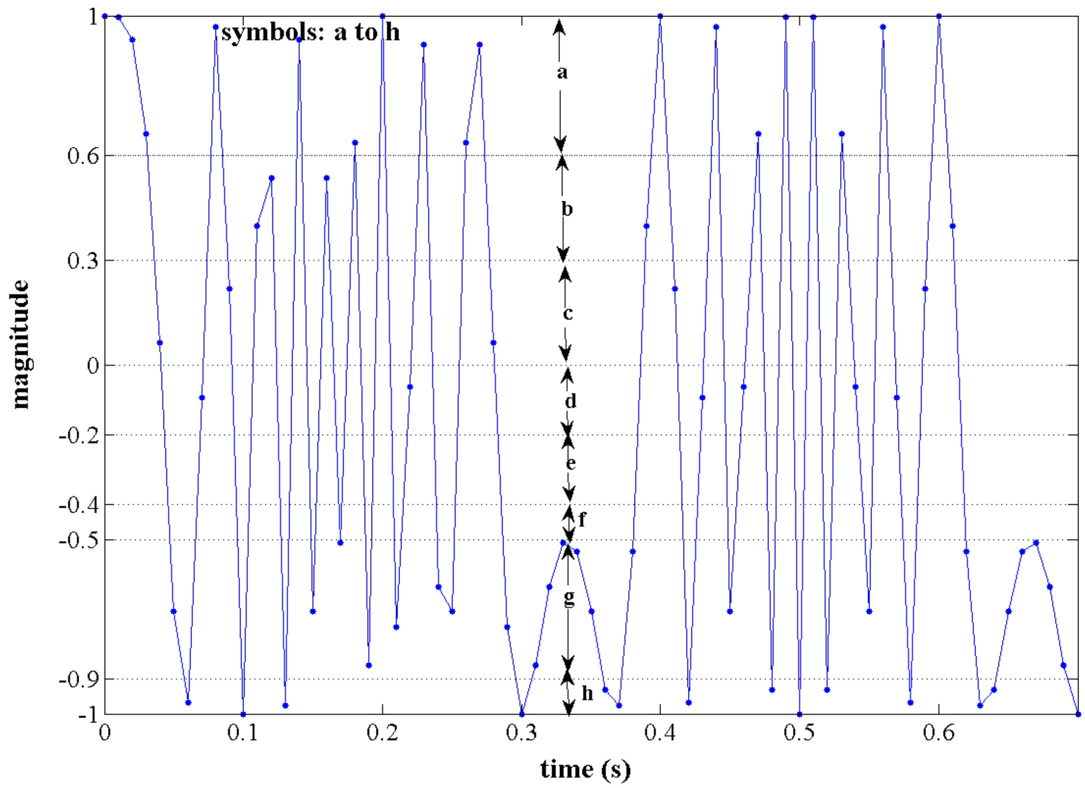

Figure 3.4 Phase space partitioning

Suppose the maximum word length is 2 and 1000 points (N). Word of single length are a,b,c,d,e,f,g and h. Word of length two- ab,ac,ad,ae,af,ag, ah,bc,bd,de,fg,… (ab and ba represent the same word). Frequency (f) of 'a' for the 1st cycle = 11. Then, fractional occurrence of 'a'= f/ total words =11/999 = 0.011. Similarly, for each word of different lengths, frequency and fractional occurrence could be calculated.

Dictionary is formed with two matrices. One is word matrix and other is fractional occurrence matrix with values obtained for the corresponding word. Possible word calculated from the consecutive symbol sequence with w_m=2 are a,aa,ac,c,cg,g,gh,h,hd,d,ad,ch,bh,b,bb,ah,ag,g,bg,dg (The repeated and same words are to be removed). Fractional occurrence of each these words are to be calculated. Common dictionary consists of three matrices. One matrix has the common words found from the two dictionaries formed from the reference and test signal. Other two are the fractional occurrence matrix, formed for each signal corresponding to the common word. The CSI are calculated from these fractional occurrence matrices using the equations (3.7) to (3.11).

Suppose,

Reference signal words are: a,aa,ac,c,cg,g,gh,h,hd,d,ad,ch,bh,b,bb,ah,ag,g,bg,dg.

Test signal words are: a,aa,ab,h,bc,hd,ad,gh,ch,bb,cc,dd,cg,ff,fg,af,bf,ac,c,cg.

Then, the common words are: a,aa,ac,c,cg,gh,h,hd,ad,ch,bb.

Based on the fractional occurrence of the common words, CSI values are obtained.

3.3 DESCRIPTION OF TEST DATA'S

3.3.1 Experimental data: Test data1

Vibration signals used in this work is acquired from the Case Western Reserve University bearing data centre [Bearing data Centre]. The experimental setup as shown in figure 3.5, consists of 2 HP three-phase induction motor connected with torque transducer, accelerometer and dynamometer. The drive end bearing (SKF 6205 series deep grove ball bearing) data is used for the analysis. Single point defect is introduced in the inner raceway, outer raceway and ball elements of different bearings using electron-discharge machining with fault diameters of 0.18, 0.36, 0.53 and 0.71 mm and a depth of 0.28 mm. Vibration data is collected at 12,000 samples/sec and for different fault sizes with load varying from 0 to 3 HP with 1HP increment. The speed varies from 1797 r/min (no-load) to 1730 r/min (3HP load). The data for the outer race fault are taken with the fault position centered at the 6 o'clock position with respect to the load zone. The bearing dimensions are: d = 7.94 mm, D = 39.04 mm, Z=9 and α = 0.

Figure 3.6 shows the recorded bearing acceleration vibration signals for healthy and faulty conditions. Bearing conditions considered for the study are: i) Healthy (H); ii) point defect on inner race (I); iii) point defect on outer race (O); iv) point defect on ball (B).

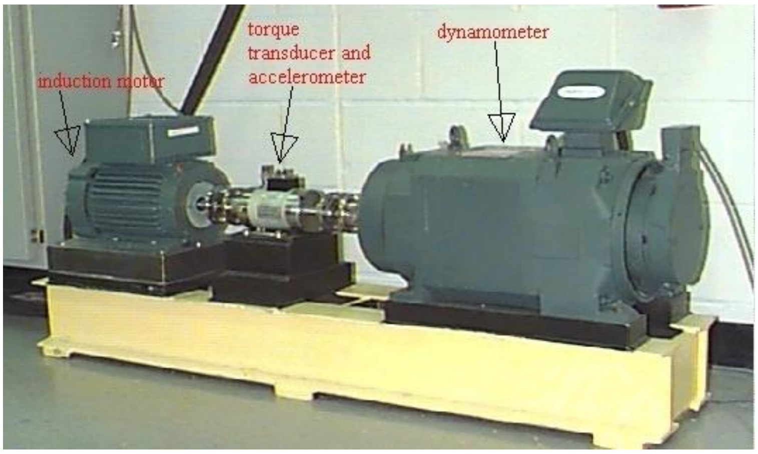

Figure 3.5 Experimental setup of test data1 [Bearing data Centre]

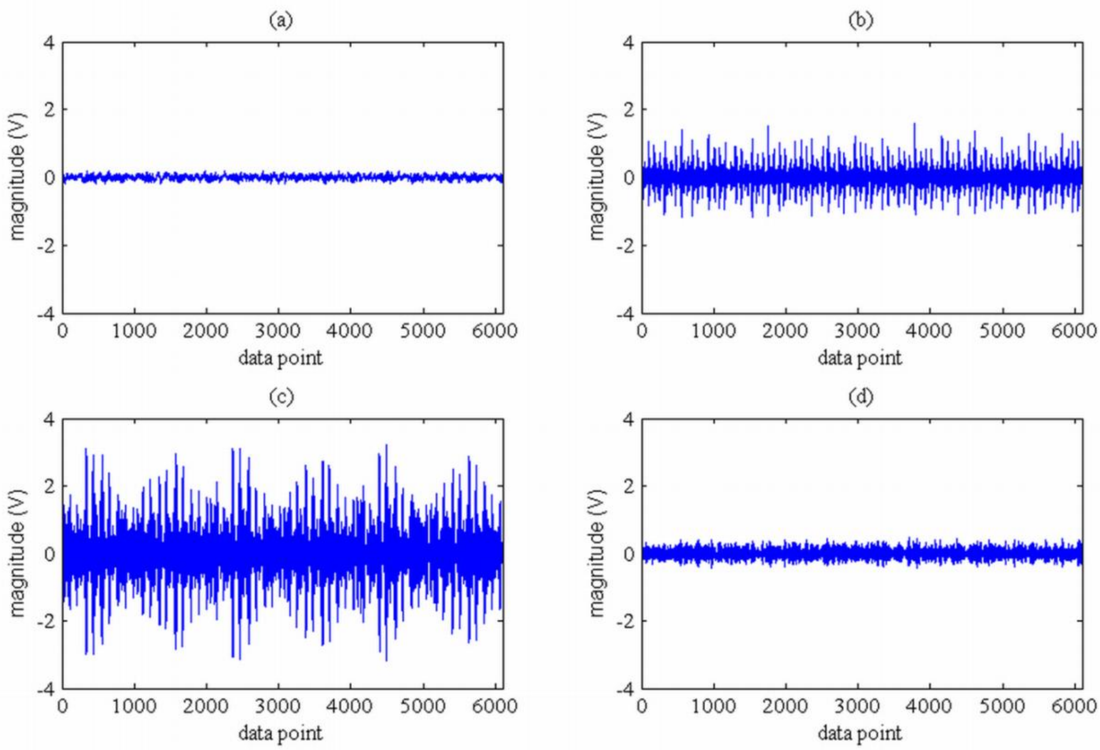

Figure 3.6 Bearing vibration signal of Test data1 (0.18mm fault, 1 HP load) under : a) Healthy; (b) Inner race fault; (c) Outer race fault; (d) Ball element fault;

3.3.2 Experimental data: Test data2

The second data in this method is obtained from the spur gear test rig [Sawalhi & Randall, 2008; Randall, 2011] of University of New South Wales (UNSW). The bearing fault data used is taken from [Randall, 2011]. Figure 3.7 gives the schematic representation of the test setup. The test rig consists of single stage spur gearbox (set with 1:1 ratio and 32 gear teeth) driven primarily by three phase motor and powered by a hydraulic pump/motor set. The shaft of the gearbox has two double row ball bearings (Koyo 1205). Total torque load on the gear was 100 Nm. The shaft speed was 6 Hz. The sampling frequency of the acceleration signal is 48 kHz. The outer race had a notch fault of width 0.8 mm and depth of 0.3 mm, while ball had a fault with both width and depth of 0.5 mm. Figure 3.8 displays the vibration signals obtained under various bearing conditions. The bearing dimensions are: d = 7.12 mm, D = 38.5 mm, Z=12 and α = 0.

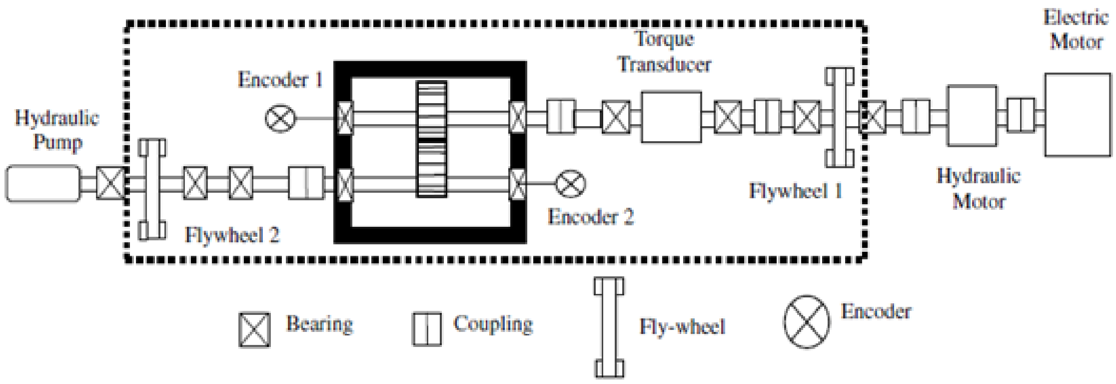

Figure 3.7 Schematic representation of Test data2 [Sawalhi & Randall, 2008]

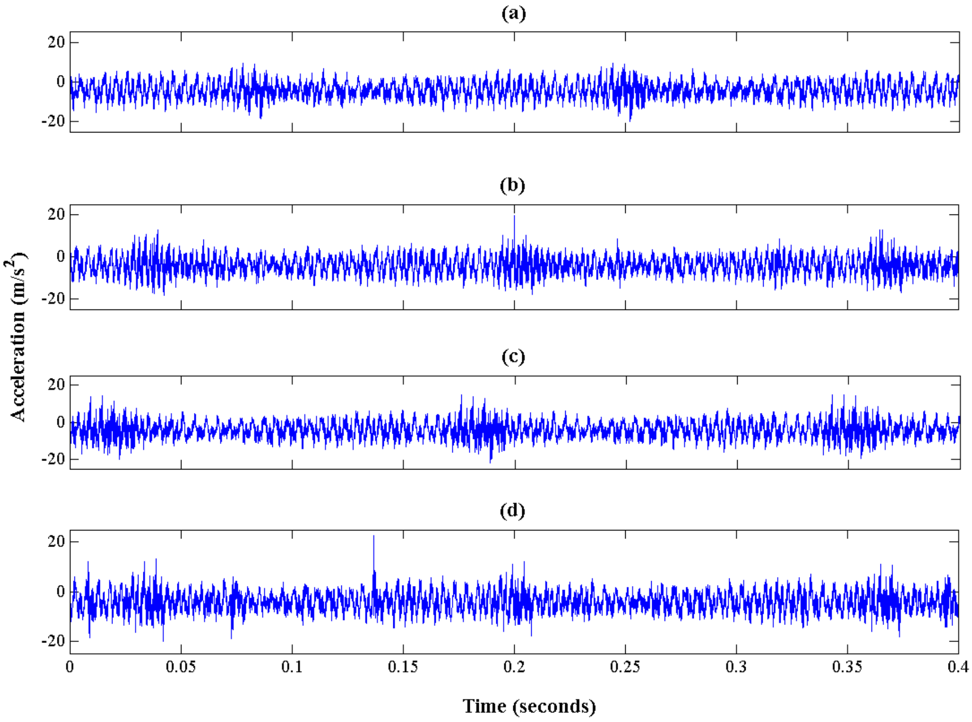

Figure 3.8 Vibration signals obtained from test data2 setup: a) Healthy; (b) Inner race fault; (c) Outer race fault and (d) Ball element fault

3.3.3 Simulation of bearing vibration signal under healthy and faulty conditions : Test data3

The bearing vibration is simulated under the presence of gearbox and additive noise. For faulty bearing signal, the signal obtained would be the summation of fault impulses and those from gear mesh.

The M-impulses produced by the faulty bearing can be expressed as [Dong & Chen, 2012]

$$b(t) = \sum_{i=1}^{M} A_i \, e^{-\beta\,(t - iT - \tau_i)} \cos\,(2\pi f_n\,(\,t - iT - \tau_i) + \varphi_2)\; u(t - iT - \tau_i\,) \quad (3.12)$$

$$A_i = A_0 \cos(2\pi f_r t + \varphi_1) + B$$

(3.13) where, A_0 is the amplitude of the fault impulse, B is constant $(B > A_0)$, f_r is shaft rotational frequency, φ_1 and φ_2 are the arbitrary phase angles, A_i denotes the amplitude modulation due to f_r, β is the structural damping constant ($\beta < f_n$), f_n is the resonant frequency of the system, T is the fault characteristic period, τ_i represents the random slippage of rollers $(0.01T \sim 0.02T)$. $u(t)$ is the unit step function.

For faulty bearing, the vibration interference produced due to gear meshing and its k harmonics are given as

$$g_f(t) = \sum_{k=1}^{G} A_{g,f} \cos(k2\pi f_g t + \varphi_3) \tag{3.14}$$

where, $A_{g,f}$ is amplitude of the gear meshing frequency, k is number of harmonics, f_g is gear meshing frequency.

The total vibration signal under faulty condition is given by

$$x_f(t) = b(t) + g_f(t) + n(t) \tag{3.15}$$

where, $n(t)$ denotes the gaussian white noise.

For healthy vibration signal,

Gear meshing vibration is given as $g_h(t) = \sum_{k=1}^{G} A_{g,h} \cos(k2\pi f_g t + \varphi_4)$ (3.16)

Shaft vibration is expressed as $s(t) = \sum_{l=1}^{S} A_s \cos(k2\pi f_r t + \varphi_5)$ (3.17)

where, $A_{g,h}$ is amplitude of the gear meshing frequency under healthy condition, A_s is the amplitude of shaft frequency components.

The total vibration signal under healthy condition is given by

$$x_h(t) = g_h(t) + s(t) + n(t) \tag{3.18}$$

Parameter values (related to different frequency components and β are taken from the experimental inner race fault vibration signals of [Liang & Soltani Bozchalooi, 2010]) used for the simulation are $A_0 = 0.3$, $f_r = 23.8$ Hz, $T = 0.00854$ s, fault frequency= 117 Hz, $\beta = 1500$, $f_n = 1750$ Hz, $\tau_i = 0.01\,T$, $M = 15$, $f_g = 167.3$ Hz, $f_s = 20$ kHz, N=4000, G=S=3, $A_{g,f} = 0.5$, B=0.4, $A_{g,h} = 0.1$, $A_s = 0.04$, $\varphi_1 = \varphi_2 = \varphi_3 = \varphi_4 = \varphi_5 = 0.0005$. $n(t)$ is added using matlab function 'awgn'such that SNR in the range of 0 to +10 dB signals are obtained. Figure 3.9 shows the healthy and faulty bearing vibration signals obtained using simulation.

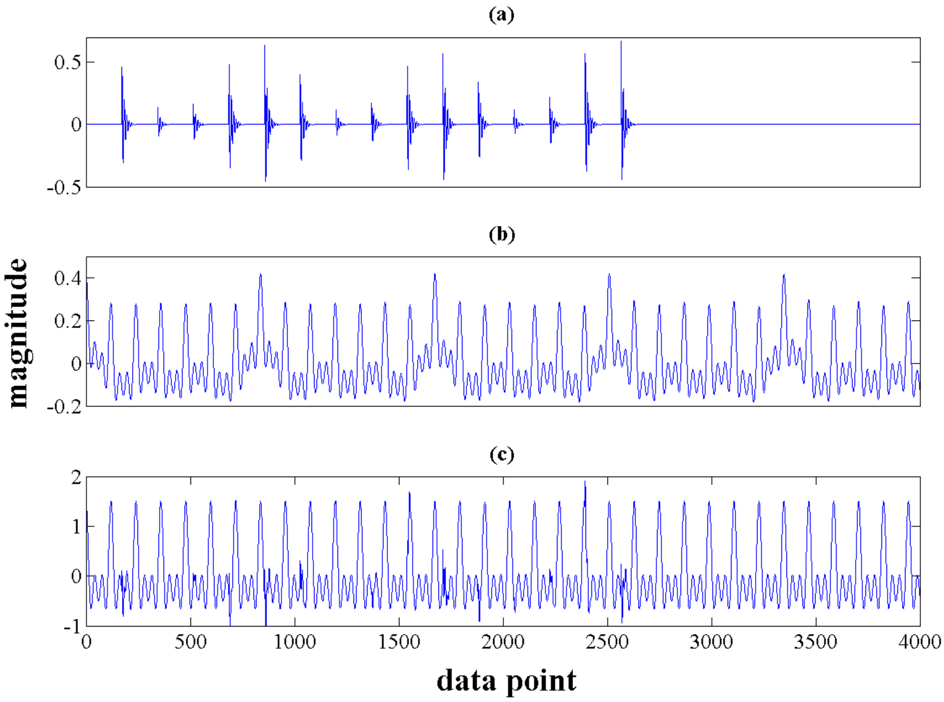

Figure 3.9 Simulated bearing vibration signals without additive noise (a) fault Impulses; (b) healthy condition and (c) faulty condition

3.4 ALGORITHM FOR BEARING FAULT DETECTION BASED ON SYMBOLIC DYNAMICS

The bearing fault detection algorithm is described below:

Step 1: Obtain the two time series data. Signal '1' to be a reference data which represents the healthy bearing condition obtained during commissioning of the machine. Signal '2' to be the test data obtained under the running condition.

Step 2: Calculate the number of partition based on maximum entropy partitioning method and obtain the symbolic series for each signal.

Step 3: Form the dictionary from the symbolic series of each signal.

Step 4: Compare the two dictionaries and list out the common word between the signals with corresponding frequency of occurrence of that word.

Step 5: Compute the suitable CSI which reflects the condition of bearing under running conditions. Using the rule formed, bearing condition is identified depending on the CSI value obtained.

3.5 TESTING OF THE METHOD

The parameters to be chosen in this method are word length (w_m), threshold value (ε) and number of symbols (K). The word length affects the accuracy and computation time of fault algorithm. ε ranges between 0 and 1 which is used in maximum entropy based partitioning algorithm. A small value of threshold leads to a large size of the symbol partition, resulting in the increased computation. Also, larger partitions will make the partitioning finer. This might increase the probability of false symbols being induced by noise. On the other hand, a large ε will lead to small partitions that may prove inadequate for condition identification. Hence, there is trade-off between accuracy and computational speed when ε is chosen. Up to a particular value of ε, K may not vary. In this work, for $\varepsilon = 0.2$, $K = 3$ was obtained. For $K = 4$, ε = 0.02 was set. In the following sub-sections, the symbolic dynamic based fault detection method is applied to the three test data's.

3.5.1. Application to test data1

From the maximum entropy based partitioning algorithm, for ε = 0.2, number of symbols (K) obtained is 3. No-load healthy bearing vibration signal is used as the reference signal for bearing condition monitoring, which could be easily obtained during the commissioning of the plant. The test signals are obtained for the various bearing conditions considered under study. Different maximum word length of 2, 3 and 4 were used to compute the fault index.

3.5.1.1 Selection of appropriate CSI

Of the various CSI's mentioned in section 3.2.3, a suitable CSI should be selected as a fault index. For this purpose, data of healthy bearing under 1 HP and no-load condition are compared with the faulty bearing data's respectively to obtain the CSI's values which are given in table 3.1. Here, results obtained using word length 3 is only shown. Based on the observations presented in table 3.1, it is seen that CSI2, CSI4 do not change much under all the bearing conditions comparison. CSI1 and CSI3 have different values for healthy bearing and faulty bearing conditions. CSI5 values are close to CSI1. When the two signals are of similar kind, the fractional occurrence of words would be equal, and then expected value of CSI1 and CSI3 are 0.5 and 0 respectively. Based on the observation, CSI1 and CSI3 are chosen as a fault index.

3.5.1.2 CSI1 and CSI3 as Fault Index

Table 3.2 shows the overall range of fault index values obtained for various maximum word lengths under different bearing conditions. CSI1 and CSI3 have different range of values for healthy and fault conditions, but they have similar range of values within the different fault conditions. Using word length of 2, the fault index has nearly same range of values for healthy and fault conditions in few cases. Hence, using word length of 2 the algorithm would give ambiguity in the bearing condition for some data. It is observed that, word lengths of 3 and 4 are suitable for the bearing condition monitoring as the fault index values clearly differentiates between healthy and fault conditions. The average time taken for the dictionary formation using word length as 4 is 2.5 times more than for word length as 3. Thus, word length of 3 is chosen as an appropriate length. Under healthy and fault conditions for varying fault severity and load level, the CSI1 and CSI3 values obtained using word length 3 are as shown in tables 3.3 and 3.4 respectively.

Table 3.1 Different CSI values under different reference and test conditions of bearing for 0.18 mm fault size.

(Note: H- Healthy, I- inner race fault, O- outer race fault, B- ball fault; numbers 0 and 1 in reference and test condition indicates load in HP)

Reference Condition	Test Condition	CSI1	CSI2	CSI3	CSI4	CSI5
	H0	0.5	0.071	0	0.06	0.483
	I0	0.411	0.054	0.418	0.046	0.399
H0	O0	0.374	0.052	0.438	0.044	0.362
	B0	0.381	0.052	0.51	0.044	0.369
	H1	0.5	0.069	0	0.059	0.484
H1	I1	0.417	0.054	0.453	0.046	0.405
	O1	0.399	0.053	0.517	0.046	0.386
	B1	0.384	0.051	0.512	0.044	0.372

Table 3.2 Overall fault Index Values for various maximum word length (w_m) under different bearing conditions

w_m	Fault Index	Healthy	Inner race Fault	Outer race Fault	Ball race Fault
2	CSI1	0.49-0.5	0.46-0.49	0.45-0.47	0.44-0.47
	CSI3	0-0.2	0.16-0.29	0.19-0.35	0.24-0.37
3	CSI1	0.49-0.5	0.4-0.47	0.38-0.44	0.37-0.43
	CSI3	0-0.14	0.29-0.53	0.37-0.6	0.43-0.61
4	CSI1	0.48-0.5	0.34-0.45	0.3-0.41	0.3-0.4
	CSI3	0-0.21	0.38-0.64	0.47-0.68	0.52-0.68

Table 3.3 Fault index for healthy bearing condition under various loads (w_m = 3)

Reference Condition	Test Condition	CSI1	CSI3
	H0	0.5	0
H0	H1	0.497	0.067
	H2	0.491	0.138
	H3	0.497	0.071

Table 3.4 Fault index for different bearing fault conditions under various fault sizes and loads (w_m= 3)
(X – Fault size vibration data not available; 0 to 3 indicates the load in HP)

Reference condition	Test condition	Fault size (mm)							
		0.18		0.36		0.53		0.71	
		CSI1	CSI3	CSI1	CSI3	CSI1	CSI3	CSI1	CSI3
	I0	0.414	0.495	0.4	0.514	0.399	0.508	0.438	0.403
	I1	0.41	0.488	0.396	0.535	0.4	0.506	0.44	0.397
	I2	0.419	0.471	0.399	0.517	0.399	0.534	0.452	0.351
	I3	0.413	0.47	0.424	0.444	0.402	0.528	0.466	0.288
	O0	0.375	0.533	0.391	0.549	0.439	0.373		
H0	O1	0.378	0.604	0.38	0.575	0.434	0.39		
	O2	0.383	0.385	0.389	0.557	0.427	0.426	X	
	O3	0.385	0.568	0.397	0.52	0.425	0.432		
	B0	0.38	0.604	0.409	0.508	0.392	0.57	0.379	0.494
	B1	0.379	0.592	0.422	0.44	0.386	0.573	0.375	0.553
	B2	0.368	0.598	0.418	0.47	0.409	0.506	0.371	0.504
	B3	0.38	0.608	0.433	0.425	0.401	0.504	0.37	0.498

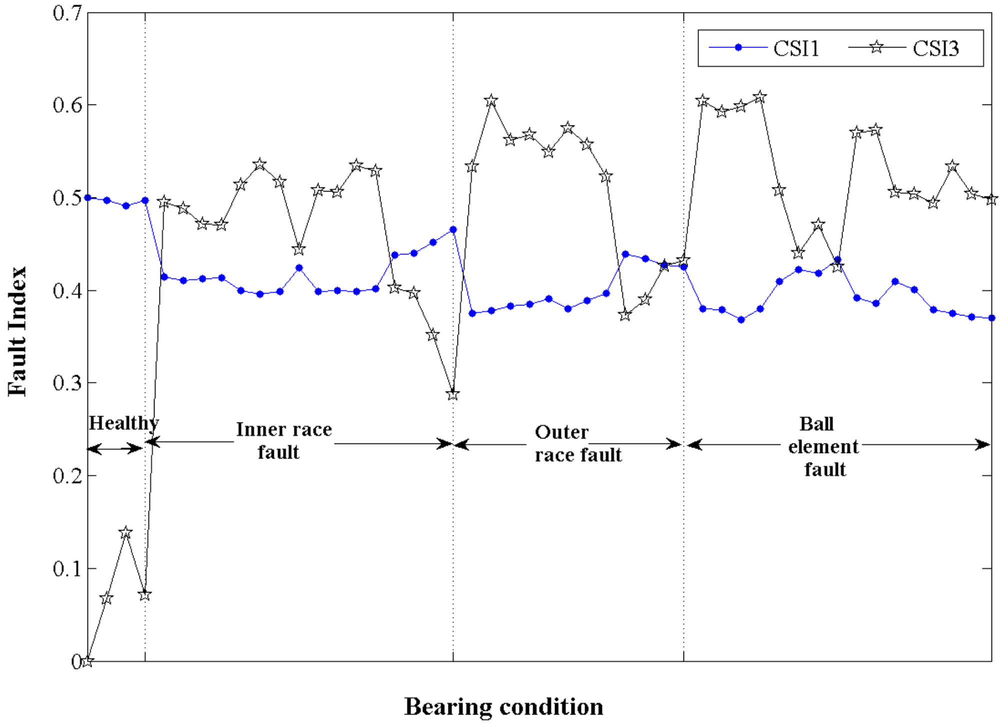

Figure 3.10 Fault index values for different bearing condition (various load and fault severity)

Figure 3.10 shows the variation of the fault index with respect to the various bearing condition based on the tables 3.3 and 3.4.

With the occurrence of the fault, CSI1 decreases and CSI3 increases (figure 3.10). As the fault occurs, the symbolic representation of the signal drastically changes, and the total number of words increases which in turn modifies the fractional occurrence of the words. The fault index is calculated based on the fractional occurrence of the common words found in the two signals been compared. When the two signals are of similar kind i.e. healthy, the fractional occurrence of words would be equal, which makes the CSI1 value close to 0.5 and CSI3 close to 0 [based on equations (3.7) & (3.9)].

When the two signals under comparison are of different nature i.e. reference is healthy and test signal is of fault condition, the fractional occurrence would be different. Few words will have the same value of fractional occurrence, while many words of fault signals show greater number of fractional occurrence and little number of words of fault signals will have less number of fractional occurrences than the healthy signal. This is due to the impulses which modify the signal on occurrence of the fault. The region of impulses will have more fractional occurrence of the word to code. Thus, statistically, based on the equations (3.7) & (3.9), the CSI1 values decrease below and CSI3 increases above healthy condition value. It is seen that out of the two fault index, CSI3 is better fault index as there is a large margin between the values for healthy and fault conditions. As seen from figure 3.10, the fault index values for inner race fault, outer race fault and ball element fault conditions are in the same range. Hence, no information about the type of fault occurred could be obtained. But, the bearing in general healthy or fault condition is identified. Bearing preliminary information is obtained which is vital from the maintenance point of view.

On the basis of the results obtained, bearing condition is classified using the rule given below.

If CSI1 = 0.48 to 0.5 or CSI3 = 0 to 0.2, Bearing is healthy else bearing has fault.

To increase the robustness of the fault algorithm above range of values is considered for fault index instead of the nominal values of 0.5 and 0 respectively for CSI1 and CSI3.

3.5.1.3 Effect of noise on fault index

The performance of the fault index in the presence of noise is vital as during the operation of the motor, mostly signals would be noisy. Assuming that the signals obtained from the experimental setup are noise free, test signals are degraded with noise in order to study the effect of noise on the CSI1 and CSI3 values. Gaussian white noise is added synthetically with SNR in the range of 10 dB (low noise) to 0 dB (highly noise). The CSI1 and CSI3 values are obtained for various combinations of reference signals such as (i) reference is noise-free; (ii) reference is noisy.

3.5.1.3.1 Under Noise-free Reference signal

CSI1 and CSI3 are computed using noise-free reference signal and noisy test signal. Figure 3.11 and 3.12 shows the fault index values obtained for the above condition. In case of healthy bearing (figure 3.11(a) and 3.11(b)), CSI1 gradually decreases with increase in noise level for 1HP and 3 HP load. For fault condition (figure 3.11), there is a less change in CSI1 values. CSI3 increases with increase in noise for healthy, while for fault condition there is less change in CSI3 as observed from figure 3.12. There is always a huge difference in fault index value obtained in case of healthy and fault conditions. The fault index does not attain the nominal values under higher noise level.

3.5.1.3.2 Under Noisy Reference signal

Figures 3.13 and 3.14 give the results for CSI1 and CSI3 respectively, obtained when the reference signal is degraded with noise of 10 dB. The test signal is also noisy with varying range (0 to 10 dB). As seen from figures 3.13(a) and 3.13(b) under healthy condition, CSI1 slowly decreases from its nominal value as noise level increases for both 1HP and 3HP load. CSI3 up to 6 dB increase slowly and thereafter it increases drastically with noise (figures 3.14(a) and 3.14(b)) for healthy bearing. For fault conditions, there is a less change in value of CSI1 and CSI3 as observed (figures 3.13 and 3.14) with the increase in the noise level.

3.5.1.3.3 Comparison of CSI values for healthy conditions with respect to noise

CSI values were obtained for various combinations: (a) When both the reference and test signals are noise free (signals obtained from test setup), (b) When reference is noise free and test signal is noisy, (c) When reference and test signals both are noisy. CSI values varying close to nominal value are vital. Hence, for healthy conditions the aforementioned three combinations of reference and test signal are compared as shown in figures 3.15 and

3.16 for CSI1 and CSI3 respectively. From figure 3.15, it is observed that, where *both the reference and test signal are noisy* the CSI1 decreases at a lower rate as compared to the case where reference *is noise-free and test signal is noisy*. In condition (c), up to 6 dB noise is tolerable, beyond which filtering would be required. Also, for CSI3 (figure 3.16), case where both *the reference and test signal are noisy* performs better than the case *where reference is noise free and test signal is noisy.* For condition (c), CSI3 sustains up to 8 dB to be within the nominal range, beyond which filtering would be necessary. In real conditions, both the signals would be noisy which would require further de-noising and as seen from the comparison, condition (c) i.e. where *both the reference and test signal are noisy* gives good results. Hence, even during the actual environment the fault index would give accurate bearing health information.

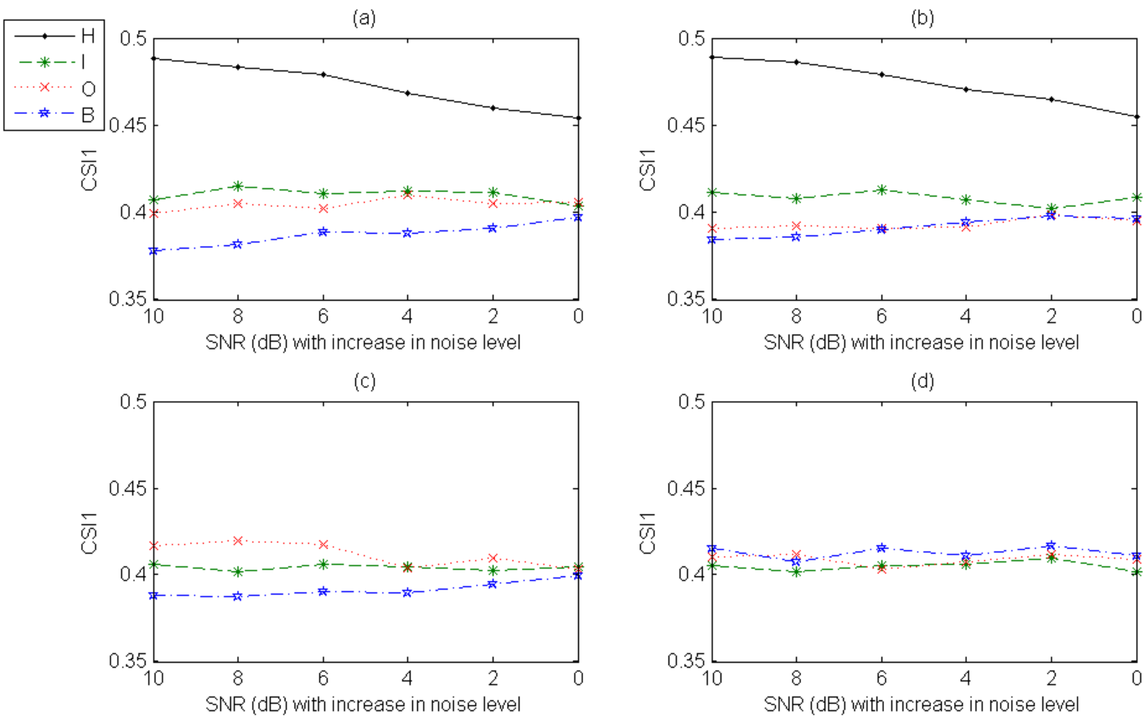

Figure 3.11 CSI1 variation with noise level under different bearing conditions where Reference is noise-free: a) 0.18 mm fault size, 1HP load; b) 0.18 mm fault size, 3HP load; c) 0.53 mm fault size, 1HP load and d) 0.53 mm fault size, 3HP load

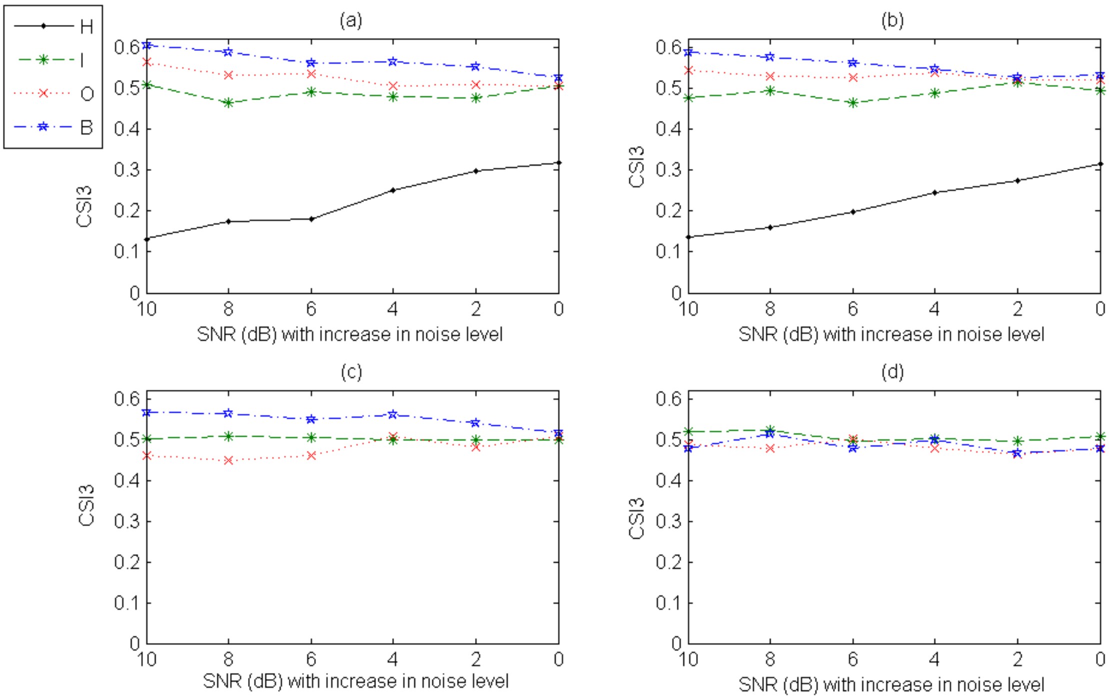

Figure 3.12 CSI3 variation with noise level under different bearing conditions where Reference is noise-free: a) 0.18 mm fault size, 1HP load; b) 0.18 mm fault size, 3 HP load; c) 0.53 mm fault size, 1 HP load and d) 0.53 mm fault size, 3 HP load

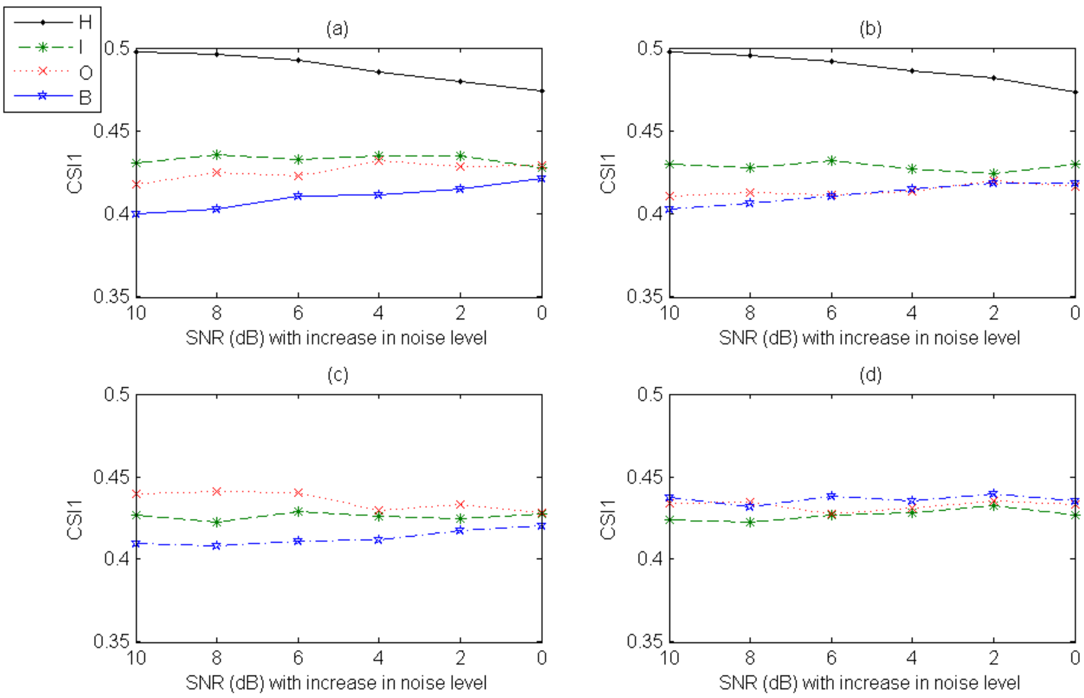

Figure 3.13 CSI1 variation with noise level under different bearing conditions when reference signal is noisy: a) 0.18 mm fault size, 1 HP load; b) 0.18 mm fault size, 3 HP load; c) 0.53 mm fault size, 1 HP load and d) 0.53 mm fault size, 3 HP load

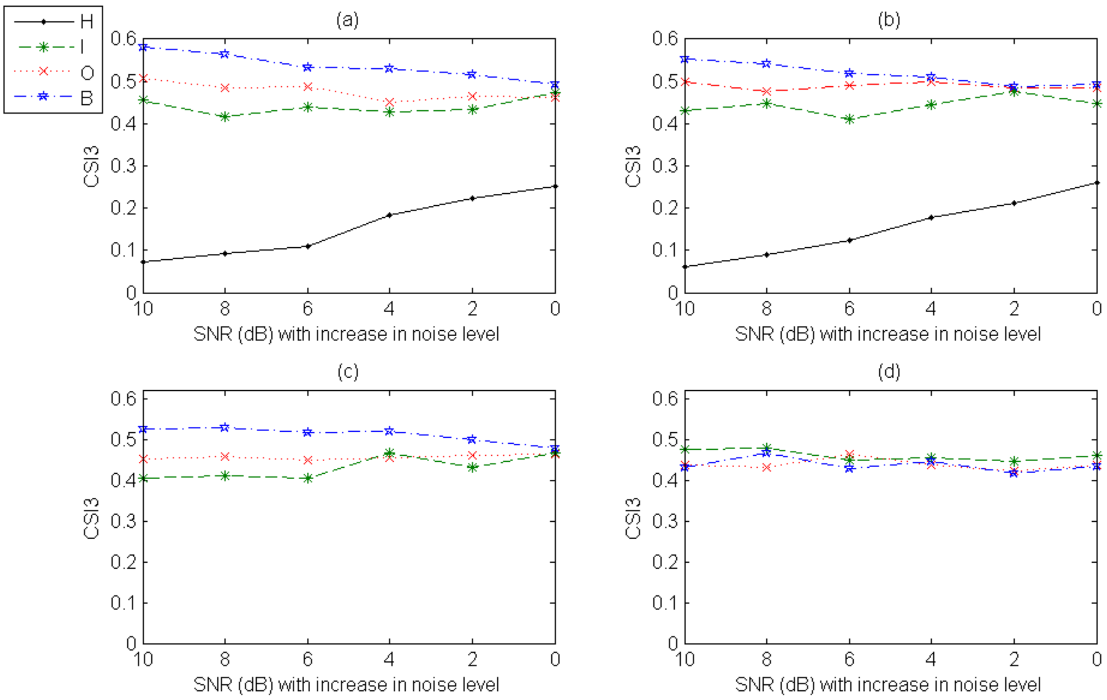

Figure 3.14 CSI3 variation with noise level under different bearing conditions when reference signal is noisy: a) 0.18 mm fault size, 1 HP load; b) 0.18 mm fault size, 3 HP load; c) 0.53 mm fault size, 1HP load and d) 0.53 mm fault size, 3 HP load

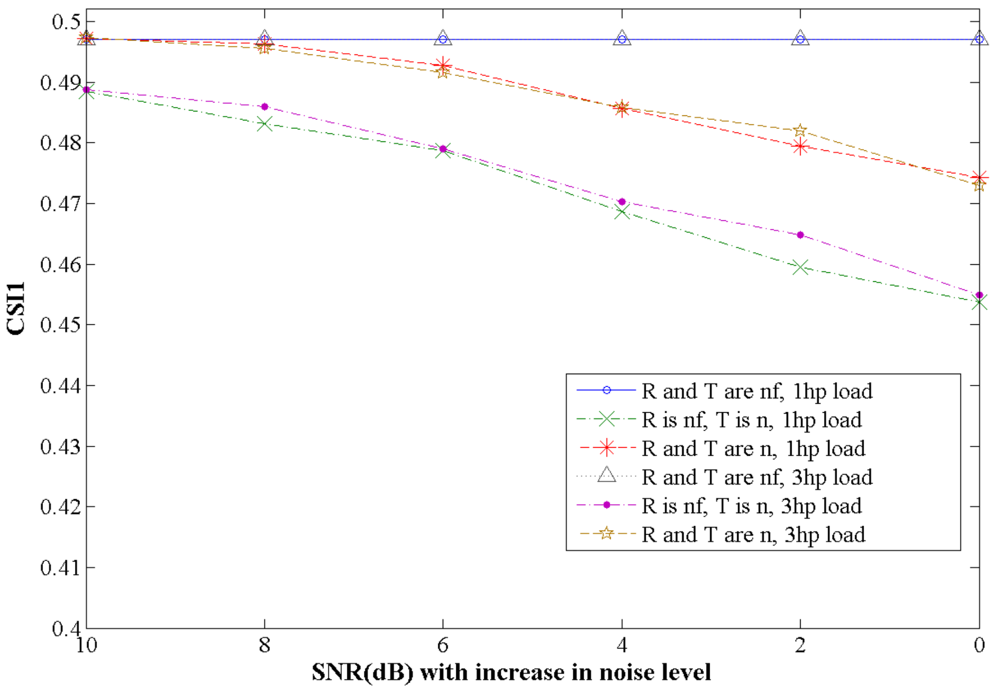

Figure 3.15 CSI1 values obtained for healthy bearing under noisy conditions at 1 HP and 3 HP load (R- reference signal, T- test signal, n- noisy, nf- noise-free)

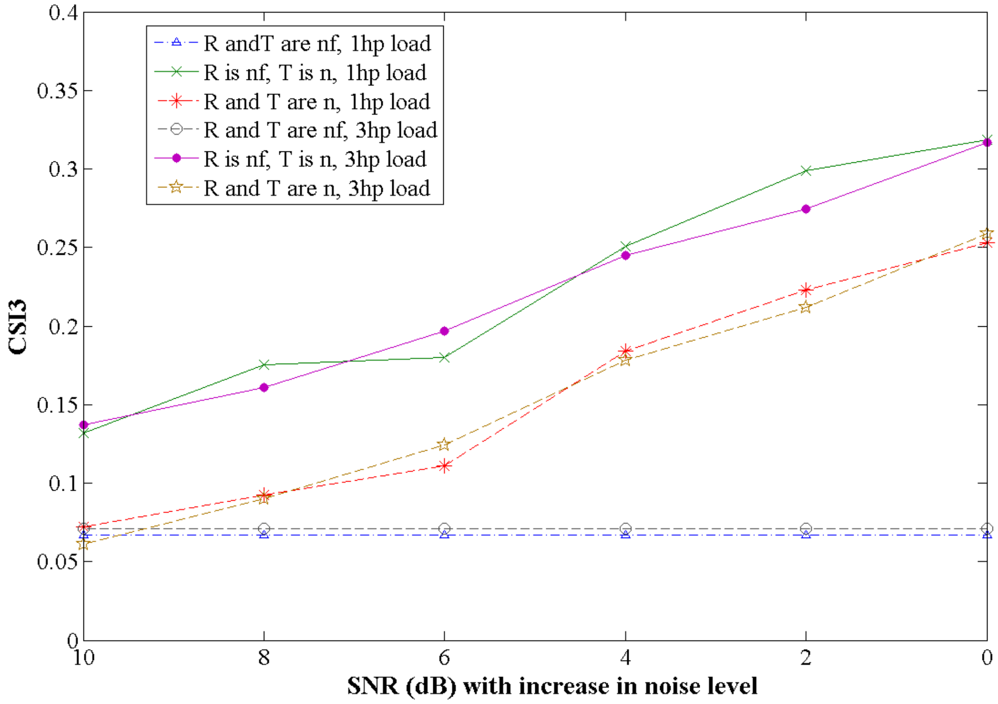

Figure 3.16 CSI3 values obtained for healthy bearing under noisy conditions at 1 HP and 3 HP load

3.5.1.4 Effect of sample points

The variation of the fault index for varying number of sample points is also studied. Figure 3.17 gives the CSI1 and CSI3 values under different bearing conditions for varying number of sample points. It is observed that CSI1 and CSI3 maintain the value of 0.5 and 0 respectively for different number of sample points. Also, the healthy and fault condition is identified.

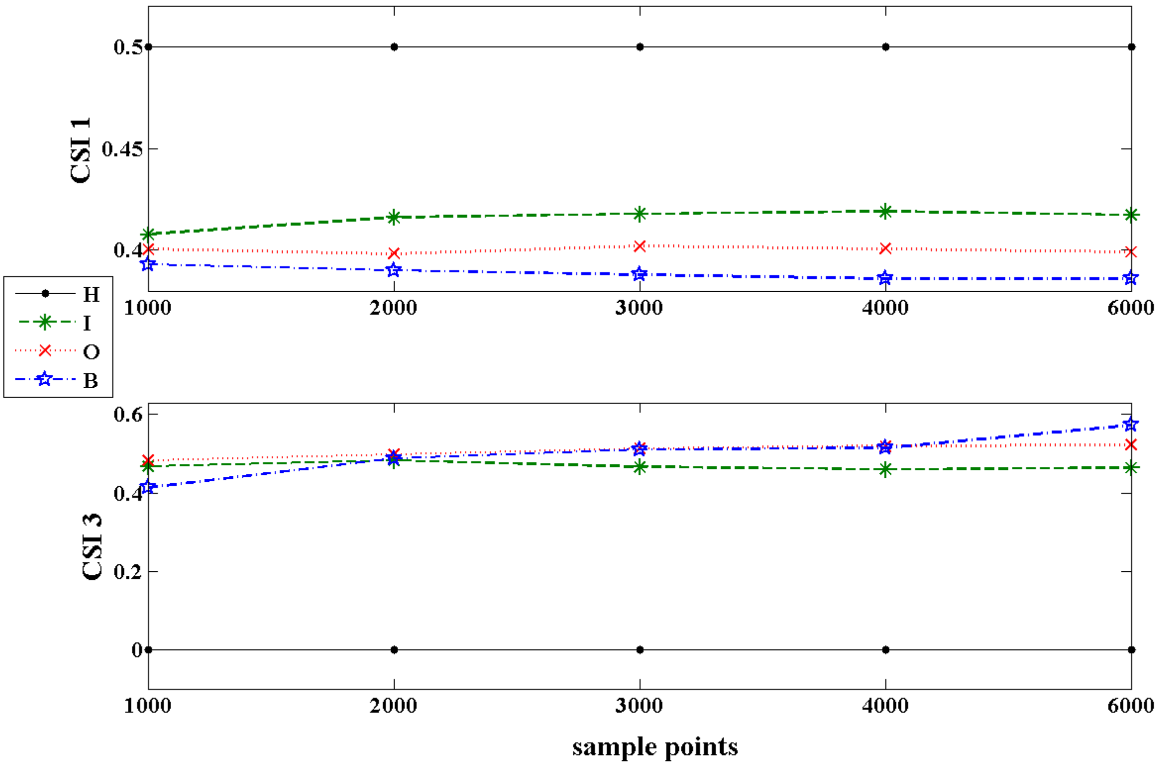

Figure 3.17 CSI1 and CSI3 values for healthy and faulty bearing with 0.18mm fault under 1HP load for different sample points

3.5.2 Application to Test data2

To check the robustness of the method, test data2 signals (under presence of gearbox) are used. Initially, $\varepsilon = 0.2$ and $K = 3$ were chosen. But accurate results could not be obtained. Hence, threshold ε was reduced further to 0.02, and number of symbols obtained using maximum entropy partitioning was 4. With $K = 4$, the method is tested using various word lengths (10, 15 and 20). The signals obtained were having background noise in the range of 15 to 25 dB. Hence, no noise was added virtually for the analysis. Similar to test data1, reference signal is healthy signal and test signal are of I, O and B conditions. CSI values obtained for the various word lengths are given in table 3.5. Table 3.5 shows that for fault condition, the CSI1 does not have values close to 0.5 and CSI3 does not does not values near to zero. Also, we observe that, word length affects the accuracy of the methods and also computation time increases with it. With the rule formed based on the analysis done for test data1, we could detect the presence of fault in bearing of test data2.

Table 3.5 CSI values obtained for bearing faulty conditions under varying ω_m : test data2 (e.g., H vs I, means healthy(H) and inner race fault (I) signals are compared)

ω_m	Fault Index	H vs H	H vs I	H vs O	H vs B
10	CSI1	0.5	0.4461	0.4312	0.4250
	CSI3	0	0.1871	0.2236	0.1788
15	CSI1	0.5	0.3772	0.3513	0.3586
	CSI3	0	0.1942	0.2307	0.1841
20	CSI1	0.5	0.3122	0.2780	0.3003
	CSI3	0	0.1735	0.1974	0.1673

3.5.3 Application to simulation data - Test data3

The simulated data was added with gaussian white noise to obtain signals with various SNR's (0 to +10 dB). Parameter used for testing are $\varepsilon = 0.2$ and $K = 3$. Similar to the test data2, various word length (10, 15 and 20) were used for analysis. The CSI1 and CSI3 values obtained for different SNR and using various ω_m are given in figures 3.18 and 3.19 respectively. Both the reference and test signals are noisy for different SNR case. For CSI1 (figure 3.18), an increase in w_m increased the deviation of value with respect to healthy condition. For CSI3 (figure 3.19), with increase in w_m, the deviation with respect to healthy condition reduced. From this figures, it is observed that CSI values obtained for faulty condition have values well below the healthy CSI threshold value. Even with increase in noise level, the faulty bearing is correctly identified with reference to the healthy value.

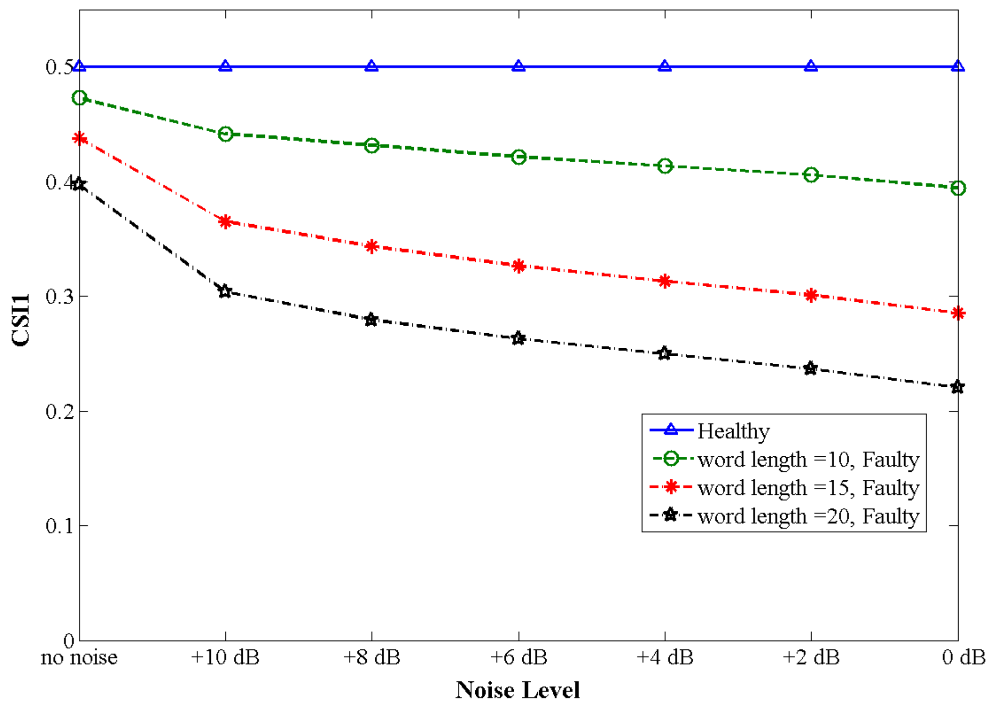

Figure 3.18 CSI1 values obtained under varying SNR and different w_m values: test data3

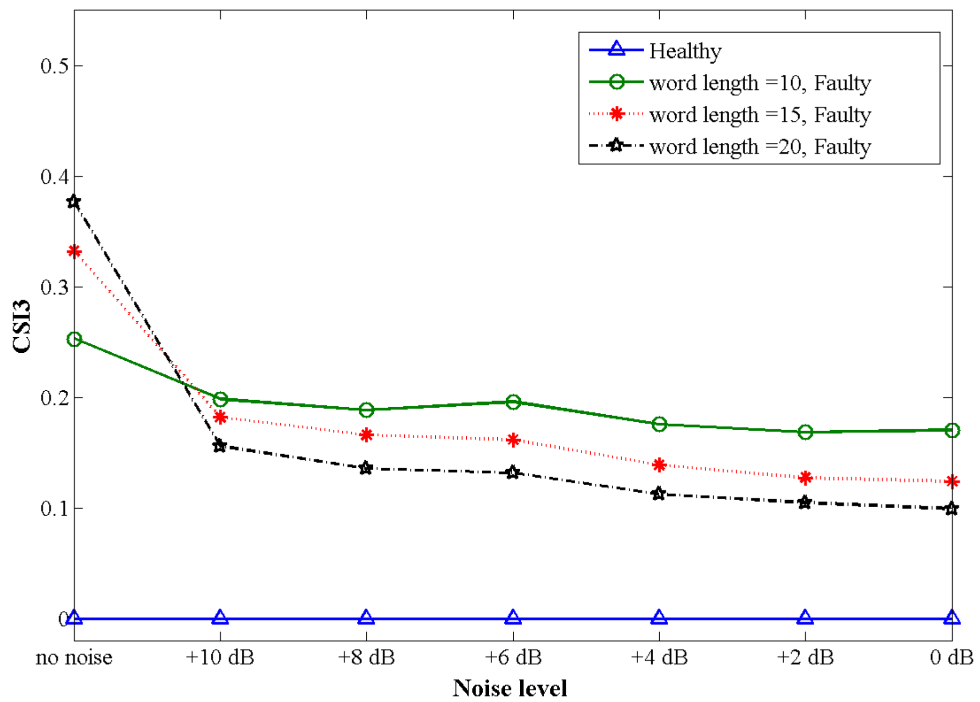

Figure 3.19 CSI3 values obtained under varying SNR and different w_m values: test data3

3.6 COMPARISONS WITH OTHER TIME-DOMAIN AND DATA BASED TECHNIQUES

As the symbolic dynamics method is based on the time series, so the comparisons are done with methods based on time-domain and data based ones. The dataset used in this work has no masking vibration sources such as gears. Thus, the comparison is done with methods where same test data are used. The works done in [Nelwamondo et al., 2006; Sreejith et al., 2008; Wang et al., 2009; Van wyk et al., 2009, Xiong et al., 2010; William & Hoffman, 2011; Li & Zhang, 2011; Boutros & Liang, 2011] uses the same bearing dataset [Bearing data Centre] as used in this chapter. Hence, they are used for comparison. Table 3.6 gives the comparison of the symbolic dynamics based method with the existing time domain and data based methods with respect to the some features of the bearing condition monitoring system.

In [Sreejith et al., 2008], no pre-processing is done and statistical features like peak, rms, and kurtosis are calculated and given to ANN for classification. Noise will affect the features which affects the accuracy.

In [Van wyk et al., 2009], difference histogram is used to identify bearing as healthy or faulty. But it required neural network, which is not needed in the symbolic dynamics based method. Also, sample size influences the classification and it has to be sufficient large (N=30,000) for high accuracy.

In [Xiong et al., 2010], Multi scale entropy feature is found to be suitable for bearing fault detection. However, in noisy condition the classification accuracy comes down from 97.42% to 73.94%. As seen from section 3.5.1.1 even in noisy condition, 100% accurate bearing health information is obtained using symbolic dynamics based method.

In [William & Hoffman, 2011], zero crossing features are used. Its calculation dependent on the signal length which required the knowledge of accurate rotation frequency and longest expected time duration between successive zero crossing. The classification accuracy of Artificial Neural Network used is affected by window length and varies from 91.5% to 97.1%.

The Performance of Supervised locally linear embedding projection based method [Li & Zhang, 2011] is very sensitive to the regularization parameter which represents the generalization capacity of algorithm. Computational and storage complexity is present as the whole data set needs to be retained when mapping new data.

In [Nelwamondo et al., 2006], mel-frequency cepstral coefficients and fractals were used along with hidden Markov model and Gaussian mixture model (GMM). Depending on the number of sample, the classification accuracy varies from 81% to 100% at different bearing location. In the symbolic dynamics method, it is observed that even on sample size variation the bearing health is accurately known (section 3.5.1.2).

In [Wang et al., 2009], reconstructive phase space is used to bring out the non linear characteristic of the signal. A bayesian classifier is used to calculate the likelihood of the test signal with the learned GMM. Each fault required separate GMM. In [Boutros & Liang, 2011], bearing fault detection is based on comparison of the monitoring index with the reference vectors which are large in number along with Hidden Markov Model. The training time is more and not fixed as the random values are used to fix the model parameters which are calculated by Viterbi algorithm [Boutros & Liang, 2011].

Based on the above comparison, the advantages of the symbolic dynamic based method are - 1) Insensitive to sample size, speed and load; 2) No fault data or speed information needed beforehand and 3) Avoids training of fault algorithm as in case of artificial intelligence based methods.

Table 3.6 Comparison of the symbolic dynamics approach with other methods based on desired features of vibration based bearing condition monitoring systems

Algorithms	Machine independent	Simple mathematical calculation	No pre-fault data requirement/ training	Speed and Bearing parameter independent
AR [Baillie & Mathew, 1996] and **ARMA** [Li et al., 2007]	X	X	X	√
Histogram [Van wyk et al., 2009]	X	√	X	√
Zero crossing [William & Hoffman, 2011]	√	√	X	speed required
Pattern classifiers, rule based [Nelwamondo et al., 2006; Wang et al., 2009; Xiong et al., 2010; Li & Zhang, 2011; Boutros & Liang, 2011]	X	X	X	√
Symbolic dynamics [In this chapter]	√	√	√	√

X- Not applicable; √ - applicable

3.7 SUMMARY

Symbolic dynamic approach has been presented for the detection of single point faults in ball bearing. Two fault indexes (CSI1 and CSI3) are calculated and bearing in healthy or faulty condition is accurately identified. The method works well against two experimental and one simulation data. It shows robustness even in presence of masking sources such as gearbox as found in test data2. Performance of the method is sample size independent. The method does not need fault data beforehand to detect the presence of fault. Hence, it overcomes the problem of training the fault algorithm from machine to machine. Also, it is machine and load independent. Even when the reference and the test signal are noisy, the fault index gives satisfactory results. This method is well suited as a start up test of the motor for bearing healthiness check before commencing the normal operation as it works even in no-load condition.

CHAPTER 4

IDENTIFICATION OF FAULTY BEARING USING SINGULAR VALUE RATIO: A CASE STUDY

MAIN CONTENTS:

- **Introduction**
- **Calculation of Singular Value Ratio (SVR)**
- **SVR based Fault Identification**
- **Robustness Study of SVR**
- **Comparison with Simple Time Domain Methods**
- **Summary**

4.1 INTRODUCTION

Chapter 4 investigates the possibility of using the ratio of singular value for bearing fault detection. The proposal of using the ratio of singular value as a fault index was developed from the work of bearing fault diagnosis method using singular spectrum analysis (it will be discussed in chapter 5).

Singular value decomposition (SVD) of the bearing vibration signal is carried out under healthy and different fault conditions. The dominant singular values are selected based on the singular value plot. The method is tested with test data1 obtained for different bearing fault types, with increasing fault severity and at various load. The effect of load, fault size, sample points and noise are studied on the fault index. The advantages of the fault index are shown in comparison with the simple time domain techniques such as Difference histogram [Van wyk et al., 2009] and zero crossing [William, P. E., & Hoffman, 2011].

4.2 CALCULATION OF SINGULAR VALUE RATIO

Singular Spectrum Analysis (SSA) is used for the calculation of singular values and then the ratios of adjacent singular value's are obtained. SSA is a non-parametric time series analysis technique which decomposes the signal into an additive set of independent time series. The steps which are part of SSA [Golyandina et al., 2010] used for the calculation of singular value ratio are given as below:

Step1- Embedding

In this step, bearing vibration signal of N data point $F = (f_0, \dots, f_{N-1})$ is mapped into a sequence of multidimensional lagged vectors called as trajectory matrix. Let L be an integer (window length), 1< L< N and K lagged vectors (K=N-L+1) $X_i = (f_{i-1,\dots\dots}f_{i+L-2})^T$, where $1 \leq i \leq K$.

The obtained trajectory matrix X is shown below.

$$X = \begin{pmatrix} f_0 & f_1 & \cdots & \cdots & f_{K-1} \\ f_1 & f_2 & \cdots & \cdots & f_k \\ . & . & \cdots & \cdots & . \\ . & . & . & \cdots & . \\ f_{L-1} & f_{L-2} & \cdots & \cdots & f_{N-1} \end{pmatrix} \tag{4.1}$$

Step 2- Singular value decomposition (SVD)

In this step, SVD of the matrix X is obtained which decomposes it into a sum of mutually orthogonal, unit-rank elementary matrix. Let $S=XX^T$ be an L x L matrix. Let λ_1, λ_2,.. λ_d be the non-zero eigenvalues of S (d= L if no eigenvalue is zero) arranged in decreasing order, and U_1, $U_2 \ldots U_d$ be the corresponding eigenvectors. The vectors $V_j = X^T \frac{U_j}{\sqrt{\lambda_j}}$ for j=1,2,…d is constructed.

The SVD of $X = X_1 + X_2 + \cdots + X_d$ (4.2)

Where $X_j = \sqrt{\lambda_j} U_j V_j^T$

The obtained singular values (SV) are the square roots of the eigenvalue of matrix S. The plot of the SV is known as Singular Spectrum (SS) plot.

4.3 SINGULAR VALUE RATIO (SVR) BASED FAULT IDENTIFICATION

Test data1 (section 3.3.1) is used in this analysis. At the end of step(2) (Section 4.2), we get L number of SV's. The important factors to be considered are window length (L) and choice of SV to be used. They are discussed in the following sub-sections.

4.3.1 Selection of Window length

Different window lengths (L= 5, 10 and 15) were used for embedding the signal and the corresponding L number of SV's were obtained based on the procedure given in section 4.2. The SS plot of bearing vibration signal obtained in healthy and faulty conditions using the chosen L values are shown in figure 4.1.

The larger SV in the SS represent the large amplitude components in the decomposition and the low-amplitude components of the signal are represented by the smallest SV. The SV should be selected such that it value differs for all the bearing conditions. For L=5 (figure 4.1a), all the SV are found to separate the different bearing conditions. If these SV are used it would result in processing the whole signal. As seen from figures 4.1(b, c), for L=10 and L=15, many of the SV differ for all the bearing conditions. With an appropriate L value the fault feature of the signal would be extracted more clearly. As compared to L=15, L=10 has less number of dominant SV with respect to total L. The singular values from the cases L=5 and L=15 could be used, but it is required to use less number of SV representing the signal in spectral domain. Hence, window length of 10 is selected.

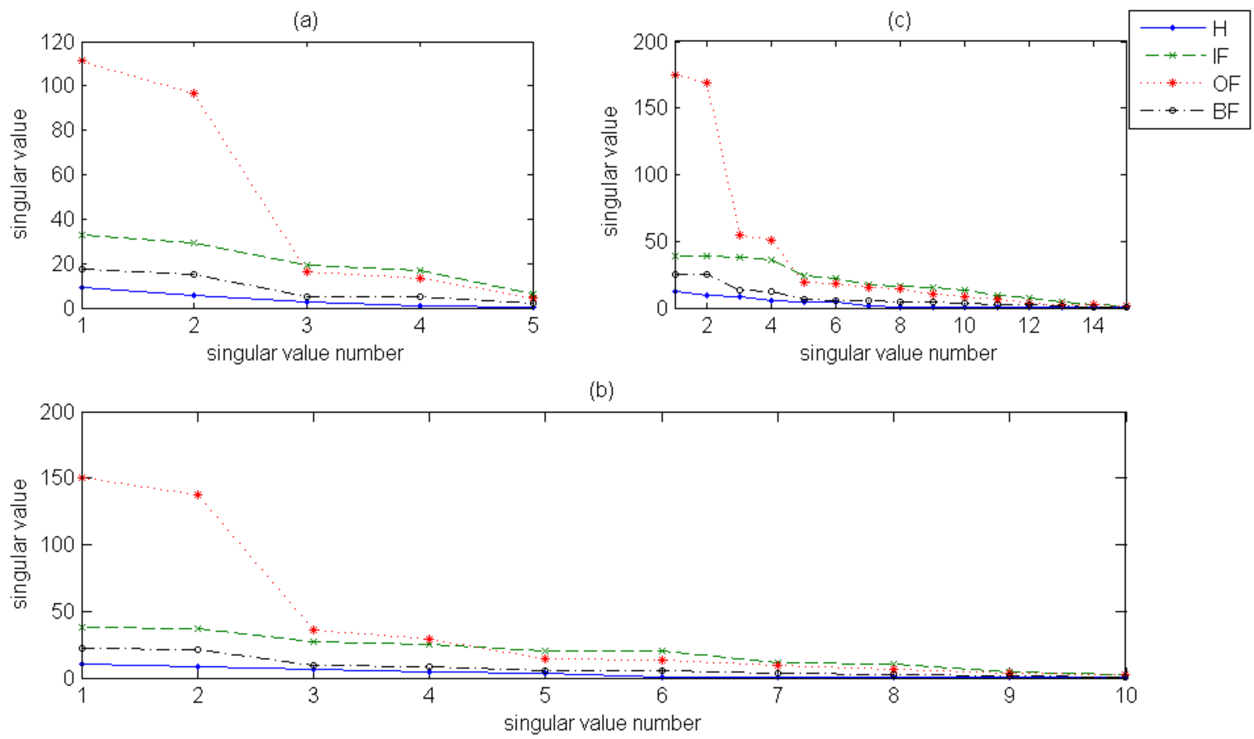

Figure 4.1 SS plot of bearing in healthy and faulty conditions (a) L=5 (b) L=10 and (c) L=15 [Fault size of 0.18mm, 1HP: Test data1]

4.3.2 Fault index and faulty bearing identification

The singular value ratio (SVR) is given by (equation 4.3)

$$SVij=SV_i/SV_j \tag{4.3}$$

Where i=1, 2…, L-1; j=i+1; SV_i is the i^{th} singular value and L is window length.

For L=10, there would be five SVR's (sv12, sv34, sv56, sv78 and sv910). Appropriate SVR for condition monitoring is to be selected among them. The selected SVR should clearly differentiate the healthy and faulty conditions i.e. it should have different range of values in healthy and faulty conditions. Figure 4.2 displays the pattern obtained for the different SVR's under healthy and faulty conditions. Bearing fault considered are inner race fault (IF), outer race fault (OF) and ball fault (BF). As seen from this figure, sv12 have similar range of values under faulty conditions. Also, there are no significant changes in the ratio for different fault sizes. Important observation is that, as the bearing becomes faulty, the ratio values diverges from the healthier ranges to a value and remain constant in that range. Similar trend is observed for sv56.

sv34 shows a constant trend for healthy and faulty condition which makes it difficult to ascertain the bearing health. sv78 in some cases shows similar range of values for healthy and faulty conditions. In most of the cases for sv910, it showed values in the range of healthy conditions for faulty conditions. Hence, sv34, sv78 and sv910 could not be used as fault index. So, sv12 and sv56 is selected. From the plots of sv12 and sv56 in figure 4.2, the bearing in faulty conditions is easily identified.

In Hankel matrix, the adjacent row vectors differ only by oe data. The trajectory matrix formed (equation 4.1) has similarity with a Hankel matrix construction. Thus, the adjacent row vectors of trajectory matrix X will be having high correlation. It is mentioned in [Carniel et al., 2006] that for sufficiently higher window lengths some of the SV tend to show some degree of coupling. It is observed that the adjacent singular values such as sv1 and sv2, sv5 and sv6 are correlated.

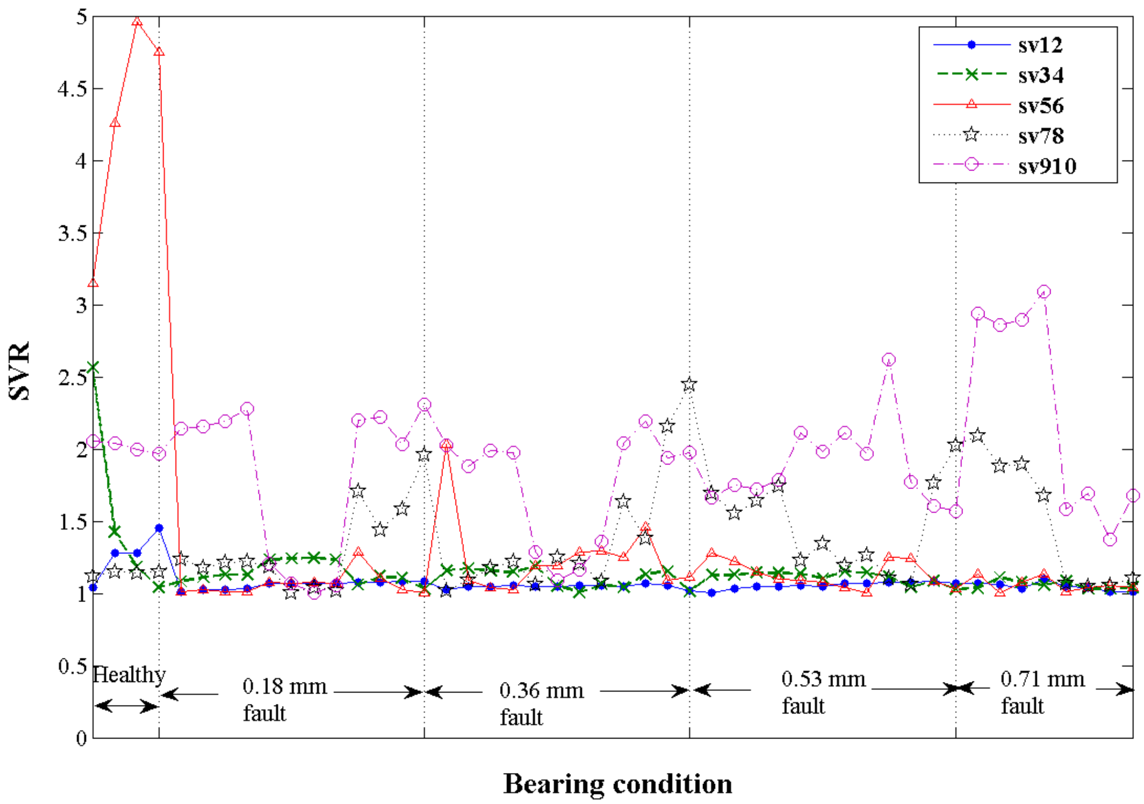

Figure 4.2 SVR values obtained for healthy and faulty conditions

To show that the singular values are in general correlated with each other, a simple sine wave signal (y=2sin8πt, sampling frequency is 100Hz) is considered. For varying window lengths (1 to 100), SV's (sv1 and sv2) are calculated and are plotted as shown in figure 4.3. As observed from this figure, sv1 and sv2 show coupling between each other.

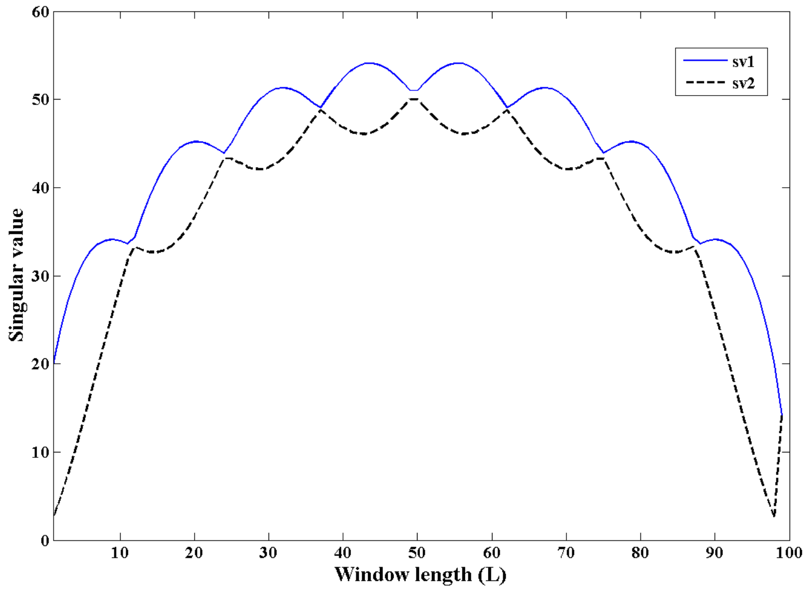

Figure 4.3 An illustration for correlation between SV's for the signal y=2sin(8πt)

4.4 ROBUSTNESS STUDY OF SVR

It is very important that the operating conditions such as load, external noise do not affect the fault index. Also, the effects of the fault size and sample size on the fault index are to be known. The following sub-sections studies the effect of above mentioned parameters on the fault index.

4.4.1 Effect of load on SVR

To study the effect of load on sv12 and sv56, the signals obtained for all the fault sizes, all fault types and 0 to 3 HP load are considered. Figures 4.4, 4.5 and 4.6 illustrates the variation of SVR with respect to changes in the load for IF, OF and BF respectively. It is observed that sv12 does not have much variation, while sv56 has little variation with respect to load. Also, sv56 has different variation for each type of fault. For some cases it increases with load and other cases it decreases with increase in load. The values obtained are well below the values obtained for healthy conditions and the faulty bearings could be still detected.

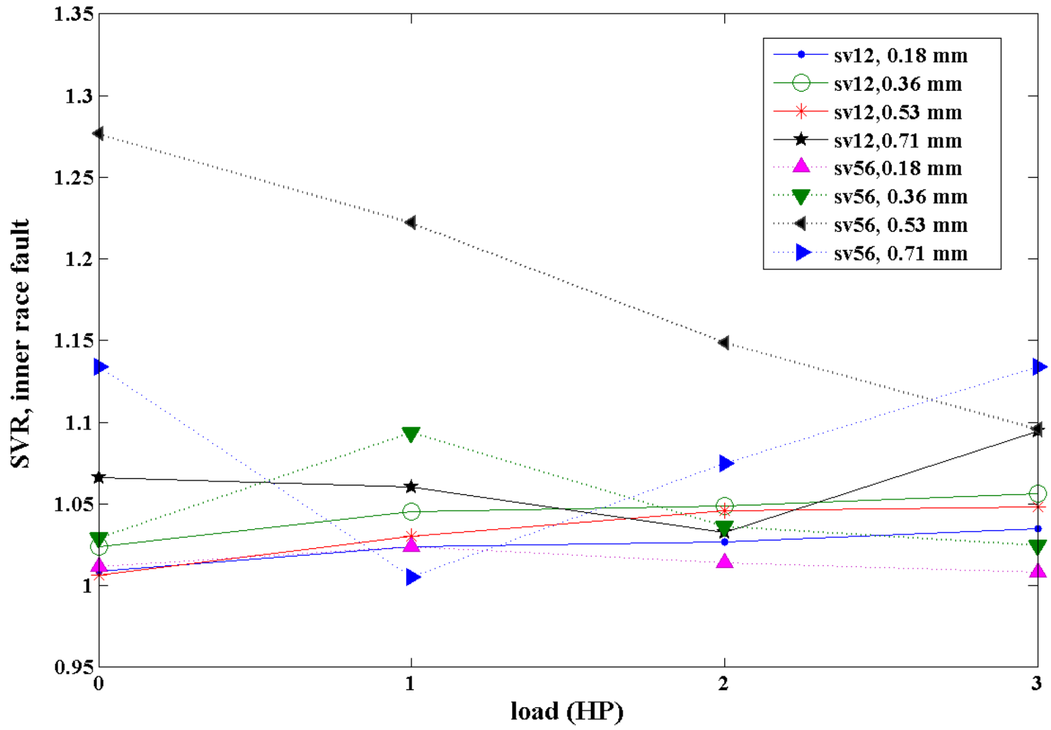

Figure 4.4 Effect of load on SVR for different fault sizes: IF

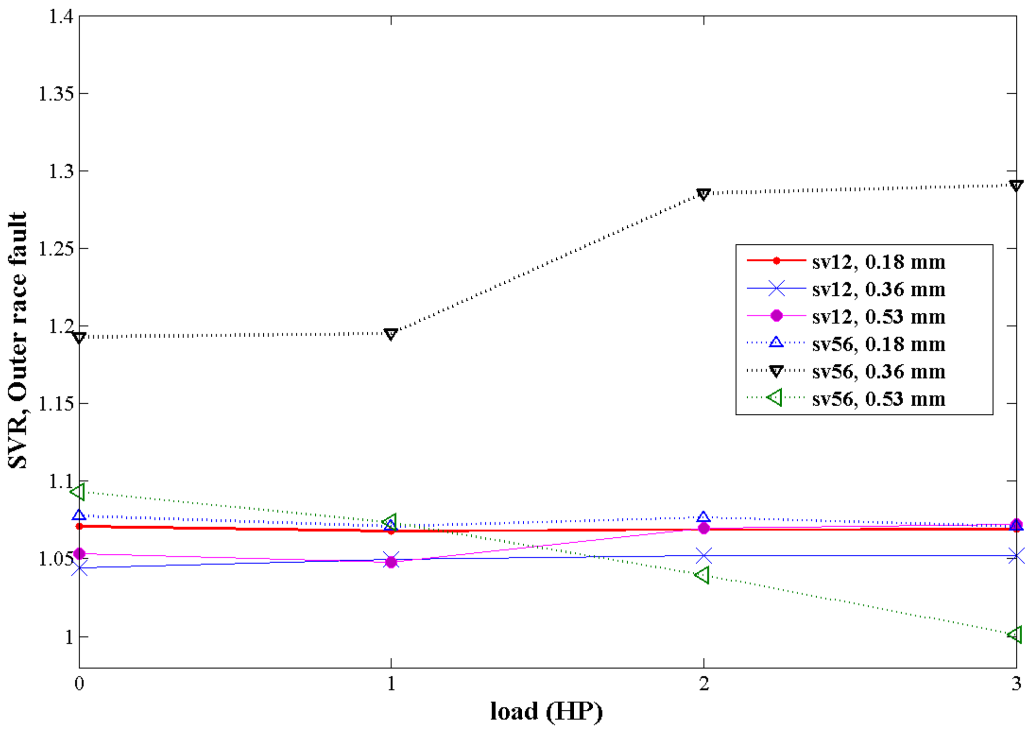

Figure 4.5 Effect of load on SVR for different fault sizes: OF

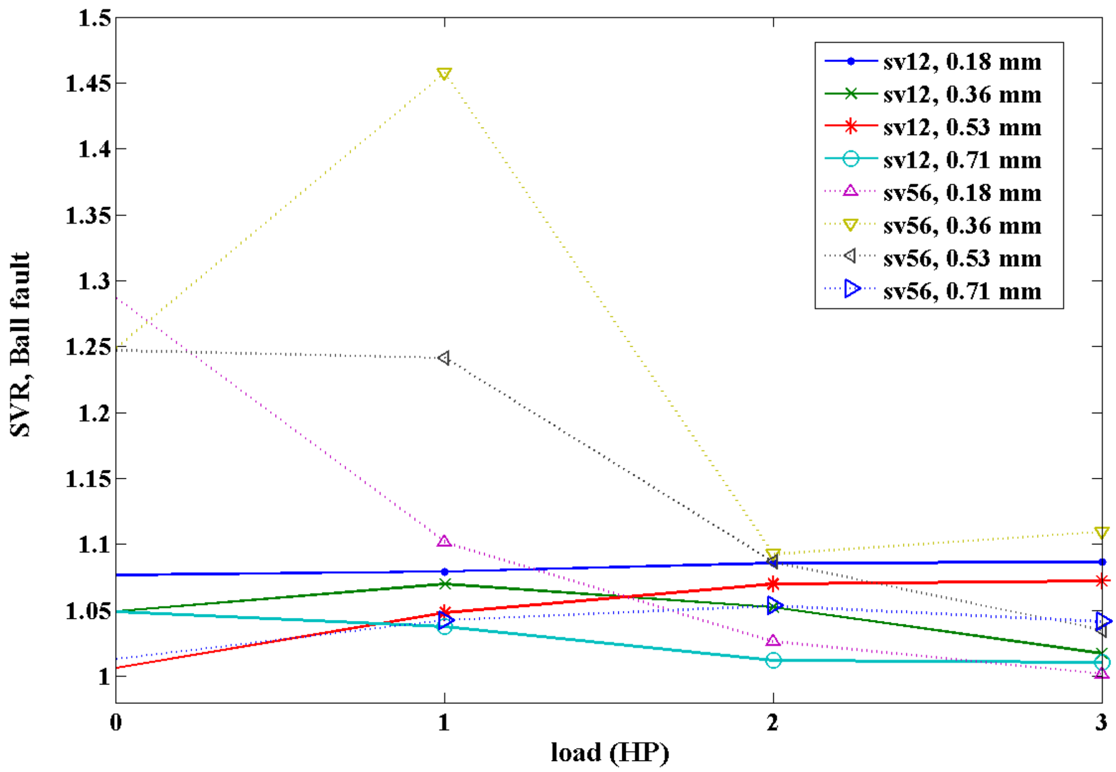

Figure 4.6 Effect of load on SVR for different fault sizes: BF

4.4.2 Effect of fault size on SVR

The signals considered for this study are: fault sizes of 0.18 mm, 0.36 mm, 0.53 mm and 0.71mm for IF, OF and BF; load varied from 0 to 3HP in all the cases. Figures 4.7, 4.8 and 4.9 display the variation of SVR with respect to the increasing fault sizes for IF, OF and BF respectively. Similar to the observation seen in the load effect study (section 4.4.1), sv12 does not vary much with the increase in fault severity, while sv56 has variation with respect to the fault size. sv56 increases for lower sizes and then decreases for higher fault sizes. The values found are well below the values of healthy conditions and one can detect the faulty bearings.

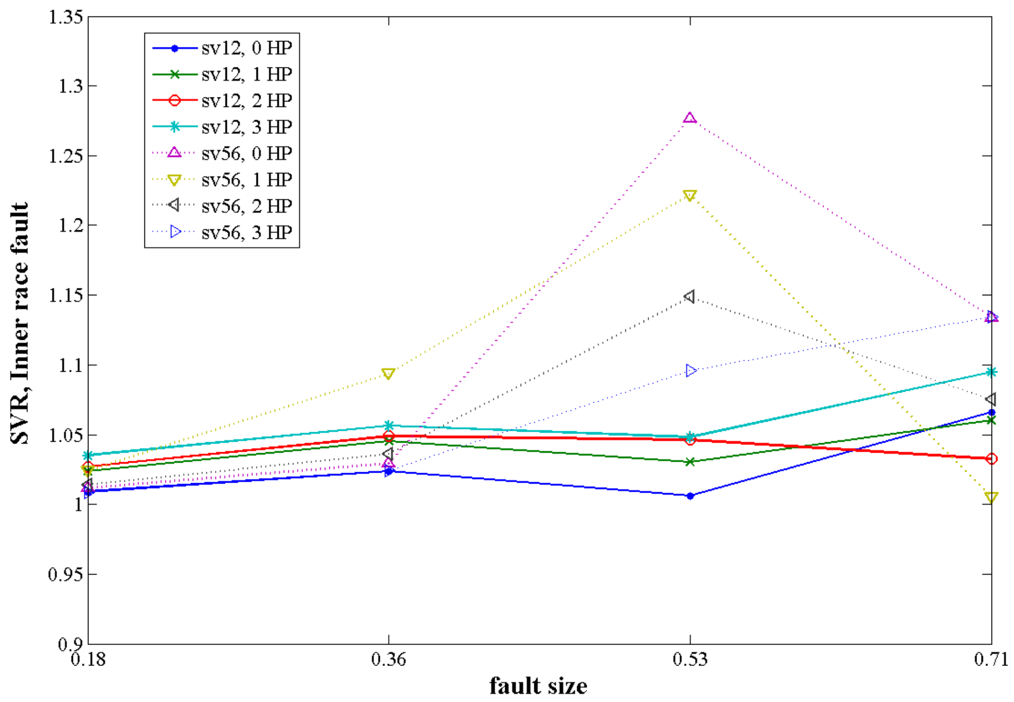

Figure 4.7 Effect of fault size on SVR for different loads: IF

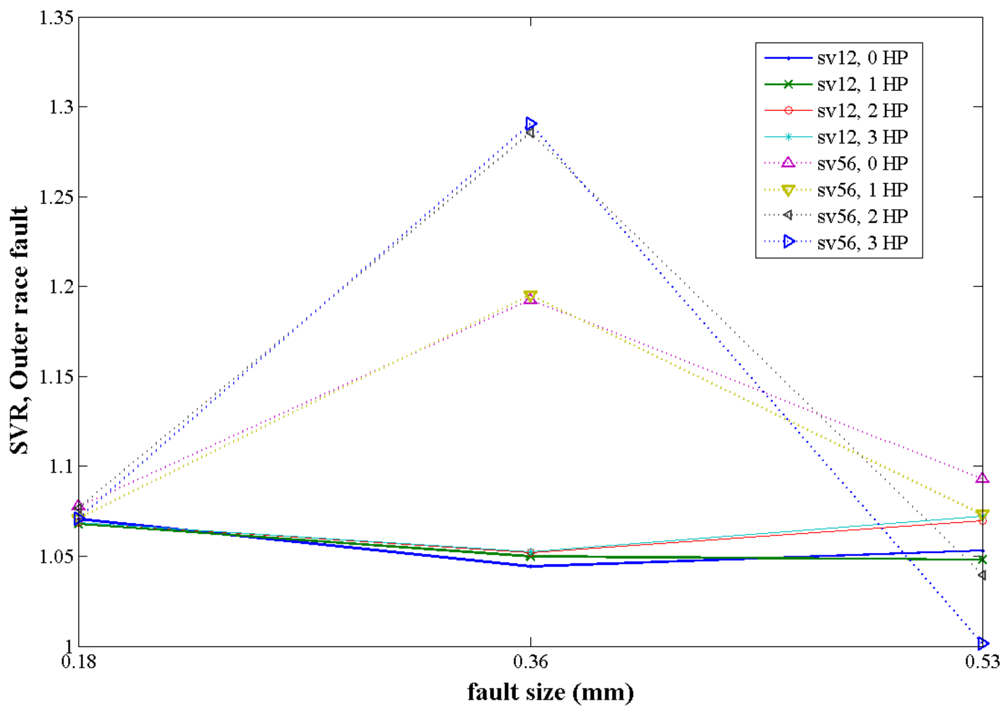

Figure 4.8 Effect of fault size on SVR for different loads: OF

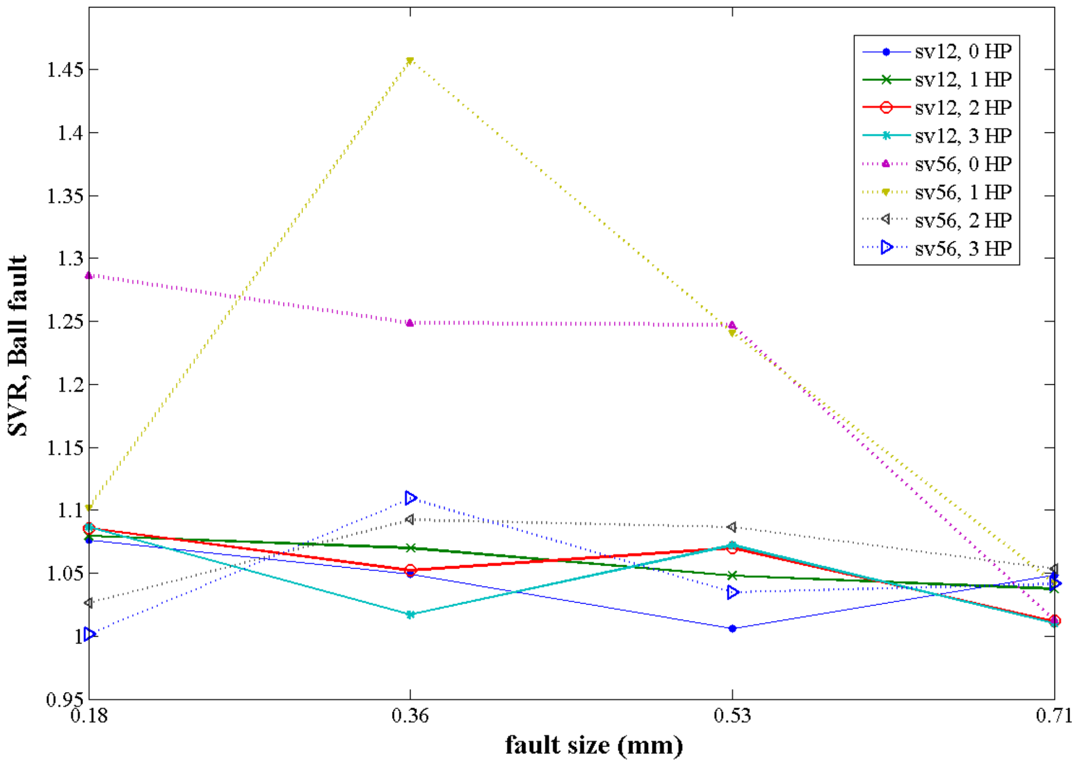

Figure 4.9 Effect of fault size on SVR for different loads: BF

4.4.3 Effect of sample size on SVR

To study the effect of the sample size (or points), vibration signals (healthy, IF, OF and BF) obtained for 0.18 mm fault size, 1 HP load are considered. The sample points are varied from 1000 to 6000. Figures 4.10 and 4.11 show the variation of sv12 and sv56 respectively with respect to the number of sample points. It is observed that sv12 and sv56 values have negligible variation with respect to sample points under different bearing conditions. Hence, the fault index is sample size invariant.

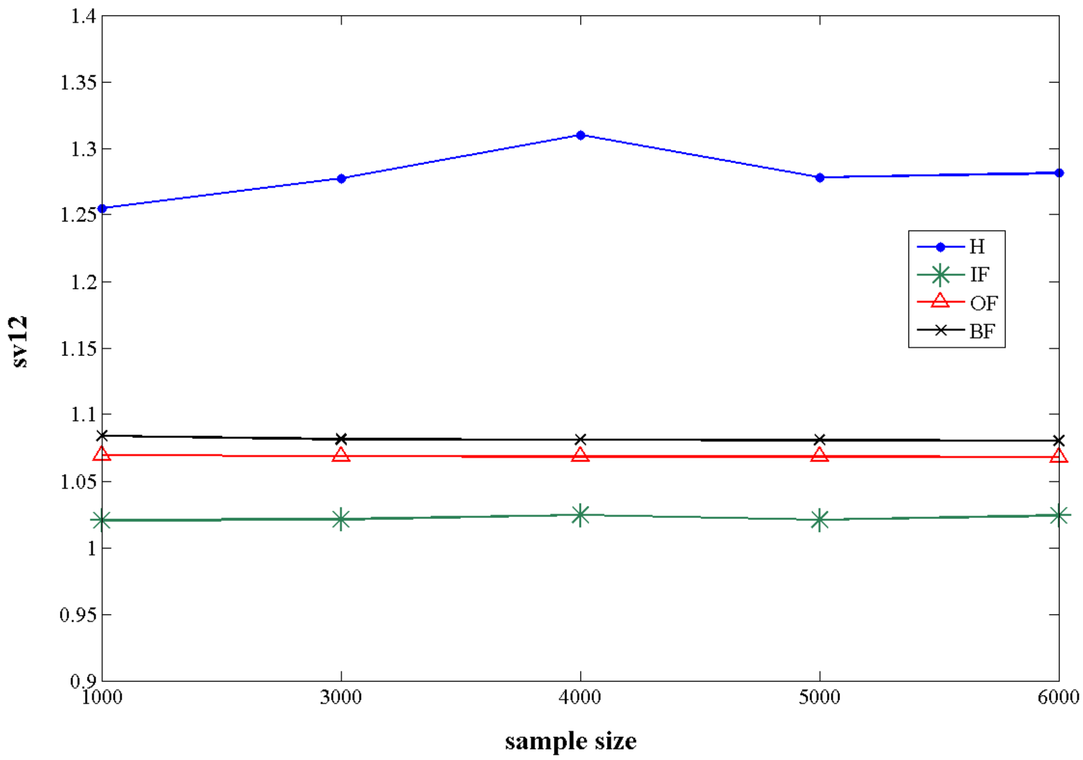

Figure 4.10 Effect of sample size variation on sv12 under different bearing conditions: 0.18mm fault size, 1 HP load

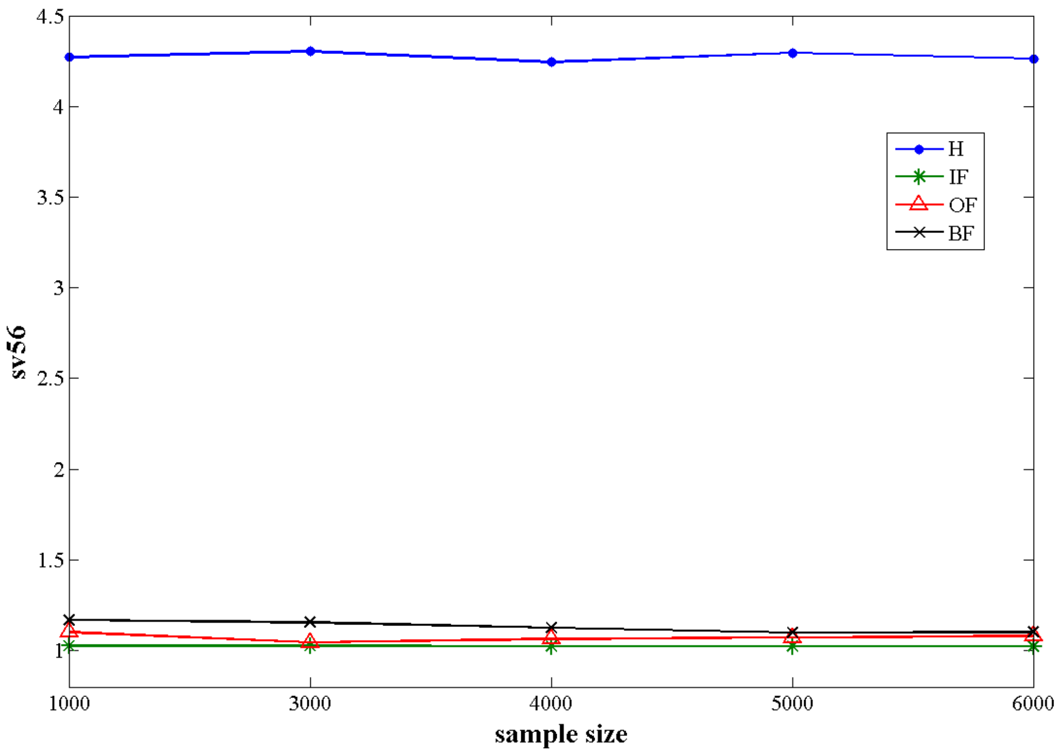

Figure 4.11 Effect of sample size variation on sv56 under different bearing conditions: 0.18mm fault size, 1 HP load

4.4.4 Effect of noise on SVR

To check the performance of the fault index in the presence of noise, all the signals obtained are virtually added with the white gaussian noise to obtained signals with SNR of +10 dB and -10 dB. Figures 4.12 and 4.13 illustrate the variation of sv12 and sv56 with respect to noise respectively. From figure 4.12, it is seen that sv12 values do not vary much for +10 dB case, but for -10 dB the values decreases as compared to pure signal (original data). Under healthy conditions, sv56 (Figure 4.13) decreases with increase in noise. In case of +10 dB, healthy and faulty bearing can be classified. For +10 dB, sv56 has values very close to those obtained under original data under faulty condition. But it is not possible in presence of -10 dB noise.

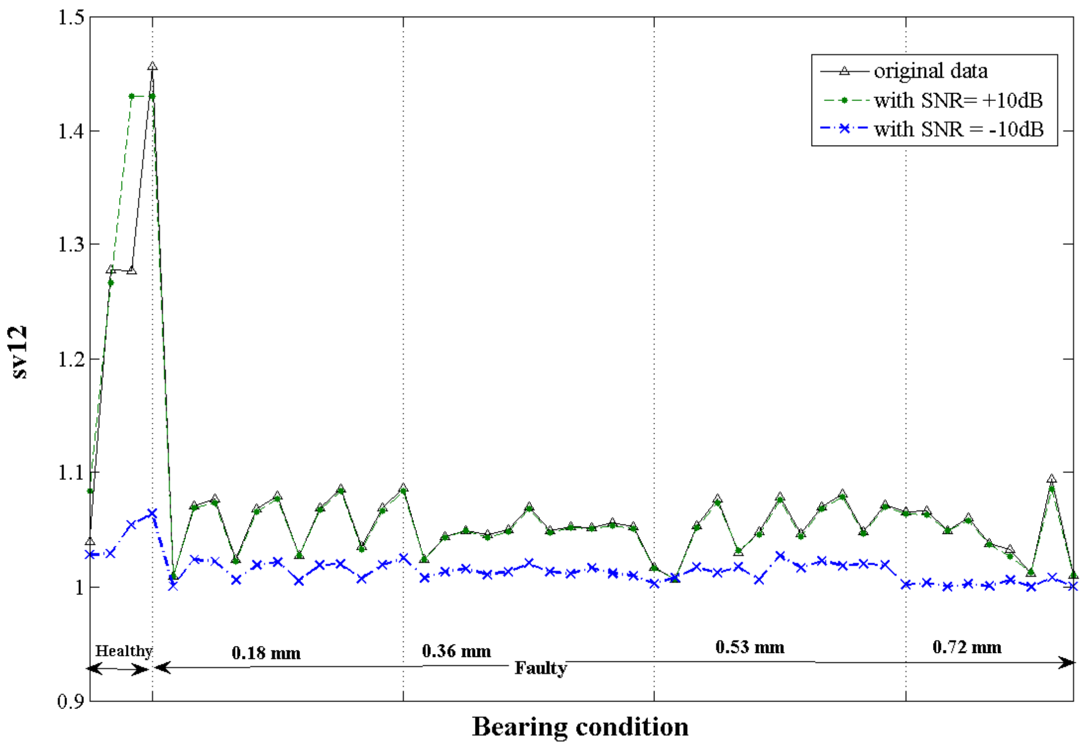

Figure 4.12 Effect of noise on sv12 under different bearing conditions

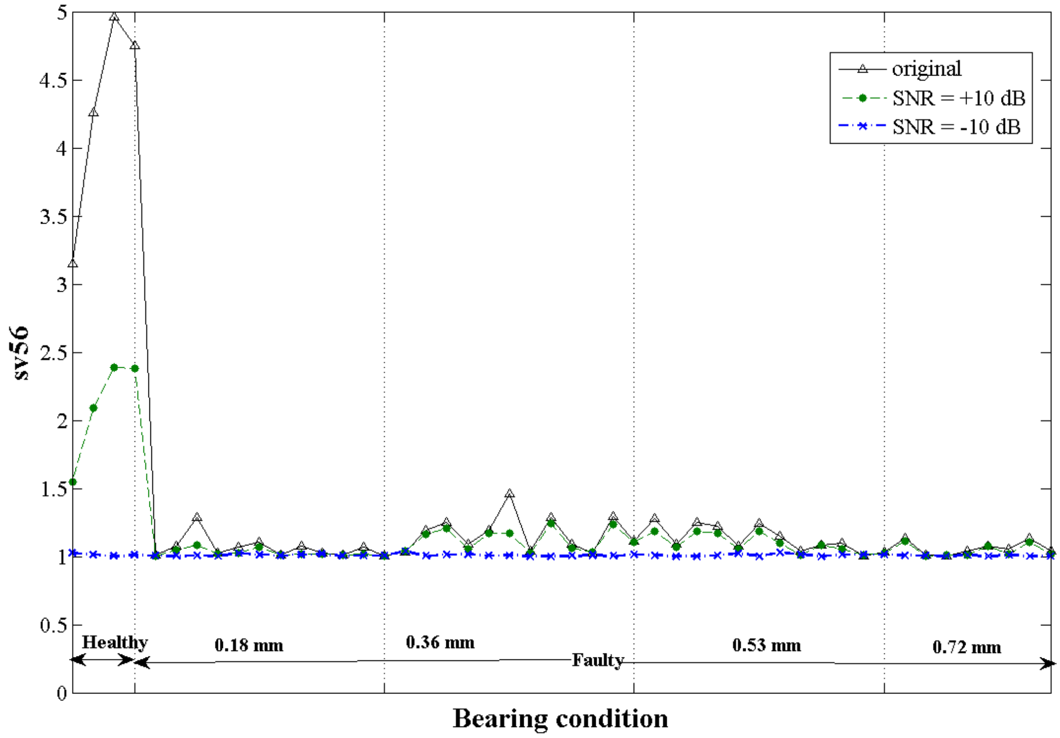

Figure 4.13 Effect of noise on sv56 under different bearing conditions

4.5 COMPARISON WITH SIMPLE TIME DOMAIN METHODS

The SVR index is compared with two simple time domain method index: Difference Histogram (DH) [Van wyk et al., 2009] and Zero crossing (ZC) interval [William, P. E., & Hoffman, 2011]. These two methods use the same test data1 as used for SVR.

In DH, histogram bin is used as fault feature and threshold value is chosen to differentiate the faulty bearings. Artificial Neural Network (ANN) is used for fault classification. Also, the size of the histogram has to be sufficiently large (N=30,000) for higher accuracy. In ZC method, ZC count and ZC duration are used as fault features. The feature calculation depend on the signal length which requires the knowledge of longest expected time duration between the successive zero crossing. ANN when trained only with higher defect size and tested for other defect sizes gave good classification.

DH is affected by sample size and the methodology used for calculating the zero crossing points can be affected by the noise. It is shown in section 4.4.3 that the fault index is sample size invariant and also works well even in presence of SNR of +10 dB (Section 4.4.4). From the above discussion, it is clear that SVR based method is superior to other simple methods. It has the added advantage of inherent noise reduction due to usage of the singular value decomposition.

4.6 SUMMARY

A time domain method using singular spectrum analysis for faulty bearing detection is discussed. It is shown that singular value ratio extracted from the time domain bearing vibration signals are useful in determination of faulty bearings. The ratio of the singular values is found to be having a constant value for faulty bearing and another range of values for healthy bearing. The fault index is not affected by sample size, load variations and the method work even in the presence of noise. But, the fault index does not show much variation with respect to fault size. Based on the comparison with the other simple time domain methods, it has advantages such as feature is sample size and load independent, method performs well for noisy signal.

PART III

FAULT DIAGNOSIS

CONTENTS:

CHAPTER 5

BEARING FAULT DIAGNOSIS USING SINGULAR SPECTRUM ANALYSIS

MAIN CONTENTS:

- **Introduction**
- **Singular Spectrum Analysis**
- **Singular Value and ANN based bearing fault diagnosis- 1st method**
- **Energy feature and ANN based bearing fault diagnosis - 2nd method**
- **Comparison with other methods**
- **Summary**

5.1 INTRODUCTION

Most of the existing time series methods for bearing fault diagnosis (section 2.7.2) involves complex algorithm and extracted features are affected by sample size and noise. Even though these methods are efficient, still need to identify a time domain approach which is useful for diagnosis with advantages such as noise immunity and sample size invariance.

In this chapter, a time domain approach based on singular spectrum analysis (SSA) is presented for bearing fault diagnosis. SSA is used for the decomposition of the acquired signals into an additive set of principal components. An approach for the selection of the principal components is also presented. Two methods of fault diagnosis based on SSA are implemented. In the first method, the Singular Values (SV) of the selected SV number are adopted as the fault features, and in the second method, the energy of the principal components corresponding to the selected SV numbers are used as features. An Artificial Neural Network (ANN) known as feed forward back propagation neural network is used for the fault classification. The algorithms are evaluated using two experimental datasets - one from a motor bearing subjected to different fault severity levels at various loads, with and without noise (test data1), and the other with bearing vibration data obtained in the presence of a gearbox (test data2). The effects of sample size, fault size and load on the fault features are studied. The advantages of the proposed method over the exiting time series method are discussed.

The block diagram of the singular spectrum analysis based roller bearing fault diagnosis is given in figure 5.1.

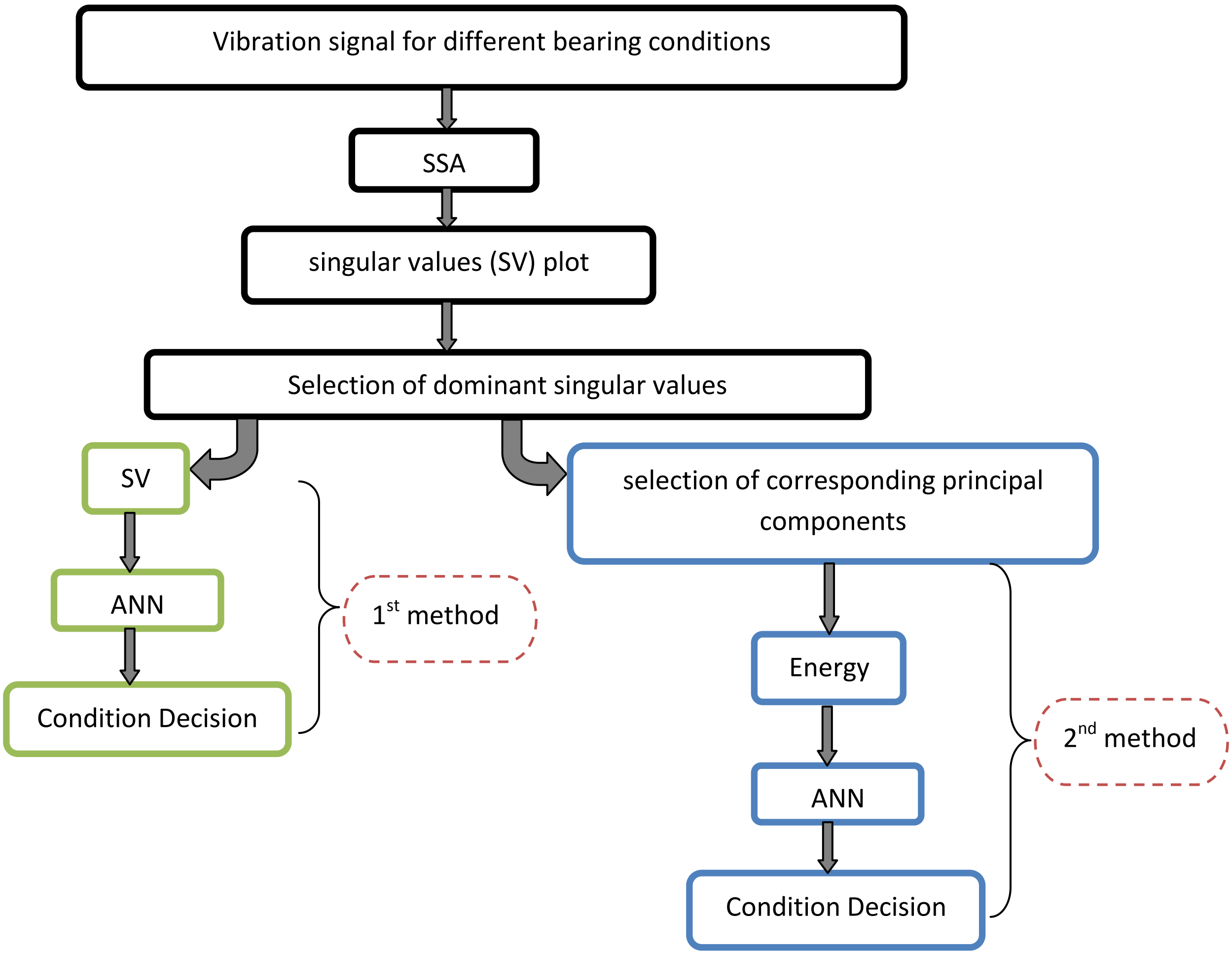

Figure 5.1 Block diagram of the roller bearing fault diagnosis method based on SSA

5.2 SINGULAR SPECTRUM ANALYSIS

SSA [Golyandina et al., 2010] is a time series analysis technique which decomposes the signal into an additive set of independent time series (principal components). The set of series resulting from the decomposition is interpreted as consisting of a trend representing the signal mean at each instant, a set of periodic series, and an aperiodic noise. SSA is applied to the vibration signals obtained under the various bearing conditions considered for the study.

The SSA algorithm is described as follows:

Step1- Embedding

In this step, the bearing vibration signal $F = (f_0, \ldots, f_{N-1})$ of N data points is mapped into a sequence of multidimensional lagged vectors. Let L be an integer (window length), $1 < L < N$ and K be the number of lagged vectors (K=N-L+1), $X_i = (f_{i-1, \ldots\ldots} f_{i+L-2})^T$, where $1 \leq i \leq K$.

The obtained trajectory matrix X is given as equation (5.1)

$$X = \begin{pmatrix} f_0 & f_1 & \cdots & \cdots & f_{K-1} \\ f_1 & f_2 & \cdots & \cdots & f_k \\ . & . & \cdots & \cdots & . \\ . & . & . & \cdots & . \\ f_{L-1} & f_{L-2} & \cdots & \cdots & f_{N-1} \end{pmatrix} \tag{5.1}$$

Step 2- Singular Value Decomposition (SVD)

In this step, the SVD of the matrix X is obtained. It is further decomposed into a sum of mutually orthogonal, unit-rank, elementary matrices. Let $S=XX^T$ be an L x L matrix. Let λ_1, λ_2,.. λ_d be the non-zero eigenvalues of S (d= L if no eigenvalue is zero) arranged in decreasing order, and U_1, $U_2 \ldots U_d$ be the corresponding eigenvectors. The vectors $V_j = X^T \frac{U_j}{\sqrt{\lambda_j}}$ for j=1,2,…d is constructed.

The SVD of $X = X_1 + X_2 + \cdots + X_d$ (5.2)

where, $X_j = \sqrt{\lambda_j} U_j \, V_j^T$

The obtained L numbers of SV's are the square roots of the eigenvalues of matrix S. The plot of the SV in decreasing order is known as Singular Spectrum (SS), and thus gives the method its name.

Step 3- Diagonal averaging

Each matrix obtained after the decomposition (equation (5.2)) is transformed into a new time series of length N by applying a linear transformation known as diagonal averaging. The matrices X_1, X_2… X_L gets converted to principal components C_1, C_2… C_L respectively. The diagonal averaging algorithm is as follows:

Let Y be a $L \times K$ matrix with elements y_{ij}, where i, j values range are $1 \leq i \leq L$ and $1 \leq j \leq K$ respectively. Diagonal averaging transforms the matrix Y into the series $g_0 \cdots g_{N-1}$ (principal component) by the formula:

$$g_k = \begin{cases} \frac{1}{k+1}\sum_{m=1}^{k+1} y_{m,k-m+2} & \text{for } 0 \leq k \leq L^* - 1 \\ \frac{1}{L^*}\sum_{m=1}^{L^*} y_{m,k-m+2} & \text{for } L^* - 1 \leq k \leq K^* \\ \frac{1}{N-k}\sum_{m=k-K^*+2}^{N-K^*+1} y_{m,k-m+2} & \text{for } K^* \leq k \leq N-1 \end{cases} \tag{5.3}$$

Where $L^* = \min(L, K)$, $K^* = \max(L, K)$

Two methods based on SSA and ANN are developed. The efficiency of the SSA for time series based bearing fault classification is illustrated using the two methods discussed in the following sections.

5.3 SINGULAR VALUE AND ANN BASED BEARING FAULT DIAGNOSIS - 1st METHOD

The singular values are the representation of the signal in the singular spectrum domain. At the end of step 2 of the SSA method (section 5.2), L number of SV's are obtained. These SV are plotted with respect to their number (SS plot). The SS plots for the different bearing conditions are compared and then the appropriate SV's are selected. They are adopted as an inputs to an ANN for the condition diagnosis. This method is tested with the vibration signals of test data1 (section 3.3.1) and test data2 (section 3.3.2), which are described in the subsequent sections.

5.3.1 TEST DATA1 ANALYSIS

5.3.1.1 Choice of window length

Different window lengths (L = 5, 10 and 15) were used for embedding the signal, and the corresponding L number of SV are obtained based on the procedure as given in section

5.2. The SS plots of the bearing vibration signal in healthy and faulty conditions for values of L are shown in figure 5.2.

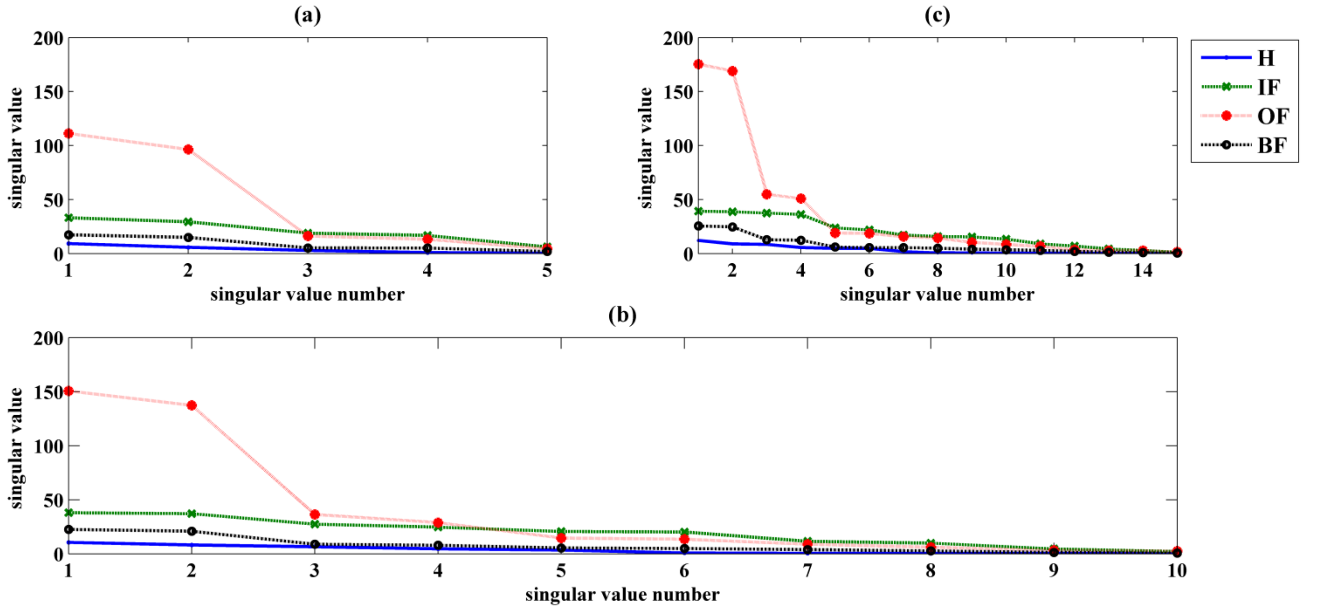

Figure 5.2 SS plot of bearing in healthy and faulty conditions (a) L=5; (b) L=10 and (c) L=15

The larger SV in the singular spectrum represent the large amplitude components in the decomposition, and the low-amplitude components of the signal are represented by the smaller SV. The SV should be selected such that they differ for all the bearing conditions. For L=5 (Figure 5.2(a)), all the SV are found to separate the different bearing conditions. If all these SV are used, it would result in processing the whole signal. As seen from figure 5.2(b) and figure 5.2(c), for L=10 and L=15, many of the SV differ for all the bearing conditions. With an appropriate L value the fault features of the signal would be extracted more clearly. As compared to L=15, L=10 requires fewer SV to be selected with respect to the total number available. We could also use the singular values obtained using L=5 or L=15, but fewer SV are used when L=10. Hence, a window length of 10 is selected.

5.3.1.2 Selection of singular values

SV selection criteria and method used : The selected SV should have distinct values for healthy, inner race fault, outer race fault and ball fault, so that not only the faulty condition is identified but also the type of fault is known (even for different combinations of load and fault sizes).Mostly, selection of the principal components obtained from the decomposition of SSA is based on either the first few eigenvalues or those components' eigenvalues which cover a predefined percentage of the variance of the total eigenvalues [Kilundu et al., 2011]. In this method, singular value plot is used for the selection of SV and the principal components.

To select the appropriate SV, the singular spectrum plots were obtained for four different fault sizes (0.18 mm, 0.36 mm, 0.53 mm and 0.71 mm) taken at 1HP load, under healthy and various types of faulty conditions, which is shown in figure 5.3.

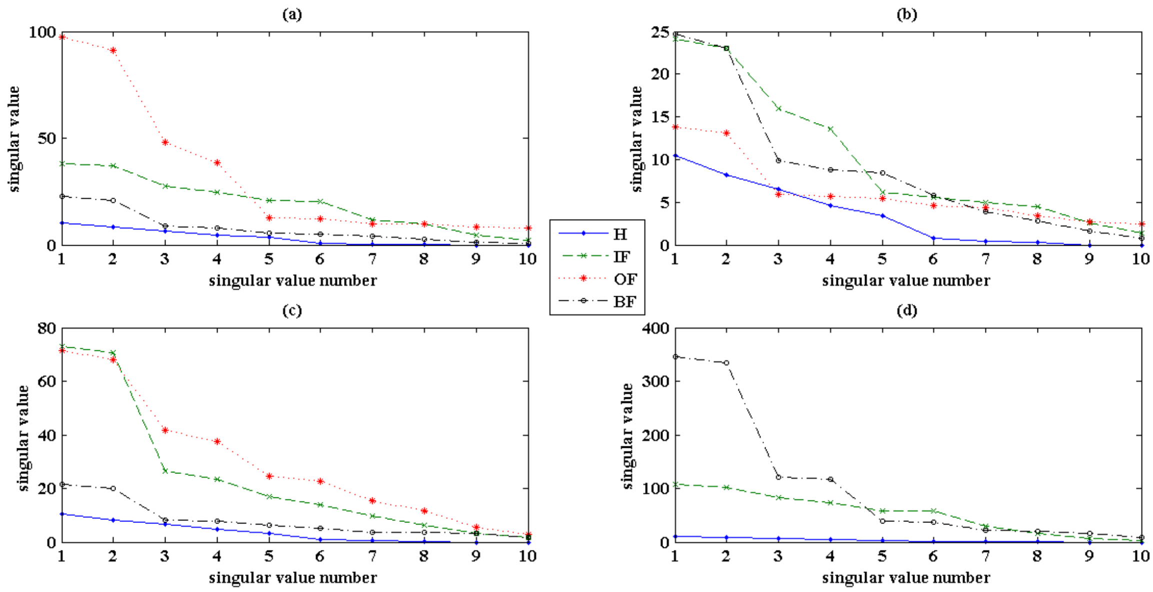

Figure 5.3 SS plot for L=10 obtained for bearing under different fault severity conditions, 1 HP load (a) 0.18 mm; (b) 0.36 mm; (c) 0.53 mm and(d) 0.71 mm

From figure 5.3, it is seen that there are many SV which differentiate the healthy and faulty conditions, i.e. these SV have distinguishable values with respect to each of the conditions. With reference to figure 5.3(a,c,d), SV1 to SV6 are able to classify the faults for 0.18 mm, 0.53 mm and 0.71 mm. However, for the 0.36 mm case (figure 5.3(b)), SV1, 2, 5 and 6 are found to classify the faults. Only, those SV which satisfy the criteria are selected. Hence, SV1, SV2, SV5 and SV6 are selected for fault classification. The selected SV are further verified, by considering the vibration signal obtained for no-load, 2 HP and 3 HP. It was found that the selected SV have different values for healthy and faulty conditions under different loads which make them suitable for the fault classification. The effects of SV1, SV2, SV5 and SV6 under varying load and fault sizes are studied in section 5.3.1.4. The pattern of the SV remains constant for varying load and fault sizes.

It is seen that SV1, SV2, SV5 and SV6 are able to classify faults even under different load and fault size conditions. Hence, they are selected.

The SS plot follows the same trend found in the power spectral density plot, as shown in figure 5.11. Hence, it is possible to use the singular spectrum to detect changes in the signal, as it represents the frequency spectrum of the signal [Alonso & Salgado, 2008]. This correspondence between the singular spectrum and the frequency spectrum is the basis of the processing technique [Alonso & Salgado, 2008], which is shown in section 5.3.3.

SV are normalized using the min-max normalization technique. These are then used as an input to an ANN. Based on the output of the ANN, bearing condition is identified as healthy or faulty, including its type.

5.3.1.3 ANN performance results using test data1

The ANN used is a feed-forward back propagation neural network (BPNN) with a single hidden layer architecture. There are four nodes in the input layer each representing the SV. There are four nodes in the output layer. The output pattern of the nodes depends on the bearing condition: healthy (H) [1 -1 -1 -1], inner race fault (IF)[-1 1 -1 -1], outer race fault (OF)[-1 -1 1 -1] and ball fault (BF) [-1 -1 -1 1]. The BPNN is created, trained and implemented using the MATLAB neural network toolbox. A total of 480 datasets of 4 normalized features (1^{st}, 2^{nd}, 5^{th} and 6^{th} SV) are obtained for the different bearing conditions, out of which 336 are used to train the network and the remaining are used to test the network. Normalization is done using min-max method in the range of [0-1]. BPNN training parameters used were: mean square error of 10^{-10}, minimum gradient of 10^{-10} and maximum iteration number (epoch) of 1000. The training process would terminate if any of the above conditions are met. Log sigmoid and tan sigmoid activation functions are used for the hidden and outer layers respectively.

The test data1 has no masking vibration source elements such as gear vibration. Hence, gaussian white noise was added using matlab function (awgn) such that noisy signals of SNR +10 dB and -10 dB are obtained for the each recorded vibration signal respectively. SV values are obtained for three cases- original data, noisy data of +10 dB SNR and noisy data of -10 dB SNR. Table 5.1 shows the BPNN overall classification accuracy. As observed from table 5.1, even in the presence of noise high classification accuracy is obtained.

Table 5.1 BPNN performance for test data1-1st method

Signal	Hidden Neuron	Classification accuracy (%)
Test data1	13	96.53
Noisy test data1 of SNR +10dB	13	98.61
Noisy test data1 of SNR -10dB	13	100

The reason for the better accuracy even under noisy condition is explained: The performance of the fault diagnosis method is highly dependent on two factors: First, how well the fault features contain information about the different fault conditions; Second, the ability of the classifier to accurately differentiate the different types of faults with respect to the input fault features. The selected singular values have distinct values for each type of bearing condition, i.e. each condition has a specific value of singular value, which makes the different conditions easily separable. Thus, they have good information about each type of condition. Even for the noisy signal, SV 1, 2, 5 and 6 has distinguishable values for each of the four conditions. The ANN is trained and tested using the k-fold cross validation technique (k=10) which gives much less chance of over training. It is the combination of the distinct SV (even under noisy conditions) and the good generalization capability of the ANN that contribute to the accurate classification of the bearing conditions even under noisy conditions.

Tables 5.2, 5.3 and 5.4 give the confusion matrix of the BPNN obtained in each case. The diagonal elements give the number of datasets correctly classified and the non diagonal elements give the misclassifications. As seen from the confusion matrices, the method gives a very high detection rate for each condition.

Table 5.2 Confusion matrix for test data1-1st method

	H	**IF**	**OF**	**BF**
H	12	0	0	0
IF	0	48	0	0
OF	0	0	35	1
BF	0	1	3	44

Table 5.3 Confusion matrix for noisy test data1 of SNR = +10 dB: 1st method

	H	IF	OF	BF
H	12	0	0	0
IF	0	47	0	1
OF	0	0	35	1
BF	0	0	0	48

Table 5.4 Confusion matrix for noisy test data1 of SNR = -10 dB:1st method

	H	IF	OF	BF
H	12	0	0	0
IF	0	48	0	0
OF	0	0	36	0
BF	0	0	0	48

5.3.1.4 Effect of load and fault size on SV

To study how the SV are affected with respect to the changes in load and with the increase in fault severity, the vibration signals from bearings with fault sizes of 0.18 mm, 0.53mm and 0.71 mm recorded at no-load and 3HP load are considered. Figures 5.4, 5.5 and 5.6 show the variation of the SV with respect to load and fault size for the inner race fault, ball fault and outer race fault respectively.

In case of inner race fault (figure 5.4), with the increase in fault severity, the SV increases; but the SV decreases with an increase in load. For the ball fault (figure 5.5), all the SV increase with increase in fault size, while for increase in load, SV1 and SV2 increase and SV5 and SV6 decrease. With an increase in outer race fault size (figure 5.6), SV1 and SV2 decrease while SV5 and SV6 increase. However, for an increase in load, SV1 and SV2 increase while SV5 and SV6 decrease. It is seen that the effect depends on the location of the fault. However, the profiles of all the SV remain same for a change in load. It is seen that the ratios SV1/SV2 and SV5/SV6 both have a constant value of 1 for all faulty conditions, while for healthy conditions, (SV1/SV2) is > 1, (SV5/SV6) is > 3. The concept of using the ratio of singular value for the fault detection emerged during this study (Chapter 4). Thus, the selected SV are able to classify different load and fault sizes. The fault size effect is more pronounced compared to that of load.

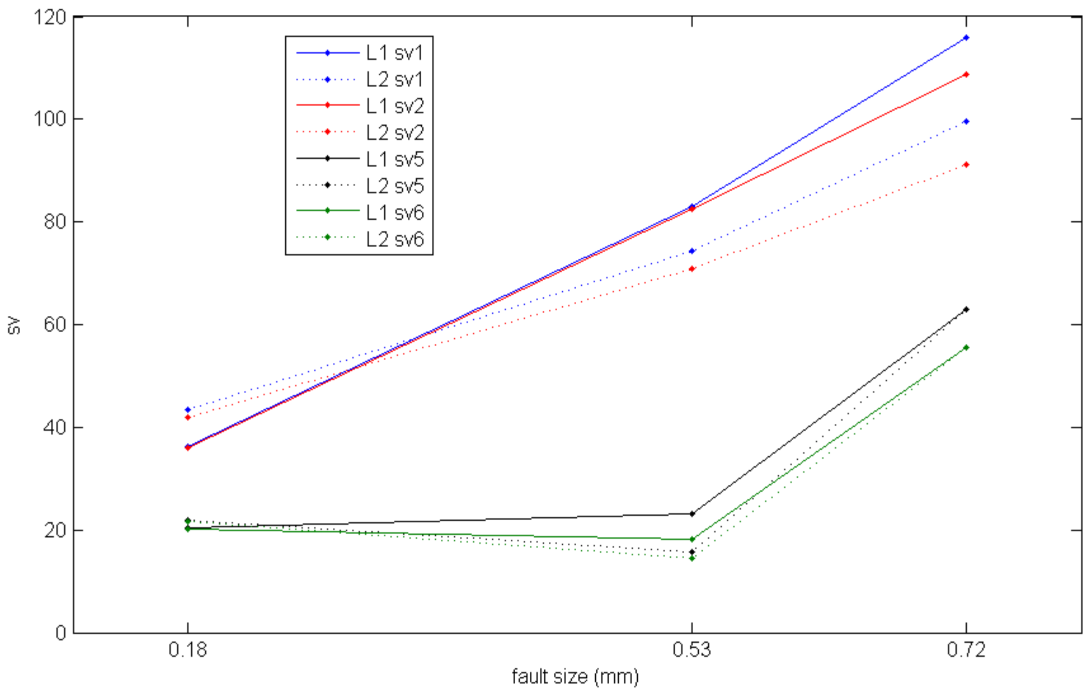

Figure 5.4 Effect of load and fault size on SV- inner race fault (L1= 0HP and L2=3HP load)

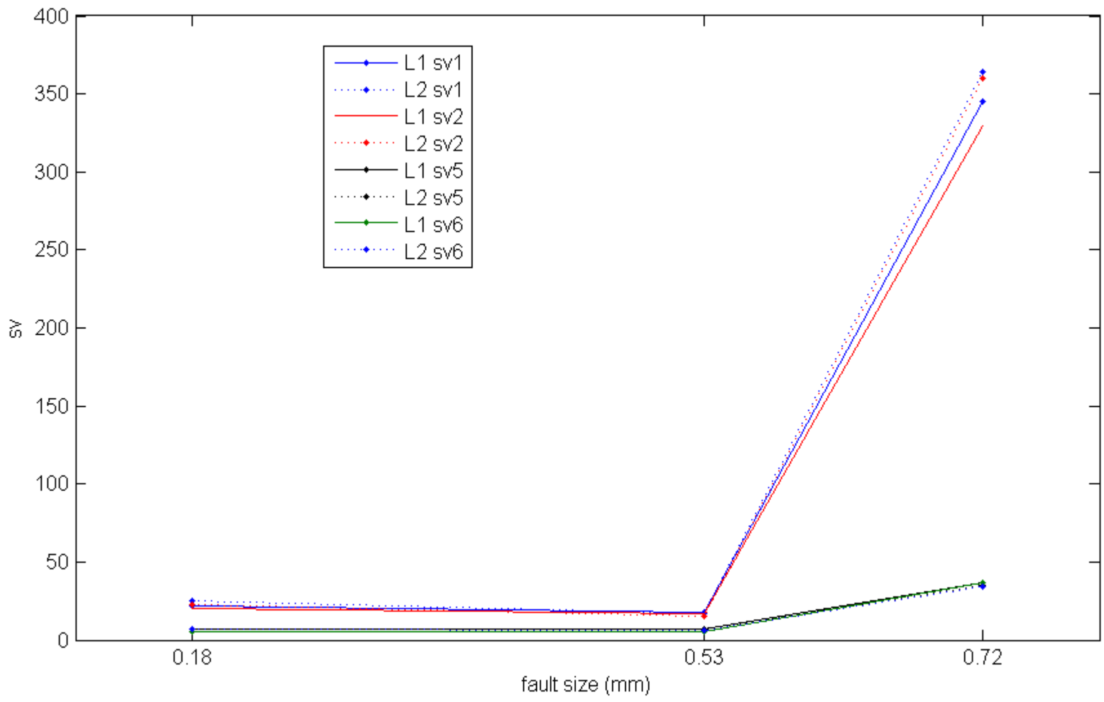

Figure 5.5 Effect of load and fault size on SV- ball fault (L1= 0HP and L2=3HP load)

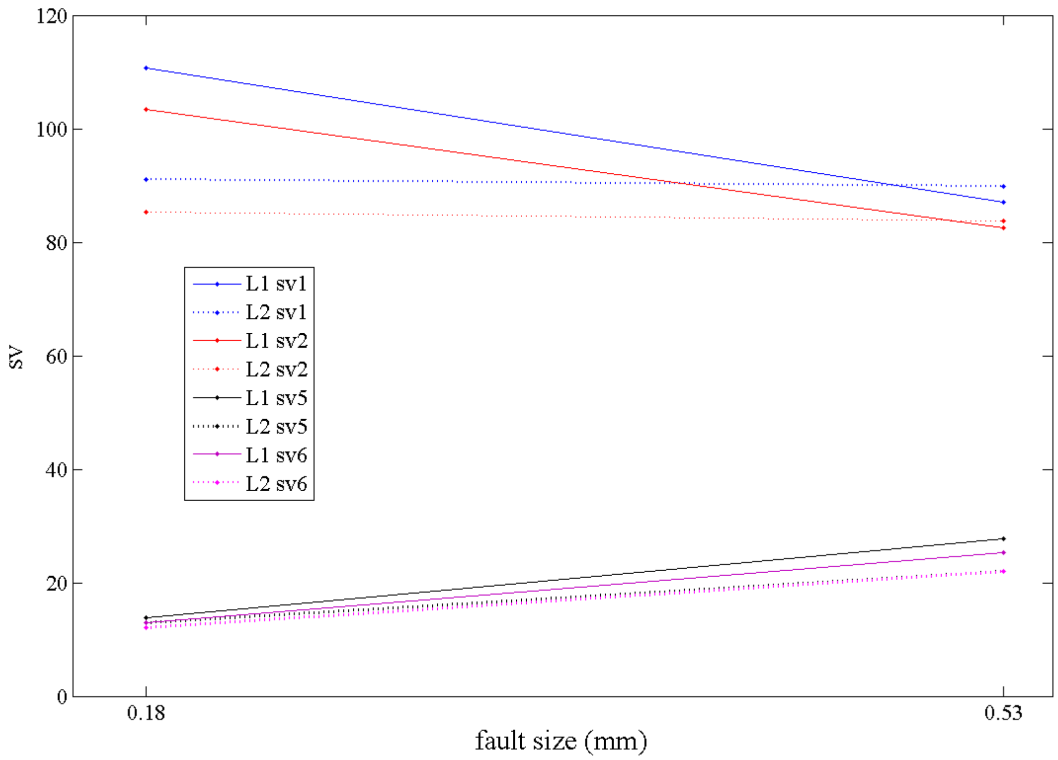

Figure 5.6 Effect of load and fault size on SV- Outer race fault (L1= 0HP and L2=3HP load)

5.3.1.5 Effect of sample size on SV

To investigate the effect of sample size on the SV, testdata1 obtained for 0.18 mm fault size taken at 1 HP load is considered. The SV values are obtained for sample sizes of 500, 1000, 2000 and 4000. Figure 5.7 shows the variation in the SV with respect to the sample size for healthy and faulty cases. As seen from this figure, as sample size increases, the SV also increase. However, it is found that the ratios (SV1/SV2) and (SV5/SV6) have a constant value of 1 for all faulty conditions, while for healthy conditions the ratio (SV1/SV2) > 1 and (SV5/SV6) > 4. This shows that the trend of the SV for healthy and faulty cases follow the same pattern for different sample sizes. The selected SV have distinct values for each condition even under sample size variation and this easily separates the healthy and different fault conditions. This shows that fault diagnosis can be done accurately and sample size variation has little affect on the classification accuracy.

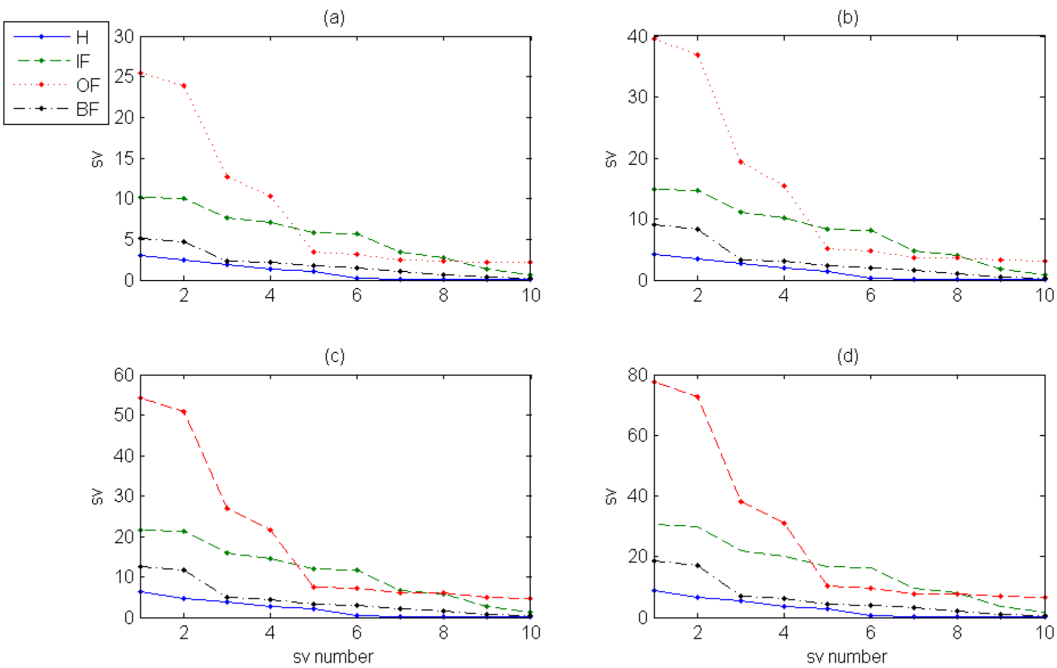

Figure 5.7 Effect of sample size (data points) on SV (a) 500; (b) 1000; (c) 2000 and (d) 4000

5.3.2 TEST DATA2 ANALYSIS

In the test data1 setup (section 3.3.1), there was no masking vibration source such as gearbox vibration. To study the method in the presence of a gearbox, signals obtained from the experimental setup of test data2 (section 3.3.2) are used. The procedure followed is similar to that of the test data1 analysis.

5.3.2.1 Selection of singular values and window length - test data2

Similar to test data1, different window lengths were used. Figures 5.8, 5.9 and 5.10 show the SS plots obtained for test data2 using L = 5, 10 and 15 respectively. As observed from the figures 5.8 and 5.10, healthy SV coincide with SV of the outer race fault. Also, SV of the inner race fault and ball fault have similar values. Hence, different bearing condition could not be easily separated using SV’s for L=5 (figure 5.8) and L=15 (figure 5.10).

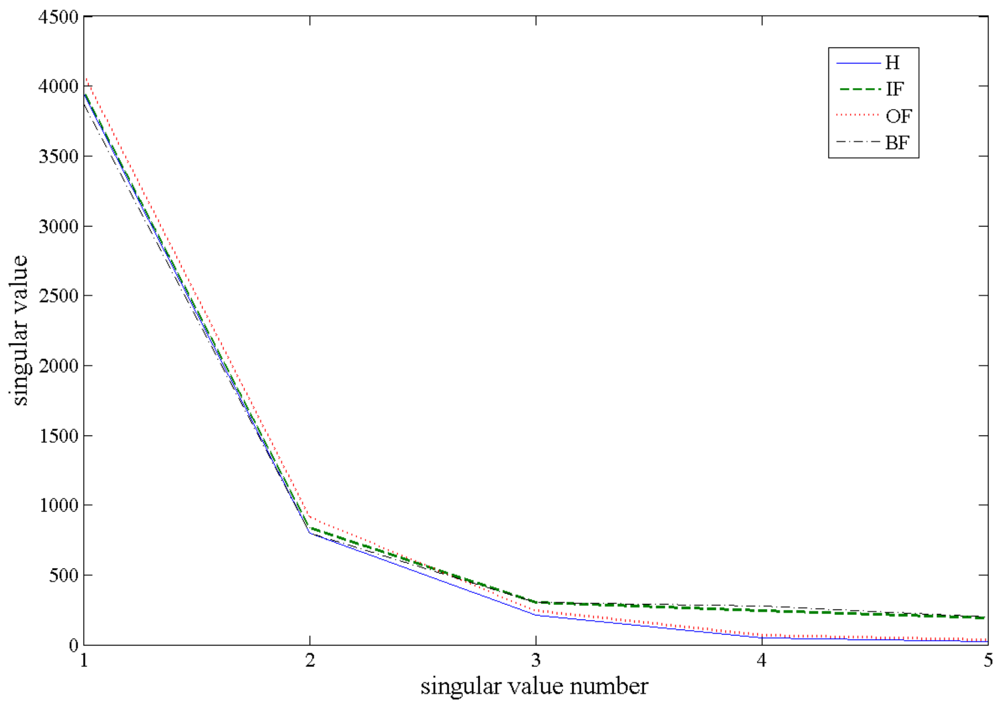

Figure 5.8 SS plot of test data2 for L=5

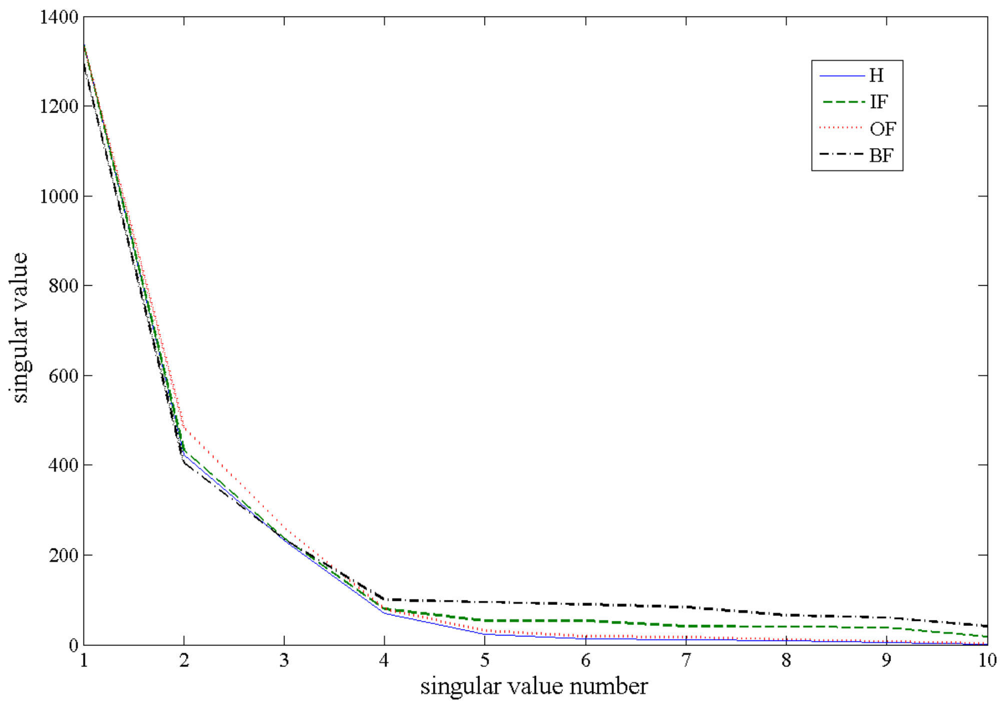

Figure 5.9 SS plot of test data2 for L=10

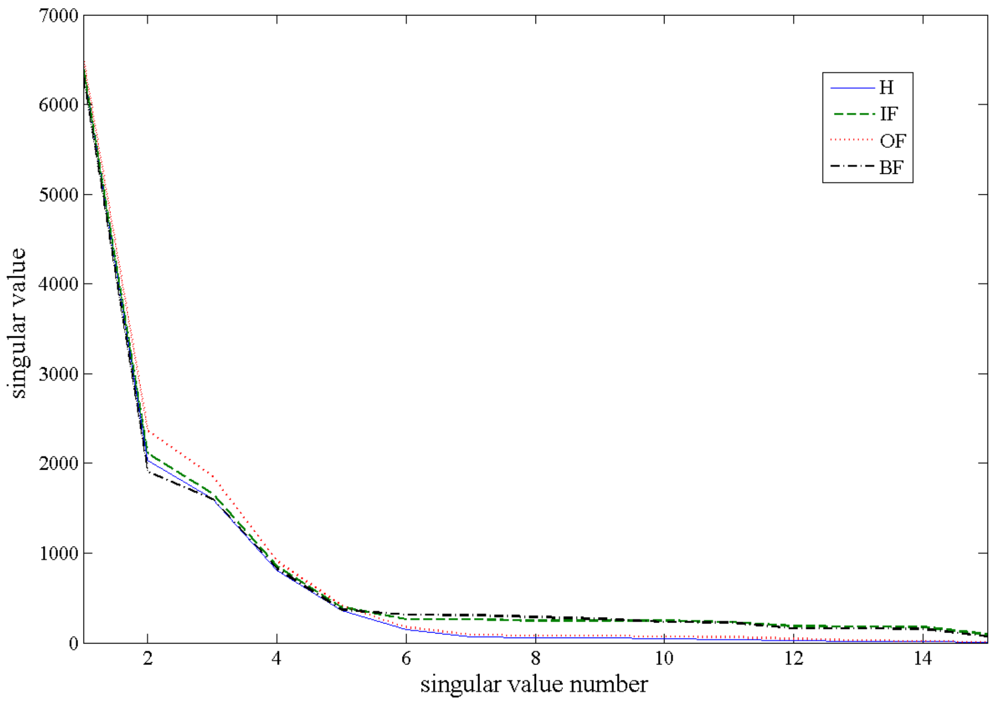

Figure 5.10 SS plot of test data2 for L=15

In the case of L=10 (Figure 5.9), the SV of healthy and outer race fault have close values, while for the inner race fault and ball fault the SV are separated, which is not observed in case of L=5 (Figure 5.8) and L=15 (Figure 5.10) plots. Hence, L=10 is used as the optimal window length for fault diagnosis. It is seen that SV number 5, 6 and 7 are sufficient to separate the different bearing conditions under study. The SV's of healthy and outer race fault, inner race fault and ball fault have close values which is consistent with the power spectra density plot shown in figure 5.12.

As shown in the analysis of test data2, the first few singular values are the same for healthy and faulty conditions (due to the presence of the gearbox) and hence the choice of these components would lead to a wrong diagnosis. Also, the choice of the amount of variance required is unknown and in the case of gearbox the amount of variance may include the masked eigenvalues.

5.3.2.2 ANN performance results using test data2

The ANN used for test data2 is same as that of the test data1 analysis (section 5.3.1.3) except that the network uses 3 inputs and 17 hidden neurons. 48 sets of 3 SV's (SV number 5, 6 and 7) are obtained for each bearing condition. The SV values are normalized (min–max normalization) in [0-1] range. 33 sets of input SV's in each condition were used for training the ANN and rest for testing. The overall classification accuracy of the BPNN obtained is 93.33%. The confusion matrix obtained for BPNN is shown in table 5.5.

Table 5.5 Confusion matrix for test data2-1st method

	H	**IF**	**OF**	**BF**
H	13	0	0	2
IF	0	15	0	0
OF	0	0	15	2
BF	0	2	0	13

5.3.3 COMPARISON BETWEEN POWER SPECTRUM AND SINGULAR SPECTRUM

The Power Spectral Density (PSD) is calculated based on welch method using the hanning window [Sawalhi & Randall, 2008] of length 512 samples. Figures 5.11 and 5.12 give the PSD plots obtained for test data1 and test data2 respectively. For test data1(figure 5.11), in the lower frequency range (up to 2200 Hz), the power spectra has very minute masking due to the motor and dynamometer, and at a few places, the PSD's intersect for healthy and faulty cases. In the region from 2200 Hz to 4000 Hz (figure 5.11), there is a large increase in the level of power spectral magnitude due to the presence of defect.

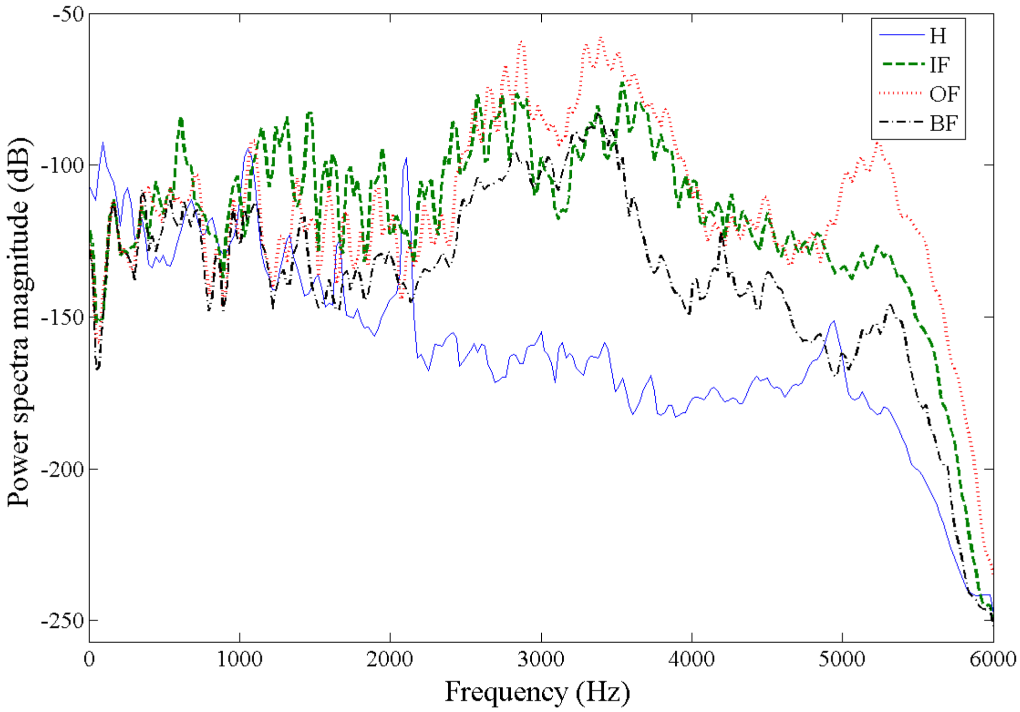

Figure 5.11 PSD of test data1 (0.18 mm fault size, 1HP load)

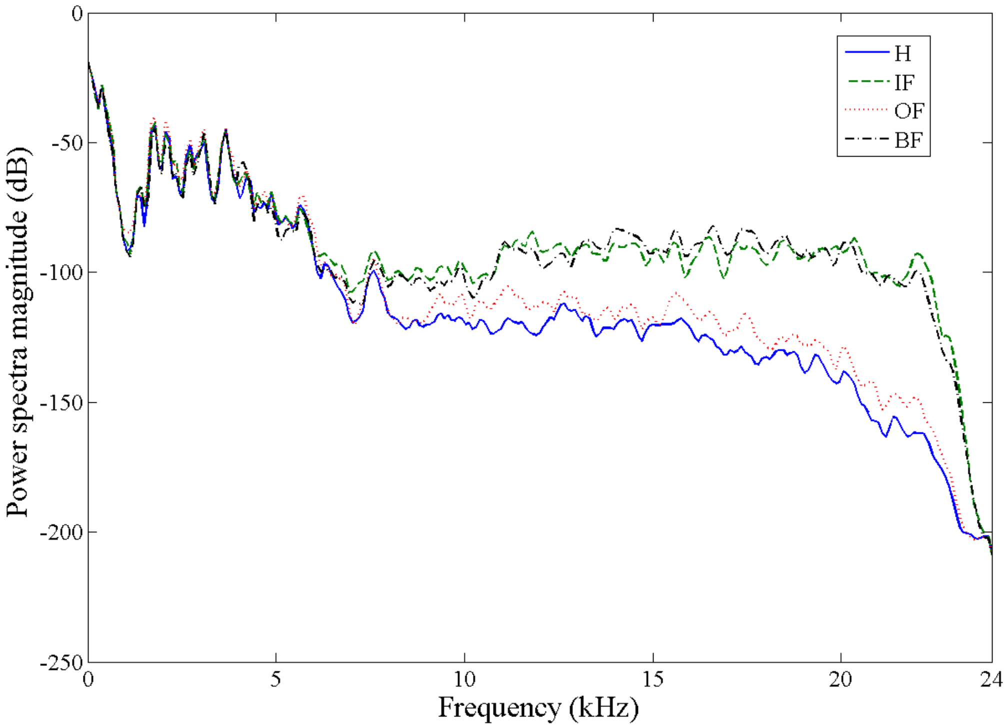

Figure 5.12 PSD of test data2

For test data2 (figure 5.12), it is seen that up to 8 kHz, there is no change in the power spectra for the healthy and fault cases. It is known that a large part of the frequency region is masked by the gearbox vibration [Sawalhi & Randall, 2008]. Only above 10 kHz, the healthy power spectra start to separate from the faulty ones. Similar to figure 5.11, there is an increase in power spectra in the higher frequency region (> 10 kHz) as a consequence of a defect in the bearing, and the power spectra can be separated for healthy and faulty cases in this region.

From the SS plot of test data1 (figures 5.2 and 5.3), SV of healthy and faulty conditions are separated in various regions of the singular spectrum. A similar trend is observed in the PSD of test data1 (figure 5.11). While for test data2, it is seen that the healthy SV and faulty SV coincide with each other in the initial part of the SS plots (figure 5.9). This is due to the masking of the signal due to gear vibration, as observed in figure 5.12. For test data2, the SV's of healthy and outer race fault, inner race fault and ball fault all have close values, which is in agreement with the PSD shown in figure 5.12. Also, for test data1, the SS plots are concurrent with the power spectra shown in figure 5.11. This shows the correspondence between the power spectrum and singular spectrum.

5.4 ENERGY FEATURE AND ANN BASED BEARING FAULT DIAGNOSIS - 2nd METHOD

At the end of step (3) of the SSA technique (section 5.2), the vibration signal is decomposed into L components-C_1, C_2,…., C_L. These principal components are time series of different frequency regions. The correlation between these components and the bearing fault is studied in this method. Based on the condition of the bearing i.e. healthy or faulty, the resonant frequency changes. The energy of the signal also changes in the different frequency regions [Yu et al., 2006]. In the 1st method described earlier, appropriate SV were obtained. The components corresponding to these SV are selected. From the total L components, m number of components are selected ($1<m<L$). The energy of the corresponding principal components is calculated as $E = \sum_{n=1}^{N}[x(n)]^2$, where, x is signal (principal component) and n=1 to N data points. Thus, energy $E = \{E_1,E_2..E_m\}$, gives the energy distribution in the frequency domain for a bearing in healthy or different faulty conditions. Each energy feature is normalized by the total energy of the m-components. These are then given as inputs to an ANN for fault diagnosis.

5.4.1 APPLICATION TO TEST DATA1-2nd METHOD

From the analysis done in section 5.3.1.1, window length L=10 is found to be suitable. Hence, the signals are decomposed into 10 components. Figure 5.13 shows the principal components obtained from the decomposition of the vibration signal for an inner race fault with a window length L = 10.

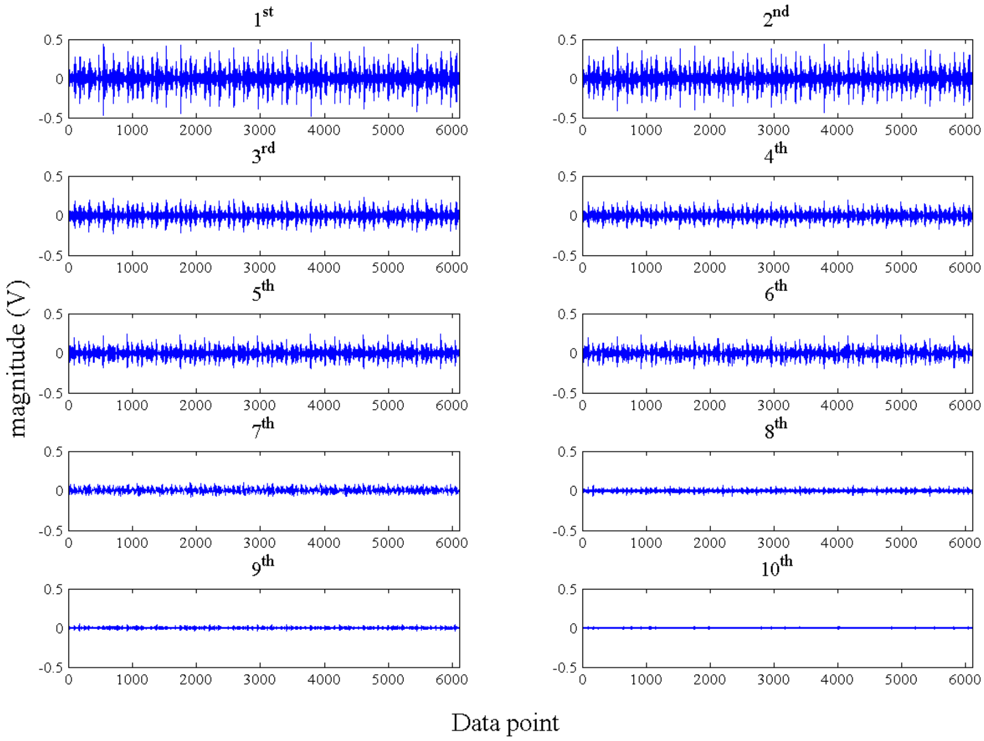

Figure 5.13 SSA decomposition of bearing vibration signal for inner race fault (0.18 mm fault size, 1HP load)

The appropriate SV are SV number 1, 2, 5 and 6 (from 1st method, section 5.3.1.2). The components (C_1, C_2, C_5 and C_6) corresponding to the selected SV are chosen from which the normalized energy (E_1, E_2, E_5 and E_6) features are obtained, which are then given as input to ANN. Similar to 1st method, gaussian white noise is added to obtain noisy signals having SNR of +10 dB and -10 dB which are separately analyzed.

5.4.1.1 ANN performance results for test data1-2nd method

The ANN consists of 4 input nodes, 13 hidden nodes and 4 outputs. The architecture, number of training and testing datasets and other parameters are the same as used in the 1st method (section 5.3.1.3). Table 5.6 gives the testing accuracy of the BPNN. Tables 5.7, 5.8 and 5.9 show the confusion matrix of the output result for the three cases of signals analyzed. For the original and noisy signal of SNR=+10 dB, the BPNN gives higher classification. However for SNR= -10 dB, the classification drops down from 95% to

65%. This is due to the energy values for the different fault conditions in the three chosen components having close values in the very low SNR case. Also, the chosen value of L was based on the analysis done on the original signal, not the signal with added noise.

Table 5.6 BPNN performance for test data1: 2nd method

Signal	Hidden Neuron	Classification Accuracy (%)
test data1	13	95.14
Noisy test data1, SNR +10dB	13	96.53
Noisy test data1, SNR -10dB	13	64.58

Table 5.7 Confusion matrix for test data1:2nd method

	H	IF	OF	BF
H	11	0	0	1
IF	0	47	1	0
OF	0	4	31	1
BF	0	0	0	48

Table 5.8 Confusion matrix for noisy test data1of SNR = +10 dB :2nd method

	H	IF	OF	BF
H	11	0	0	1
IF	0	47	1	0
OF	0	1	34	1
BF	0	0	0	48

Table 5.9 Confusion matrix for noisy test data1 of SNR= -10 dB:2nd method

	H	IF	OF	BF
H	12	0	0	0
IF	0	23	13	12
OF	0	6	22	8
BF	0	4	8	36

5.4.2 APPLICATION TO TEST DATA2- 2nd METHOD

From the analysis done in section 5.3.2.1, window length of 10 and SV numbers are 5, 6 and 7 are selected. The principal components (C_5, C_6 and C_7) corresponding to the selected SV numbers are obtained and their energy features (E_5, E_6 and E_7) are calculated. ANN is then used for diagnosis with the normalized energy features as an input.

5.4.2.1 ANN performance results for test data2- 2nd method

The ANN used is same as for test data1 (section 5.4.1.1) except that 17 hidden neurons are used. Similar to the 1st method applied to test data2 (section 5.3.2), the number of training and test datasets are the same. On testing, the classification accuracy is found to be 100%. Table 5.10 gives the confusion matrix obtained.

Table 5.10 Confusion matrix for testdata2: 2nd method

	H	**IF**	**OF**	**BF**
H	15	0	0	0
IF	0	15	0	0
OF	0	0	15	0
BF	0	0	0	15

5.5 COMPARISON WITH OTHER METHODS

Table 5.11 shows the comparison of the discussed method on SSA with some of the published works [Sreejith et al., 2008; Van wyk et al., 2009; William & Hoffman, 2011 ; Xiong et al., 2010; Abbasion et al., 2007; Nelwamondo et al., 2006; Nelwamondo et al., 2006; Boutros & Liang, 2011; Li & Zhang, 2011] which are based on time series and data based fault diagnosis approaches. All these studies use the same test data1 [Bearing data Centre] as used. The classification rate calculated depends on the number of datasets used for training and testing of the classifier. The works including this chapter have used different numbers of data sets ranging from 63 to 940.

In [Sreejith et al., 2008, Abbasion et al., 2007; Nelwamondo et al., 2006], the algorithm is applied to data consisting of only one fault size at a particular load and used fewer samples for training and testing of the classifier. Time domain features used are affected by noise [Sreejith et al., 2008].

The Difference Histogram (DH) based method [Van wyk et al., 2009] is a simple method, but the size of histogram bin influences the classification and it has to be sufficiently large for higher accuracy. The DH bins along with an ANN were used to discriminate between the faults, but the healthy condition was not included.

William and Hoffman [William & Hoffman, 2011] implemented a simple technique based on a Zero Crossing (ZC) feature. Similar to the SV feature, the ZC feature also represents the information present in the frequency domain. The feature calculation depends on the signal length which requires knowledge of the longest expected time duration between the successive zero crossing. The classification accuracy was affected by the length and varied from 91.5% to 97.1%. Also, the BPNN when trained only with higher defect sizes and tested for other defect sizes gave good classification. The effects of noise on ZC features were not studied.

In [Xiong et al., 2010], multi scale entropy as a feature was found to be suitable for bearing fault detection. However, in noisy conditions (white noise power is between [0.25, 1] times signal power), the classification accuracy comes down from 97.42% to 73.94%. The method1 of this chapter works even in noisy conditions.

Hidden Markov Model (HMM) and Gaussian Mixture Model (GMM) were employed for fault detection by Nelwamondo et.al [Nelwamondo et al., 2006]. Sample size influenced the classification and an accuracy of 81% to 100% was obtained for different bearing fault locations. The average accuracy is less than the one obtained in this chapter (1^{st} method) using BPNN.

Complex calculation is used in [Abbasion et al., 2007] and separate GMM was constructed for each bearing fault type along with a Bayesian classifier used for fault detection [Nelwamondo et al., 2006].

In [Boutros & Liang, 2011], HMM was used for bearing fault detection which was based on comparison of monitoring index with the reference vectors which are large in number. It required more training time and it was not fixed, as random values are used to fix the model parameters which are calculated by the Viterbi algorithm [Boutros & Liang, 2011]. Over fitting of data occurs in HMM due to usage of the Baum –Welch method [Garamani, 2001].

Li and Zhang [Li & Zhang, 2011] used a non linear dimension reduction method known as Supervised Locally Linear Embedding Projection (SLLEP), which transforms the original signal (assumed to be in a higher dimension) to a low dimension feature space. The performance of SLLEP is very sensitive to the regularization parameter which represents the generalization capacity of algorithm.

In all the above described methods, a high classification rate is achieved, but the method discussed (mainly 1st method) in this chapter does not suffer from the limitations of the above described methods such as parameter dependent performance, and features affected by noise and sample sizes. Of all the methods discussed so far, the methods based on ZC and DH are simple. In the DH method, discriminating between healthy and faulty bearings was found to be trivial using a single histogram bin.

Sample size affects DH and ZC based methods. It was shown in section 5.3.1.5 that fault diagnosis using the method1 is not affected by sample size variation. The effect of noise on classification and the performance in the presence of gearbox vibration is not studied in the ZC and DH methods. The methods in this chapter, work well even in presence of noise (test data1) and masking sources such as gears (test data2).(2nd method did not perform well for SNR = -10dB). Also, the methods are evaluated using the data obtained for many fault sizes and at different loads which very few of the above mentioned published works have tested.

Table 5.11 A study between the discussed method (this chapter) and some of the recent published works which uses bearing data set [Bearing data Centre]

Method	Dataset (single point defect size width ; load; signal length)	Training and Testing datasets	Condition classified	Average testing accuracy (%)	Fault features
BPNN [Sreejith et al., 2008]	0.18 mm, 1 HP load; 6000 data points	Train- 48 Test-32	H, IF, OF and BF	100	Kv, normal negative log-likelihood value
DH and BPNN [Van wyk et al., 2009]	0.18, 0.36, 0.53 mm; 0-3HP load; 30000 data points	Both 144	healthy and faulty	92 (IF, OF and BF classification only)	6 histogram bins
ZC and BPNN [William & Hoffman, 2011]	0.18, 0.36, 0.53 mm; 0-3HP load; 1024-4096 data points	-	H, IF, OF and BF	91.5–97.1	ZC count and ZC duration
Multi scale entropy and Support Vector machine (SVM) [Xiong et al., 2010]	0.18, 0.36, 0.53, 0.71 mm; no-load ; 2048 data points	Train-525 Test- 237	H, IF, OF and BF	97.42	6 entropies at different time scale
Time domain feature and SVM [Xiong et al., 2010]				75.64	rms, skewness, kurtosis, max
Wavelet denoising and SVM [Abbasion et al., 2007]	0.18 mm, 2HP load; 12000 data points	Testing-63	H, IF, OF and BF	100	2 weibull negative log-likelihood values
HMM and GMM [Nelwamondo et al., 2006]	0.18 mm	-	H, IF, OF and BF	HMM-99-100 GMM-94-99	mel-frequency cepstral coefficients, multi-scale fractal dimension, kurtosis (Kv)
Reconstructed phase space, GMM and Bayesian classifier [Wang et al., 2009]	0.18, 0.36, 0.53 mm; 1HP load; 1024 data points	384	H, IF, OF and BF	81–100	4 GMM
k-means clustering and HMM [Boutros & Liang, 2011]	0.18, 0.36, 0.53, 0.71 mm; 0-3 HP load.; 3000 data points	940	H, IF, OF and BF	96	power index and 17 reference vector's
SLLEP with Minimum distance, k-NN and SVM [Li & Zhang, 2011]	0.53 mm; 3HP load; 1030 data points	Train -150 Test -100	H, IF, OF and BF	96.64-99.67	low dimension feature space of original signal
SSA and BPNN [This chapter]	0.18, 0.36, 0.53, 0.71 mm; 0-3HP load; 6100 data points	Train -336 Test -144	H, IF, OF and BF	96.53-100 95-100%	4 singular values 3 energy features

5.6 SUMMARY

This chapter discussed a new technique for bearing fault feature extraction based on singular spectrum analysis. A new fault feature (singular value) was introduced for bearing fault detection. A new approach for selection of the principal components was employed. Two methods were discussed. In the first method, singular values extracted from the bearing vibration signal are used as fault features which are given to ANN for automated fault diagnosis. This method is simple, detects faults even in a signal with a low SNR and also with masking sources such as gears with higher classification accuracy. In the second method, the correlation between the principal components corresponding to the selected SV and the bearing fault has been investigated. It shows that the features obtained from the principal components corresponding to SV numbers are useful for fault detection. An energy feature was used for fault identification. The correspondence between the singular spectrum and the power spectrum has also been shown. The method is found to have more advantages over the existing time series and data based methods. The experimental results demonstrate that the singular spectrum analysis based bearing fault diagnosis method is simple, noise tolerant and efficient.

CHAPTER 6

GENERALIZED TEAGER KAISER ENERGY OPERATOR BASED BEARING FAULT DIAGNOSIS

MAIN CONTENTS:

- **Introduction**
- **Demodulation Methods**
  - Teager Kaiser energy Operator (TKEO)
  - Generalized Teager Kaiser energy Operator (GTKEO)
- **Demodulation using GTKEO and signal improvement ratio**
- **Testing of the GTKEO method in comparison with TKEO method**
  - Application to Test data1: IF detection
  - Application to Test data2: OF and BF detection
- **Discussion based on Test data1 and Test data2 results**
- **Validation of GTKEO Method using industrial data's**
- **Summary**

6.1 INTRODUCTION

Frequency based method to diagnose a bearing fault involves detection of the fault characteristic frequencies (FCFs) related to faults on the different bearing parts. FCFs are mainly amplitude modulated due to: i) transfer function of the transmission path between the vibration source and sensor; ii) load carried by the rolling elements. It has also some amount of frequency modulation due to variation in the instantaneous rotating frequency of shaft. At the incipient stage of a fault, FCFs contains very little energy as compared to the stage of a high fault severity. Also, the measured vibration signal not only contain the FCF's but also the background noise and the interference vibration signals generated due to gearboxes, shaft imbalance or misalignment and bent or cracked shaft. Due to roller slippage [Randall, 2004], noise and vibration interferences, the FCF's are smeared and masked across wide frequency bands. Thus, the detection of a fault in its incipient stage is slightly difficult as compared to the severe fault condition.

The existing methods of fault diagnosis (chapter 2, section 2.7.2) require either designing the band pass filter or denoising or involves decomposition of the signal. There are few requirements which a spectrum analysis method should satisfy. Firstly, it should be simple in implementation. Secondly, the method should perform efficiently under the presence of masking vibration sources and background noise. But, most of the efficient methods developed are not simple in implementation. Thus, a simple and efficient method to diagnose the fault is required.

In this chapter, a method which satisfies the above requirements of a spectrum analysis based method is presented. It is based on the concept of energy operator, which is known as Generalized Teager Kaiser Energy Operator (GTKEO). The fault diagnosis method involves the transformation of the signal using GTKEO, followed by spectral analysis. A method based on the energy operator known as Teager Kaiser Energy Operator

(TKEO) has been developed and patented by Liang and Bozchalooi (Liang and Bozchalooi, 2010). TKEO based method has advantages such as simple in implementation, elimination of enveloping step and involves demodulation. But, high frequency noise amplification occurs due to TKEO. Thus, for signals with low SNR, it may not perform efficiently. GTKEO based method which is discussed in this chapter includes the advantages of TKEO and additionally performs efficiently even for signals with low SNR, as compared to TKEO.

GTKEO is similar to TKEO but requires calculation of a parameter known as lag parameter which is easily calculated using a suitable method. Capability of GTKEO to detect fault under very low SNR is shown in comparison to TKEO. TKEO method is chosen for comparison because it is shown in [Liang and Bozchalooi, 2010] to perform better than the conventional high frequency resonance technique. The block diagram of the GTKEO based diagnosis method is shown in figure 6.1.

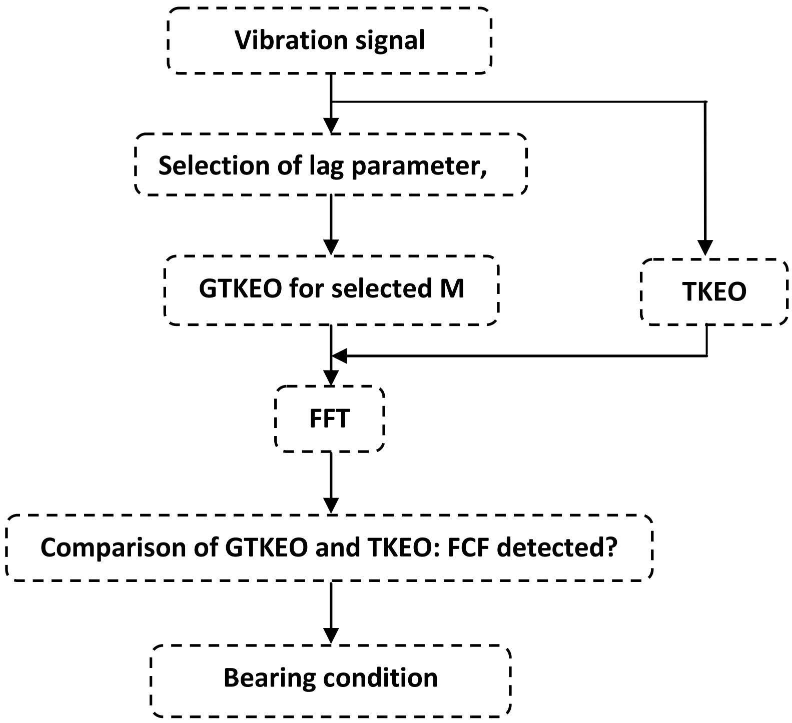

Figure 6.1 Block diagram of the GTKEO based bearing fault diagnosis method in comparison with the TKEO method

6.2 DEMODULATION METHODS

6.2.1 Teager Kaiser Energy Operator

Teager Kaiser Energy Operator (TKEO) was first conceptualized by Teager [Teager, 1980] in his work on non linear modelling and Kaiser developed it [Kaiser, 1990] for the energy calculation. It has also been used for demodulating the speech signals [Maragos et al., 1993].

The TKEO for discrete time signal x(n) is defined as [Kaiser, 1990]:

$$\Psi\,[x(n)] = x^2(n) - x(n+1)\,x(n-1) \tag{6.1}$$

For the signal, $x(n) = a(n)\ cos(\phi(n))$

(6.2)

where, $a(n)$ and $\phi(n)$ are the discrete time varying amplitude and time varying phase of signal $x(t)$.

On applying TKEO [Maragos et al., 1993] to $x(n)$,

$$\Psi[x(n)] \approx [a(n)\ sin(\Omega(n))]^2 \tag{6.3}$$

where, $\Omega(n) = \phi(n) - \phi(n-1)$

6.2.2 Generalized Teager Kaiser Energy Operator

The generalized form of Generalized Teager Kaiser Energy Operator (GTKEO) [Lin et al., 1995] (also referred here as M-TKEO) is expressed as

$$\Psi_M[x(n)] = x^2(n) - x(n+M)\,x(n-M) \tag{6.4}$$

where, M is an integer (M>1), known as Lag parameter.

On applying, M-TKEO to signal (equation 6.2), we get [Lin et al., 1995]

$$\Psi_M[x(n)] \approx [a(n)\ sin(\Omega(n)\ M)]^2 \tag{6.5}$$

6.2.2.1 Selection of Lag parameter

The lag parameter, M is chosen by calculating an index known as Energy Ratio (ER) [Al Regib and Ni, 2010].

ER is calculated as

ER(M) = Energy calculation using M-TKEO/ Conventional equation of energy

$$ER(M) = \frac{\frac{1}{N_M}\sum_{n=1}^{N_M}\Psi_{\mathrm{M}}[\mathrm{x(n)}]}{\frac{1}{N}\sum_{n=1}^{N}x^2(n)} \tag{6.6}$$

Where N and N_M are the number of samples of $x(n)$ and $\Psi_M[x(n)]$ respectively.

The M value at which the peak will be observed in ER is considered as the optimal one and using this value, M-TKEO is calculated (will be shown in section 6.4). The concept of GTKEO for bearing fault diagnosis is explained in the following section.

6.3 DEMODULATION OF FAULT SIGNAL USING GTKEO AND SIGNAL IMPROVEMENT RATIO

To illustrate the concept of GTKEO and to simplify the analysis, a simple bearing fault model is considered. The bearing fault vibration signal obtained under the presence of vibration interference (e.g. gearbox) and background noise is used. This is same as used for TKEO [Liang and Bozchalooi, 2010] analysis except the noise component which was not considered.

Bearing fault vibration signal is given as

$$X(n) = \underbrace{I_f\, e^{-\beta n}\cos(\omega_n n + \varphi)}_{\text{fault impulses}} + \underbrace{V_i\cos(\omega_v n)}_{\text{vibration interferences}} + Noise \tag{6.7}$$

where, I_f is the amplitude of the fault impulse, β is the damping constant of the system, φ is the initial phase angle, $\omega_n = 2\pi f_n$, f_n is the resonant frequency, V_i is the amplitude of the vibration interference, $\omega_v = 2\pi f_v$, f_v is the frequency of vibration interference such as gear meshing frequency.

The GTKEO is applied to $X(n)$,

$$\Psi[X(n)] = \Psi[I_f\, e^{-\beta n} \cos(\omega_n n + \varphi) + V_i \cos(\omega_v n)] + \Psi[Noise]$$

$$\Psi[X(n)] = \Psi\big[I_f e^{-\beta n} \cos(\omega_n n + \varphi)\big] + \Psi[V_i \cos(\omega_v n)] + \Psi\big[I_f\, e^{-\beta n} \cos(\omega_n n + \varphi)\,, V_i \cos(\omega_v n)\big] + \Psi[Noise] \tag{6.8}$$

where, $\Psi_c = \Psi\big[I_f\, e^{-\beta n} \cos(\omega_n n + \varphi)\,, V_i \cos(\omega_v n)\big]$ denotes the cross term energy operator between fault impulses and vibration interference signal.

Cross term energy operator is given as

$$\Psi_c = [I_f e^{-\beta(n+M)} \cos(\omega_n(n + M) + \varphi)\; V_i \cos \omega_v(n - M) - 2I_f\, e^{-\beta n} \cos(\omega_n n + \varphi)\; V_i \cos \omega_v n + I_f e^{-\beta(n-M)} \cos(\omega_n(n - M) + \varphi)\; V_i \cos \omega_n(n + M)] \tag{6.9}$$

$$\Psi_c = V_i I_f e^{-\beta n}\, L(n) \tag{6.10}$$

where,

$$L(n) = \{e^{-\beta M}[\cos[(\omega_n + \omega_v)n + (\omega_n - \omega_v)M + \varphi] + \cos[(\omega_n - \omega_v)n + (\omega_n + \omega_v)M + \varphi]] - 2(\cos[(\omega_n + \omega_v)n + \varphi] + \cos[(\omega_n - \omega_v)n + \varphi]) + ([\cos[(\omega_n + \omega_v)n - (\omega_n - \omega_v)M + \varphi] + \cos[(\omega_n - \omega_v)n - (\omega_n + \omega_v)M + \varphi]])\} \tag{6.11}$$

GTKEO of fault impulses is given as

$$\Psi[I_f\, e^{-\beta n} \cos(\omega_n n + \varphi)] = \big(I_f \cos(\omega_n + \varphi)\big)^2\, \Psi\big[e^{-\beta n}\big] + \big(e^{-\beta n}\big)^2 \Psi[I_f\, \cos(\omega_n + \varphi)]$$
$$= {I_f}^2\, e^{-2\beta n} \sin^2(\omega_n M) \tag{6.12}$$

GTKEO of vibration interference is given as

$$\Psi[V_i \cos(\omega_v n)] = V_i^2 \sin^2(\,\omega_v M) \tag{6.13}$$

The energy operator for white gaussian noise (WGN) gives an output signal as white noise with variance directly proportional to that of background noise. Mean value of the operator transformed noise is equal to the order of the variance of the actual noise [Dutoit et al., 2009].

$$\Psi[Noise] = \Psi[WGN] = {\sigma_1}^2 = K\sigma^2 \tag{6.14}$$

where, ${\sigma_1}^2$ represent the variance of the energy transformed noise signal, σ^2 is variance of the WGN and K is the constant of proportionality.

Using equations (6.10), (6.12), (6.13) and (6.14), equation (6.8) becomes

$$\Psi[X(n)] = {I_f}^2\, \mathrm{e}^{-2\beta n} \sin^2(\omega_n M) + V_i^2 \sin^2(\omega_v M) + V_i I_f e^{-\beta n} L(n) + K\sigma^2 \quad (6.15)$$

The signal obtained after the application of GTKEO ($\Psi[X(n)]$) consists of three terms along with the noise component. The first and the third term are the transient components denoted by the exponential decaying term. First term gives the squared envelope of the fault signal and it represents the demodulated signal. The second term shows the vibration interference component and the third term represents the high frequency component. Thus we see that the energy operator demodulates the signal under the presence of external vibration and background noise. As shown in equation (6.15), GTKEO gives the square of the envelope of the fault signal. Hence, the fault characteristic frequencies could be detected in the GTKEO spectrum.

The enhancement in detection of the fault impulse component due to the energy operator with respect to vibration interferences is studied by calculating the signal enhancement ratio (SER). Only the demodulated term is considered. The high frequency component will not contribute in fault diagnosis. Hence, it is neglected. SER is defined as

SER= (Power of fault impulse signal) / (Power of external interferences)

$$SER\big[\Psi[X(n)]\big] = \frac{\frac{1}{N_f}\int_0^{N_f} ({I_f}^2\, \mathrm{e}^{-2\beta n} \sin^2(\omega_n M))^2\, dn}{(V_i^2 \sin^2(\omega_v M))^2 + ({\sigma_1}^2)^2}$$

$$\approx \frac{{I_f}^4 \sin(2\pi f_n \mathrm{M})^4}{4\mathrm{N_f}\beta[{\mathrm{V_i}}^4 \sin(2\pi f_v \mathrm{M})^4 + K^2\sigma^4]} \quad (6.16)$$

Where, N_f denotes the signal length.

Similar to SER, the signal to interference ratio (SIR) of the original bearing fault vibration signal (equation (6.7)) is given as

$$SIR[X(n)] = \frac{\frac{1}{N_f}\int_0^{N_f}\left(I_f\, e^{-\beta n}\ \cos(\omega_n n+\varphi)\right)^2 dn}{\frac{1}{N_v}\int_0^{N_v}(V_i \cos(\omega_v n))^2\, dn+\sigma^4}$$

$$SIR[X(n)] \approx \frac{I_f^{\,2}}{2N_f\beta({V_i}^2+2\sigma^4)} + \frac{{I_f}^2(\beta\ \cos 2\varphi-2\pi f_n \sin 2\varphi)}{2N_f({V_i}^2+2\sigma^4)(\beta^2+4\pi^2{f_n}^2)} \qquad (6.17)$$

To compare the equations (6.16) and (6.17), relationship between the resonant frequency (f_n) and damping constant (β) is considered. This relationship is explained in [Liang and Bozchalooi, 2010]. For $\beta \approx f_n$, critical damping condition occurs. For $\beta > f_n$, fault impulses would not be clear. Only for the case $\beta \ll f_n$, the fault impulses would be found in the vibration signal. The equations (6.16) and (6.17) are calculated for two cases: $\beta \approx f_n$ and $\beta \ll f_n$.

For $\beta \approx f_n$

$$\left.\begin{aligned} SER\big[\Psi[X(n)]\big] &\approx \frac{{I_f}^4\ \sin(2\pi f_n \mathrm{M})^4}{4\mathrm{N_f} f_n\big[{\mathrm{V_i}}^4 \sin(2\pi f_v \mathrm{M})^4+K^2\sigma^4\big]} \\ SIR[X(n)] &\approx \frac{1.025{I_f}^2}{2N_f f_n({V_i}^2+2\sigma^4)} \end{aligned}\right\} \qquad (6.18)$$

For $\beta \ll f_n$,

$$\left.\begin{aligned} SER\big[\Psi[X(n)]\big] &\approx \frac{{I_f}^4\ \sin(2\pi f_n \mathrm{M})^4}{4\mathrm{N_f}\beta\big[{\mathrm{V_i}}^4 \sin(2\pi f_v \mathrm{M})^4+K^2\sigma^4\big]} \\ SIR[X(n)] &\approx \frac{{I_f}^2}{2N_f\beta({V_i}^2+2\sigma^4)} \end{aligned}\right\} \qquad (6.19)$$

The improvement in the signal after applying the GTKEO with respect to the original vibration signal is given by the ratio of $SER\big[\Psi[X(n)]\big]/SIR[X(n)]$ which is known as Improvement Ratio (IR). It is calculated for the above two cases considered.

For $\beta \approx f_n$,

$$IR = \frac{\frac{I_f^{4}\ \sin(2\pi f_n \mathrm{M})^4}{4\mathrm{N_f} f n\left[\mathrm{V_i}^4 \sin(\omega_{\mathrm{V}}\mathrm{M})^4 + \sigma_1{}^4\right]}}{\frac{1.025 I_f{}^2}{2N_f f n (V_i{}^2 + 2\sigma^4)}}$$

$$= \frac{1.025}{2}\frac{I_f{}^2(\mathrm{V_i}^2+2\sigma^2)\sin(2\pi f_n \mathrm{M})^4}{\mathrm{V_i}^4 \sin(2\pi f_v \mathrm{M})^4 + K^2\sigma^4} \tag{6.20}$$

For $\beta \ll f_n$,

$$IR = \frac{\frac{I_f^{4}\ \sin(2\pi f_n \mathrm{M})^4}{4\mathrm{N_f}\beta\left[\mathrm{V_i}^4 \sin(2\pi f_v \mathrm{M})^4 + \sigma_1{}^4\right]}}{\frac{I_f{}^2}{2N_f \beta (V_i{}^2 + 2\sigma^4)}}$$

$$= \frac{1}{2}\frac{I_f{}^2(\mathrm{V_i}^2+2\sigma^2)\sin(2\pi f_n \mathrm{M})^4}{\mathrm{V_i}^4 \sin(2\pi f_v \mathrm{M})^4 + K^2\sigma^4} \tag{6.21}$$

Therefore, IR for lower ($\beta \approx f_n$) and upper ($\beta \ll f_n$) limits are given as

$$\frac{1.025}{2}\frac{I_f{}^2(\mathrm{V_i}^2+2\sigma^2)\sin(2\pi f_n \mathrm{M})^4}{\mathrm{V_i}^4 \sin(2\pi f_v \mathrm{M})^4 + K^2\sigma^4} \le IR \le \frac{1}{2}\frac{I_f{}^2(\mathrm{V_i}^2+2\sigma^2)\sin(2\pi f_n \mathrm{M})^4}{\mathrm{V_i}^4 \sin(2\pi f_v \mathrm{M})^4 + K^2\sigma^4} \tag{6.22}$$

For the two limits, $SER\big[\Psi[X(n)]\big]$ is given as

$$\frac{1.025}{2}\frac{I_f{}^2(\mathrm{V_i}^2+2\sigma^2)\sin(2\pi f_n \mathrm{M})^4}{\mathrm{V_i}^4 \sin(2\pi f_v \mathrm{M})^4 + K^2\sigma^4} SIR[X(n)] \le SER\big[\Psi[X(n)]\big] \le$$

$$\frac{I_f{}^2(\mathrm{V_i}^2+2\sigma^2)\sin(2\pi f_n \mathrm{M})^4}{2(\mathrm{V_i}^4 \sin(2\pi f_v \mathrm{M})^4 + K^2\sigma^4)} SIR[X(n)] \tag{6.23}$$

Without noise, equation (6.23) is given as

$$\frac{1.025}{2}\left(\frac{I_f}{\mathrm{V_i}}\right)^2 \frac{\sin(2\pi f_n \mathrm{M})^4}{\sin(2\pi f_v \mathrm{M})^4} SIR[X(n)] \le SER\big[\Psi[X(n)]\big] \le$$

$$\frac{1}{2}\left(\frac{I_f}{\mathrm{V_i}}\right)^2 \frac{\sin(2\pi f_n \mathrm{M})^4}{\sin(2\pi f_v \mathrm{M})^4} SIR[X(n)] \tag{6.24}$$

6.3.1 Role of Lag parameter in the enhancement of the fault signal

To explain the importance of the lag parameter in the enhancement of the fault signal, IR is numerically calculated for $\beta \ll f_n$ excluding the noise component. As for M=1 and M >1, $\Psi[WGN]$ remains almost the same. Hence, noise is not considered.

Assuming that vibration interference has an amplitude of 10 times that of fault impulses ($\frac{V_i}{I_f} = 10$) and the resonant frequency to be 5 times that of vibration interfering frequency (f_n=1000 Hz; f_v=200 Hz), figure 6.2 shows the values of IR obtained for M varied from 1 to 100. As seen from this plot, for some M values (M=51, 89), IR value obtained is very much higher than that is obtained for M = 1. Also, some M values (3, 5, 6, 9) give lower IR than obtained for M=1. While, few M values (2, 4, 8) give same value of IR as seen for M=1. Thus, by an appropriate choice of M, signal could be enhanced better than when using M = 1. This suggests that GTKEO (M>1) could perform better than TKEO (M=1) using an appropriate value of M. Also, the improvement in fault detection ability depends on: SIR of actual fault vibration signal, the ratio of impulse amplitude to the vibration interference amplitude, resonant frequency, vibration interfering frequencies and the level of noise present. If the IR term is very much higher than the SIR term, then even for very low SNR signal, FCFs could be identified. This has more probability for GTKEO than for TKEO, as IR value of GTKEO is more than for TKEO for an appropriate value of M (figure 6.2).

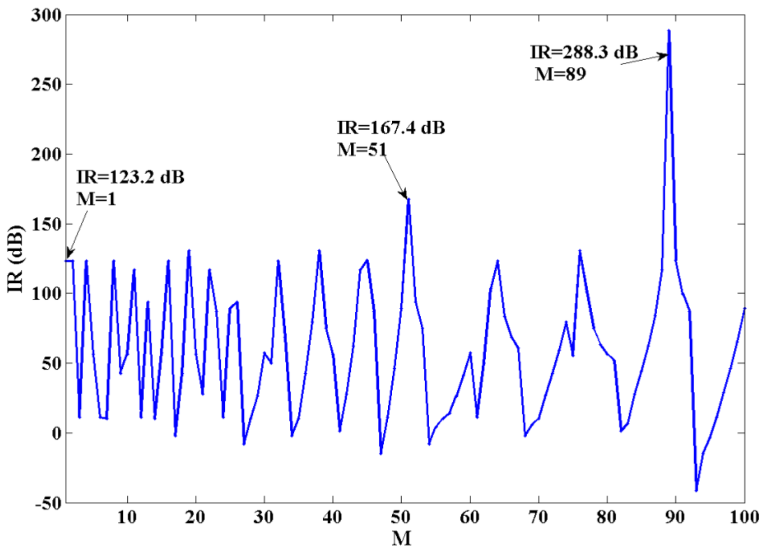

Figure 6.2 Improvement Ratio obtained for different Lag parameter ($\beta \ll f_n$ and without noise)

6.4 TESTING OF THE GTKEO METHOD IN COMPARISON WITH THE TKEO METHOD

6.4.1 APPLICATION TO TEST DATA1: Inner race fault detection

Test data1's setup (section 3.3.1) has no vibration interference sources. Hence, white gaussian noise (WGN) is added virtually using the matlab function 'awgn' to the recorded signal to emulate the real plant environment. Inner race fault (IF) signal is considered in this analysis.

Vibration data for IF was collected for the single point defect of diameter of 0.18 mm and depth of 0.28 mm at the load of 1HP. Rotational frequency of shaft was 29.53 Hz. The theoretical fundamental fault frequency calculated for IF is 159.6 Hz. The vibration signal obtained for the inner race fault is shown in figure 6.3(a). WGN is added to the recorded fault signal to obtain a noisy signal with SNR of -15 dB (figure 6. 3(b)) and SNR of -30 dB (figure 6.3 (c)).

The performances of the M-TKEO (or GTKEO) and TKEO methods are studied for three cases: without noise, SNR= -15dB and SNR= -30 dB.

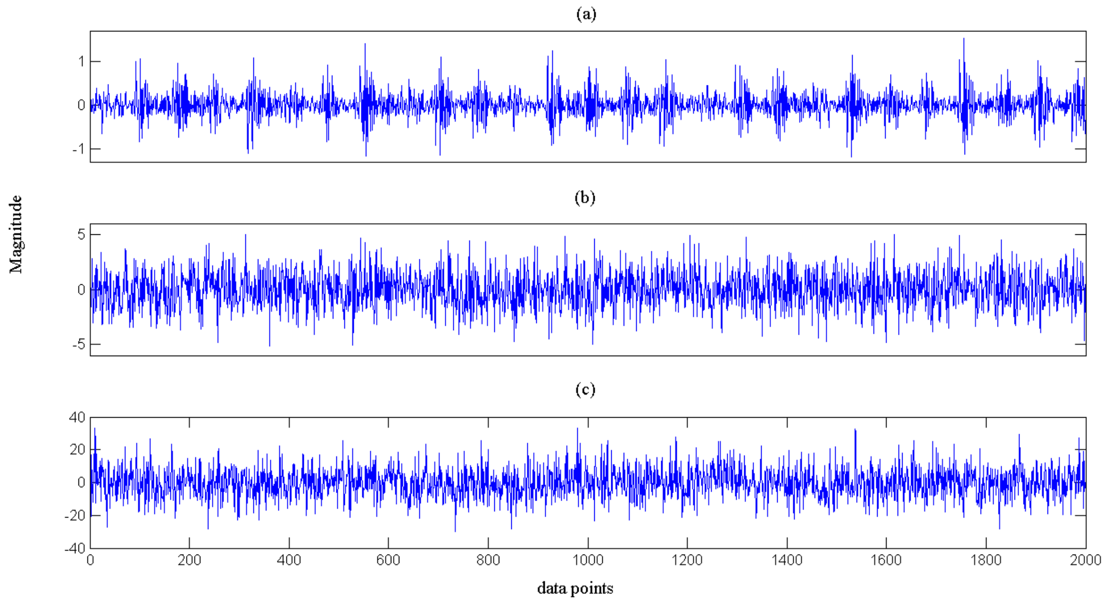

Figure 6.3 Bearing vibration signals for IF: (a) without noise; (b) SNR= -15 dB and (c) SNR= -30 dB

6.4.1.1 IF signal : without any additive noise

TKEO (equation (6.1)) was applied to the obtained IF signal and its spectrum is shown in figure 6.4. First six harmonics (at 159.6, 319.2, 478.8, 638.4, 798, and 957.6 Hz) of the FCFs are clearly detected from the spectrum. To apply M-TKEO, the lag parameter M is required to be known. For that, Energy ratio (equation 6.6) is calculated for different M values and plotted as shown in figure 6.5. At M=1, maximum value of ER is observed. Other than M=1, the next dominant value of ER is seen at M=6. With M=6, M-TKEO (equation (6.4)) is applied (referred as 6-TKEO) and its spectrum is given in figure 6.6. As observed from the figure 6.6, 6-TKEO also gives the same FCFs related to inner race fault as seen for TKEO. To see whether other M value (at which peaks are also observed) show any FCF components, 3-TKEO is calculated and its spectrum is shown in figure 6.7. It also shows the FCF and its harmonics. One can infer that, non dominant M values at which peak are seen could be for diagnosis.

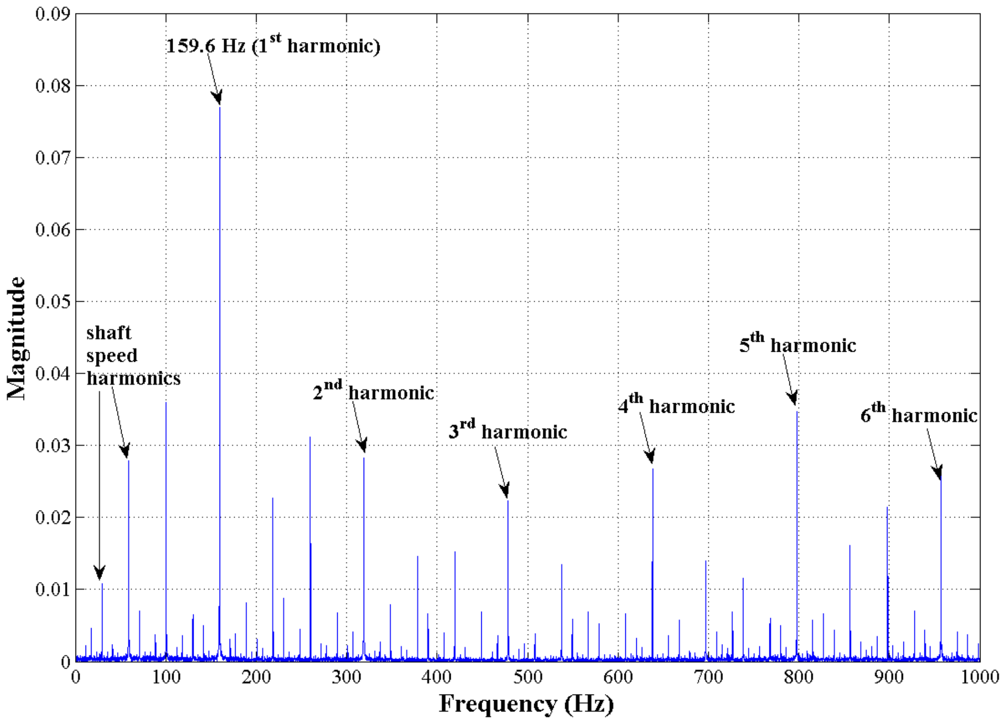

Figure 6.4 TKEO spectrum for IF: without noise

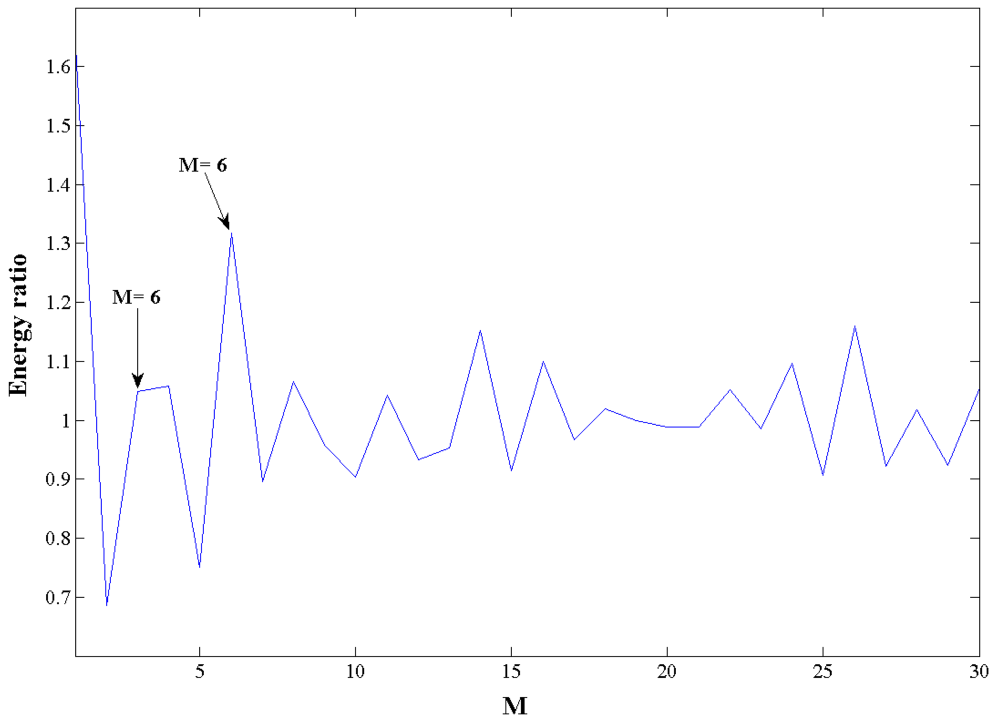

Figure 6.5 ER plot for IF: without noise

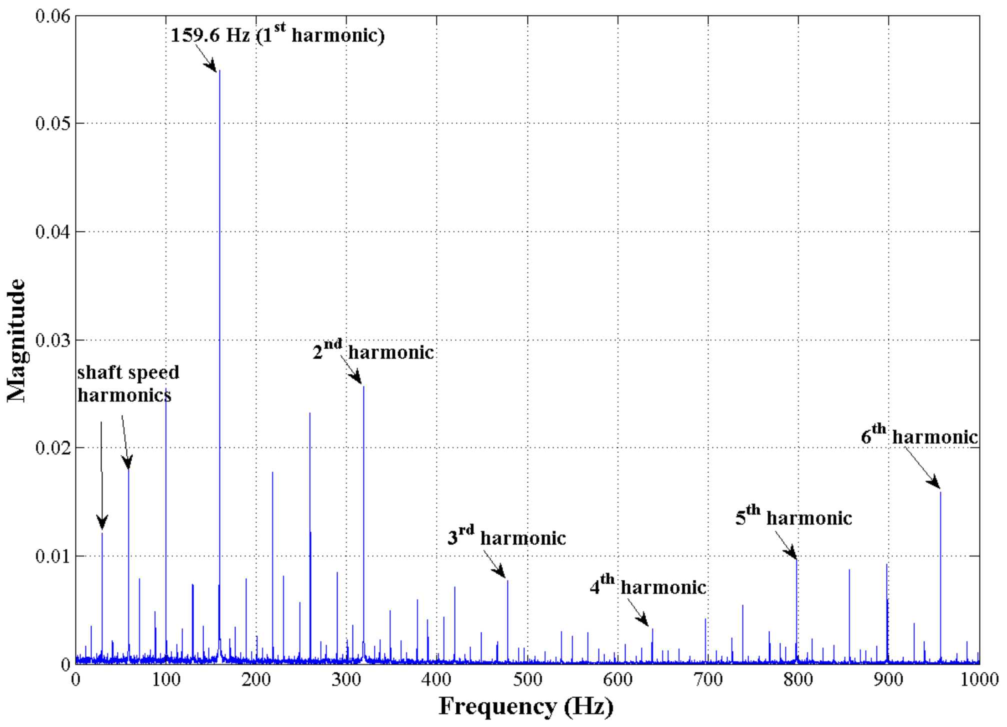

Figure 6.6 6-TKEO spectrum for IF: without noise

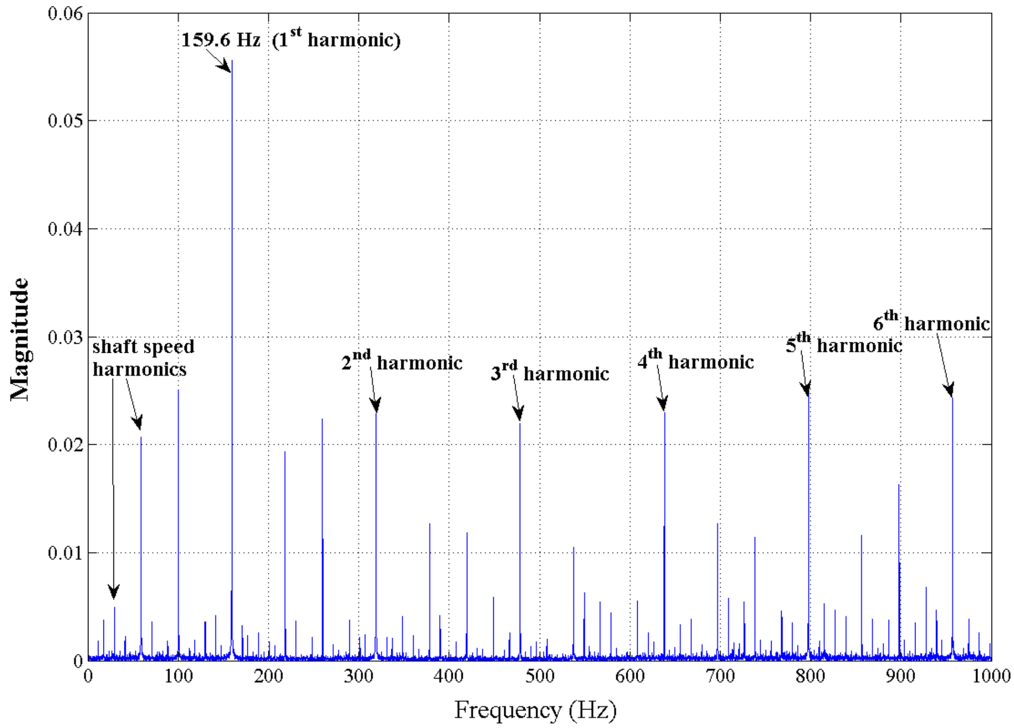

Figure 6.7 3-TKEO spectrum for IF: without noise

6.4.1.2 IF signal : SNR=-15 dB

ER is calculated and plotted as shown in figure 6.8. For M=6, we get the highest value of ER and thus it is chosen for M-TKEO calculation. First, TKEO is applied to the IF signal. Figure 6.9 gives the spectrum plot of TKEO. From this plot, we see that only the fundamental fault frequency is observed and it is also not dominant. As one can see from this figure, the spectrum is noisy and the frequency components corresponding to the shaft speed are found to be dominant. As a result, the other fault harmonics are not visible. It was shown in [Liang and Bozchalooi, 2010] that repetitive TKEO could increase the fault detection capability. Hence, TKEO is applied to the signal for two iterations i.e. $\Psi\{\Psi[x(n)]\}$. Figure 6.10 gives the representation of the TKEO (applied twice) transformed signal in the frequency domain. Only, first (159.6 Hz) and fifth harmonic (797.7 Hz) are observed after this operation.

M-TKEO is calculated for M=6. Its spectrum is shown in figure 6.11. It is observed that first five harmonics (at 159.6, 319.2, 478.8, 638.4 and 798 Hz) are detected. Though the FCF can be detected from the spectrums of TKEO and that of M-TKEO (M=6), only one fault frequency harmonic is observed in TKEO (figures 6.9), two in twice TKEO (figures 6.10), while five number of FCFs are seen in M-TKEO (figures 6.11). One may further appreciate the performance of the M-TKEO method, as it performs better than even the repetitive application TKEO.

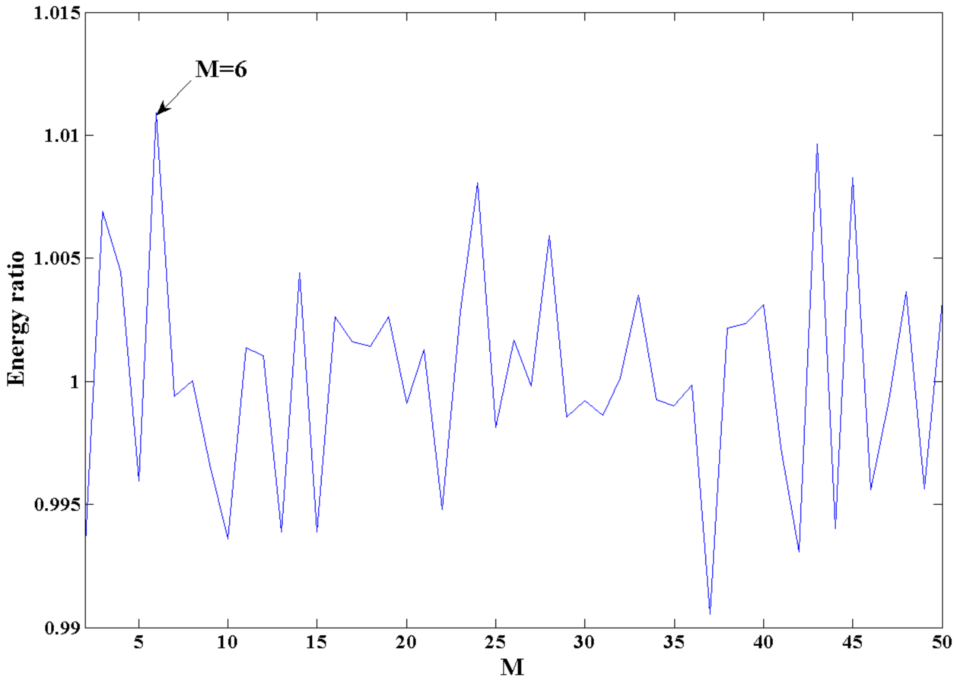

Figure 6.8 ER plot for IF: SNR= -15 dB

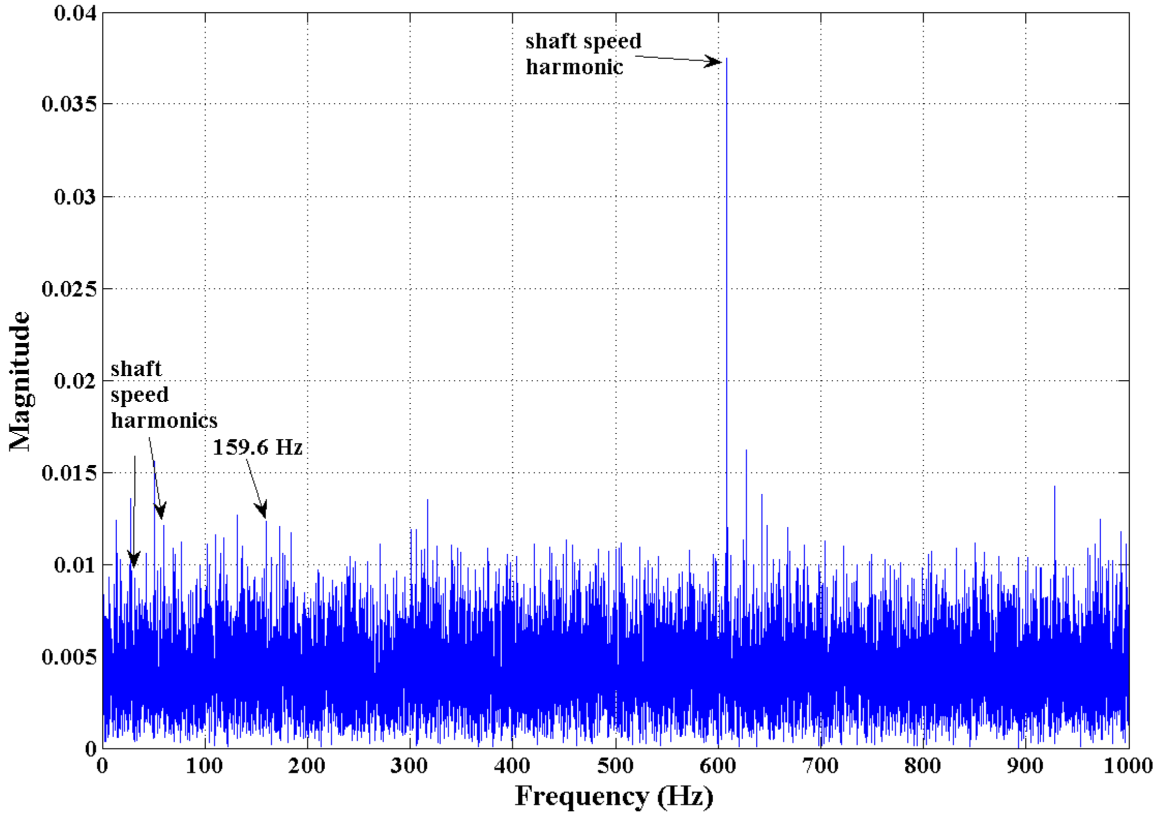

Figure 6.9 TKEO spectrum for IF: SNR= -15 dB

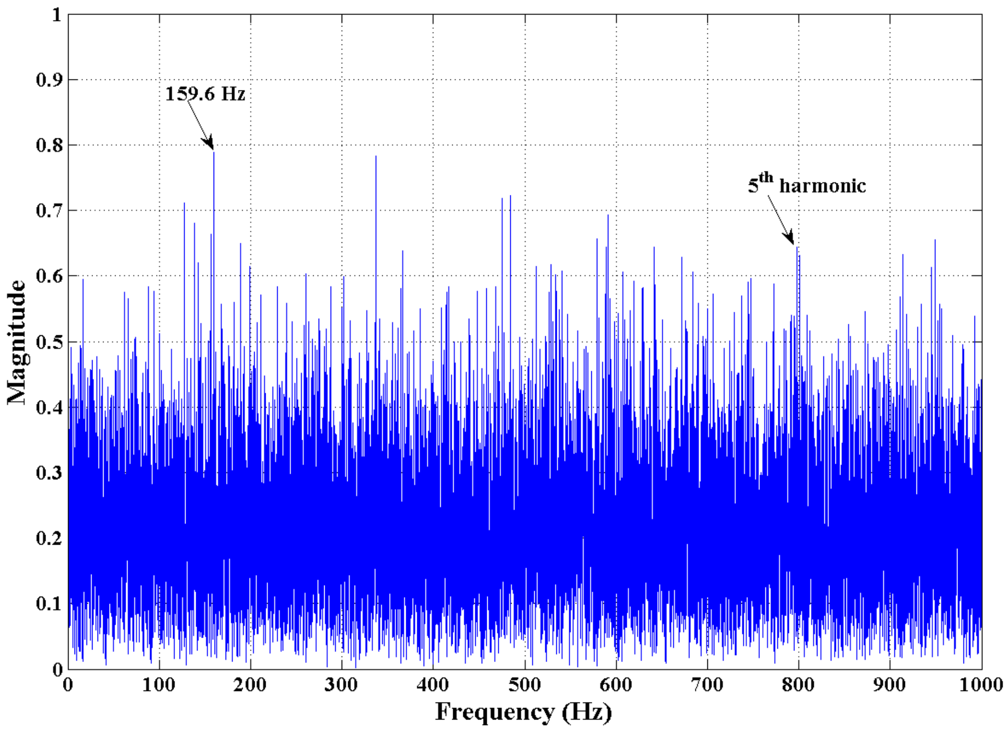

Figure 6.10 Twice TKEO operation spectrum for IF: SNR= -15 dB

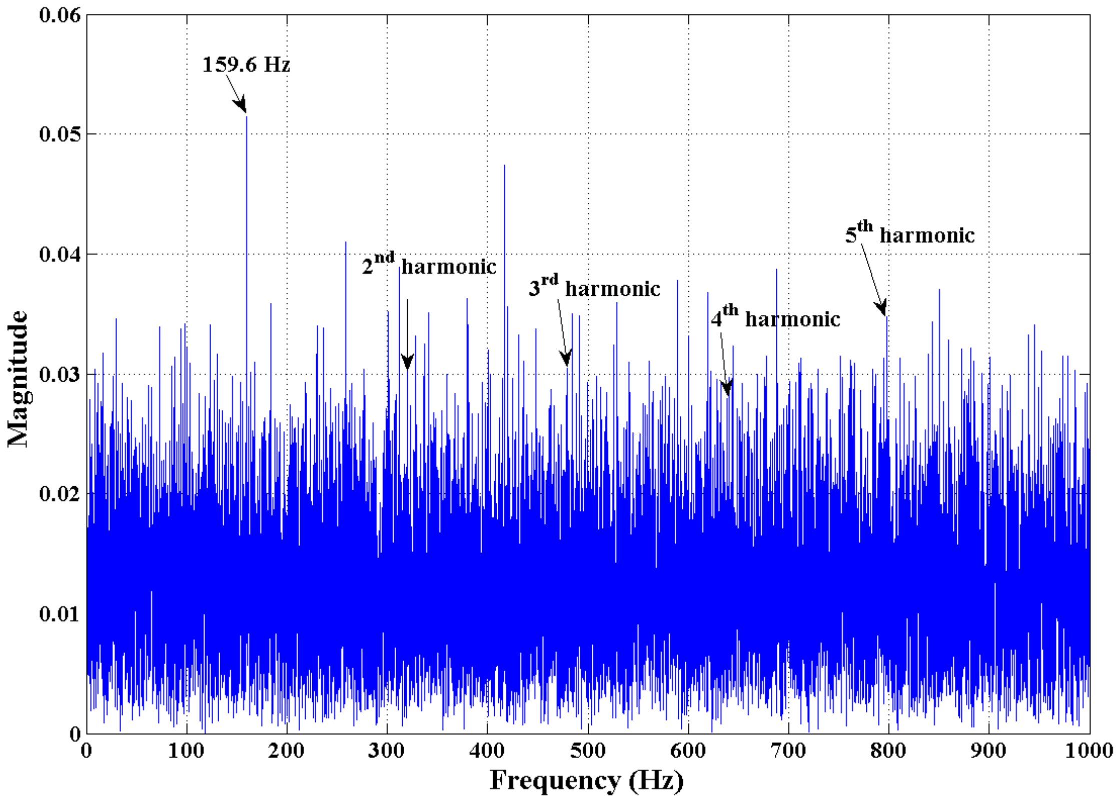

Figure 6.11 6-TKEO spectrum for IF: SNR= -15 dB

6.4.1.3 IF signal : SNR= -30 dB

M= 27 gives the maximum value in the ER plot (figure 6.12). TKEO is applied to the signal and its spectrum is given in figure 6.13. As seen from this figure, the FCF's are not detected. TKEO is now applied to the signal for two iterations. Its spectrum is displayed in figure 6.14. As observed from this figure, that even twice operation of TKEO does not show up the FCF harmonics as it showed up for SNR= -15 dB (Figure 6.10). Even the three and four consecutive TKEO spectrums failed to show the FCF's (results are not shown). The performance of the repetitive TKEO depends on the SNR. As the number of TKEO iterations increases, the noise level also increases [Bozchalooi and Liang, 2009].

M-TKEO (M=27) is also applied to the signal and its spectrum is plotted in figure 6.15. The first three FCF harmonics (at 159.6, 319.5, 478.8 Hz) are detected. When 27-

TKEO is applied twice to the signal, its spectrum (figure 6.16) also showed the first three harmonics but better than the single iteration of 27-TKEO (figure 6.15).

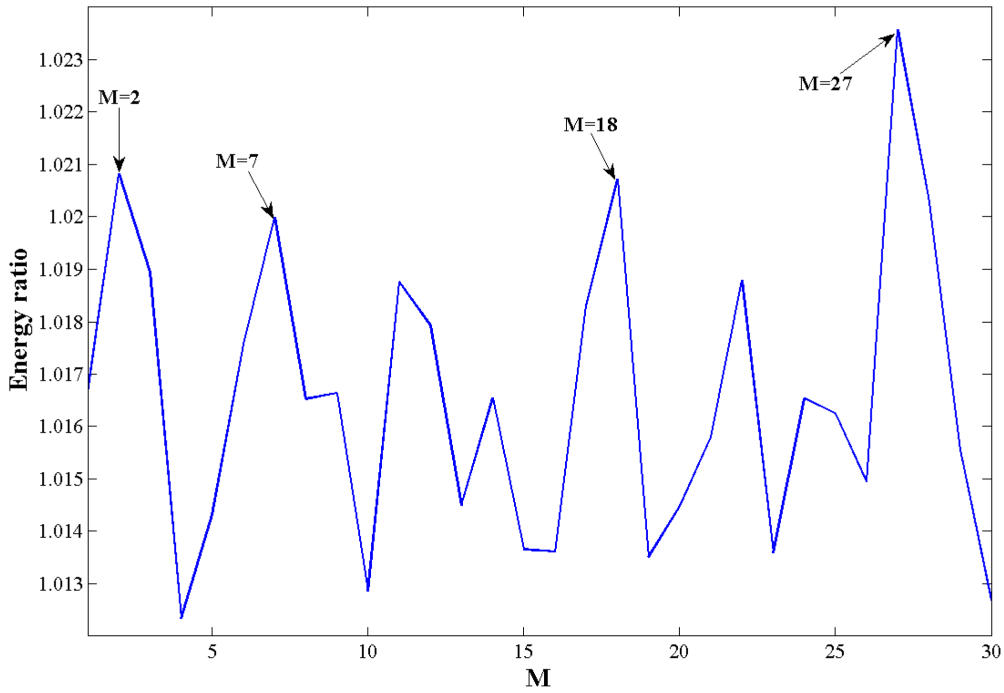

Figure 6.12 ER plot for IF: SNR= -30 dB

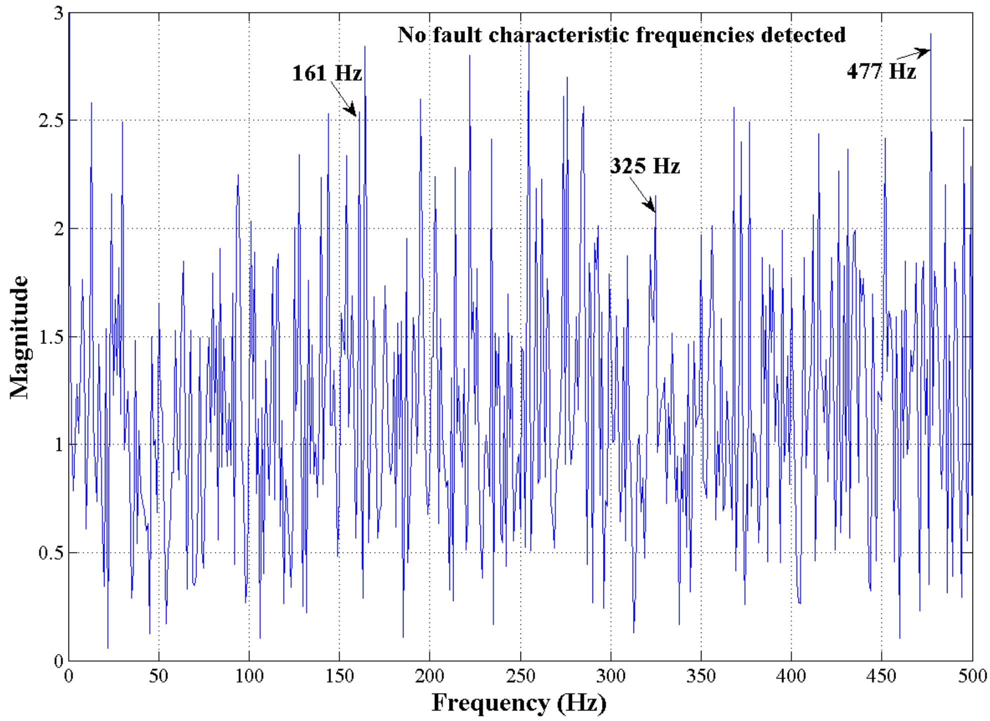

Figure 6.13 TKEO spectrum for IF: SNR= -30 dB

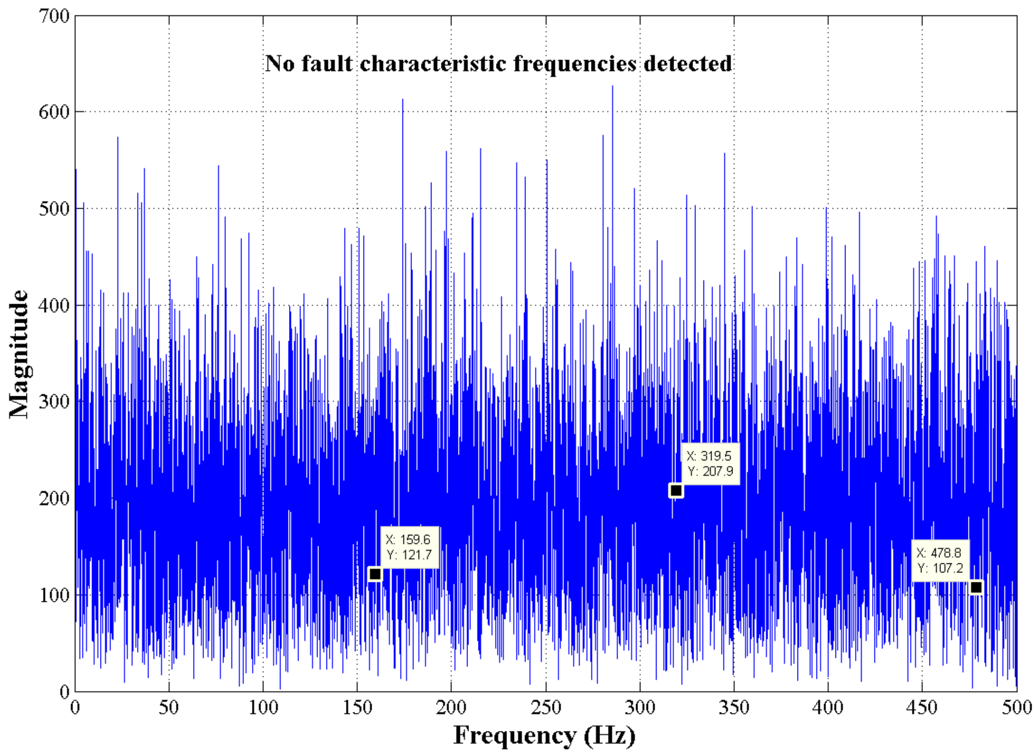

Figure 6.14 Twice applied TKEO spectrum for IF: SNR= -30 dB

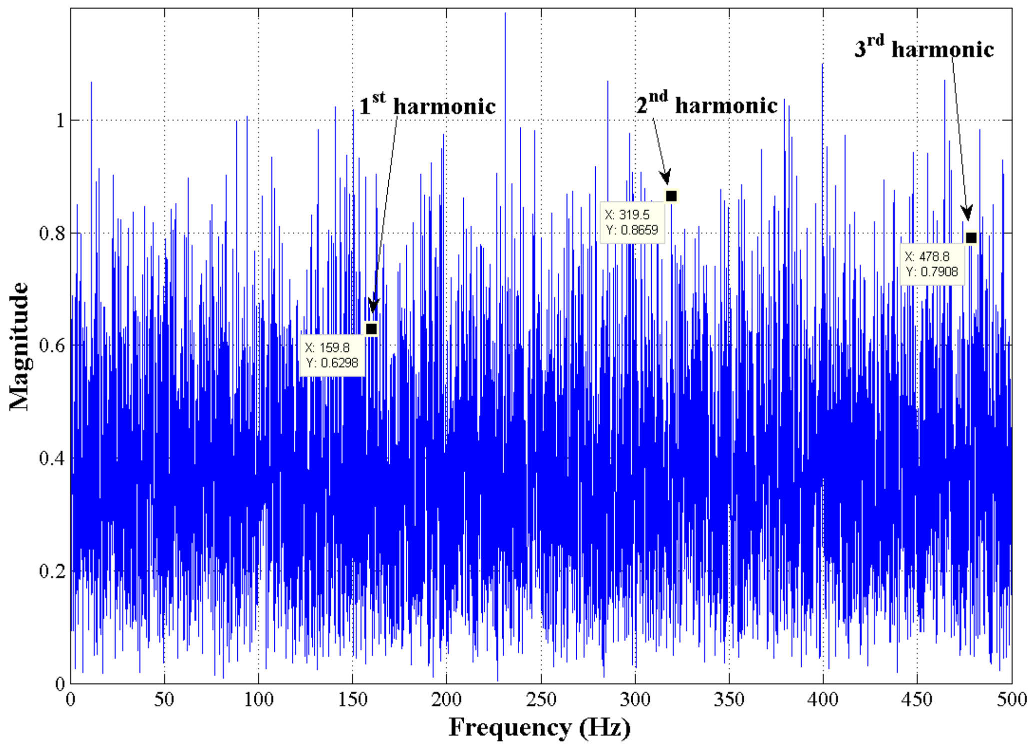

Figure 6.15 27-TKEO spectrum for IF: SNR= -30 dB

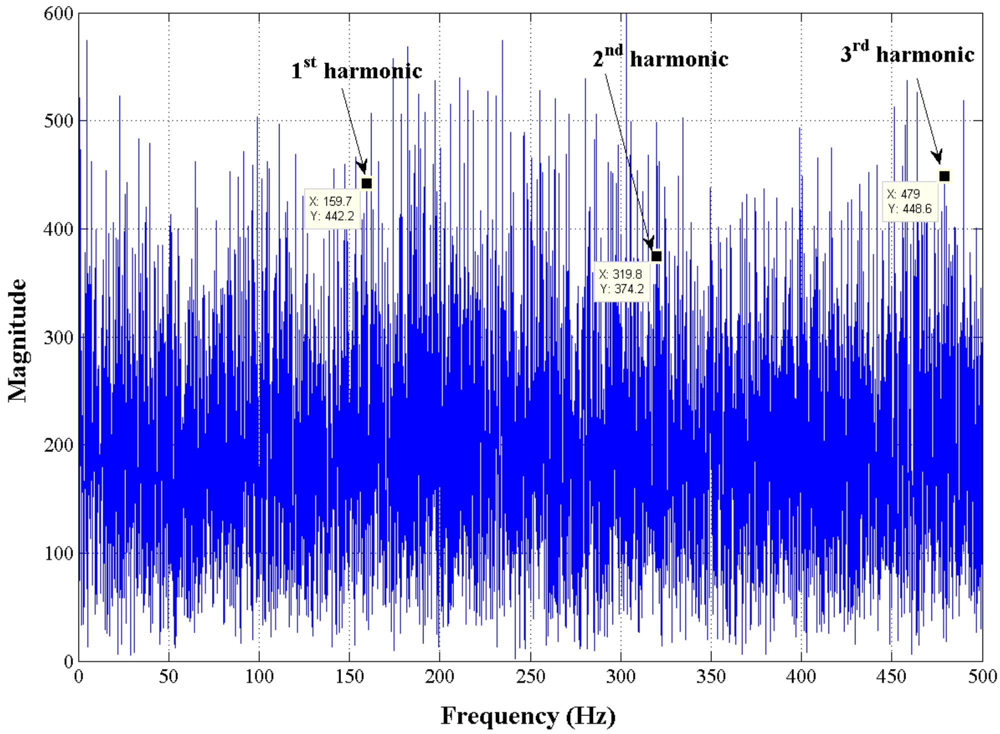

Figure 6.16 Twice applied 27-TKEO spectrum for IF: SNR= -30 dB

6.4.2 APPLICATION TO TEST DATA2

Test data2 setup (section 3.3.2) consists of vibration interference source of gearbox. The number of teeth in gearbox is 32. The shaft speed is 6 Hz. In this chapter, Test data2 signals of outer race fault and ball fault are considered. In addition to the recorded signals, white gaussian noise is added (similar to Test data1) to it to obtain signals with SNR=-15 dB. The recorded signals already has a background noise, hence only SNR of -15dB is considered. Two cases of signals: without additive noise and SNR of -15 dB are analyzed for the two fault conditions considered.

6.4.2.1 Outer race fault detection

The theoretical fundamental fault frequency for bearing with outer race fault (OF) is 29.34 Hz. The gear meshing frequency is 192 Hz (No. of teeth's x shaft speed).

6.4.2.1.1 OF signal: without any additive noise

First, TKEO is applied to the signal. No FCF's are visible in its spectrum (figure 6.17). Then, to check whether repetitive TKEO can provide any fault information, TKEO is applied twice and its spectrum is given in figure 6.18. From this plot, the outer race fault is detected as FCF harmonics are detected (29.28, 59.04, 88.32, 117.6, 146.9, 176.6 and 205.9 Hz). Also, the shaft speed and gear mesh frequency are also seen.

M=89 is obtained from the ER plot (figure 6.19). M-TKEO (M=89) is applied and its spectrum is calculated (figure 6.20). FCF harmonics are detected (29.28, 88.32 and 146.9 Hz). It is observed that, both twice operation of TKEO and single M-TKEO easily detect the outer race fault. But, the frequencies obtained in twice operation of TKEO (figure 6.18) are more dominant and more number of frequencies are detected as compared with M-TKEO (figure 6.20).

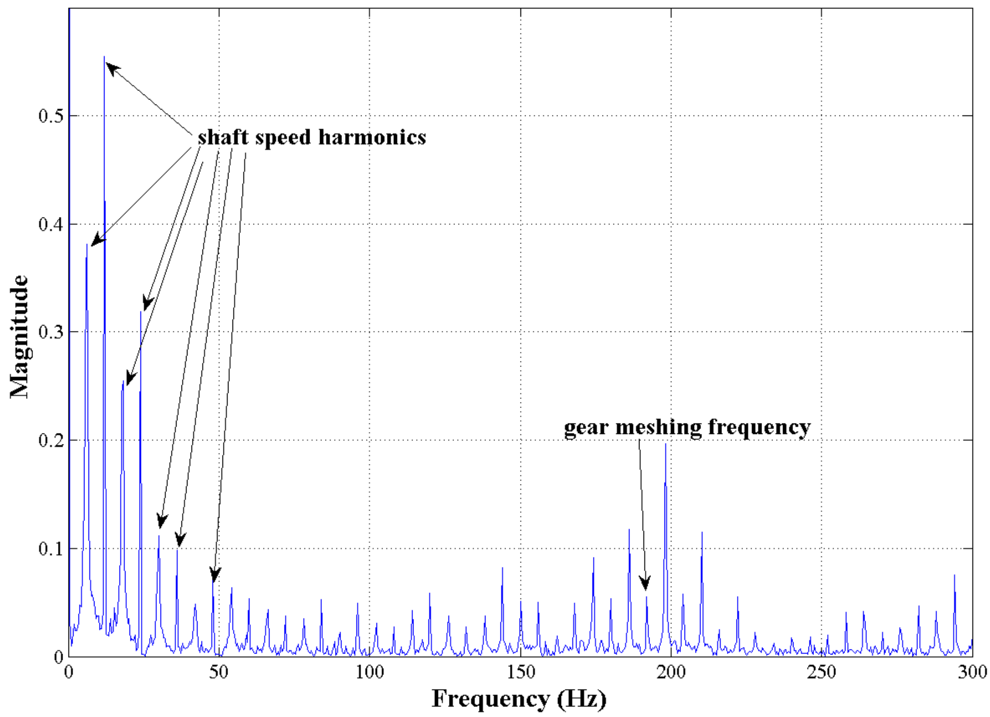

Figure 6.17 TKEO spectrum for OF: no noise added

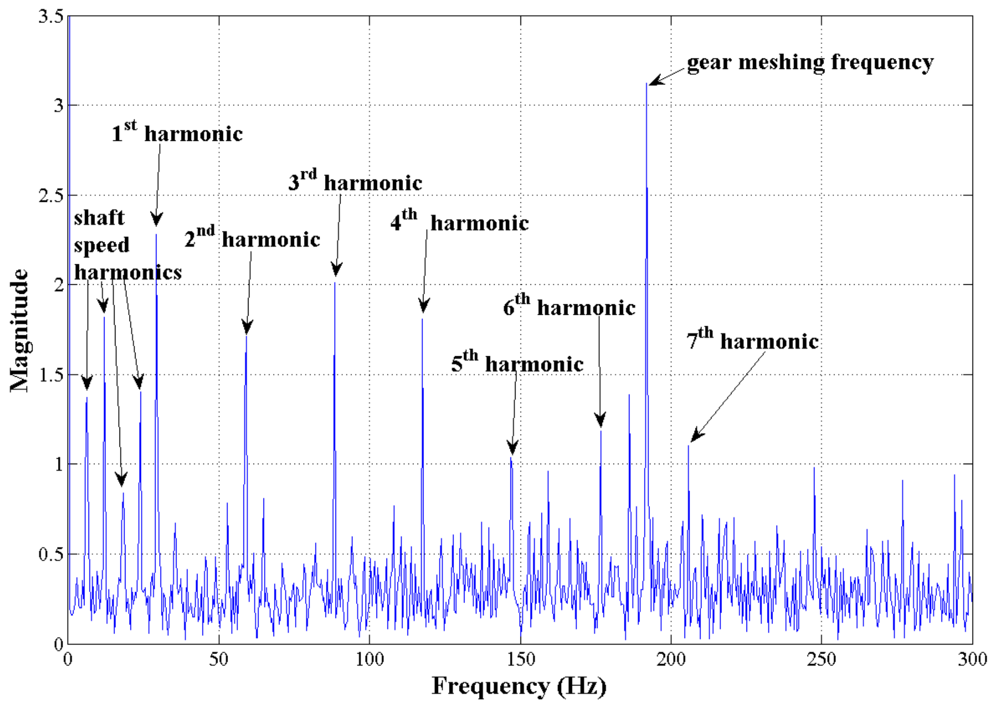

Figure 6.18 Twice applied TKEO spectrum for OF: no noise added

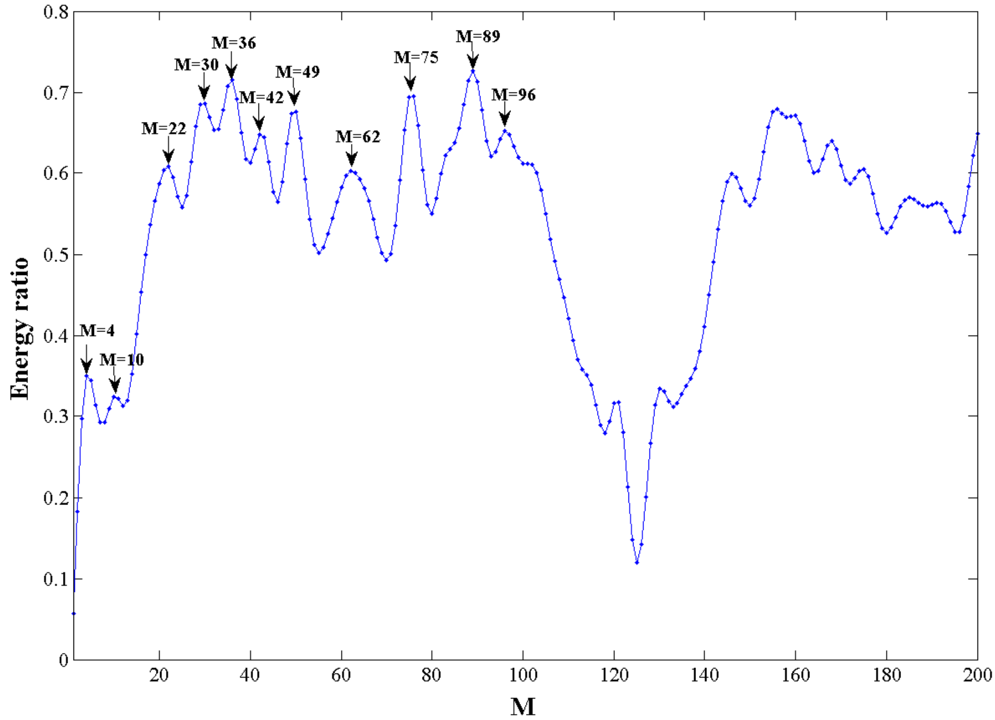

Figure 6.19 ER plot for OF: no noise added

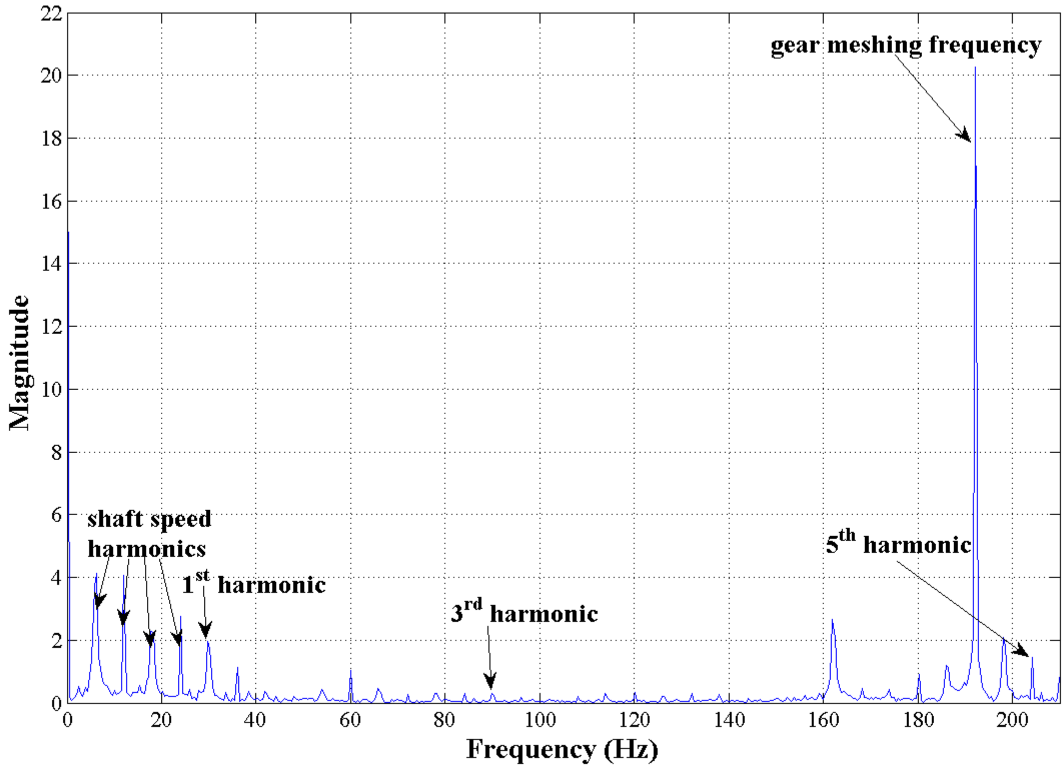

Figure 6.20 89-TKEO spectrum for OF: no noise added

6.4.2.1.2 OF signal: SNR= -15 dB

TKEO spectrum obtained for the signal is shown in figure 6.21 and only 3rd harmonic (88.32 Hz) is seen in this spectrum. Also, TKEO is applied twice to the signal and its spectrum is displayed in figure 6.22. In this plot, 4th and 5th fault harmonics are visible. M-TKEO (M=11) spectrum (figure 6.23) shows many FCF's (1st, 2nd, 4th, 5th and 7th). In this case, M-TKEO gives more fault information than TKEO.

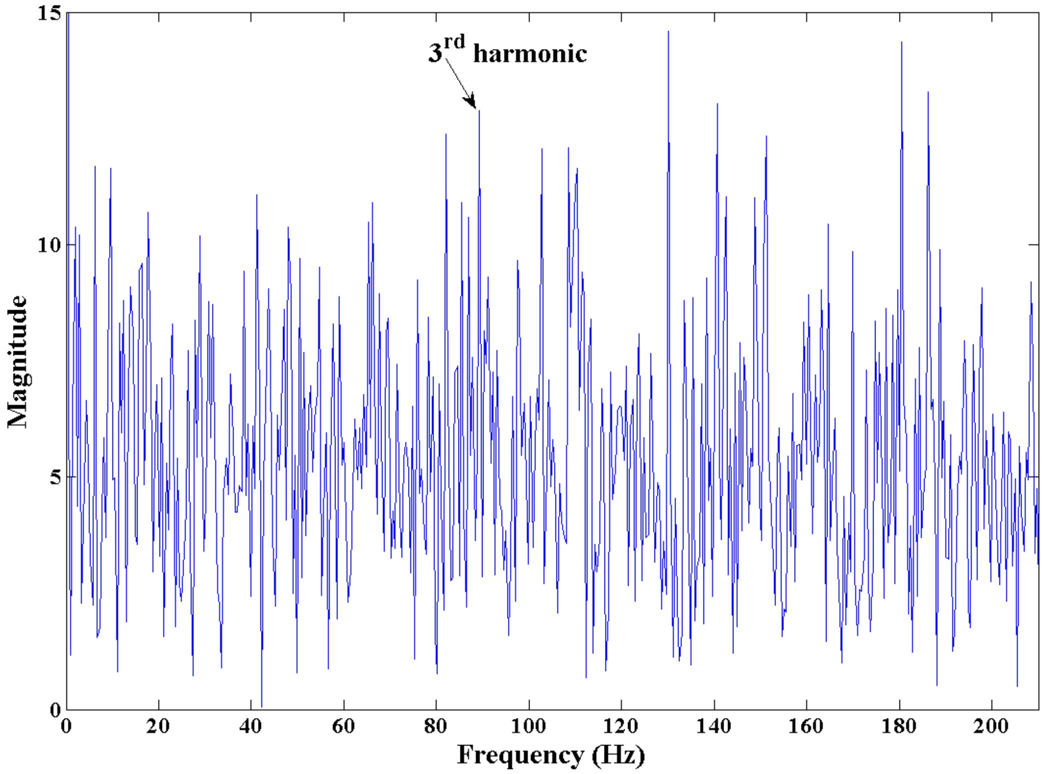

Figure 6.21 TKEO spectrum for OF: SNR= -15 dB

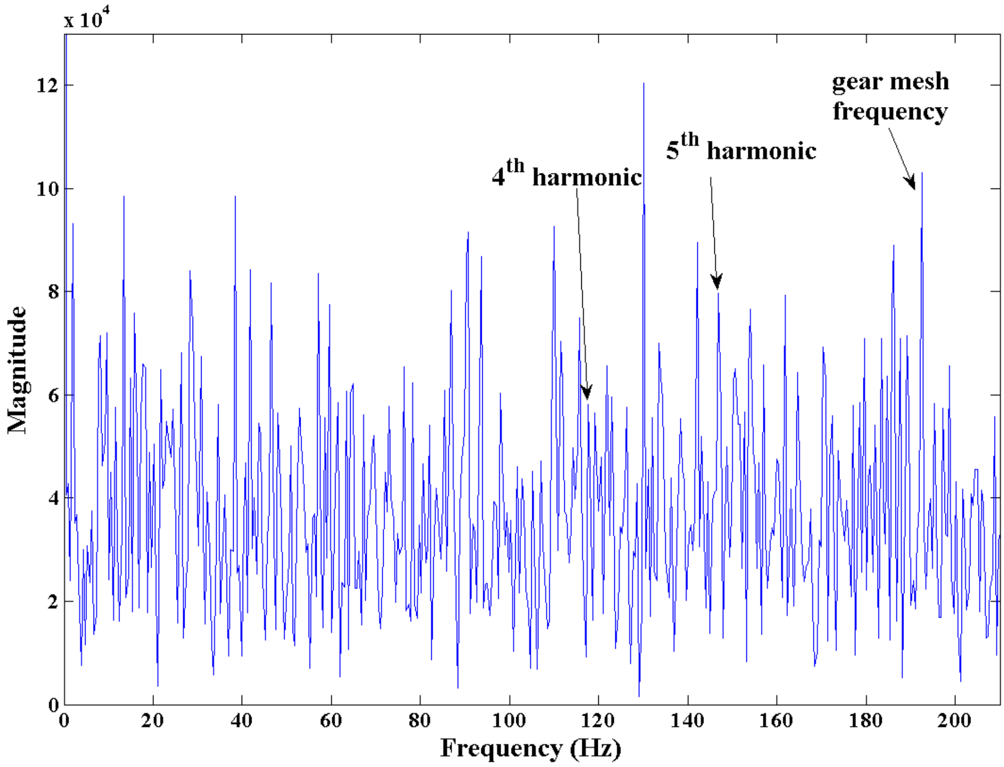

Figure 6.22 Twice applied TKEO spectrum for OF: SNR= -15 dB

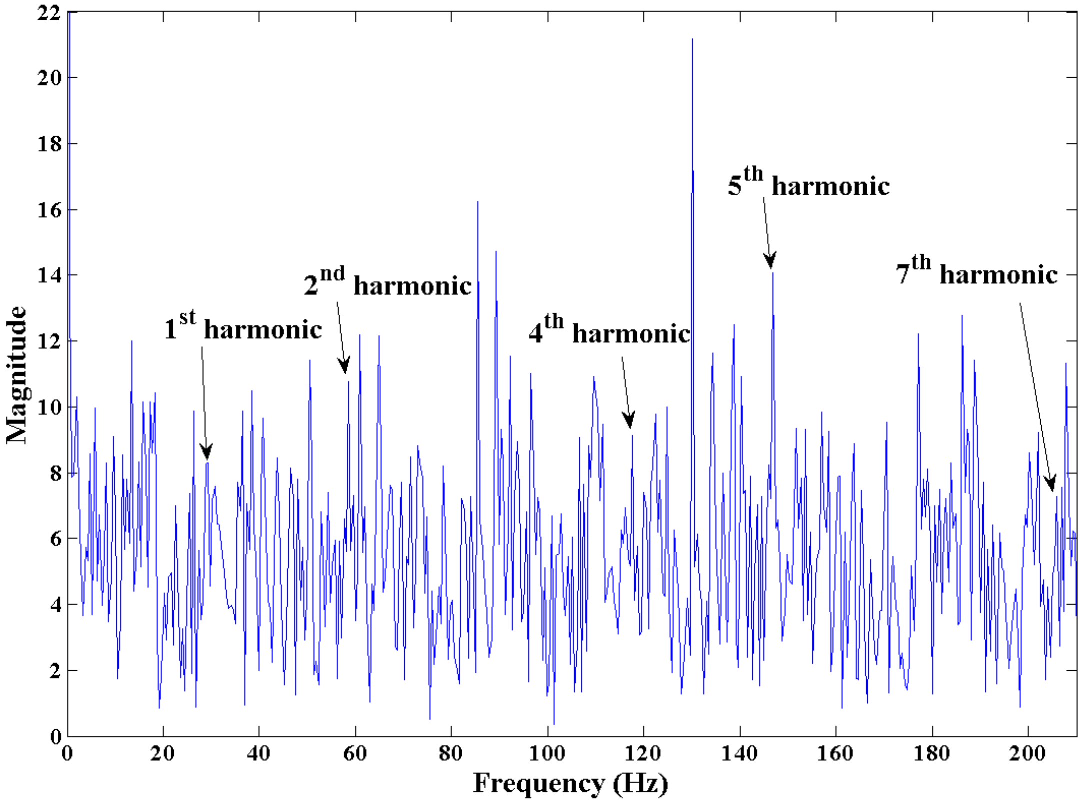

Figure 6.23 11-TKEO spectrum for OF: SNR= -15 dB

6.4.2.2 Ball fault detection

The fundamental fault characteristic frequency for ball fault (BF) is 31.33 Hz. The shaft speed is 6 Hz.

6.4.2.2.1 BF signal: without any additive noise

With no noise added, TKEO identifies the BF easily and fault harmonics from number 1 to 10 are detected as shown in figure 6.24. While for M-TKEO (M=11), 2nd, 5th, 6th, 8th and 10th harmonics are seen in the spectrum (figure 6.25). In this case, it is seen that in comparison with M-TKEO, the fault frequencies are dominant and very much clear in TKEO.

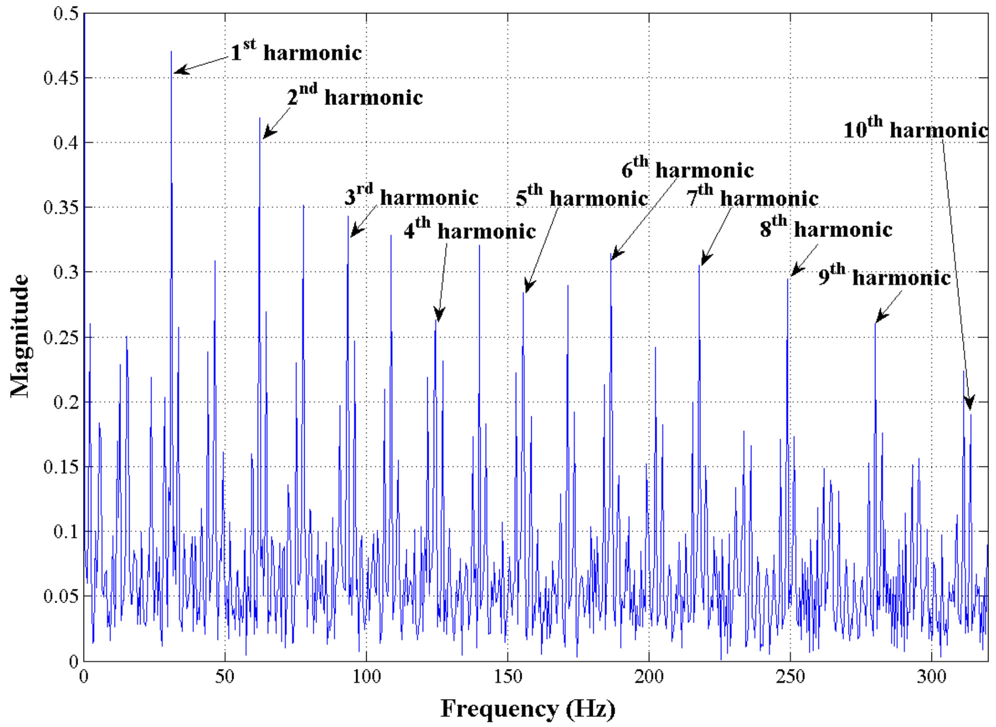

Figure 6.24 TKEO spectrum for BF: no noise added

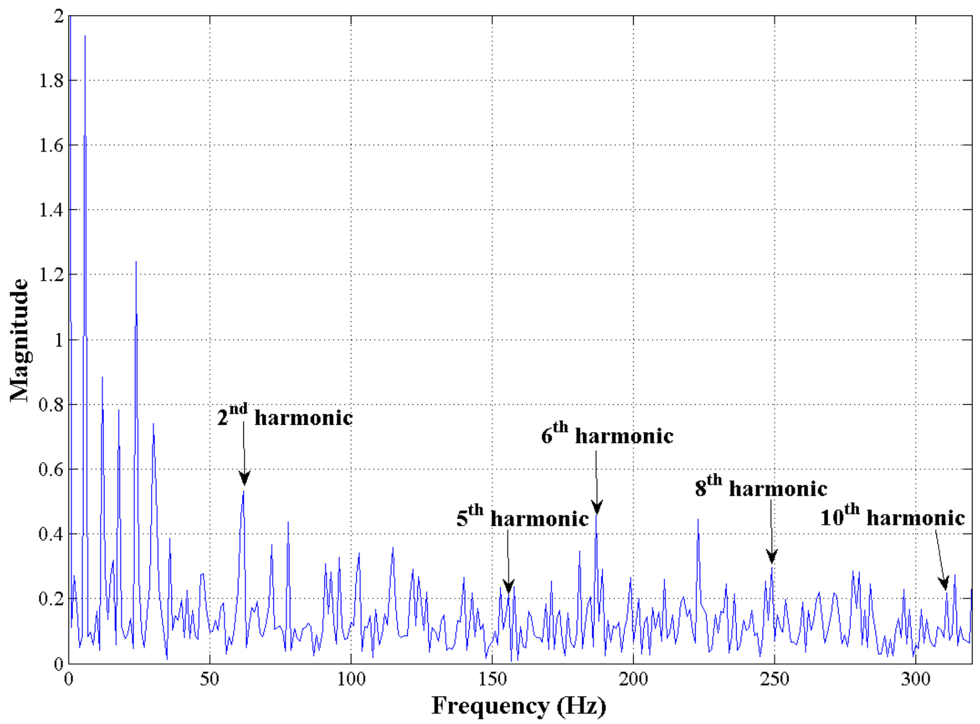

Figure 6.25 11-TKEO spectrum for BF: no noise added

6.4.2.2.2 BF signal: SNR= -15 dB

The spectrum of TKEO is shown in figure 6.26 and it shows the presence of 3rd and 7th FCF harmonics. To check whether further improvement could be obtained, repetitive TKEO is carried out. TKEO is applied twice and thrice to the signal and their spectrums are displayed in figures 6.27 and 6.28 respectively. No increase in number of fault frequencies was observed in these figures: 1st and 7th harmonic in twice TKEO (figure 6.27), while only 7th harmonic in thrice TKEO (figure 6.28) are detected. M-TKEO (M=14) spectrum (figure 6.29) is plotted for the signal and various fault frequencies harmonics are detected (2nd, 4th (low amplitude), 5th, 6th, 8th and 9th). As seen from these results, M-TKEO detects fault easily and better than TKEO.

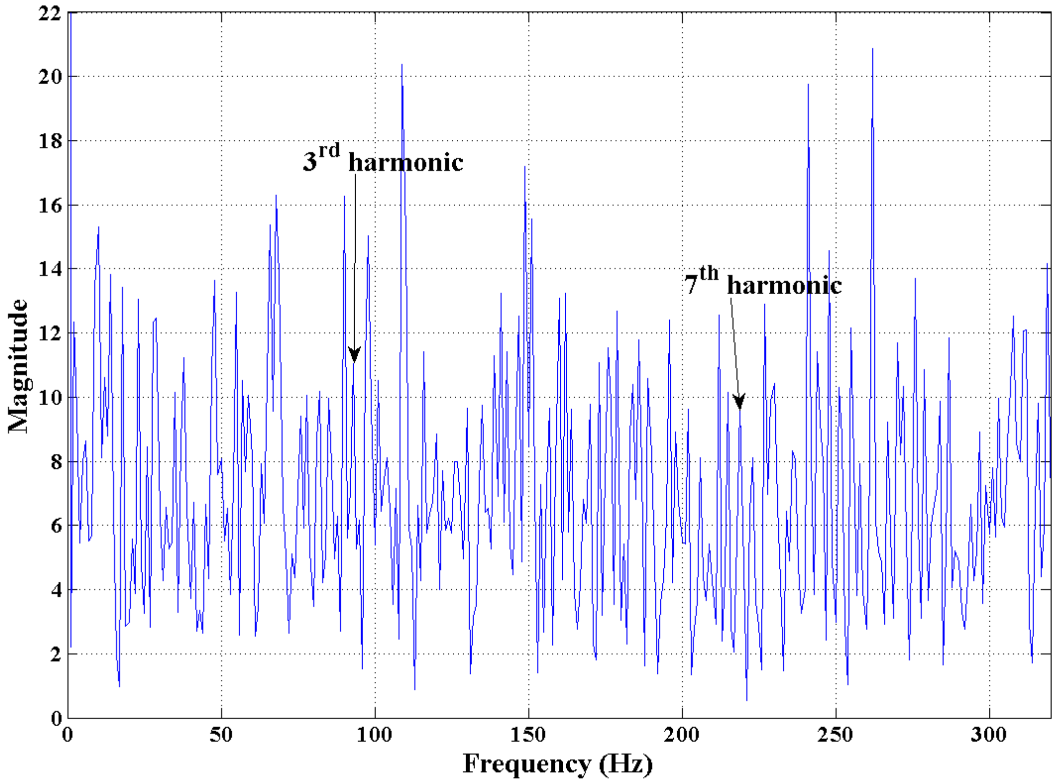

Figure 6.26 TKEO spectrum for BF: SNR= -15 dB

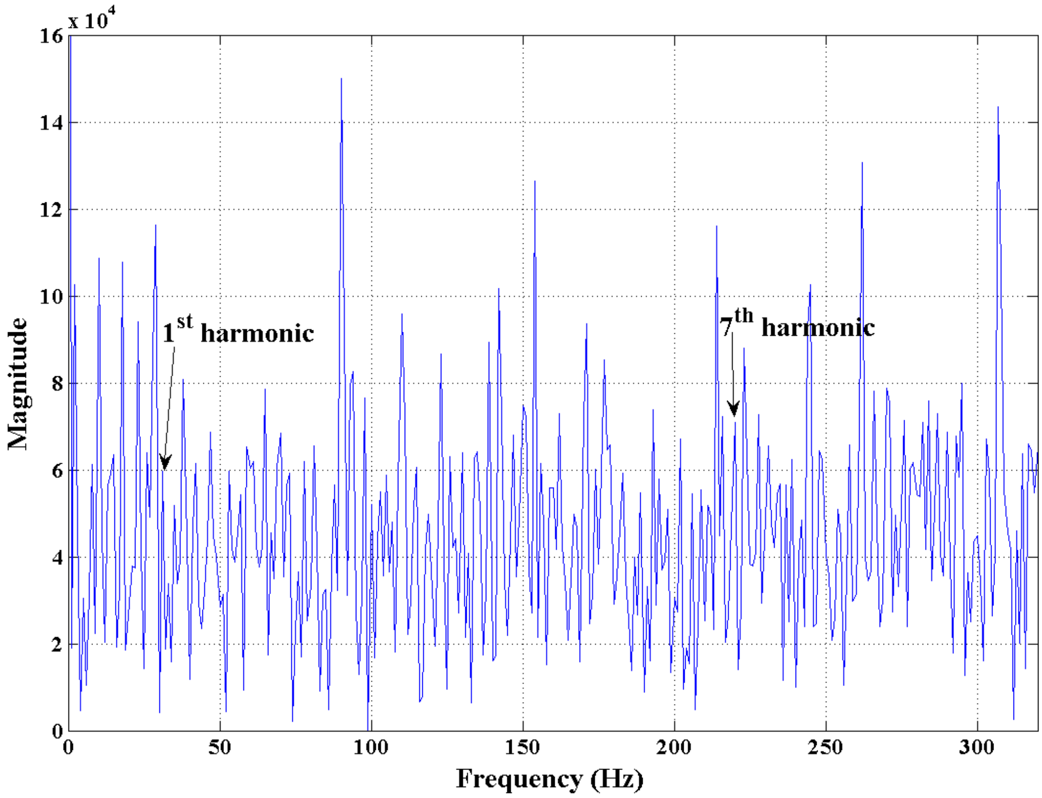

Figure 6.27 Twice applied TKEO spectrum for BF: SNR= -15 dB

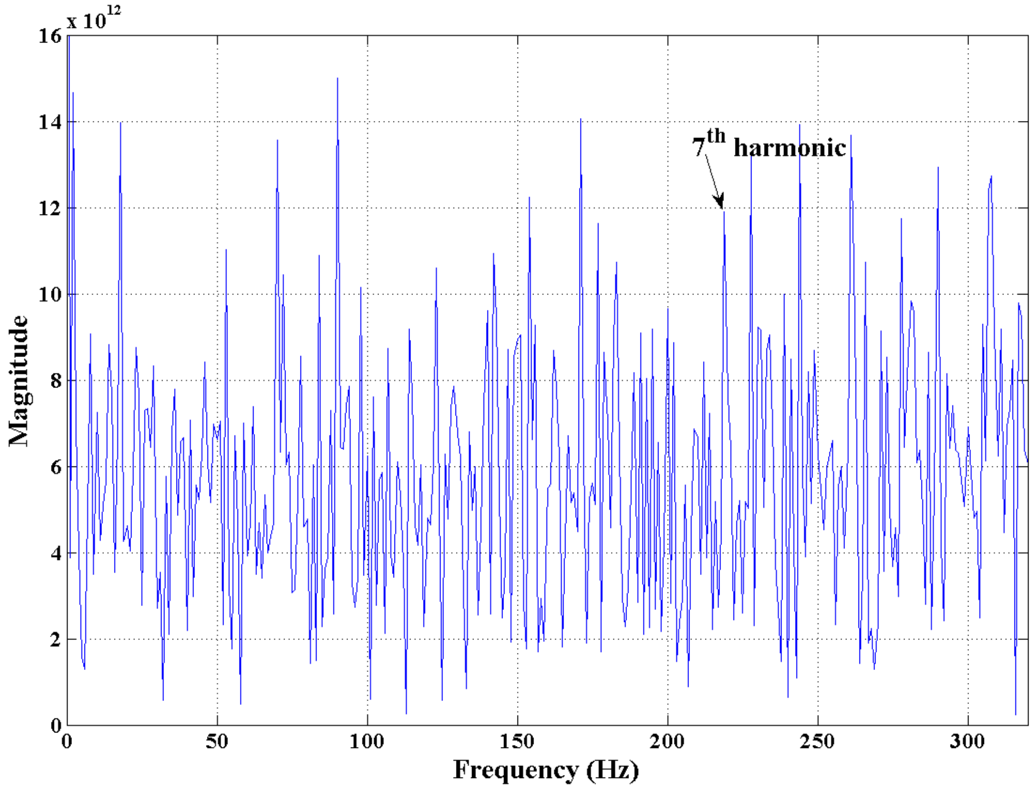

Figure 6.28 Thrice TKEO spectrum for BF: SNR= -15 dB

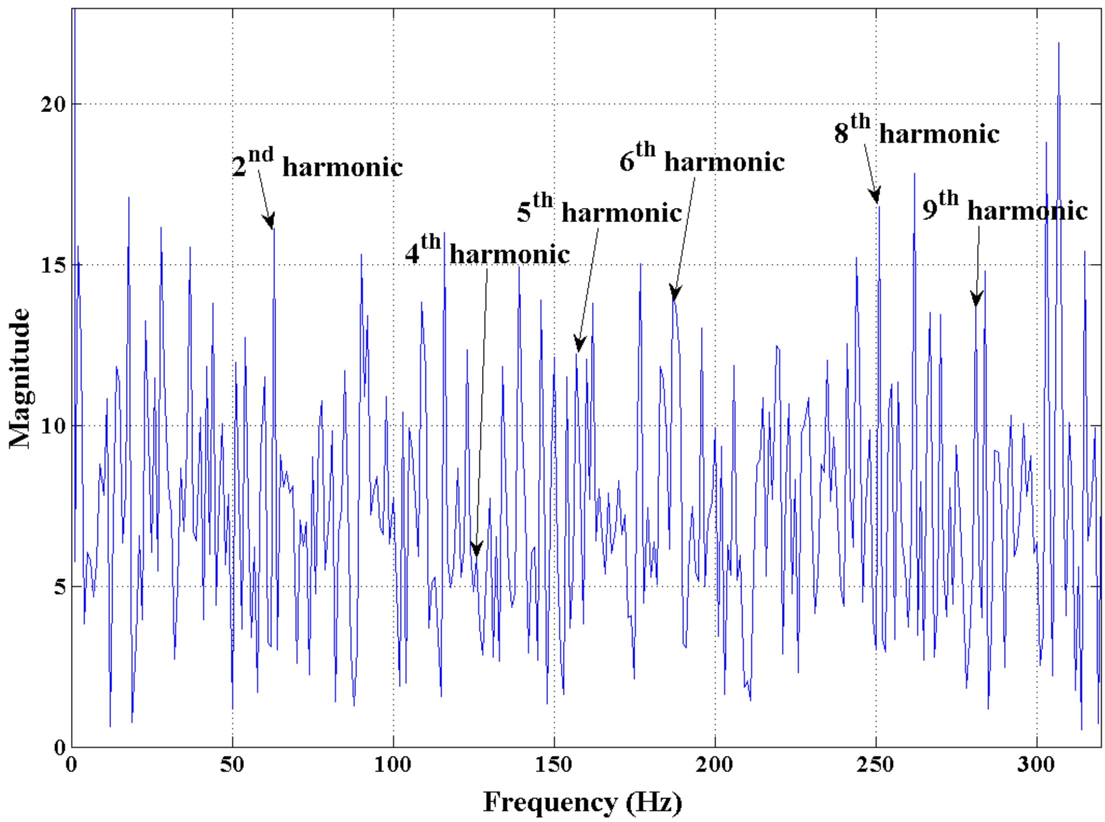

Figure 6.29 14-TKEO spectrum for BF: SNR= -15 dB

6.5 DISCUSSION BASED ON TEST DATA1 AND TESTDATA2 RESULTS

The performance comparison of M-TKEO and TKEO methods are done on the basis of the experimental results obtained which are summarized in the tables 6.1 to 6.3.

From these tables (6.1, 6.2 and 6.3), for no additive noise case, TKEO detects fault better than M-TKEO. However, in very low SNR conditions, M-TKEO outperforms TKEO. For signal of SNR = -30 dB (table 6.1), TKEO and repetitive TKEO failed to show any of the FCFs, whereas M-TKEO was able to detect in that case. For SNR= -15 dB case, M-TKEO showed more number of FCFs as compared to TKEO (tables 6.2 and 6.3). In case of low SNR signal obtained in the presence of gearbox (test data2), repetitive TKEO did not show much improvement in its fault detection capability. As the number of TKEO applied increased, it increased the noise level in the spectrum. This made the FCFs to be masked by the noise in the repetitive TKEO spectrum (table 6.3, SNR = -15 dB). M-TKEO clearly identifies the bearing faults in all the cases. No repetitive M-TKEO application is required.

From the results of obtained, it is seen that M-TKEO has better fault detection ability than TKEO for signals with very low SNR.

Table 6.1 Comparison of TKEO and M-TKEO: IF signal (Test data1)

Signal	**Energy operator**	**Fault harmonics detected**
without noise	TKEO	1^{st} to 6^{th}
	3-TKEO and 6-TKEO	1^{st} to 6^{th}
SNR= -15 dB	TKEO	1^{st}
	TKEO (twice applied)	1^{st} and 5^{th}
	6-TKEO	1^{st} (dominant), 2^{nd}, 3^{rd}, 4^{th} and 5^{th}
SNR= -30 dB	TKEO	no detection
	TKEO (twice, thrice and four consecutive application)	no detection
	27-TKEO	1^{st} , 2^{nd} and 3^{rd}
	27-TKEO (twice applied)	1^{st} , 2^{nd} and 3^{rd} (more clear than single 27-TKEO)

Table 6.2 Comparison of TKEO and M-TKEO: OF signal (Test data2)

Signal	Energy operator	Fault harmonics detected
without noise	TKEO	no detection
	TKEO (twice applied)	1^{st} to 7^{th}
	89-TKEO	1^{st}, 3^{rd} and 5^{th}
SNR= -15 dB	TKEO	3^{rd}
	TKEO (twice applied)	4^{th} and 5^{th}
	11-TKEO	1^{st} , 2^{nd} , 4^{th} , 5^{th} and 7^{th}

Table 6.3 Comparison of TKEO and M-TKEO: BF signal (Test data2)

Signal	Energy operator	Fault harmonics detected
without noise	TKEO	1^{st} to 10^{th}
	11-TKEO	2^{nd} , 5^{th} , 6^{th}, 8^{th} and 10^{th}
SNR= -15 dB	TKEO	3^{rd} and 7^{th}
	TKEO (twice applied)	1^{st} and 7^{th}
	TKEO (thrice applied)	7^{th}
	14-TKEO	2^{nd}, 4^{th} , 5^{th} , 6^{th} , 8^{th} and 9^{th}

6.6 VALIDATION OF THE GTKEO METHOD

Industrial data is used for validating the GTKEO or M-TKEO method of fault diagnosis. It is obtained from the Society for Machinery Failure Prevention Technology [MFPT]. There are three real world cases: an oil pump shaft bearing from a wind turbine (figure 6.30(a)), an intermediate shaft bearing from a wind turbine (figure 6.30(b)) and a planet bearing fault (figure 6.30(c)).

(a)

(b)

(c)

Figure 6.30 Industrial data's: a) Oil Pump location; b) Intermediate shaft location and c) planet bearing

Two of these industrial data's are obtained from a 2 MW wind turbine. Red dot (figure 6.30a) shows the location of the low speed shaft accelerometer, which is used for the oil pump analysis. The pump is out of the frame - its low and to the left of the red dot. The shield (figure 6.30b) is covering the high speed shaft - the intermediate shaft is lower and to the left. Planet bearing is shown in figure 6.30c. The three cases which are diagnosed using M-TKEO are given below:

6.6.1 Intermediate Shaft Gearbox bearing

The data was obtained at a speed of 6.3289 Hz and load of 300 Nm. The sampling frequency is 48 kHz. The fault characteristic frequencies given in its data site [MFPT] are: f_o=51.9 Hz; f_c=2.76 Hz; f_i= 67.84 Hz; f_b= 24.3 Hz.

Figure 6.31 displays the signal obtained from the bearing of intermediate shaft gearbox of wind turbine. Energy ratio plot (figure 6.32) gives the optimal value of M as 8. At this value, M-TKEO spectrum was obtained and the dominant frequency of 23.4 Hz was observed (figure 6.33). This frequency value is close to fault characteristic frequency (24.3 Hz) for ball fault. Thus, ball fault is detected in the bearing of intermediate shaft gearbox.

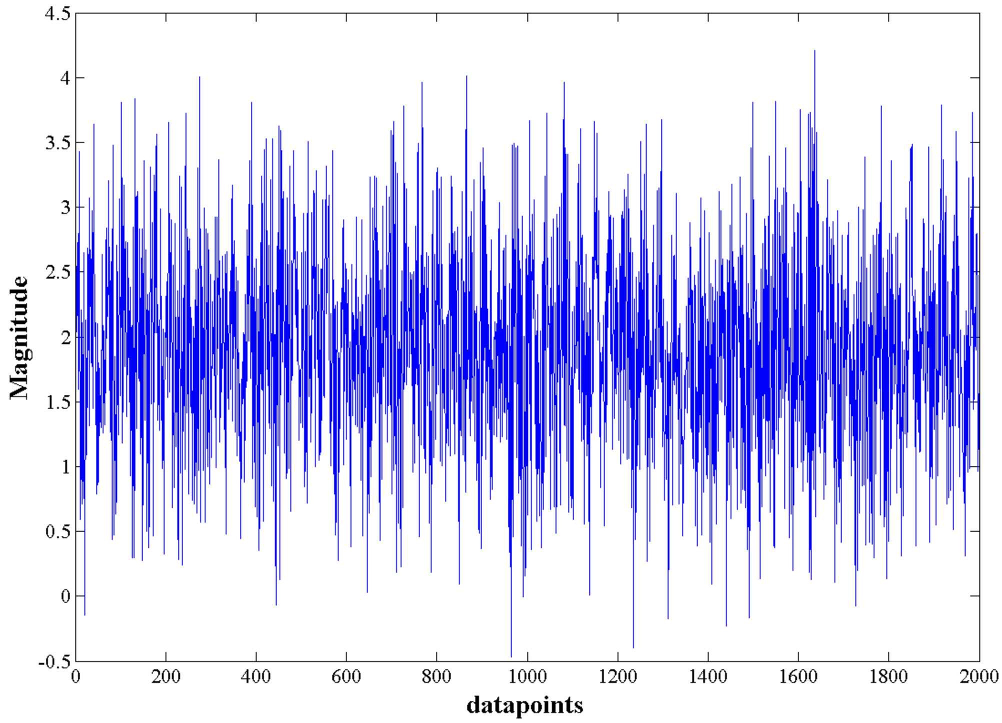

Figure 6.31 Signal obtained for bearing fault in intermediate shaft gearbox

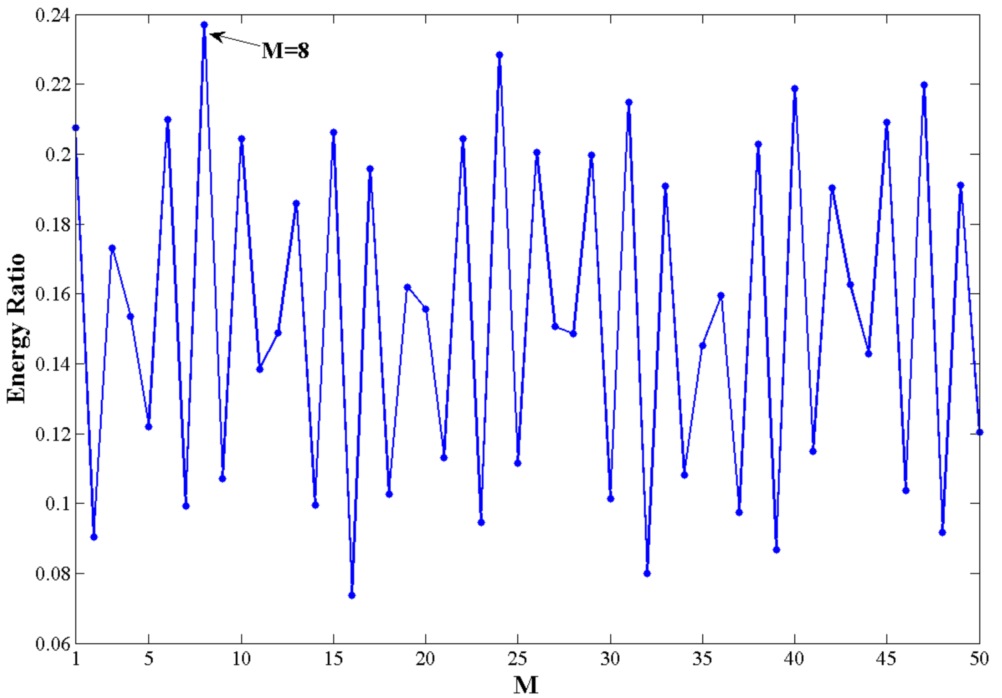

Figure 6.32 ER plot for intermediate shaft gearbox bearing signal

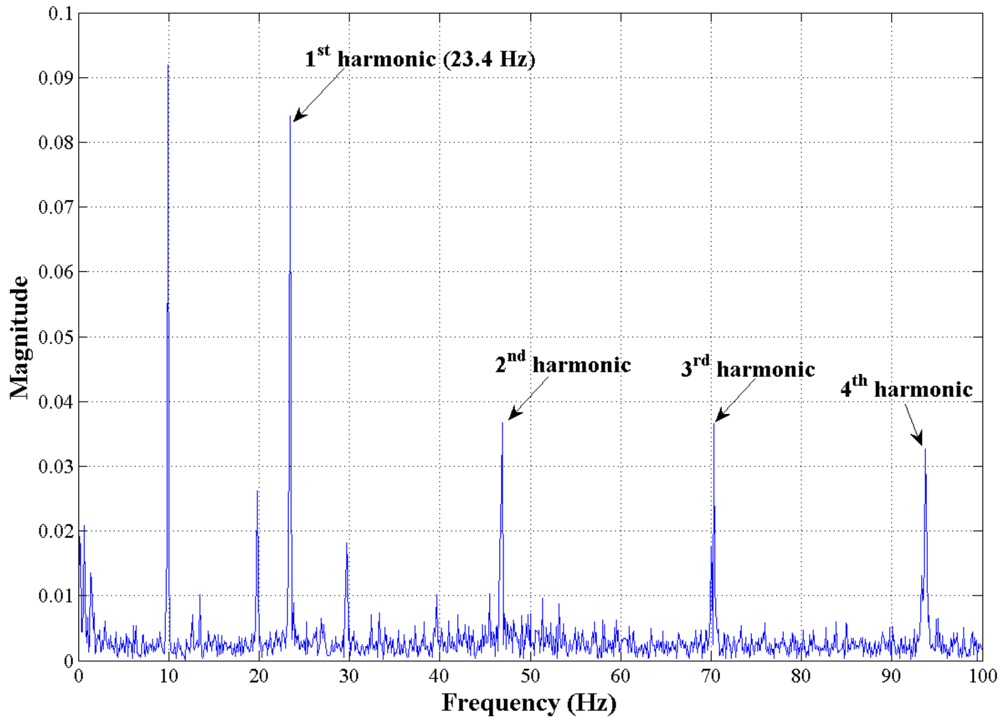

Figure 6.33 8-TKEO spectrum for intermediate shaft gearbox bearing signal

6.6.2 Oil pump shaft bearing

The signal of the oil pump shaft bearing is obtained at a shaft speed of 9.5155 Hz using the sampling frequency of 24 kHz under a load of 300 Nm. The theoretical fault characteristic frequencies given in its data site [MFPT] are: f_o=78.5 Hz; f_c=7.89 Hz; f_i= 114.19 Hz; f_b= 35.68 Hz.

The vibration signal obtained from the shaft of oil pump is given in figure 6.34. Energy ratio plot is shown in figure 6.35, it shows the optimum value of M as 4. Initially, 4-TKEO spectrum was obtained but no dominant frequency was obtained. Hence, two times the 4-TKEO signal spectrum was obtained (figure 6.36). A dominant frequency of 114.4 Hz was observed. This matches with inner race fundamental fault characteristic frequency. Hence, it was concluded that an inner race fault has occurred in the bearing of the oil pump.

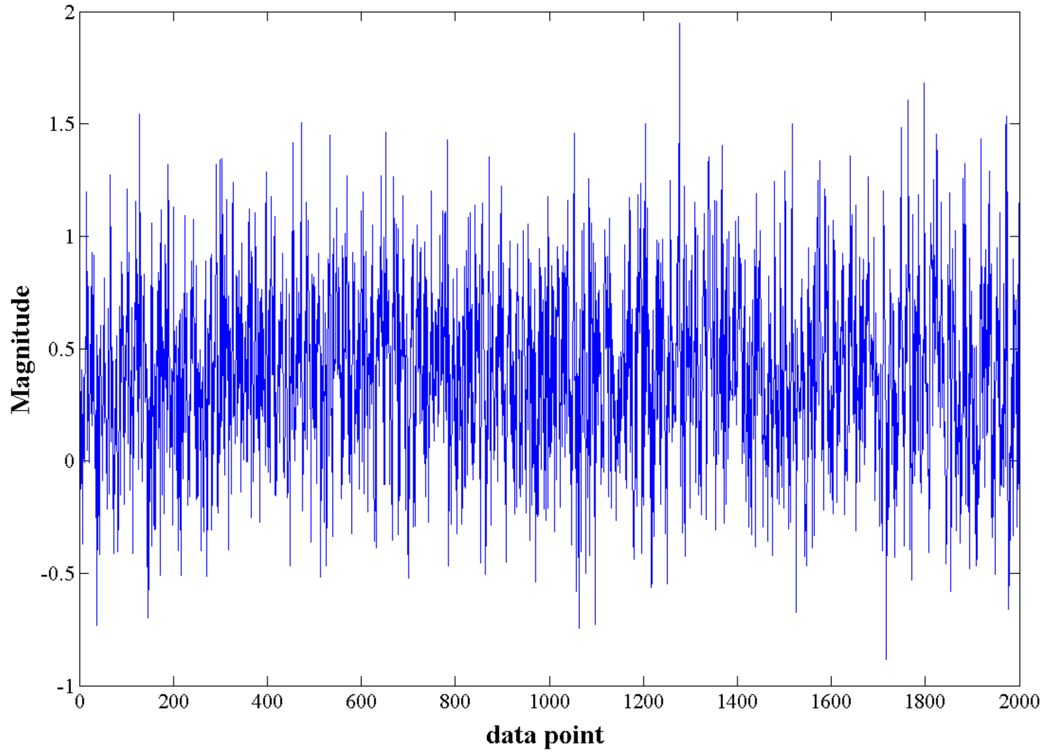

Figure 6.34 Signal obtained for bearing fault in oil pump shaft

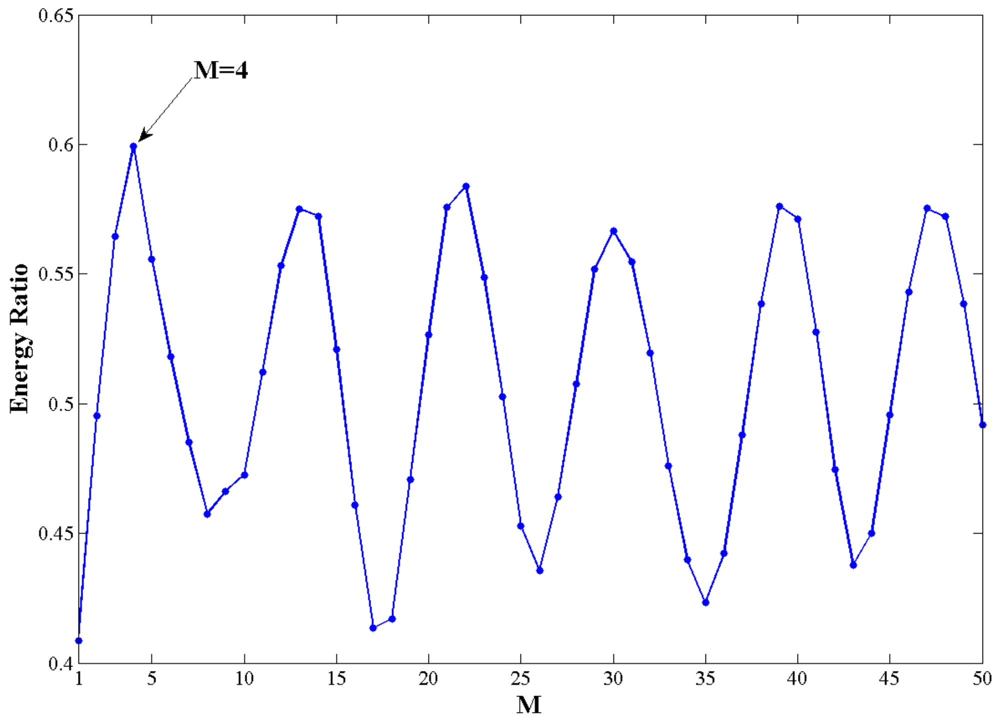

Figure 6.35 ER plot for oil pump shaft bearing

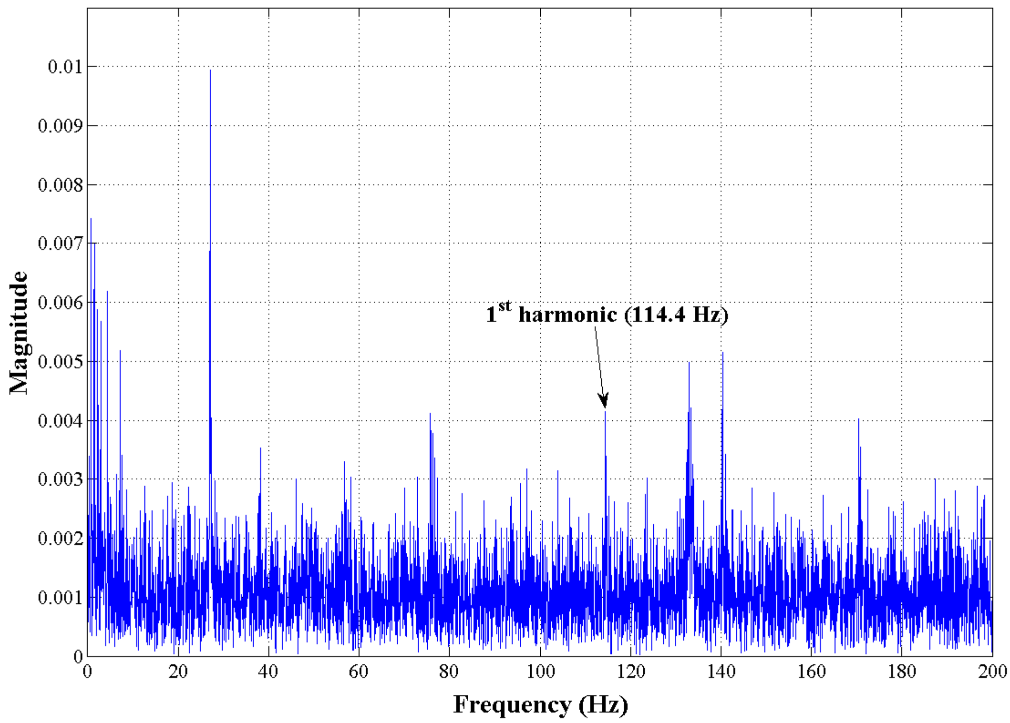

Figure 6.36 Twice applied 4-TKEO spectrum: oil pump shaft bearing

6.6.3 Planet Bearing

The planet bearing data is obtained at a speed of 0.6229 Hz. The sampling frequency is 6 kHz. The theoretical fault characteristic frequencies given in its data site [MFPT] are: f_o=6.38 Hz; f_c=0.69 Hz; f_i= 8.12 Hz; f_b= 2.94 Hz.

Figure 6.37 provides the vibration signal obtained from the planet bearing. An optimum value of M as 12 (figure 6.38) is obtained from the energy plot of the obtained signal. 12–TKEO spectrum (figure 6.39) shows two dominant frequencies of 2.95 Hz and 6.33 Hz. Referring to the theoretical fault characteristic frequencies, it is observed that there is a occurrence of ball fault (2.95 Hz) and the outer race fault (6.33 Hz).

The results of the above three cases were verified with Dr. Eric Bechhoefer, NRG Systems, who has prepared these industrial datasets on behalf of the Society for Machinery Failure Prevention Technology. The accuracy in diagnosing the fault of industrial data's shows the efficiency and applicability of the GTKEO method for real life applications.

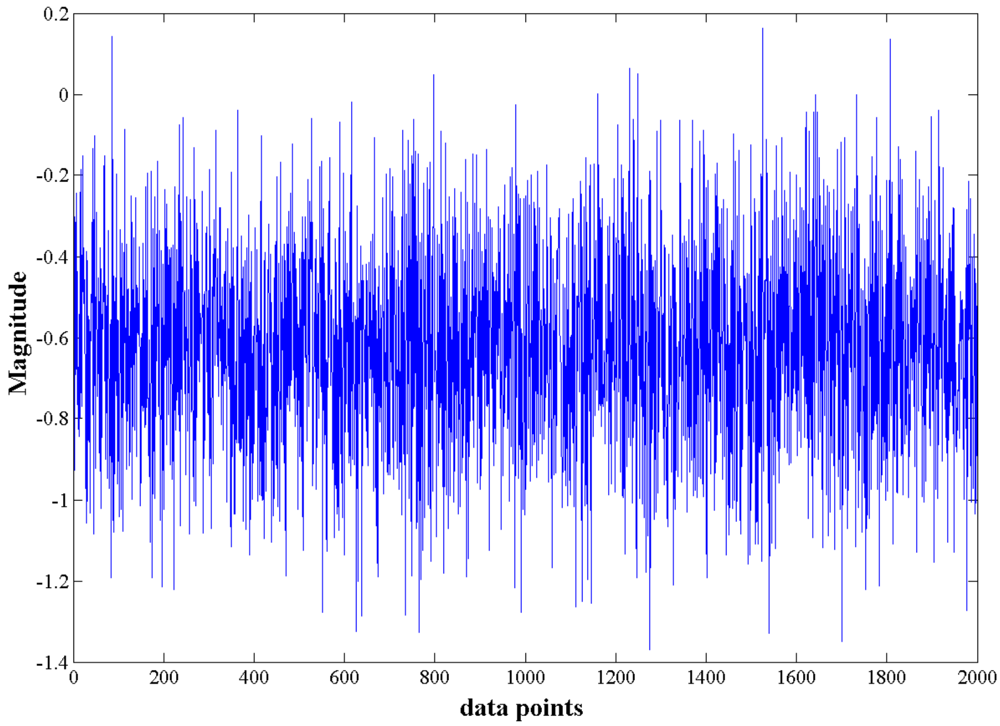

Figure 6.37 Signal obtained for fault in planet bearing

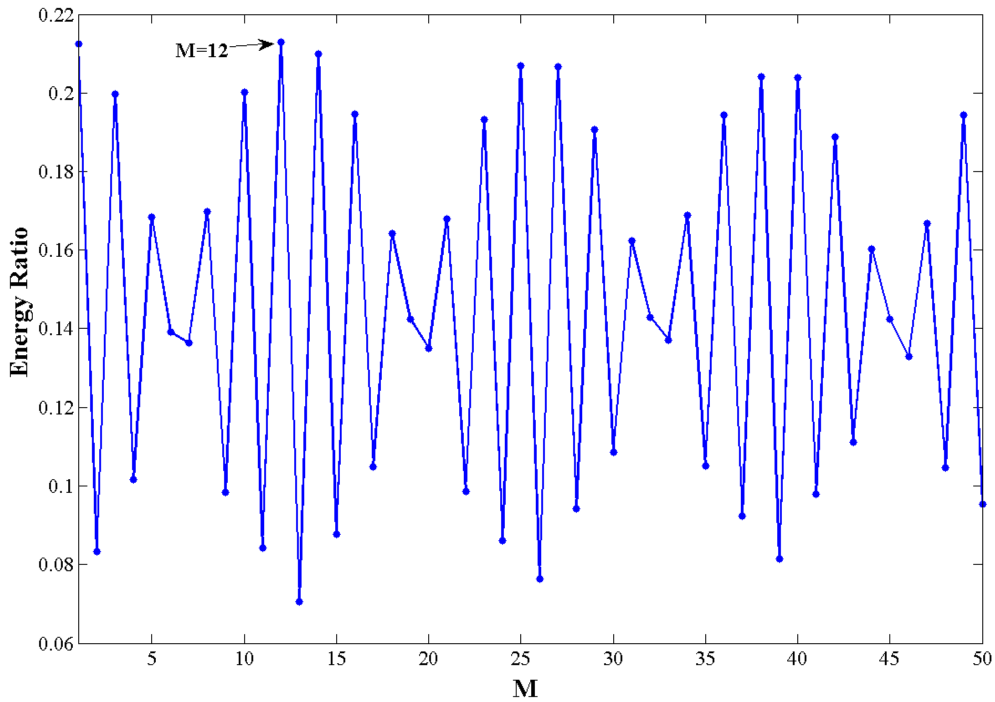

Figure 6.38 ER plot for planet bearing fault

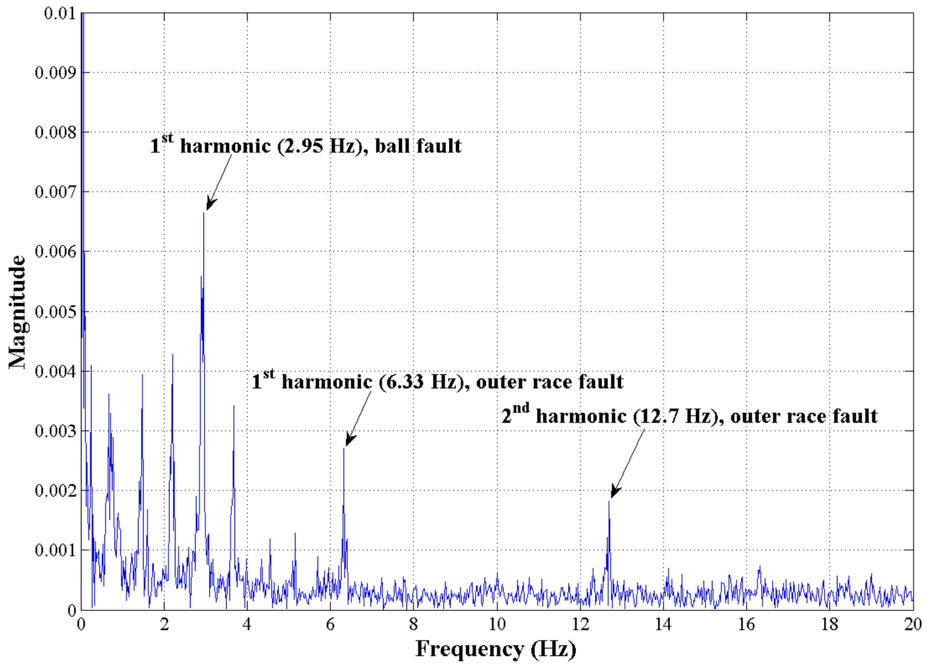

Figure 6.39 12-TKEO spectrum of planet bearing fault

6.7 SUMMARY

This chapter discussed a simple method for bearing fault diagnosis based on Generalized Teager Kaiser Energy Operator (GTKEO) which incorporates demodulation. The diagnosis method involves the transformation of the signal using GTKEO and then spectral analysis. The presented method (GTKEO or M-TKEO) is compared with a parameter-free method (TKEO).The deficiency of the TKEO method for fault diagnosis under very low SNR is shown through experimentally obtained bearing fault data's: with and without gearbox. The fault detection ability of energy operator is improved for signals with low SNR using the M-TKEO approach. Only one parameter (M) is required for calculation which is easily obtained by using Energy Ratio plot. The M value is adaptive according to the signal and interfering components such as noise and gearbox.

From the experimental results, it is seen that M-TKEO suppresses the effects of additive noise. No repetitive operation of M-TKEO is needed as required for TKEO. The effectiveness of M-TKEO over TKEO in locating the bearing fault in low SNR and also in the presence of vibration interference component such as from gears is demonstrated.

M-TKEO satisfies the requirements of a spectrum based fault diagnosis method. It is simple in calculation and requires only one parameter which is also easily calculated. It works very well under the presence of gearbox and even under very low SNR scenario.

PART IV

FAULT PROGNOSIS (FAULT DEGRADATION)

CONTENTS:

CHAPTER 7

PERFORMANCE INDEX DEVELOPMENT FOR FAULT DEGRADATION USING THE SUPPORT VECTOR DATA DESCRIPTION METHOD

MAIN CONTENTS:

- **Introduction**
- **Support Vector Data Description**
- **Experimental Test data**
- **Fault Features and its Trend**
- **Bearing Fault Degradation Indicator Development**
  - Procedure for the Performance Index Calculation
  - Performance Index Calculation
  - Comparison with other Index
- **Summary**

7.1 INTRODUCTION

Fault prognosis has more efficiency in obtaining the near zero downtime performance than fault diagnosis [Jardine et al., 2006]. It is carried out in two steps: fault degradation evaluation and calculation of the remaining useful life (RUL). Fault degradation evaluation study provides a performance index to trend the actual condition of a machine. This index is combined with the regression methods such as ANN and Support Vector Machines to calculate the RUL.

There are a few challenges in the fault degradation evaluation or performance degradation assessment. One of them is the selection of fault features which can reflect the bearing condition. Another challenge is the development of an intelligent evaluation method based on these fault features. Some of the fault features used are rms, kurtosis, crest factor, shape factor, impulse factor, clearance factor, skewness, approximate entropy and spectral entropy. These features have certain advantages and limitations which were discussed in the chapter 2 (section 2.7.3).

This chapter describes a method to assess the bearing health using the combination of new fault features and support vector data description (SVDD) classifier. A performance index is developed to trend the bearing condition from its healthy to fault initiation and then till its failure. The fault features used are common signal indexes (CSI1 and CSI3) and ratio of singular values (SVR) which are calculated using the previously discussed methods of symbolic dynamics (chapter 3) and singular spectrum analysis (chapter 4) respectively.

The method is tested using the vibration signals obtained from the accelerated life test of the rolling element bearing. The fault features are calculated for healthy conditions and using SVDD, a hyper sphere is formed using the training data. SVDD requires only healthy data during the training. The test data contains both healthy and fault data.

Performance index is formed based on the distance of the test data to the boundary of hyper sphere.

7.2 SUPPORT VECTOR DATA DESCRIPTION

Support vector data description method (SVDD) [Tax & Duin, 2004] is one of the boundary based method of one–class classifier. It does the classification based on the distance between the test data and the boundary built using the training data's. In SVDD, a hypersphere shaped decision boundary with minimum volume containing the complete training dataset is built. Its schematic diagram is shown in figure 7.1, where target (✧) represents data used for training, outlier◇) represents the data other than the target one and those on the boundary are known as support vectors.

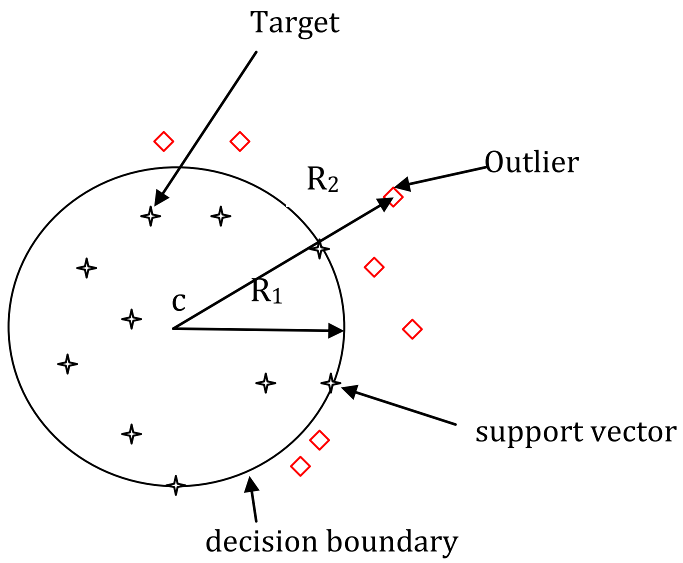

Figure 7.1 Simple representation of SVDD method

For a training dataset {x_i, i=1,2……n} consisting of N normal data objects (targets), a hypersphere with centre c and radius R_1 is described which satisfies the following :

$$\left.\begin{array}{c} \min\ L(R_1,c,\xi) = {R_1}^2 + P\sum_{i=1}^{n}\xi_i \\ s.t\begin{cases}(x_i-c)^T(x_i-c) \leq {R_1}^2+\xi_i \\ \xi_i \geq 0, i=1,2\ldots\ldots n\end{cases}\end{array}\right\} \tag{7.1}$$

where, ξ_i is slack variable which allows some of the target object outside the sphere and P is constant which gives the trade-off between volume of sphere and number of the target objects rejected. The limiting conditions are included into the function by the following Lagrangian:

$$L(R_1, c, \propto_i, \xi_i, \gamma_i) =$$

$$R_1{}^2 + P\sum_{i=1}^{n}\xi_i - \sum_{i=1}^{n}\propto_i \left\{R_1{}^2 + \xi_i - (x_i - 2cx_i + c^2)\right\} - \sum_{i=1}^{n}\gamma_i\,\xi_i \qquad (7.2)$$

where, $\propto_i \geq 0, \gamma_i \geq 0$ are the Lagrange multipliers. L is minimized. The new limiting conditions are obtained by the partial derivative of L with respect to $R_1, c, \propto_i, \xi_i, \gamma_i$ and setting them to 0. They are as follows:

$$\left.\begin{array}{l} \frac{\partial L}{\partial R_1} = 0: \quad \sum_{i=1}^{n}\alpha_i = 1 \\ \frac{\partial L}{\partial c} = 0: \quad c = \sum_{i=1}^{n}\alpha_i x_i \\ \frac{\partial L}{\partial \xi_i} = 0: \quad P - \propto_i - \gamma = 0 \end{array}\right\} \qquad (7.3)$$

subsituting in equation (7.2) by equations (7.3), one gets

$$\left.\begin{array}{l} \max\; L(\propto) = \sum_{i=1}^{n}\propto_i (x_i\,.\,x_i) - \sum_{i,j=1}^{n}\propto_i\propto_j \left(x_i . x_j\right) \\ s.t \begin{cases}\sum_{i=1}^{n}\alpha_i = 1 \\ 0 \leq \alpha_i \leq P\end{cases} \end{array}\right\} \qquad (7.4)$$

Those target objects with $\alpha_i > 0$ are known as the support vectors (x_j). They lie on the boundary of the hypersphere. The radius R_1 of the hypersphere is obtained using any of the support vector.

$$R_1{}^2 = \left(x_j . x_j\right) - 2\sum_{i=1}^{n}\propto_i (x_i . x_i) + \sum_{i,j=1}^{n}\propto_i\propto_j \left(x_i . x_j\right) \qquad (7.5)$$

For test data y, its distance to the centre c is given as

$$R_2{}^2 = \|y - c\|^2 = (y . y) - 2\sum_{i=1}^{n}\propto_i (y . x_i) + \sum_{i,j=1}^{n}\propto_i\propto_j \left(x_i x_j\right) \qquad (7.6)$$

Generally, the training data in the input space are not linearly predicted, hence a non linear function, K is required to map the orginal non linear input space to linear input space. Thus, equations (7.4–7.6) becomes

$$\max\; L(\propto) = \sum_{i=1}^{n}\propto_i K(x_i\,.\,x_i) - \sum_{i,j=1}^{n}\propto_i\propto_j K\left(x_i . x_j\right) \qquad (7.7)$$

$$R_1{}^2 = K(x_j.x_j) - 2\sum_{i=1}^{n} \propto_i K(x_i.x_i) + \sum_{i,j=1}^{n} \propto_i \propto_j K(x_i.x_j) \tag{7.8}$$

$$R_2{}^2 = \|y-c\|^2 = K(y.y) - 2\sum_{i=1}^{n} \propto_i K(y.x_i) + \sum_{i,j=1}^{n} \propto_i \propto_j K(x_i x_j) \tag{7.9}$$

Different kernel function could be used. Here, gaussian kernel function is used. It is given by

$$K(x_i.x_j) = exp\,(-(x_i - x_j))^2/\sigma^2 \tag{7.10}$$

where, x_i, x_j are the training data and σ is the width of the gaussian function.

Distance to the boundary, $\Delta = R_2 - R_1$ (7.11)

The test data is classified based on the following condition:

If $\Delta \leq 0$, test data is target, else test data is an outlier.

7.3 EXPERIMENTAL TEST DATA (Test data5)

In the test data used in the previous chapters (chapters 3 to 6), defects in the bearing were introduced using artificial methods such as electrical discharge machining, scratching or drilling. These defects are simulated faults and differ from the ones occurring naturally during the operation of a machine. To collect the whole service life data of bearing, it would consume very long time. To save this time, bearing life is accelerated (through accelerated life test rigs) and its vibration data is collected from healthy to fault initiation and finally till failure condition.

To evaluate the proposed method, an accelerated bearing life test data [Qiu et al., 2003] of University of Cincinnati [NASA Ames Prognostics Data Repository] is used. The bearing is operated under constant load conditions using a specially designed accelerated life test rig (figure 7.2). Four Rexnord ZA-2115 double row bearings are installed on a shaft and are oil force lubricated. A magnetic plug is installed in the lubrication system to collect the debris found in the oil. The test is stopped until the amount of debris collected exceeds a limit. Dimensions of the bearing are: N=16 (single row), d = 8.41 mm, D = 71.5 mm, tapered contact angle= 15.7 degree. The shaft speed of 2000 r/min is maintained constant by an AC motor coupled to shaft via rub belts. Radial load of 26.69 kN is applied onto the shaft and the bearing using a spring mechanism. A high sensitivity quartz ICP accelerometer (PCB 353B33) is used for collecting the vertical and horizontal vibration readings. Sampling frequency used is 20 kHz and the data is collected for duration of 1 sec. Vertical vibration readings are used for the analysis.

Two test sets of accelerated life data are used in this chapter. In set1 (S1), there are 2156 data files with first 43 are collected with an interval of 5 min and the rest are collected with a 10 min interval. At the end of the test1, inner race defect occurred in bearing 3 and rolling element defect in bearing 4. Bearing number 3 data is used for the evaluation in S1. Set2 data (S2) consists of an outer race defect occurring in the bearing number 1 and there are 984 data files collected with 10 min interval. Figure 7.3 provides the photo of the various defects found in different bearings under S1 and S2 test data. Figure 7.4 shows the vibration signal obtained for the bearing number 1 of S2 test corresponding to stages of its accelerated life test.

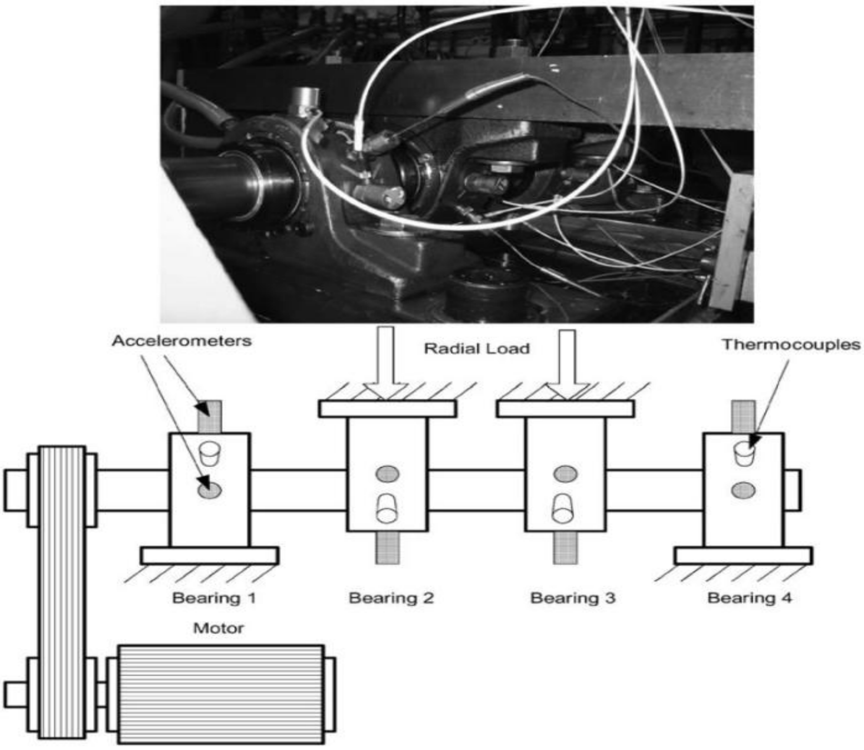

Figure 7.2 Accelerated life test rig: Test data5 [Qiu et al., 2006]

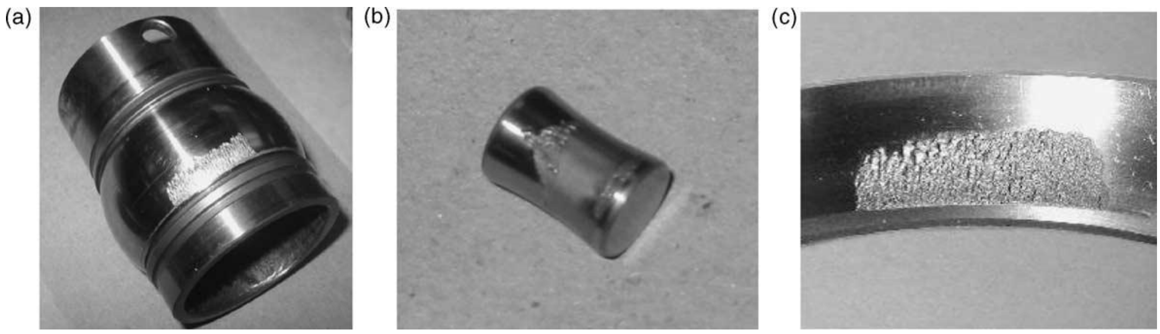

Figure 7.3 Picture of bearing failure after accelerated life test [Qiu et al., 2003] **(a) inner race defect in bearing 3, S1; (b) roller element defect in bearing 4, S1 and (c) outer race defect in bearing 1, S2**

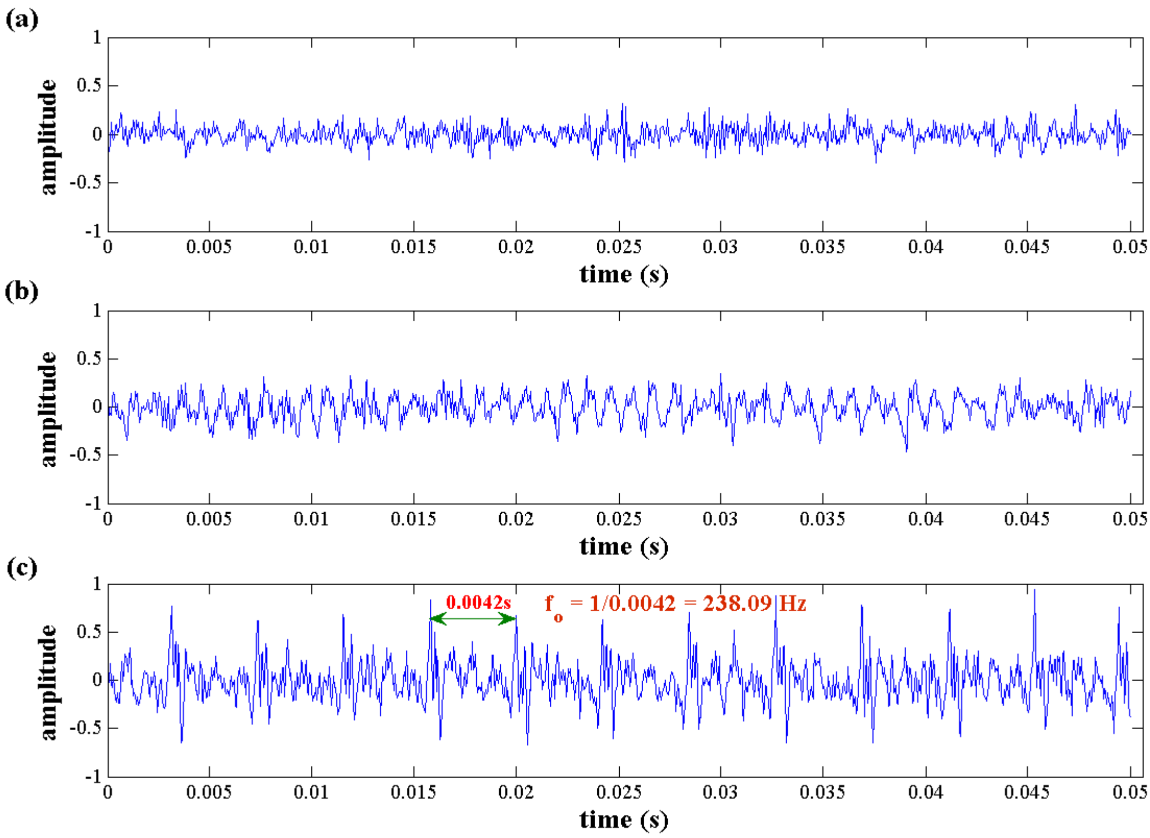

Figure 7.4 Bearing 1's vibration signals of S2 under different conditions: (a) healthy (b) fault propagation and (c) failure

7.4 FAULT FEATURES AND ITS TREND

The three fault features developed in this thesis are used for the fault degradation study. Common Signal Index (CSI1 and CSI3) discussed in chapter 3 and Singular Value Ratio discussed in chapter 4 are used. Similar to the analysis done in chapter 4, for L=10, ratio of first two singular values (being dominant) called as SV12 is used as the third feature. Thus, new fault features (CSI1, CSI3 and SV12) are calculated for the whole life test data of the bearing. The fault features used in the literature are also calculated to study their trend in comparison with the new fault features. They are root mean square (rms) value, kurtosis value (Kv), crest factor (Crf), Approximate Entropy (ApEn) [Yan and Gao, 2007], Spectral Entropy (SpEn) [Pan et al., 2009] and K-S statistic distance (D) [Cong et al., 2011].

Total 9 features (CSI1, CSI3, SV12, rms, Kv, Crf, ApEn, SpEn and D) are calculated for S1 and S2 signals. Figures 7.5 to 7.13 show the variance of the nine features for S1. Figures 7.14 to 7.22 show the trending of the nine features for S2. Each figure has two plots: one is the complete trend over the entire bearing life and the second is the zoomed last stage of the bearing life.

From the figures obtained for S1 (figures 7.5 to 7.13) and S2 (figures 7.14 to 7.22), it is observed that:

a) The time period from the point of fault initiation to failure is less. This is also verified in [Williams et al., 2001]. For S1: there is an abrupt change in value between the periods 20985-21095 min. For S2, it is between 9800-9810 min.

b) The variation in the trend remains almost same for S1 and S2 especially D (figures 7.10 and 7.19), CSI1 (figures 7.11 and 7.20) and CSI3 (figures 7.12 and 7.21).

c) CSI1 (figures 7.11 and 7.20) remains constant and then decreases abruptly at the time of failure. CSI3 (figures 7.12 and 7.21) is steady initially then increases slightly and jumps to higher value at the final stages. Behaviour of SV12 and rms seems to be reciprocal in the failure stage. (For S1, SV12 decreases (figure 7.13) and rms increases (figure 7.5); For S2, SV12 increases (figure 7.22) and rms decreases (figure 7.14)). Kurtosis value remains steady but it has some random fluctuations during the period from the fault initiation to failure (figure 7.6 and 7.15). Crest factor (figure 7.7 and 7.16) shows different behavior in the two cases. Approximate entropy has similar values during normal period, but it decreases for S1 (figure 7.8) and increases for S2 (figure 7.17) at the failure time. Spectral entropy is found to decrease in S2 (figure 7.18), while there is no clear indication in S1 (figure 7.9). D remains steady, then increases slightly and finally jumps to higher value (figures 7.10 and 7.19).

From the above results, it is observed that the new features (CSI1, CSI3 and SV12) could reflect the degradation trend. Some of the literature methods such as kurtosis value, approximate entropy and spectral entropy do not show clear trend as the fault progresses. CSI1 and CSI3 are better indexes and give similar trend as obtained with the other existing features such as rms and K-S statistic distance. However, it is better to have a single parameter which would reflect the status of the bearing. Thus, a combined index is necessary which would be sensitive to incipient defect and increases steadily as the defect severity increases. Hence, a parameter known as Performance Index (PI) based on the three features (CSI1, CSI3 and SV12) and Support Vector Data Description method is developed, which is discussed in the next section.

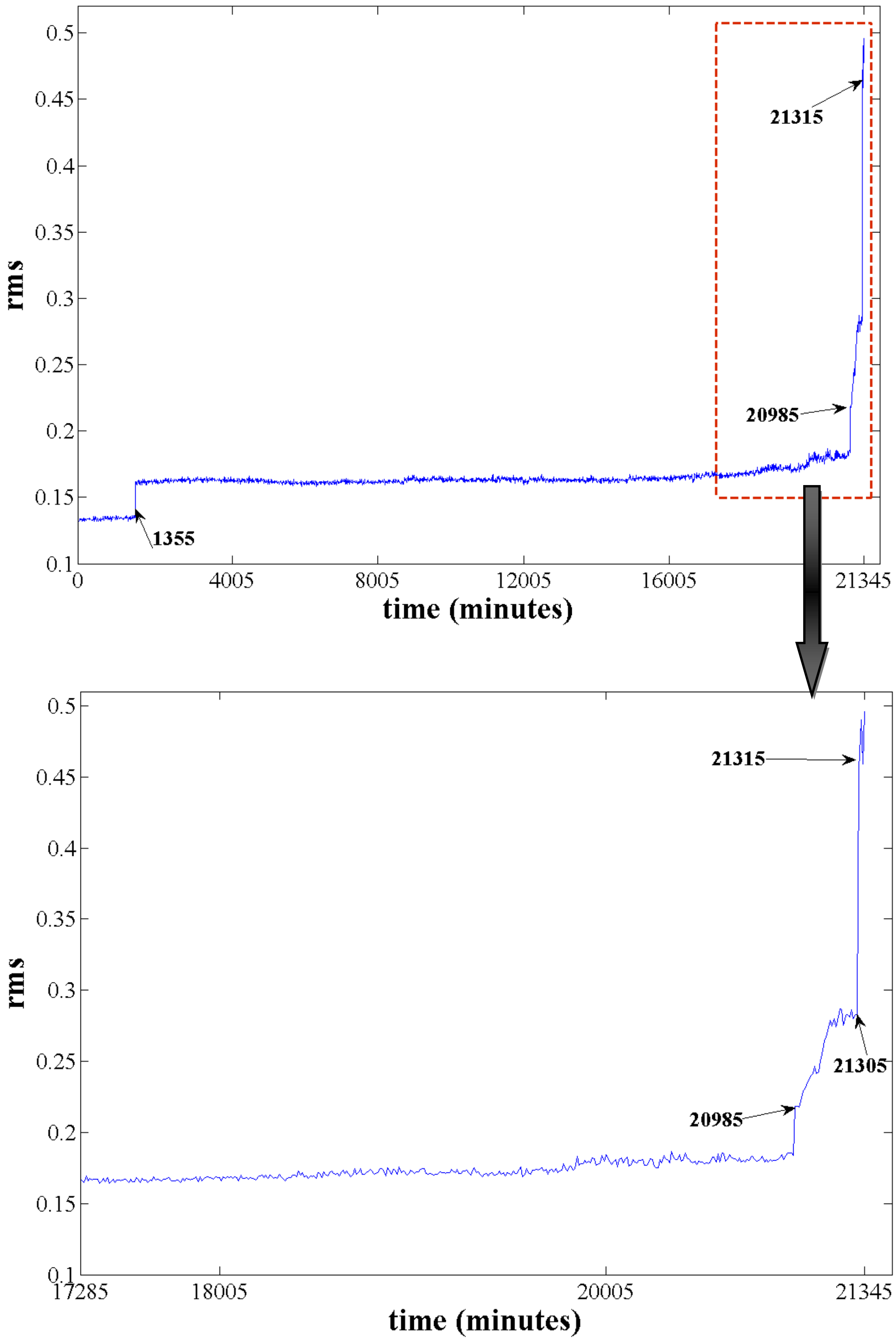

Figure 7.5 rms trend value during whole life time: S1

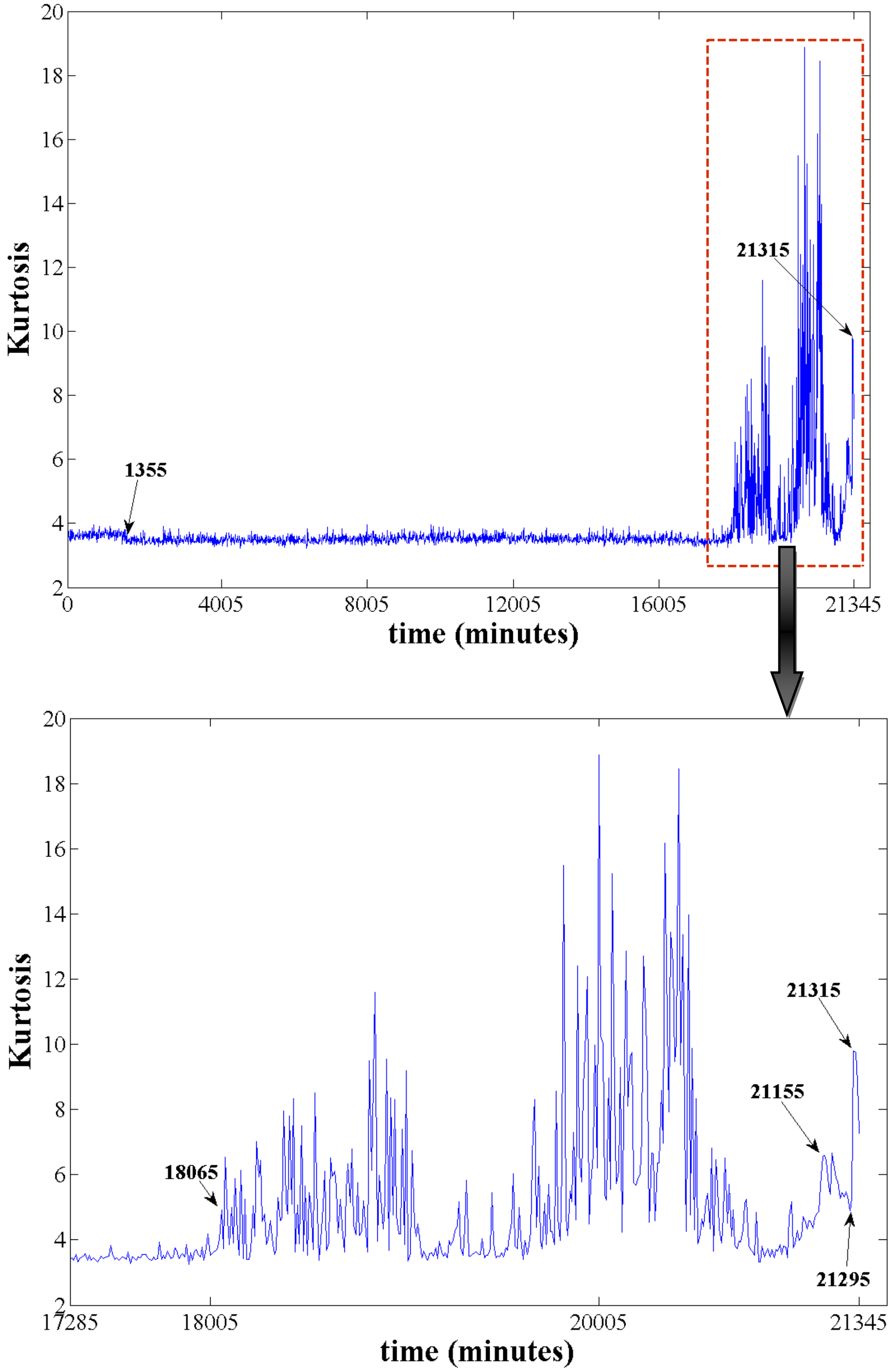

Figure 7.6 Kurtosis trend value during whole life time:S1

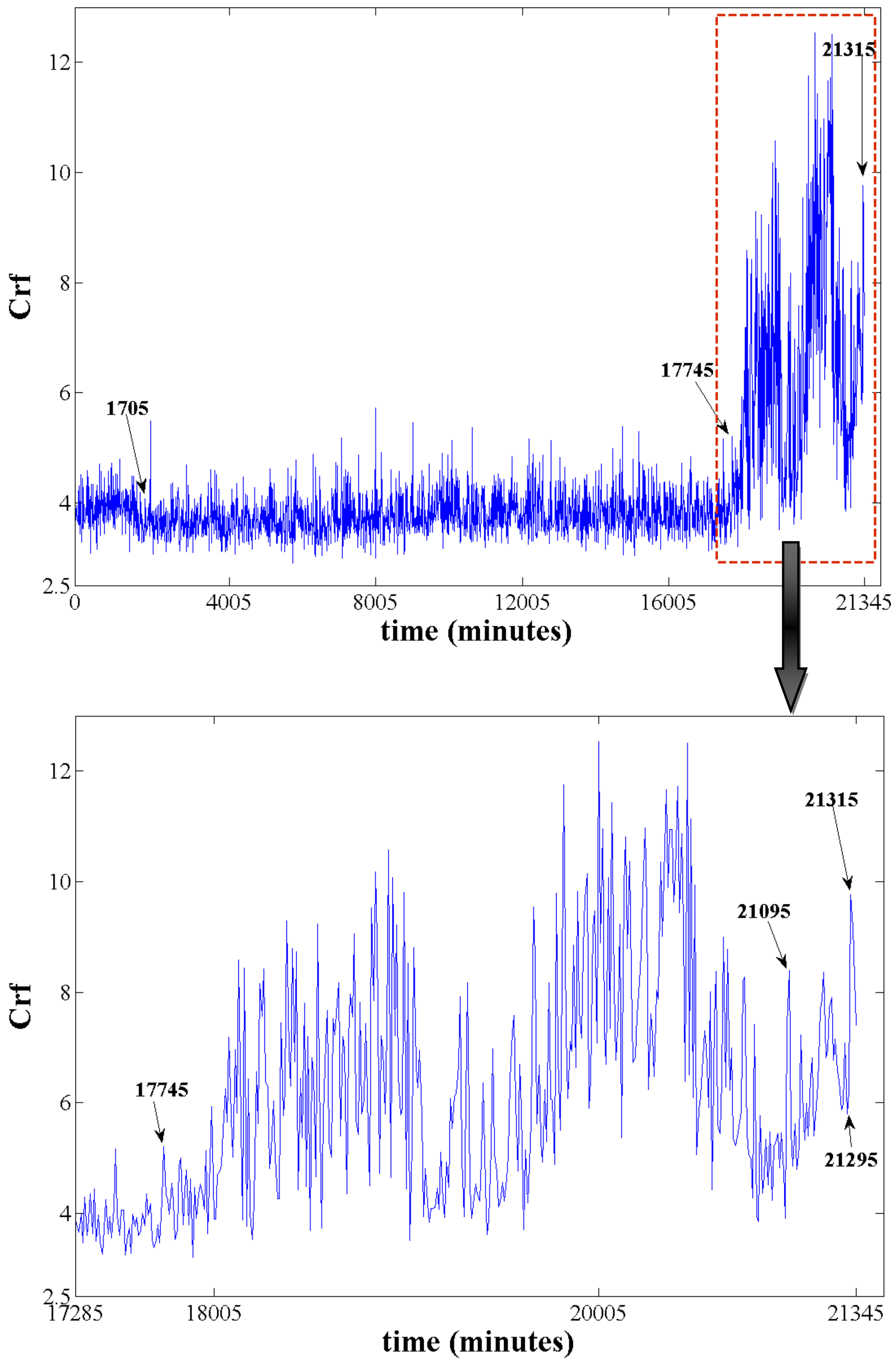

Figure 7.7 Crest factor (Crf) trend value during whole life time:S1

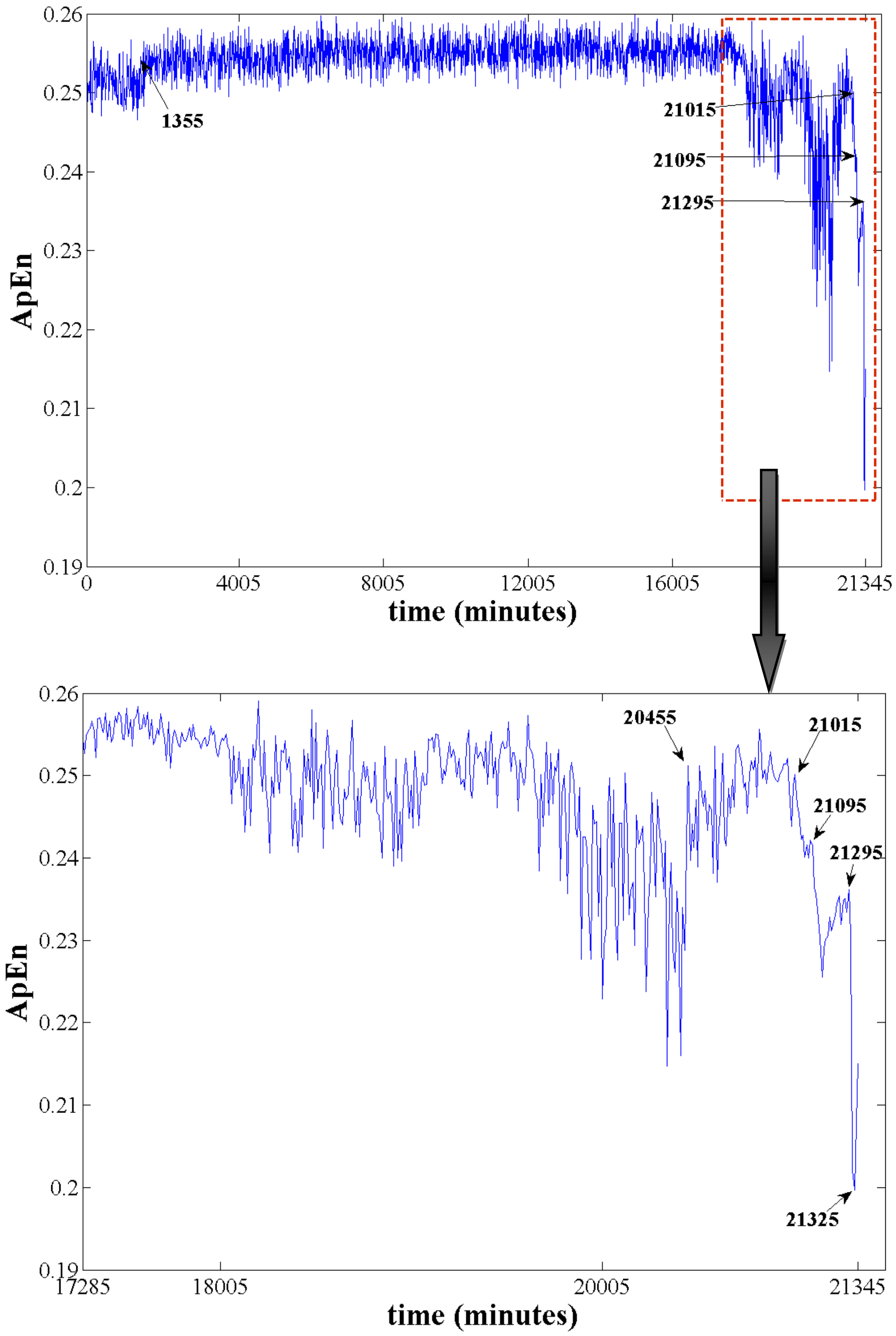

Figure 7.8 Approximate entropy (ApEn) trend value during whole life time:S1

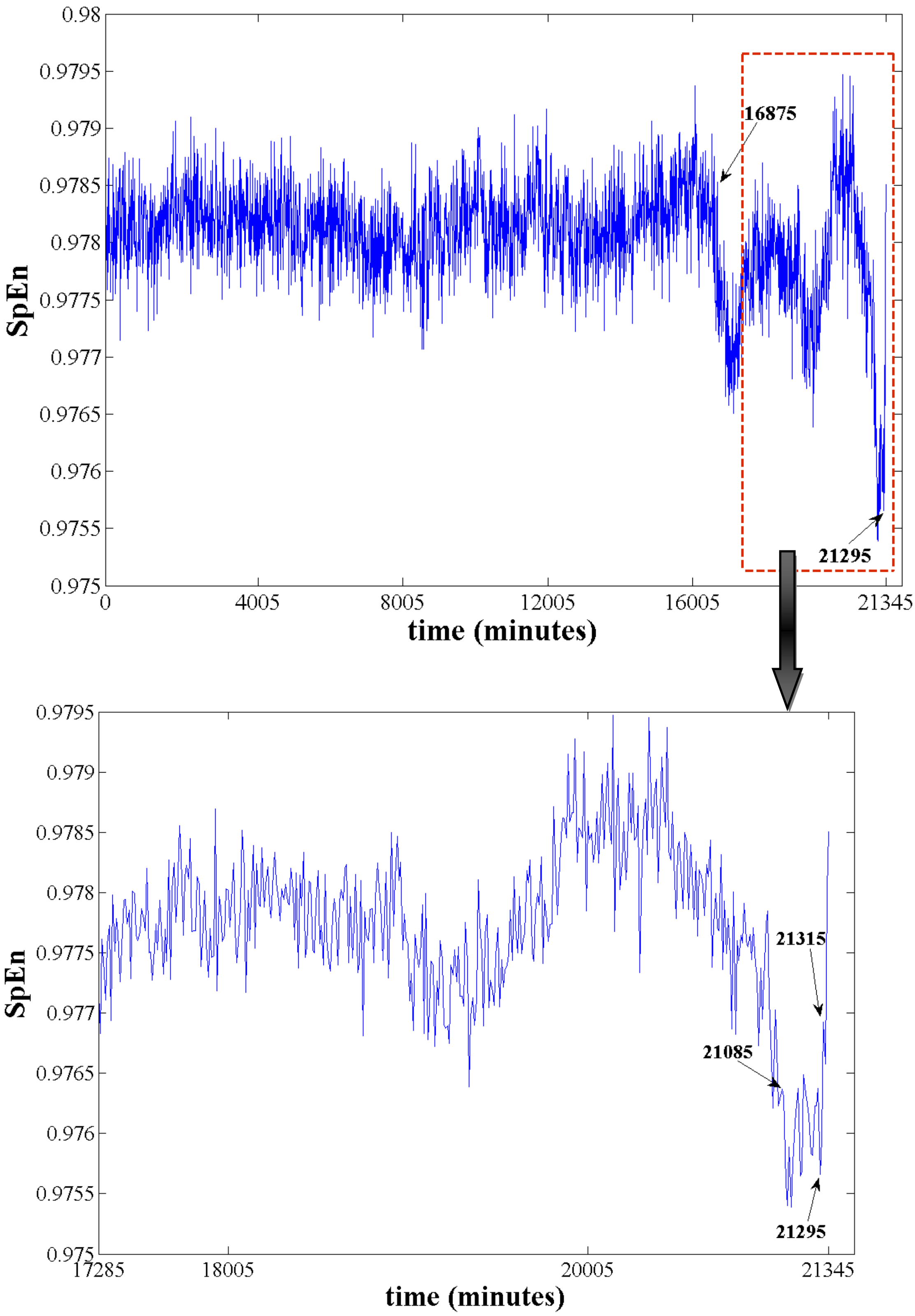

Figure 7.9 Spectral entropy (SpEn) trend value during whole life time:S1

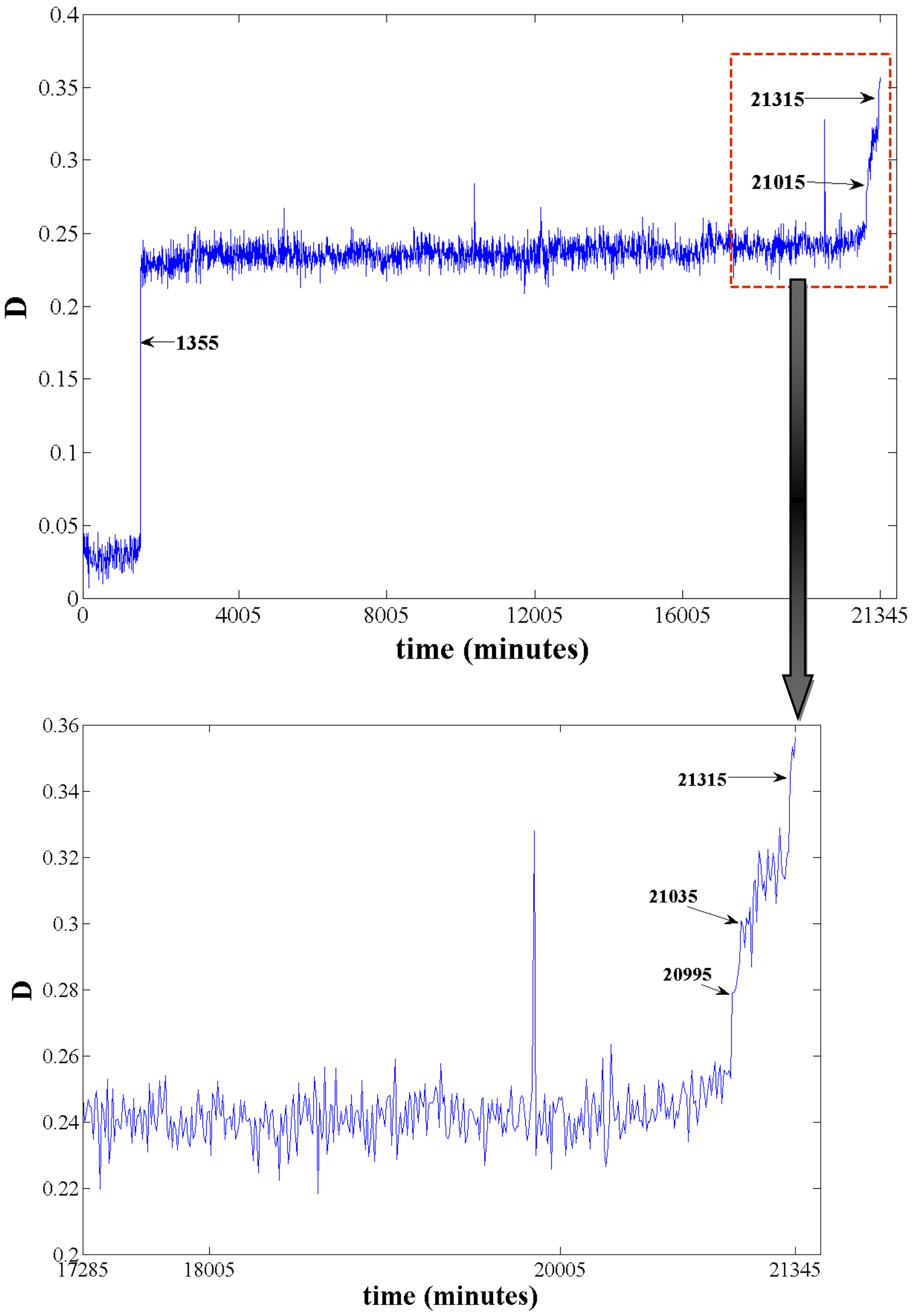

Figure 7.10 K-S statistic distance (D) trend value during whole life time:S1

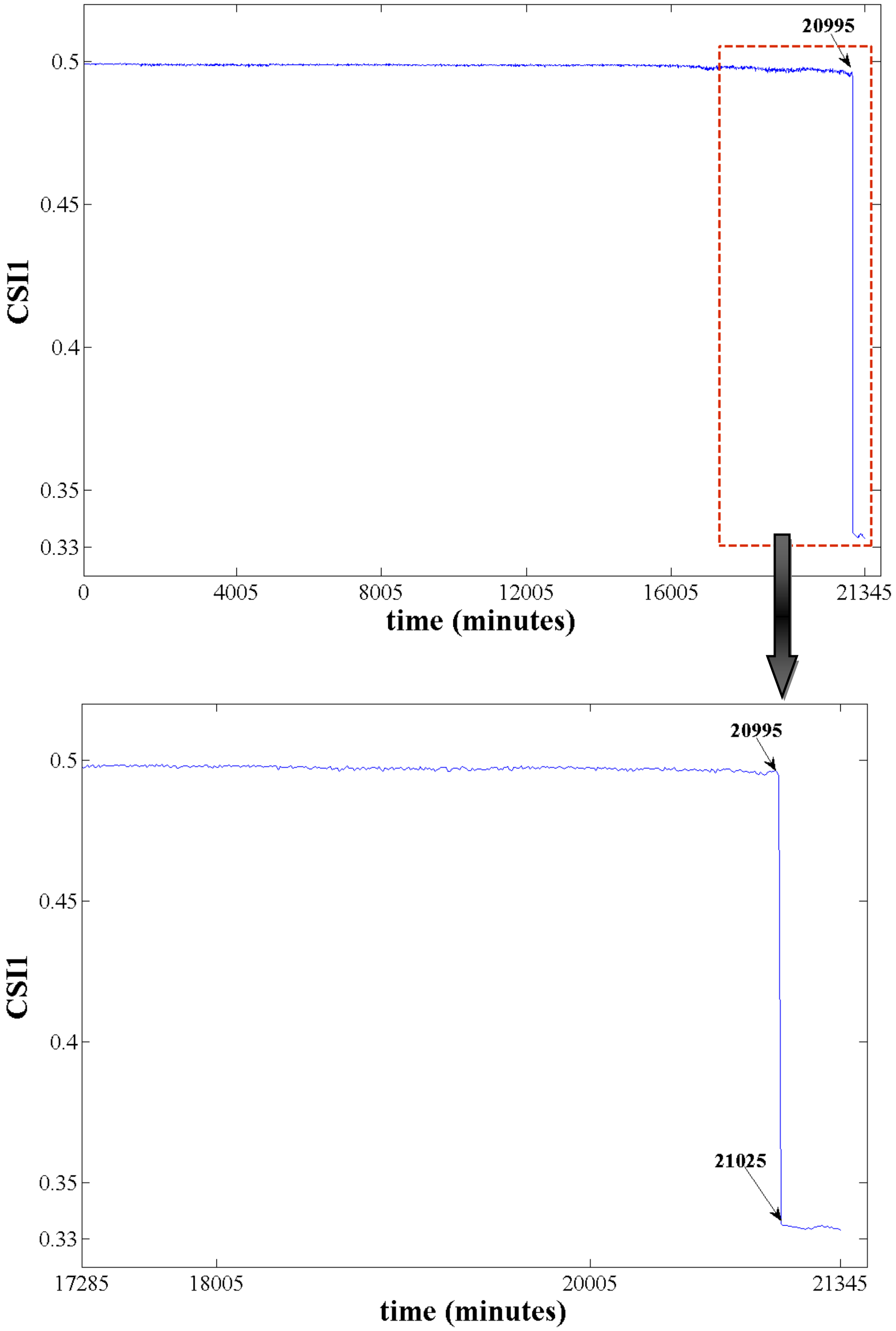

Figure 7.11 CSI1 trend value during whole life time:S1

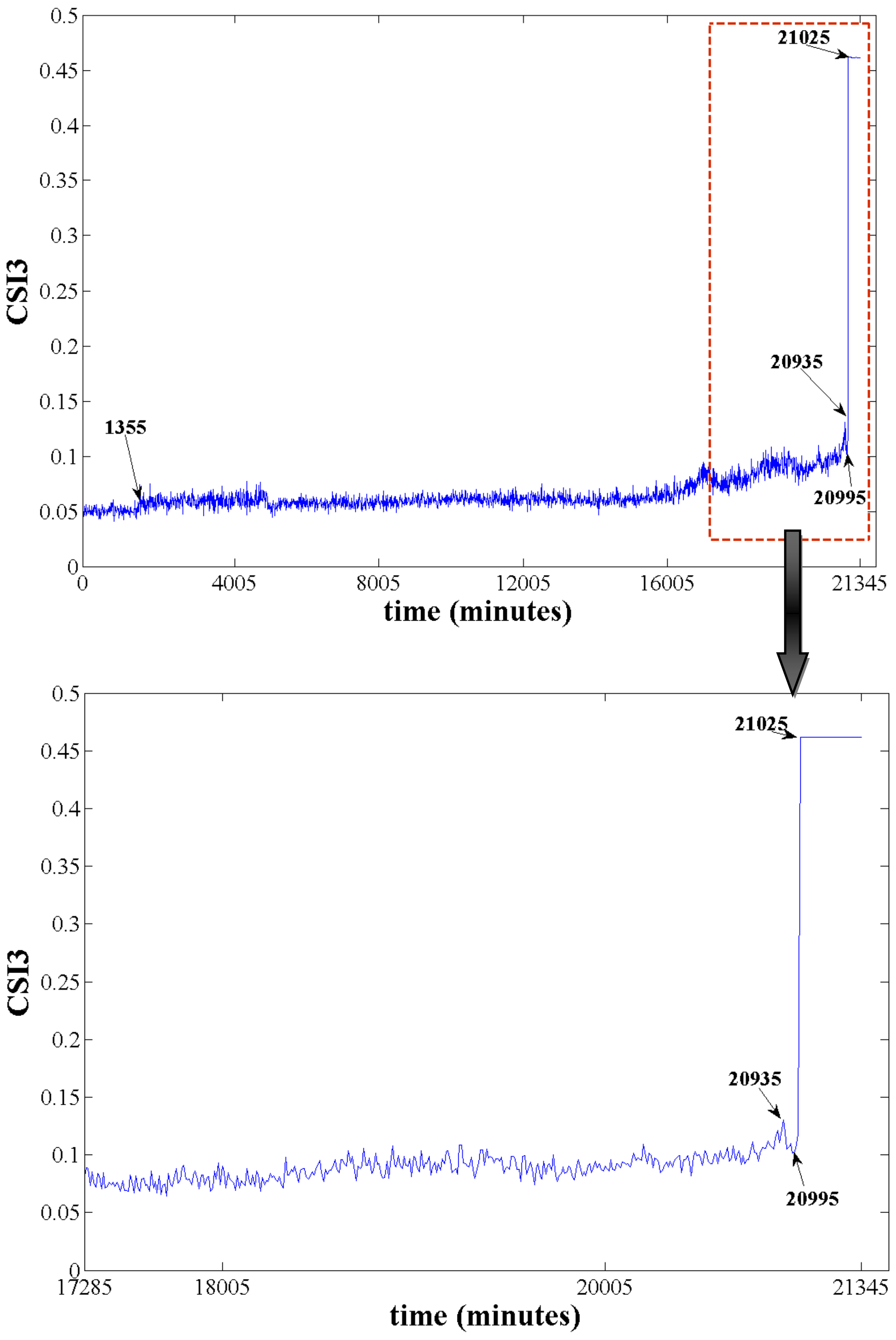

Figure 7.12 CSI3 trend value during whole life time:S1

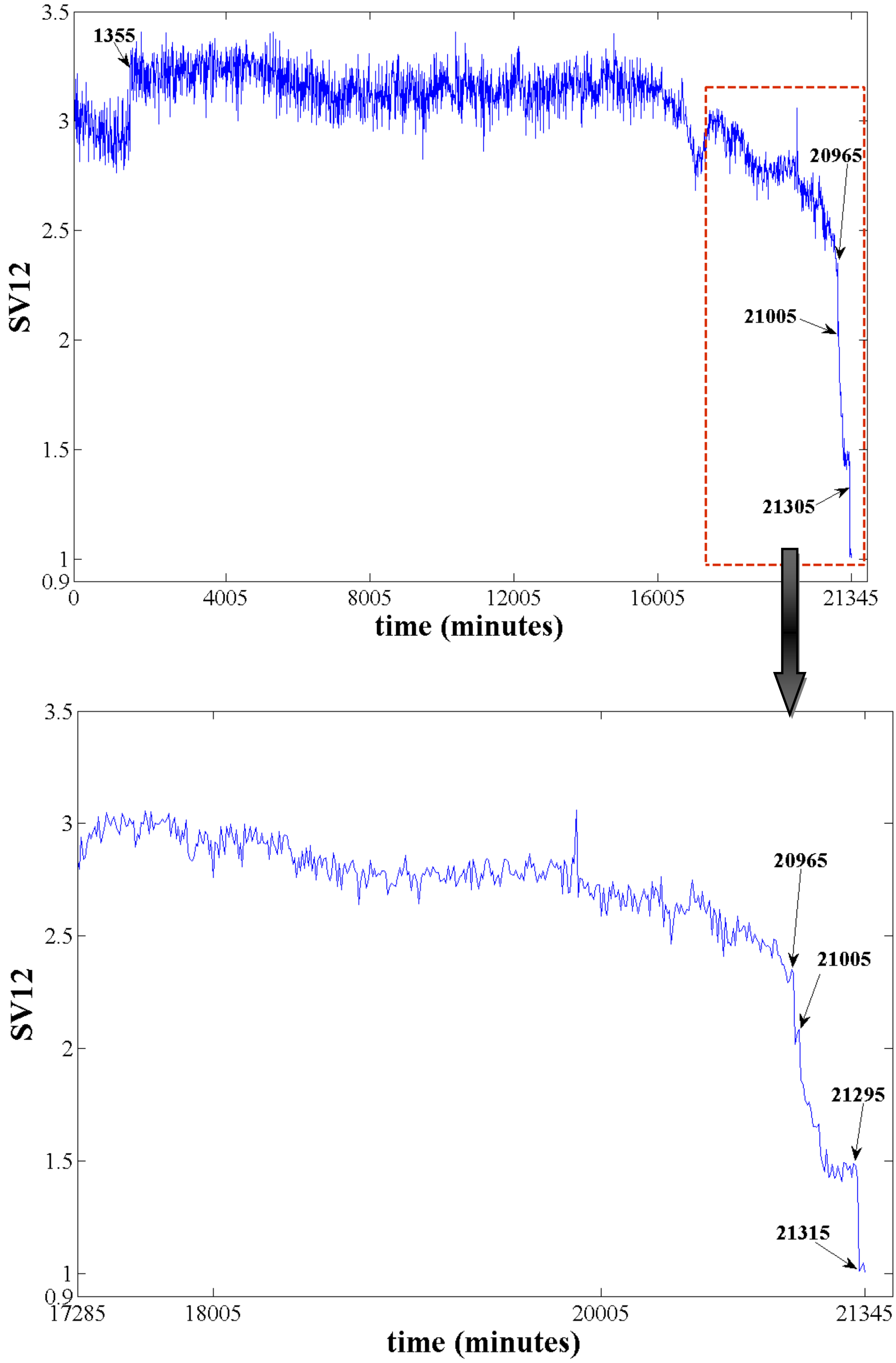

Figure 7.13 SV12 trend value during whole life time:S1

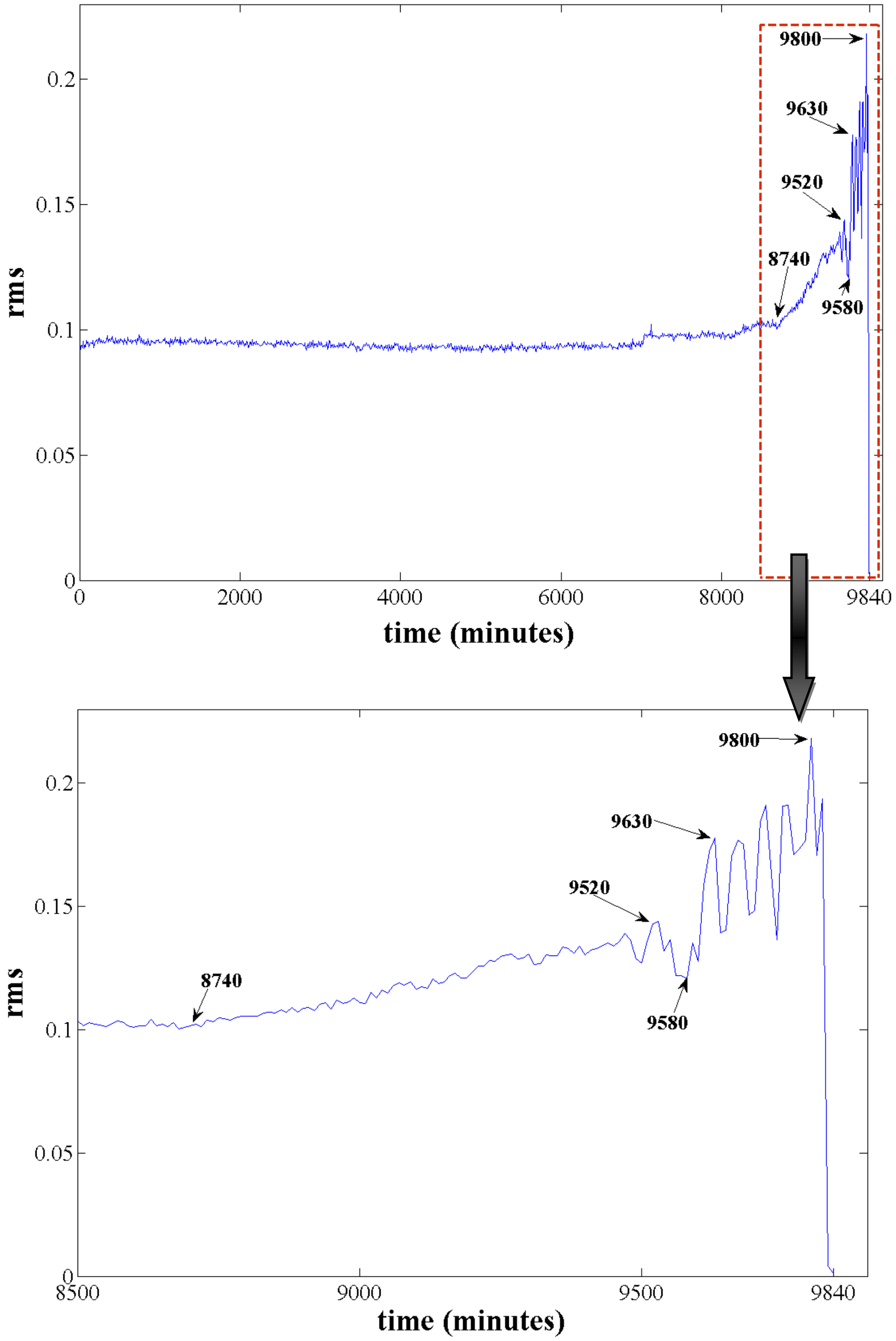

Figure 7.14 rms trend value during whole life time: S2

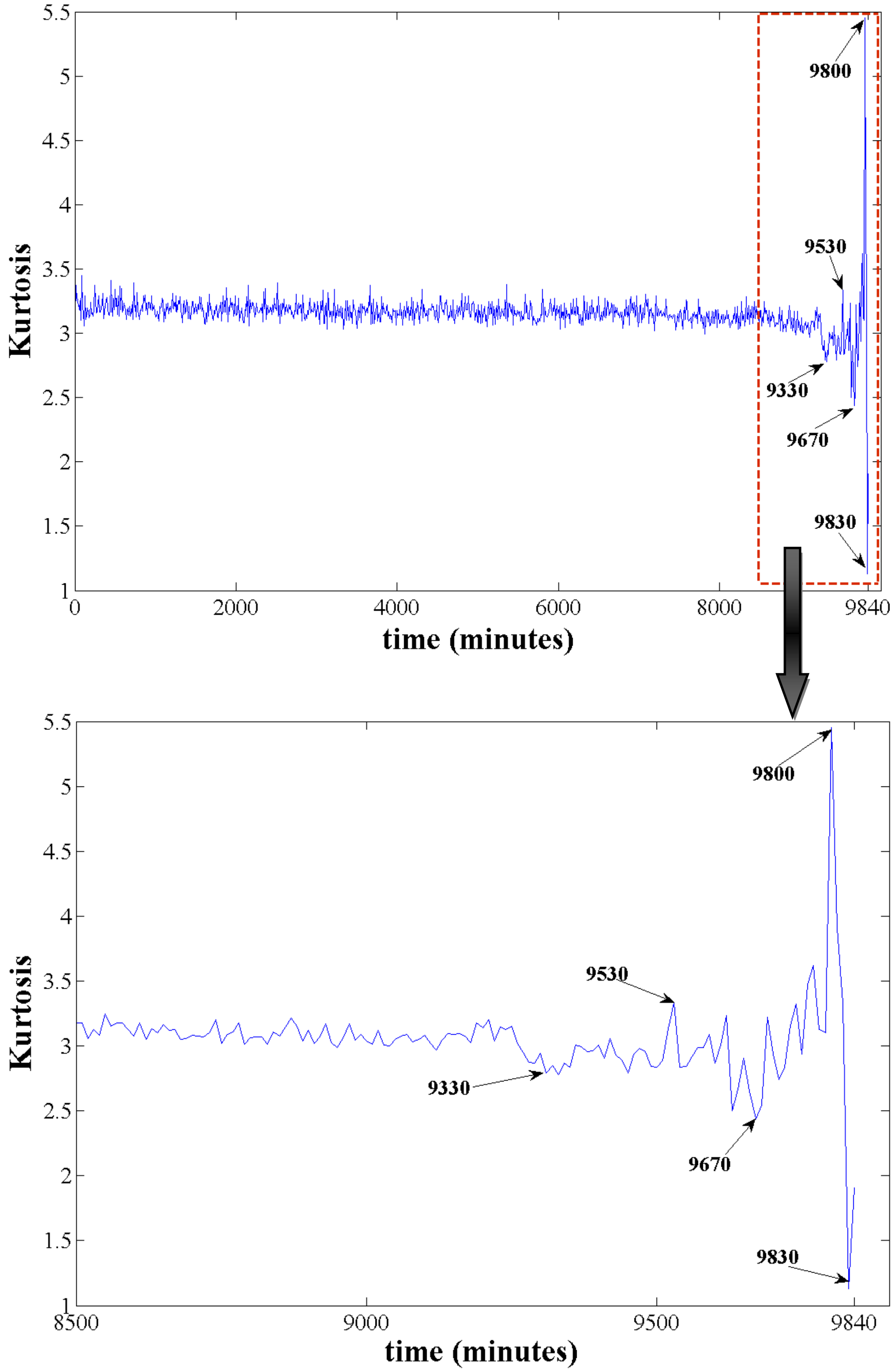

Figure 7.15 Kurtosis trend value during whole life time: S2

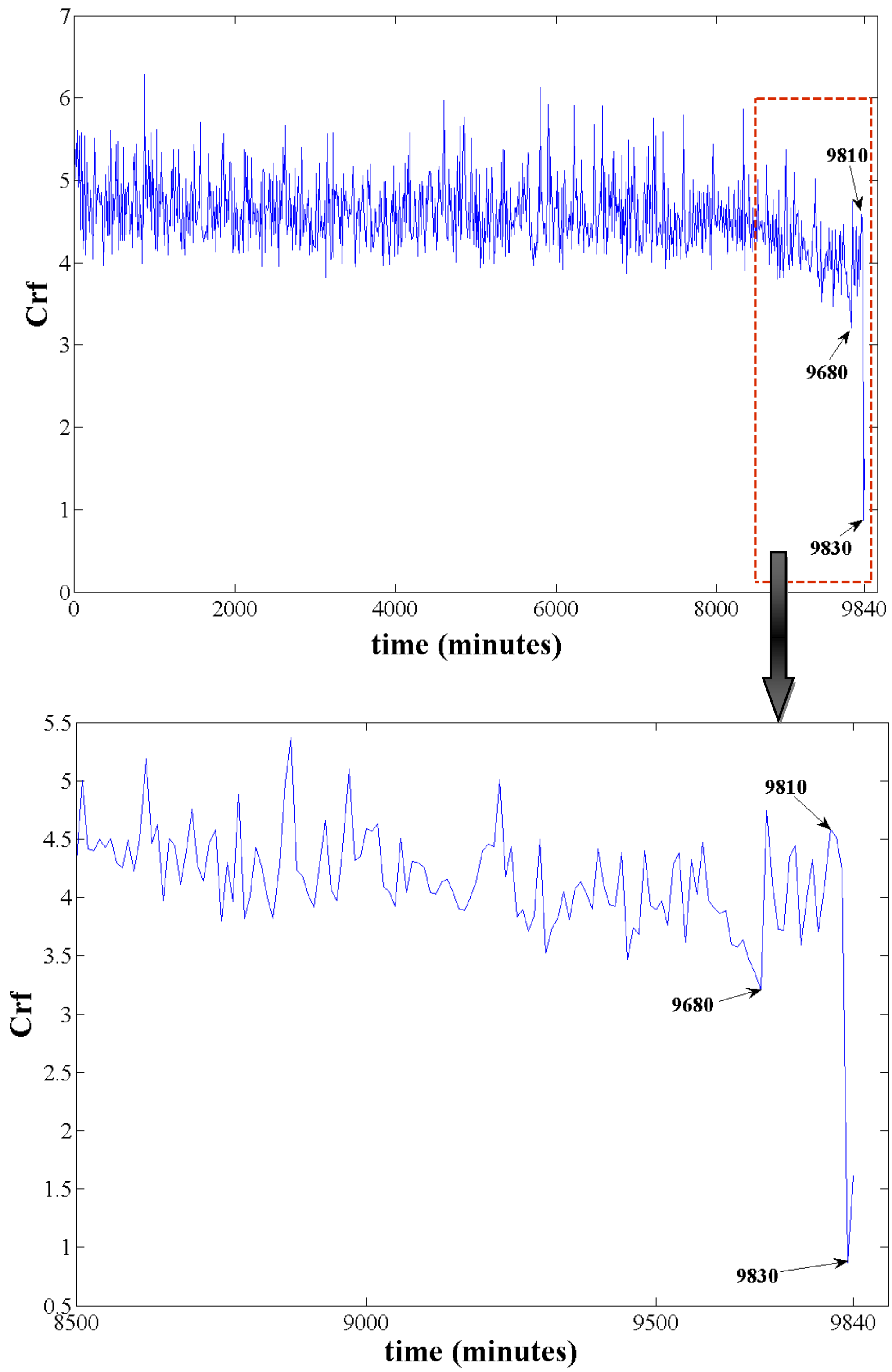

Figure 7.16 Crest factor (Crf) trend value during whole life time: S2

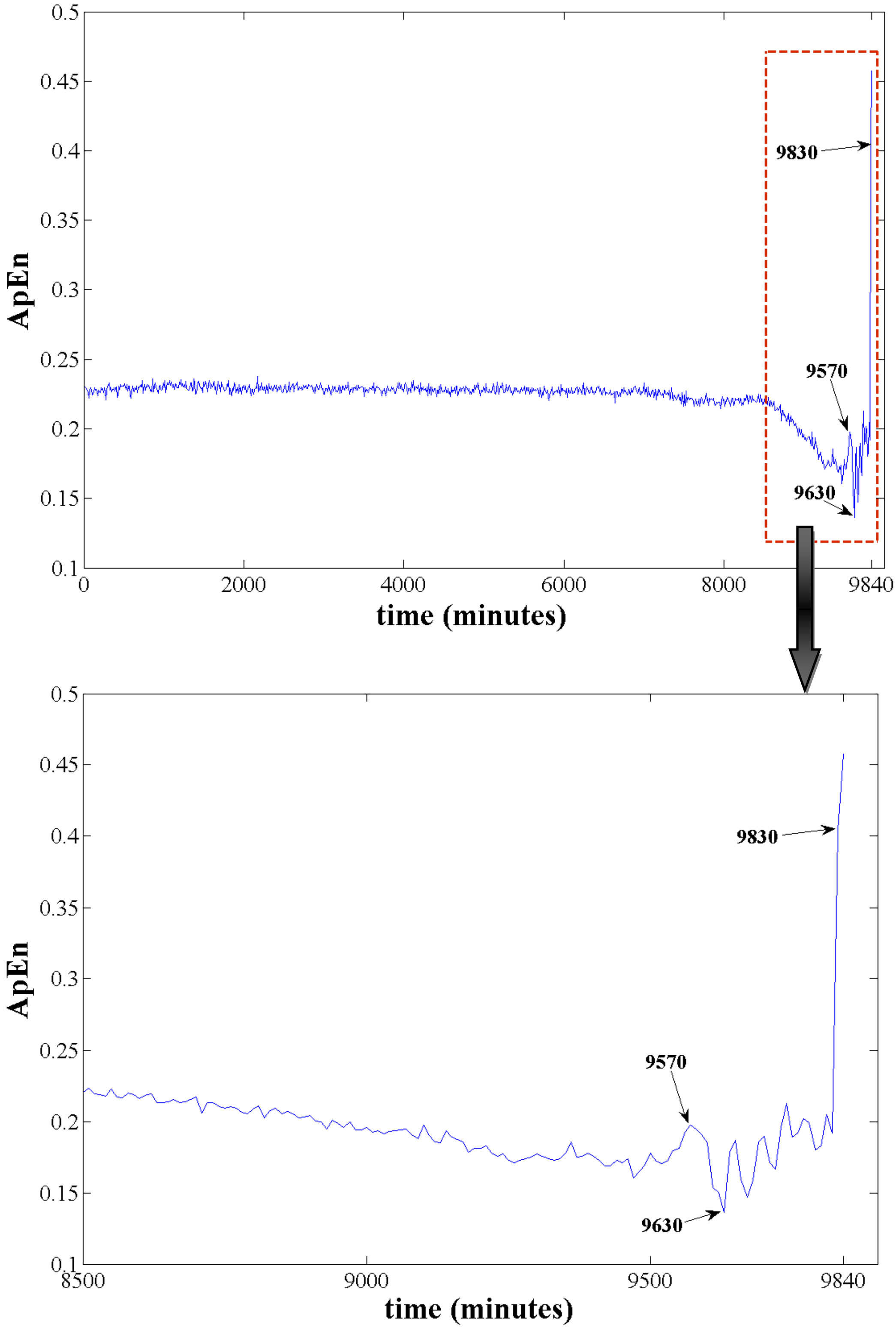

Figure 7.17 Approximate Entropy (ApEn) trend value during whole life time: S2

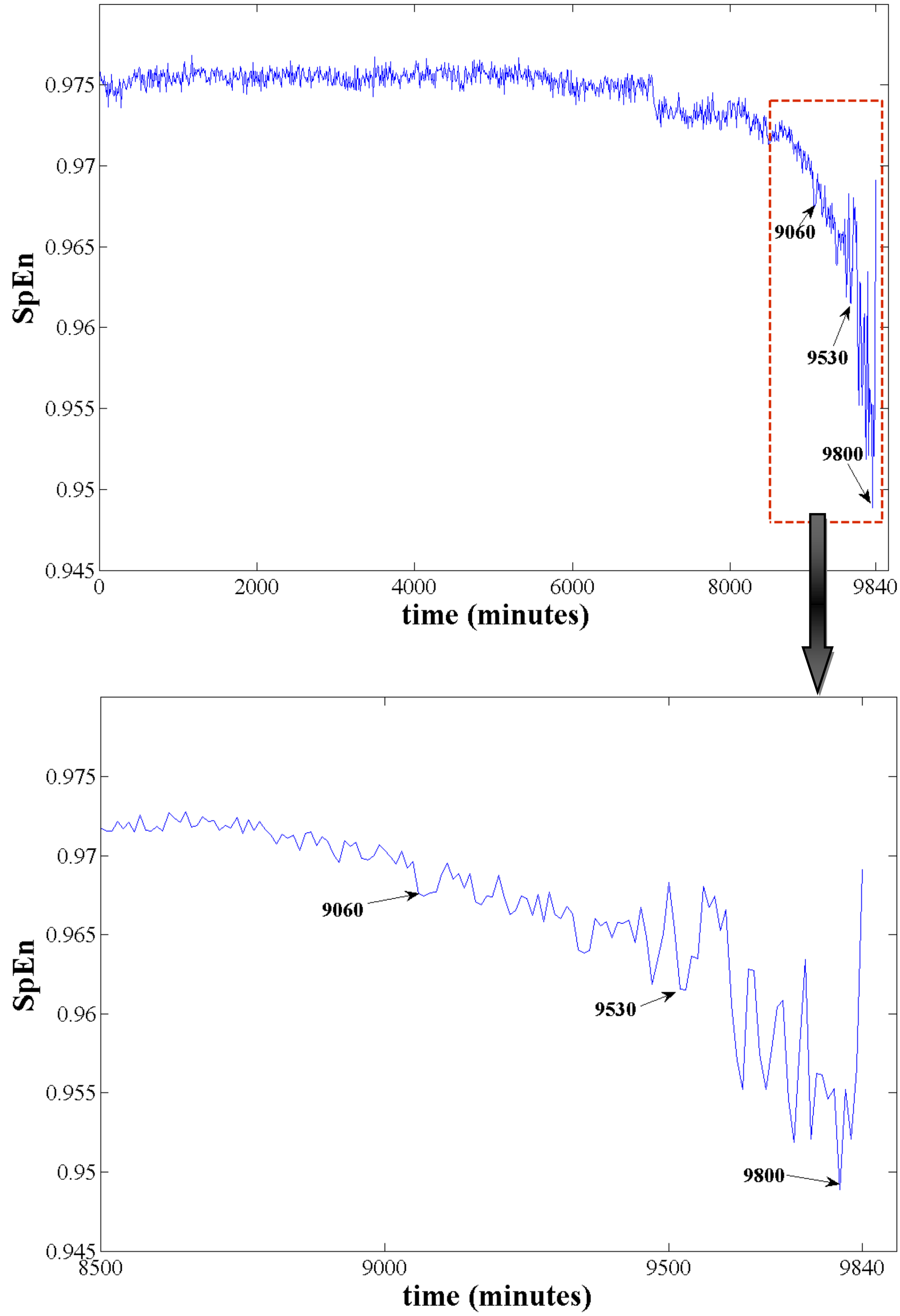

Figure 7.18 Spectral Entropy (SpEn) trend value during whole life time: S2

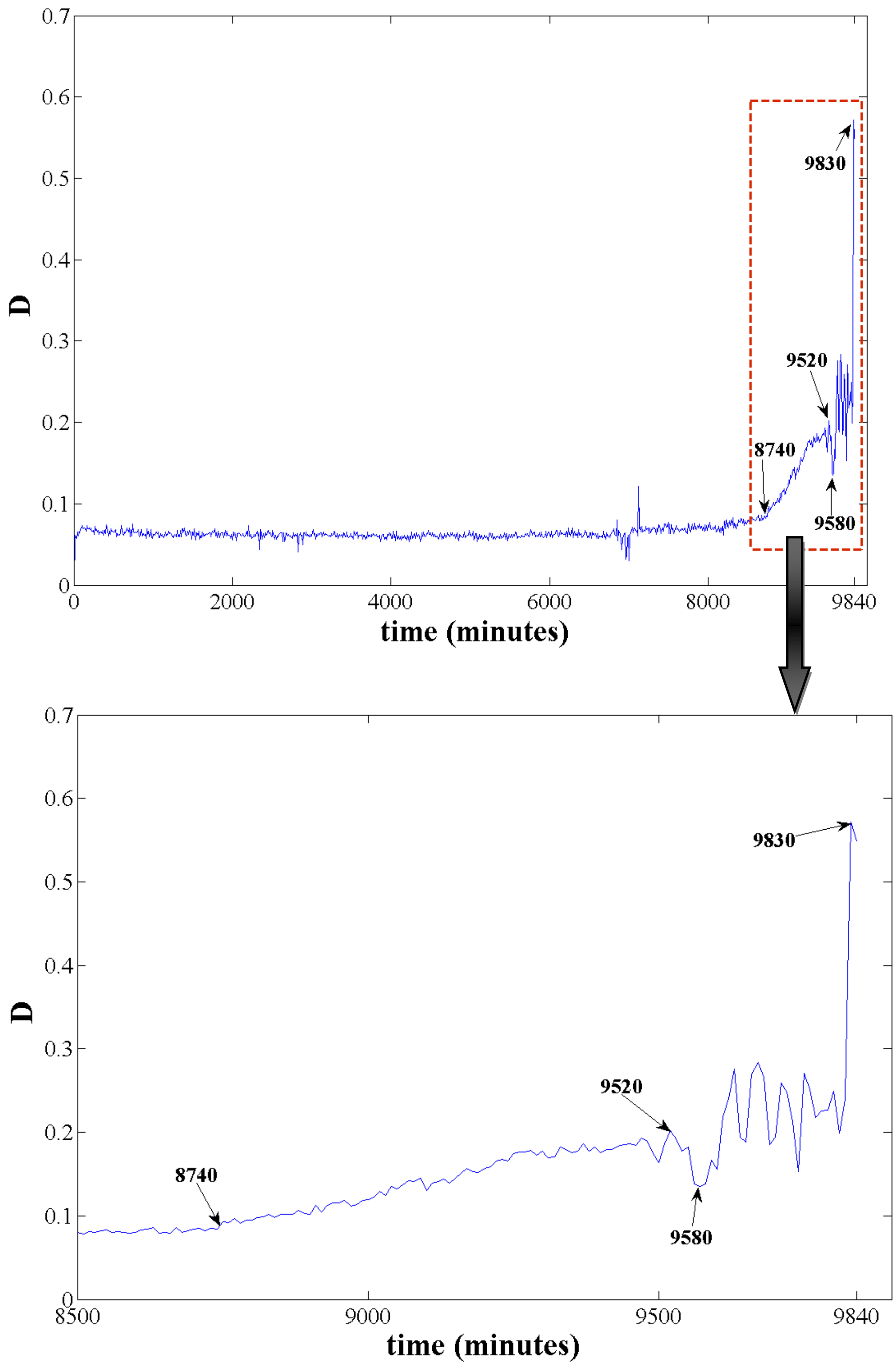

Figure 7.19 K-S statistic distance (D) trend value during whole life time: S2

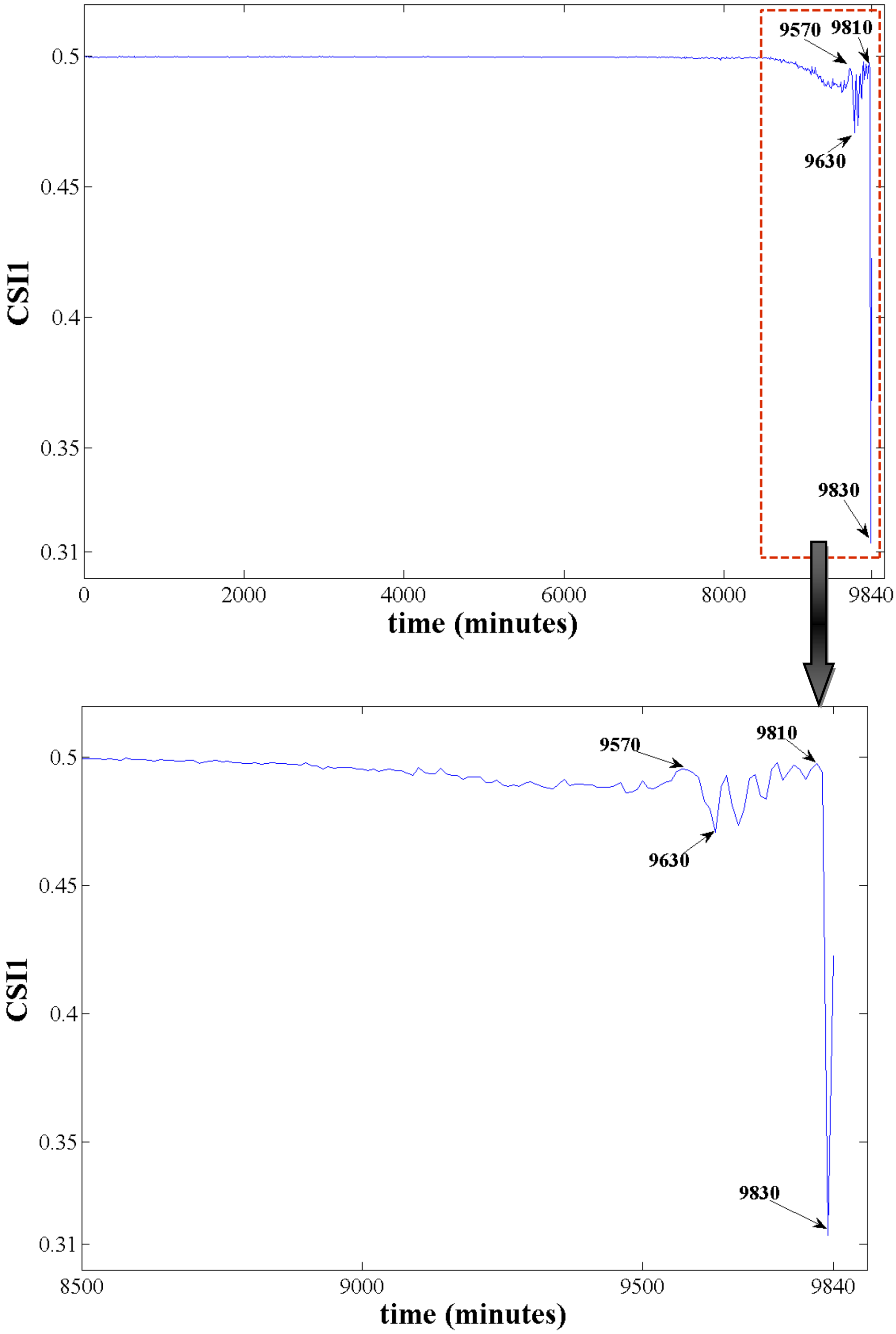

Figure 7.20 CSI1 trend value during whole life time: S2

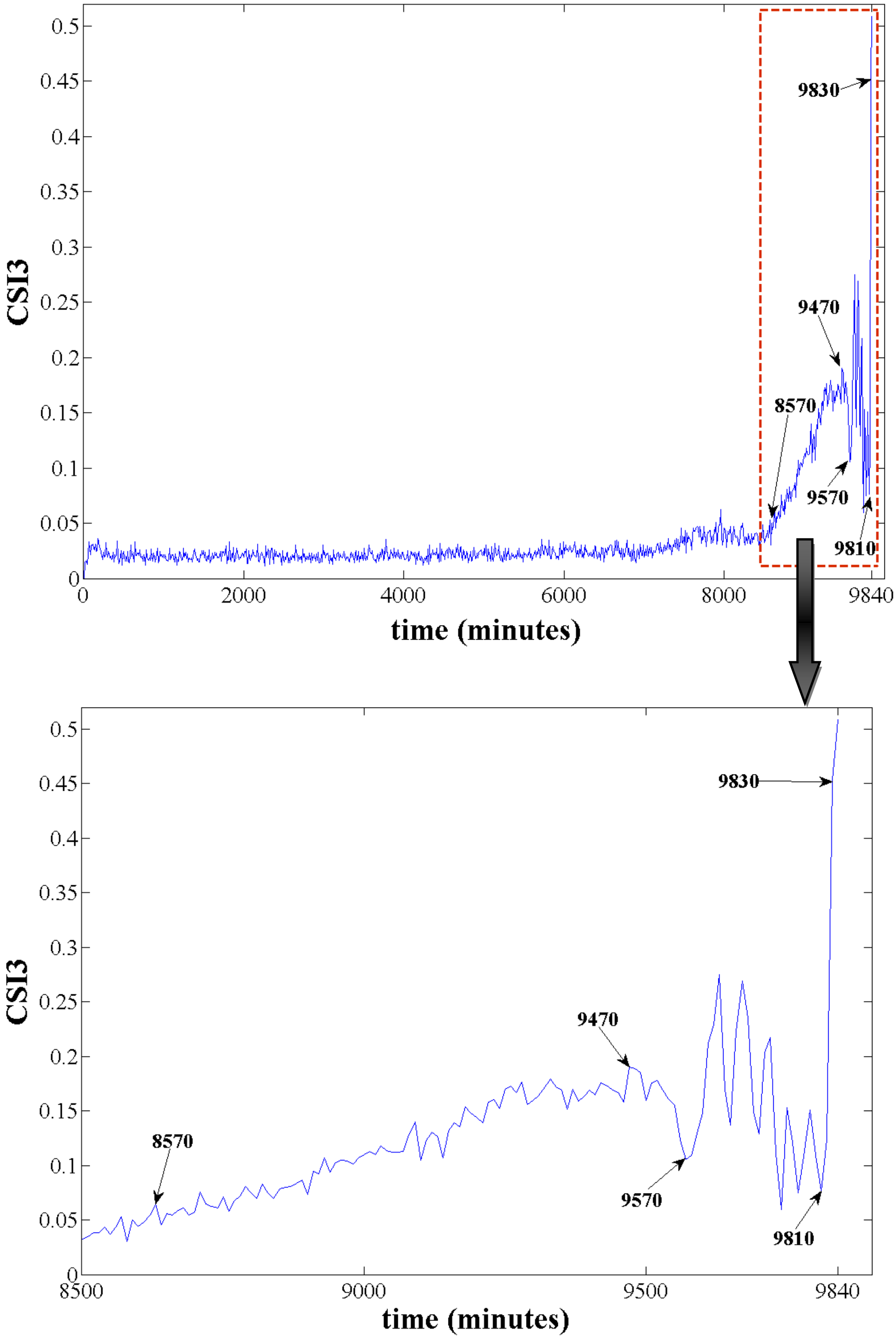

Figure 7.21 CSI3 trend value during whole life time: S2

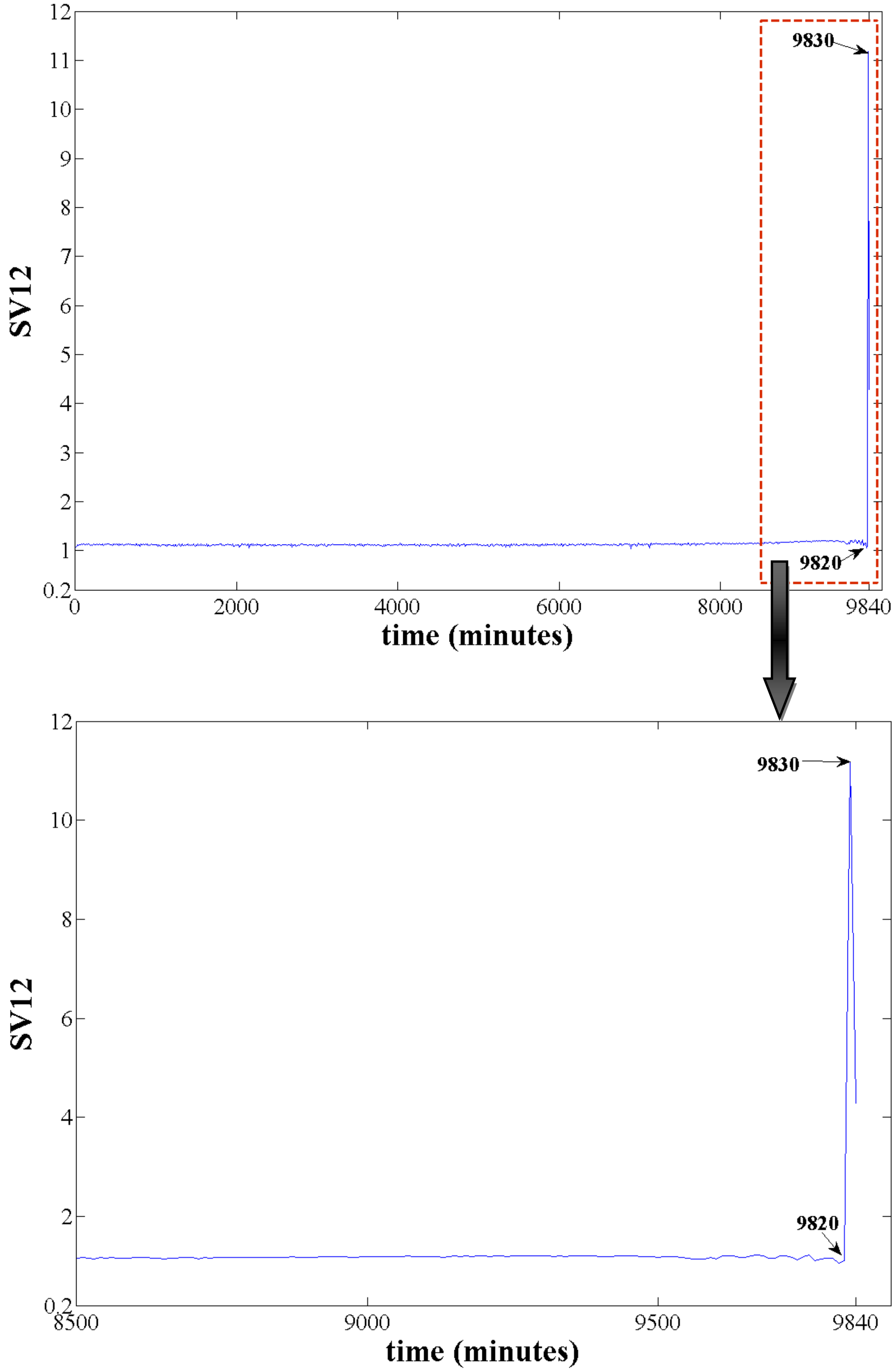

Figure 7.22 SV12 trend value during whole life time: S2

7.5 BEARING FAULT DEGRADATION INDICATOR DEVELOPMENT

7.5.1 PROCEDURE FOR THE PERFORMANCE INDEX CALCULATION

The operating life of a bearing could be divided into three stages: healthy, fault initiation and failure. During the initial period of bearing installation, it would have a short run-in period. After that, it goes into longer constant operation period. With the development of incipient fault, its health starts degrading and finally the bearing fails to provide the required performance. A performance index (PI) which would reflect the above stages is developed using SVDD. Figure 7.23 describes the steps involved in this method, which are as follows:

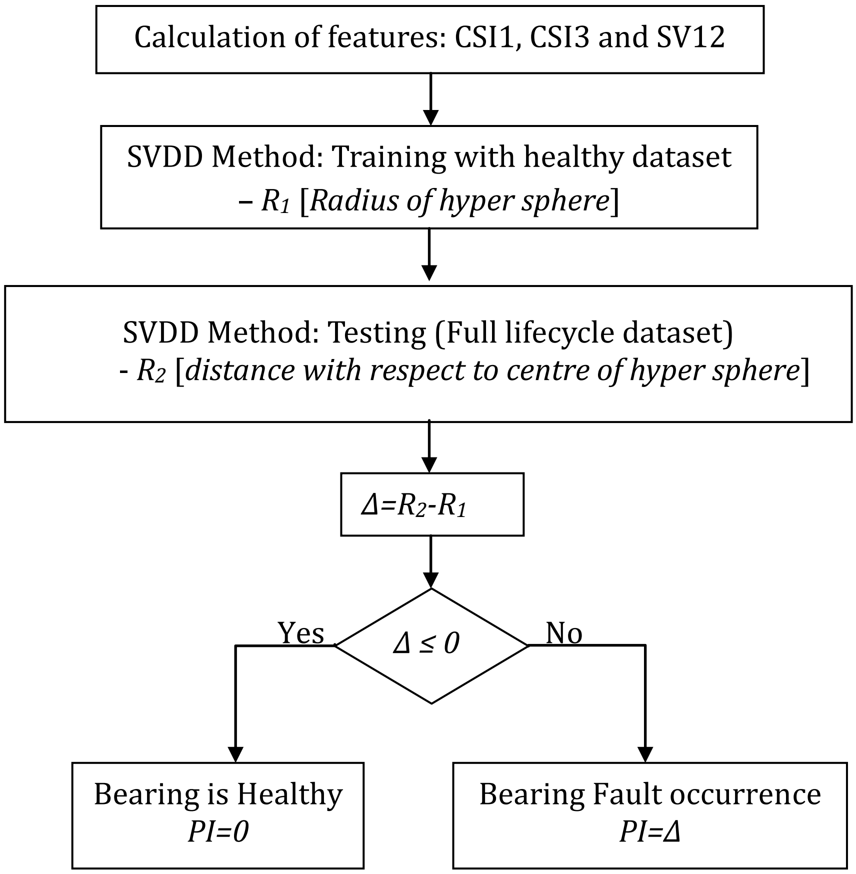

Figure 7.23 Flow diagram of the bearing fault degradation index development

Step1: *Feature Extraction*

Three features (CSI1, CSI3 and SV12) are calculated from the vibration signals for the complete operating life of bearing.

Step2: *SVDD Training and Testing*

SVDD model is developed using gaussian function as the kernel. Healthy features datasets are used for the training and a hyper sphere is built around them. Radius, R_1 of hyper sphere (equation (7.8)) is calculated. During the testing phase, R_2 which is the distance of the test dataset to the center of hyper sphere (equation (7.9)) is obtained for the dataset of complete lifecycle.

Step 3: *Performance Index (PI) for healthiness evaluation*

Performance Index is calculated based on the difference between R_1 and R_2. $\Delta=R_2-R_1$. If $\Delta \leq 0$, then test data is healthy and PI=0; Else, test data is of fault condition and PI= Δ. Large Δ value indicates more degradation of health.

7.5.2 PERFORMANCE INDEX CALCULATION

The three features are calculated for the S1 and S2 dataset's. Total of 2156 and 984 datasets were obtained from the accelerated life test rig in S1 and S2 respectively. The features were normalized in the range 0 to 1. During the training of SVDD, the number of healthy datasets chosen for S1 and S2 are 1000 and 600 respectively. Part of SVDD method is done using the data description toolbox [DD toolbox] and the gaussian kernel function is used (σ = 0.1 and σ =0.05 for S1 and S2 respectively). Using the trained SVDD, the features value for the whole life time of bearing are tested and Δ values are obtained. Performance Index is calculated using step (3) given in the procedure (section 7.5.1). Figures 7.24 and 7.25 show the PI value obtained for S1 and S2 respectively.

7.5.2.1 S1 data

From the figure 7.24, it is seen that during 17855-18955 min, PI increases with the bearing fault, then remains steady up to 19865 min and after that it increases further with big jump in values as it fails. There is drop in the value from 19825 to 19855 min, this could be due to the smoothing of the spall or edge of crack which reduces the amplitude of the fault impulses [Rubini and Meneghetti, 2001]. PI value increase slowly during 20455-20875 min with an increase in degradation and there is a sharp increase in value during 20875-21125 min which could be attributed for the occurrence of crack [Sunnersjo, 1985]. It further increases until failure around 21315 min.

7.5.2.2 S2 data

As observed from the PI plot (figure 7.25), PI values start to increase around 8740 min. It continues to increase till 9520 min, thereafter there is a drop in the value up to 9570 min. This could be due to the smoothing of the spall or some edge of the crack. PI further increases till 9630 min and further there are some random fluctuations till 9810 min. After 9810 min, there is a big jump in its value which could be associated with the formation of a big crack leading to the bearing failure.

Based on the plots obtained for S1 and S2, the Performance Index provides an assessment of the degradation trend.

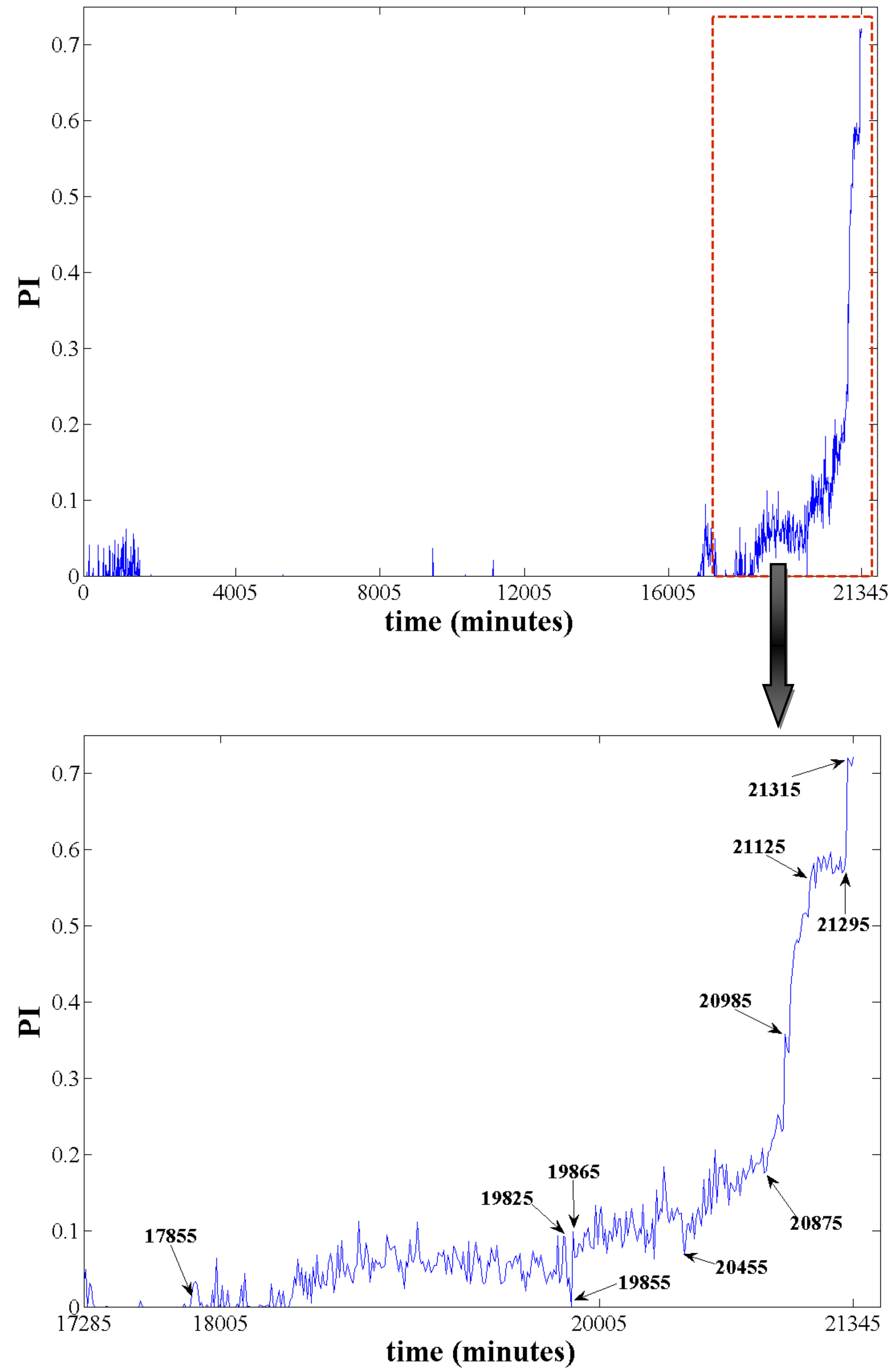

Figure 7.24 PI trend value during whole life time: S1

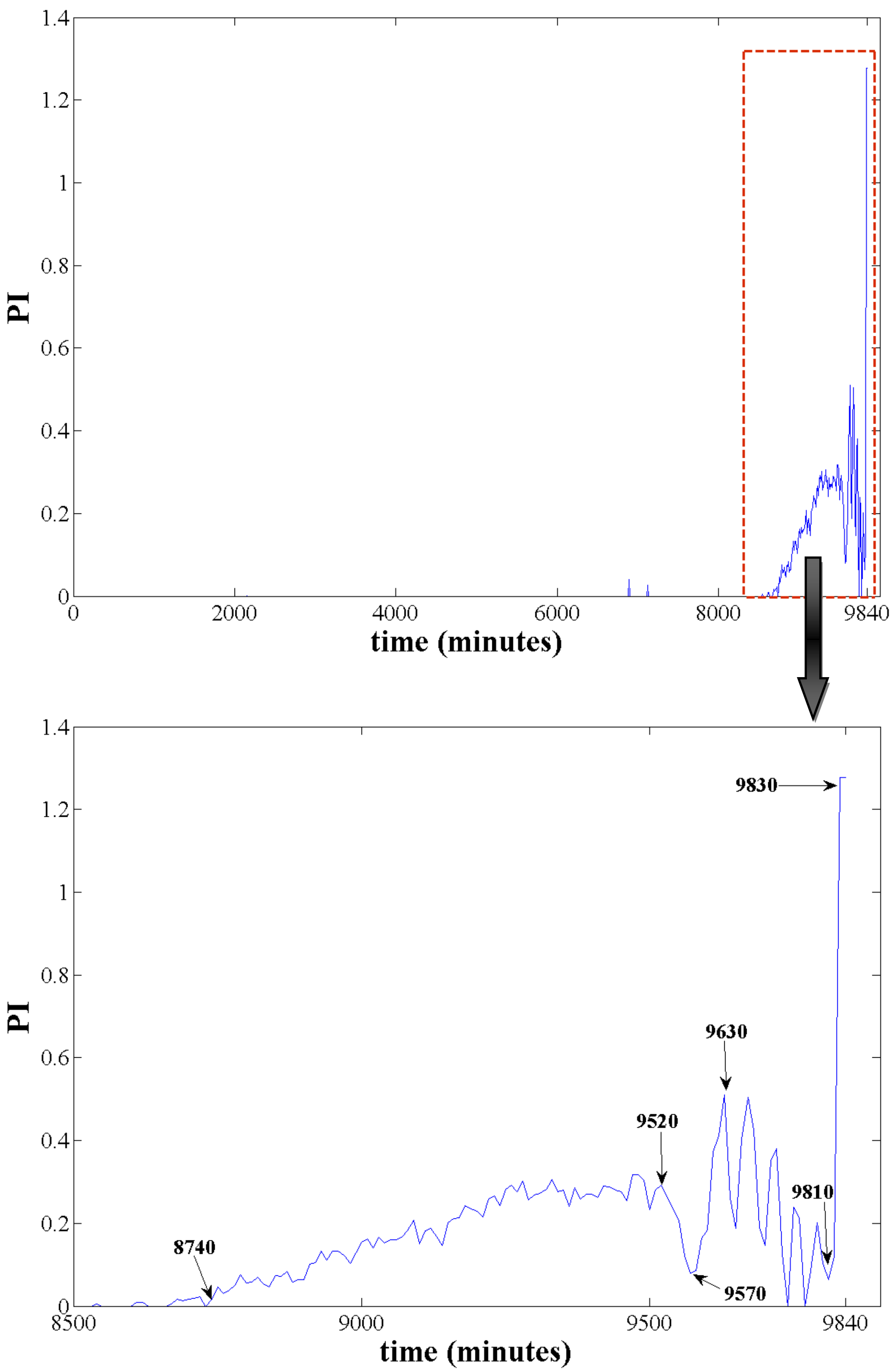

Figure 7.25 PI trend value during whole life time: S2

7.5.3 Comparison with other Index

PI is compared with another index known as H statistic [Yu, 2012]. H statistic is computed using the dynamic local and nonlocal preserving projection (DLNPP) and multivariate statistic process control approach [Yu, 2012]. DLNPP is a feature extraction technique which extracts both the local and nonlocal information of the data. Total eleven features were used for the calculation of H statistic: rms, kurtosis, skewness, crest factor, peak-to-peak, square mean root, waveform index, power ratio of maximal defective frequency to mean (PMM), Envelope PMM and two wavelet energies (level1 and level2 from the five level using daubechies wavelet, db5).

In DLNPP method, the datasets used are the same as those used for calculation of PI. H statistics which were calculated in [Yu, 2012] for S1 and S2 data's are shown in figures 7.26 and 7.27 respectively. There is an issue with time axis of the plots of H statistic used by authors of [Yu, 2012]. In the version of the data used for H statistic, it was mentioned in the data repository [NASA Ames Prognostics Data Repository] that the each dataset has an interval of 20 mins. Actually, based on the file information, it is observed that in the case of S1, first few data's (1 to 43) are of 5 mins interval and the rest are of 10 min interval. For S2, all the datasets are of 10 min interval. These information was reported to the person in-charge of the dataset and it has now been updated in the current version. To avoid any ambiguity, the author of this thesis has marked the dataset number on the H statistic plots (figures 7.26 and 7.27) which were not present in the referred work for the comparison purpose. These marking were done using data extraction software known as '*xyExtract'*. [XYExtract], as the author of H-statistic [Yu, 2012] did not provide the original plots to know the exact dataset number. The markings are nearly correct to the actual ones.

The correct time duration for S1 data is calculated by

$S1_{corrected}$ = (dataset number *10) - (43*5)

For e.g., if dataset number is 2116, then the corresponding time is $S1_{corrected}$ = 21160-215 = 20945 min. The reader must not consider 2116*20 as the real value of the corresponding time. For S2's corrected time duration is $S2_{corrected}$ = (dataset * 10) min. The time axis unit of 20 min should be neglected in figures 7.26 and 7.27.

7.5.3.1 Comparison for S1 data

On comparing the figures 7.24 and 7.26, it is seen that PI starts to increase around 18365 min, while H statistics around 20185 min (2040 dataset number). In H statistics, during the period 17295- 18785 min (1751-1900 dataset), its value is above the threshold but later it remains below the threshold till 20185 min. PI gives an early indication of fault initiation than H statistics.

7.5.3.2 Comparison for S2 data

The H statistics for S2 data (figure 7.27) shows the fault initiation time around 8720 min, while PI shows around 8740 min (figure 7.25). This shows that the PI reflects the fault degradation as tracked by the other index. The H-statistic increases till it reaches the time around of 9490 min, a similar trend is seen for PI till 9520 min. Both the indices decrease further till they reach 9570 min. Thereafter, a series of fluctuations is seen in both the indices, till the bearing failure point is reached.

The comparison shows that the PI reflects the bearing fault degradation on par with the other developed index (H statistics). It shows the correctness of PI in trending the bearing healthiness.

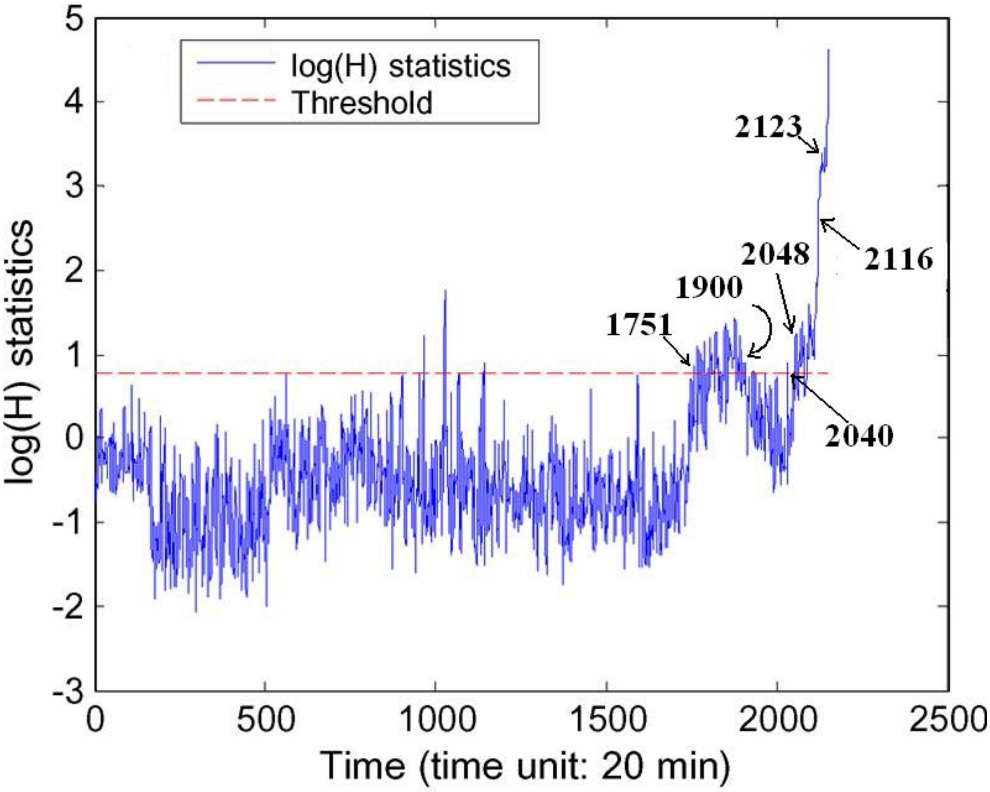

Figure 7.26 H statistics using DLNPP method [Yu, 2012]: S1

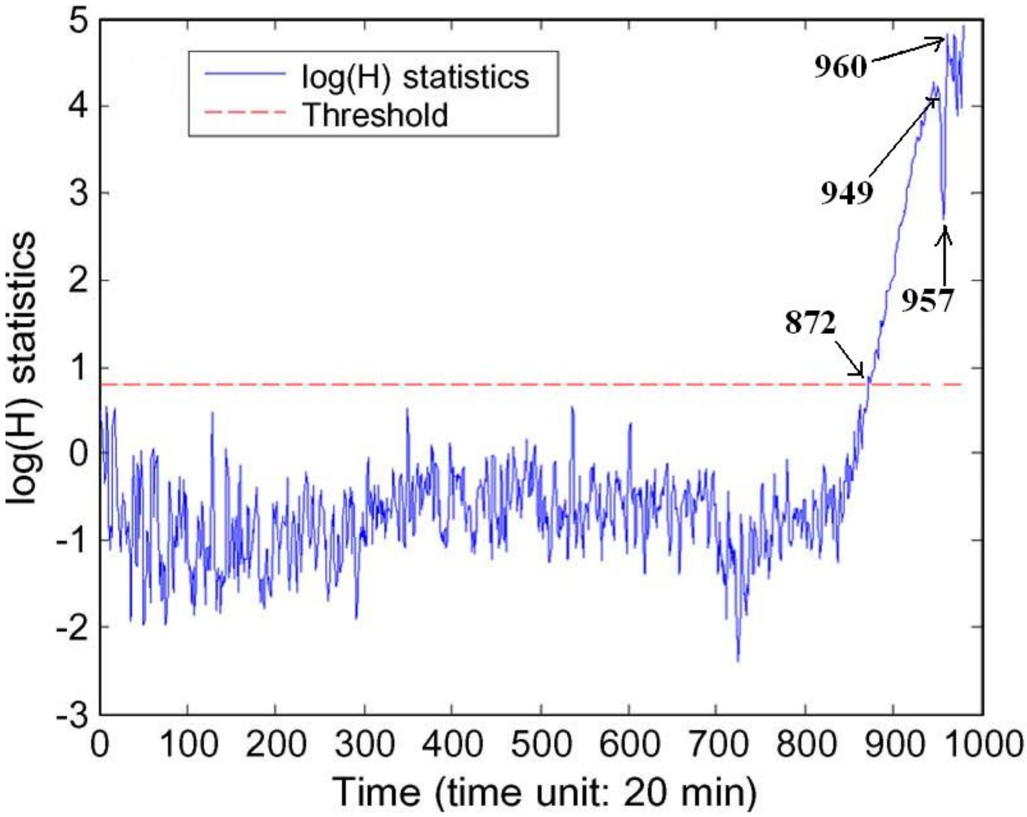

Figure 7.27 H statistics using DLNPP method [Yu, 2012]: S2

7.6 SUMMARY

A bearing fault degradation method using the support vector data description classifier and features (singular value ratio and CSI) is discussed. Degradation indicator known as performance index (PI) is developed. SVDD has the advantage of requiring only the healthy bearing data during its training. The accelerated life test results show that the developed performance index clearly reflects the different stages of bearing degradation. Comparison of PI with a recently developed index known as H statistic shows that PI shows similar trending feature as shown by H statistic. This shows the suitability of PI for reliable trend analysis. There is no need for fixing the fault threshold (varies with signal) as needed for the H-statistic. Combining PI with some regression methods such as neural networks, support vector machines and particle filter, the remaining useful life of a bearing could be computed.

PART V

HIGHLIGHTS AND FORESIGHT

CONTENTS:

CHAPTER 8

SUMMARY, CONTRIBUTIONS AND FURTHER SCOPE/GAP AREAS

MAIN CONTENTS:

- **Summary of the work**
- **Contributions of the research**
- **Further Scope/ Gap Areas**

8.1 SUMMARY OF THE WORK

The work presented in this thesis covers the important areas of the bearing condition monitoring: fault detection, fault diagnosis and fault prognosis (fault degradation). The works carried out in each of these areas are summarized below:

8.1.1 FAULT DETECTION

8.1.1.1 DETECTION OF FAULTY BEARING USING SYMBOLIC DYNAMICS

Due to the modulation occurring in fault signal, the statistics of the signals changes which are detected using the symbolic dynamic approach. The time series data is converted into a symbolic series. The symbolic series generation is done using the maximum entropy based partitioning approach. The measure of deviation called as Common Signal Index (CSI), is the parameter which compares the fractional occurrence of the symbols for healthy and faulty conditions. Based on the CSI (CSI1 and CSI3) value, faulty condition of bearing is detected.

In this method, two signals are used. One is a reference signal which is a healthy data. Other is a signal (test signal) whose condition is to be determined. A common signal index was calculated by using the fractional occurrences of the symbols in both the signals. On the basis of the results obtained, bearing condition is classified using the rule formed: If CSI1 = 0.48 to 0.5 or CSI3 = 0 to 0.2, Bearing is in healthy else faulty.

The method works well for experimental conditions (test data1 and 2) and simulation data (test data3). The results show the robustness of method even in presence of masking sources such as gearbox (test data2). Even when the reference and the test signal are noisy, the fault index gives satisfactory results. This method is well suited as a start up test of a motor for bearing healthiness check before commencing the normal operation as it works even in no-load condition.

8.1.1.1.1 Advantages

i. The performance of this method is sample size independent.
ii. The method does not need fault data beforehand to detect the presence of fault. Hence, it overcomes the problem of training the fault algorithm from machine to machine.
iii. It is load independent.

8.1.1.1.2 Limitations

i. Computational complexity is high.

8.1.1.2 IDENTIFICATION OF FAULTY BEARINGS USING SINGULAR VALUE RATIO: A CASE STUDY

A time domain method using singular spectrum analysis for faulty bearing detection was discussed. It was shown that the ratio of adjacent singular value extracted from the time domain bearing vibration signals are useful in determination of the faulty bearings. The ratio of the singular values is found to be having a constant value (one) for fault condition and another range of values (much greater than one) for healthy condition (SV). Based on the comparison with the other simple time domain methods (Difference Histogram and Zero crossing methods), it has advantages such as feature is sample size and load independent, method performs well even for noisy signal.

8.1.1.2.1 Advantages

i. The fault index is not affected by sample size, load variations and the method work even in the presence of noise.

8.1.1.2.2 Limitations

i. The fault index does not show much variation with respect to fault severity.

8.1.2 FAULT DIAGNOSIS

8.1.2.1 BEARING FAULT DIAGNOSIS USING SINGULAR SPECTRUM ANALYSIS

Bearing fault feature extraction based on singular spectrum analysis (SSA) was presented. The signals were decomposed into the number of principal component signals using SSA. A new fault feature (singular value (SV)) was introduced for bearing fault detection. A new approach for selection of the principal components was employed using singular value plot. Two methods were discussed. In the first method, singular values extracted from the bearing vibration signal are used as fault features which are given to feed forward back propagation neural network (BPNN) for automated fault diagnosis. In the second method, the correlation between the principal components corresponding to the selected SV and the bearing fault were investigated. It showed that the features obtained from the principal components corresponding to SV numbers are useful for fault detection. An energy feature was used for the fault identification in combination with BPNN. The method is found to have more advantages over the existing time series and data based methods. The experimental results demonstrate that the singular spectrum analysis based bearing fault diagnosis method is simple, noise tolerant and efficient.

8.1.2.1.1 Advantages

i. The method is simple, detects faults even in a signal with a low SNR and also with masking sources such as gearbox.

8.1.2.1.2 Limitations

i. It requires history of fault signals for training of the classifier.

8.1.2.2 GENERALIZED TEAGER KAISER ENERGY OPERATOR BASED BEARING FAULT DIAGNOSIS

A simple method for bearing fault diagnosis based on Generalized Teager Kaiser Energy Operator (GTKEO) which incorporates demodulation was developed. The diagnosis method involves the transformation of the signal using GTKEO and followed by spectral analysis. The developed method (GTKEO or M-TKEO) is compared with a parameter-free method (Teager Kaiser Energy Operator (TKEO)).The efficiency of the GTKEO method in comparison with TKEO method under very low SNR conditions was shown through experimentally obtained bearing fault data's: with and without gearbox. The fault detection ability of energy operator is improved for signals with low SNR using the M-TKEO approach. Only one parameter (M) is required for calculation which is easily obtained by using energy ratio plot. The M value is adaptive according to the signal and interfering components such as noise and gearbox.

From the experimental results, it was seen that M-TKEO suppresses the effects of additive noise. No repetitive operation of M-TKEO is needed as required for TKEO. The effectiveness of M-TKEO over TKEO in locating the bearing fault in low SNR and also in presence of vibration interference component such as from gears was demonstrated. M-TKEO satisfies the requirements of a spectrum based fault diagnosis method.

8.1.2.2.1 Advantages

i. Simple calculations involved.

ii. Works well under presence of masking sources such as gearbox and even under very low SNR (-30 dB) scenario.

iii. Suitable for handheld vibration analyzer.

8.1.2.2.2 Limitations

i. Denoising may be required for combination of extremely low SNR signals (below -30 dB) in gearbox applications.

8.1.3 FAULT PROGNOSIS (FAULT DEGRADATION)

8.1.3.1 PERFORMANCE INDEX DEVELOPMENT FOR FAULT DEGRADATION USING THE SUPPORT VECTOR DATA DESCRIPTION METHOD

The bearing fault degradation method based on support vector data description classifier and features (singular value ratio and CSI) were discussed. Degradation indicator known as performance index (PI) was developed. SVDD has the advantage of requiring only the healthy bearing data during the training. The accelerated life test results showed that the developed performance index clearly reflects the different stages of bearing degradation. Comparison of PI with a recently developed index known as H statistic showed that PI has similar trending feature as shown by H statistic. This showed the accurateness of PI in trending the bearing health. There is no need of fixing the fault threshold (varies with signal) as needed for H-statistic.

8.1.3.1.1 Advantages

i. Performance Index trends the bearing condition from its healthy to fault initiation and then till its failure.

ii. There is no need of fixing the fault threshold.

8.1.3.1.2 Limitations

i. The index does not have a perfect monotonous trend.

8.1.4 OVERALL WORK

The complete work presented in the thesis is been summarized in table 8.1.

Table 8.1 Overall work of the thesis

Condition Monitoring Stage	Methodology	Based on
Fault Detection	Symbolic dynamics (SD)	Fault Index - Common Signal Index (CSI)
	Singular Spectrum Analysis (SSA)	Fault Feature – Singular Value Ratio (SVR)
Fault Diagnosis	SSA and Back Propagation Neural Network (BPNN)	Fault Feature – Singular Value, Energy Value
	Generalized Teager Kaiser Energy Operator (GTKEO)	Fault characteristic frequencies detection
Fault Prognosis (Degradation)	SSA, SD, Support Vector Data Description (SVDD)	Performance Index based on SVDD using CSI and SVR

The developed methods are also illustrated in the form of a block diagram which is shown in figure 8.1.

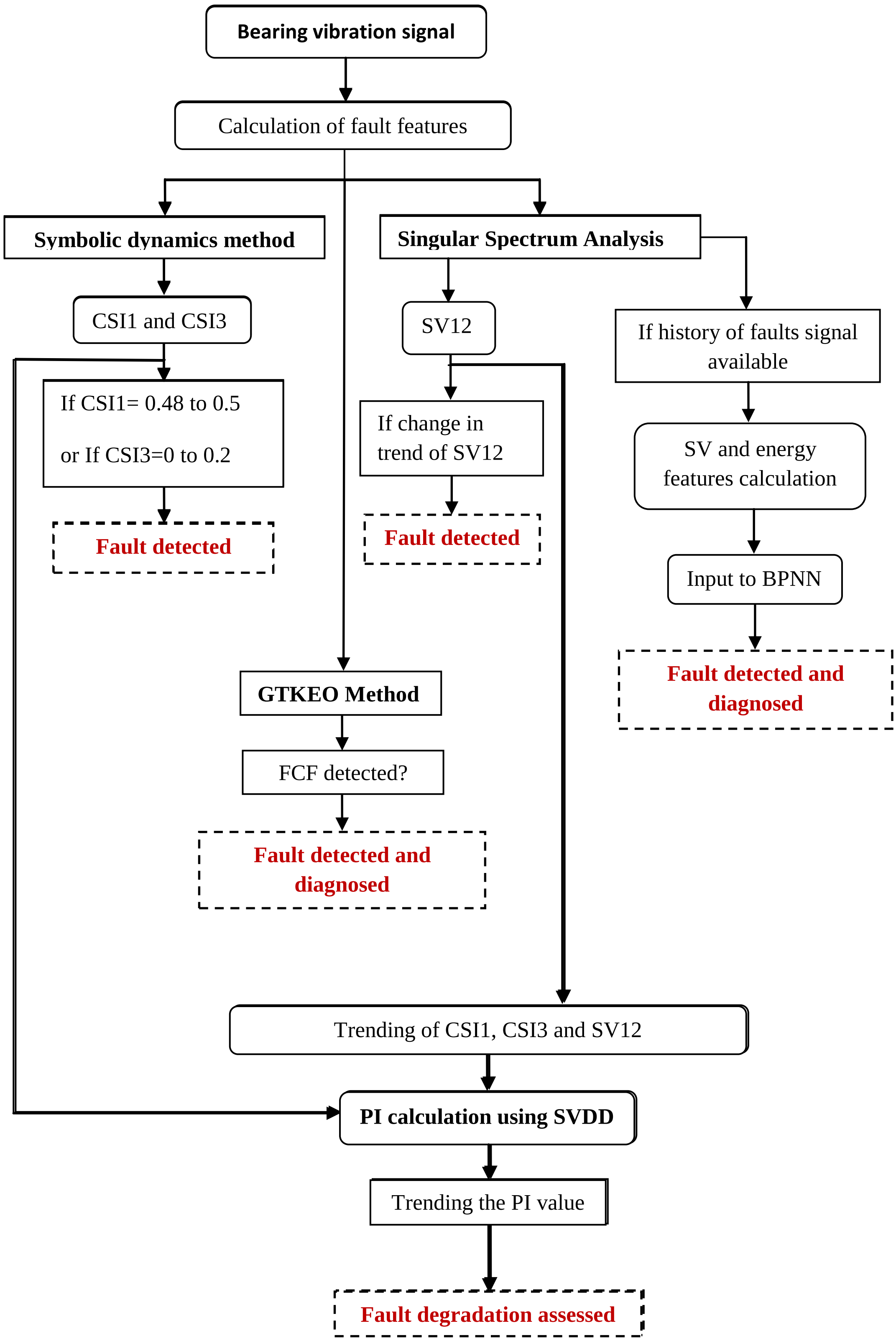

Figure 8.1 Bearing condition monitoring methods developed in this thesis

8.2 CONTRIBUTIONS OF THE RESEARCH

The work presented in this thesis includes novel approaches and improved the state-of-the-art in vibration based rolling element bearing condition monitoring. They are listed below:

i. A first approach based on symbolic dynamics for detection of faulty bearing using vibration signal is implemented. It overcomes the shortcomings of existing time domain and data based methods.
ii. Noise immune and sample size invariant bearing fault detection methods based on new fault indices (Common Signal Index, Singular Value Ratio) are presented.
iii. A simple online fault diagnosis method based on Generalized Teager Kaiser Energy Operator is developed and effectively verified. It does not require the band pass filter (conventional approach) and works well even for a low SNR signals (-30 dB). It is a useful method for a handheld vibration analyzer.
iv. A first of its kind method based on singular spectrum analysis is discussed for fault feature extraction and successfully diagnosed the faults of the tested bearings.
v. Performance Index (degradation condition indicator) for bearing fault prognosis is developed.

8.3 FUTURE SCOPE / GAP AREAS

8.3.1 FAULT DETECTION

8.3.1.1 DETECTION OF FAULTY BEARING USING SYMBOLIC DYNAMICS

i. In symbolic dynamics method, maximum entropy based partitioning approach was used. Development of an automatic method for the setting of threshold is desirable.
ii. Other methods of symbolic series generation such as symbolic false nearest neighbor partitioning [Kennel & Buhl, 2003], wavelet space partitioning [Rajagopalan & Ray, 2006] and analytic signal space partitioning (ASSP) [Subbu & Ray, 2008] could also be used.
iii. Systematic analysis to backup the classification rules used for CSI1 and CSI3.
iv. To study the statistical dependency between CSI1 and CSI3 and exploiting it for fault detection.

v. To study the error when a) Fault is treated as healthy; b) Healthy is treated as faulty. Characterizing these errors depending on the statistics of CSI1 and CSI3.

8.3.1.2 IDENTIFICATION OF FAULTY BEARINGS USING SINGULAR VALUE RATIO: A CASE STUDY

i. Singular value coupling is used for the fault detection. Physical explanation of singular value coupling could be explored.

8.3.2 FAULT DIAGNOSIS

8.3.2.1 BEARING FAULT DIAGNOSIS USING SINGULAR SPECTRUM ANALYSIS

i. In Singular spectrum analysis method, the window length was chosen based on comparison of the singular value plots. The possibility to have an automatic method for selection of window length should be explored.

8.3.2.2 GENERALIZED TEAGER KAISER ENERGY OPERATOR BASED BEARING FAULT DIAGNOSIS

i. The lag parameter, M was calculated using energy ratio plot. Other methods for selection of M could be explored.

ii. Hardware implementation of the Generalized Teager Kaiser Energy Operator (GTKEO) method can be done.

iii. Analyzing the GTKEO method under the presence of other masking sources such as compressors and pump could be considered.

iv. There is a possibility of having a single method applicable in all the three stages of condition monitoring using GTKEO method. Using the online GTKEO method, both fault detection and diagnosis is carried out. Energy of the signal obtained after the application of GTKEO could be used for fault trending. The author has studied its applicability (results are not included). Further work using this energy to be carried out.

v. Verifying the applicability of GTKEO method even for low speed machines (< 10 rpm)

8.3.3 FAULT PROGNOSIS (FAULT DEGRADATION)

i. Gaussian kernel function was used in the Support Vector Data Description method. Performance comparison using other kernel functions such as polynomial function and sigmoid function could be studied.

ii. The hypersphere of the SVDD is little sensitive to outliers and may result in over fitting problems. Solutions to overcome the over fitting issue could be studied.

iii. SVDD model is fixed using the healthy data's. But, in real time the SVDD model should be updated to the current health status. An incremental algorithm for SVDD [Tax & Laskov, 2003] model could be used to improve the method.

iv. Performance index (PI) tracks the bearing health efficiently. The PI increases with defect severity but it is also oscillatory. However, a monotonic degradation index which reflects the bearing defect severity more efficiently is needed.

v. Singular values used for fault diagnosis could be used for developing a degradation index.

vi. Remaining useful life of bearing could be computed by combining the performance index with appropriate regression methods such as neural networks, support vector machines and particle filter.

Some of the common future works involve:

i. Developing a GUI to enable the use of algorithms easily and efficiently.

ii. Calculating the computational complexity of the methods.

APPENDIX

I. Demodulation of Fault Signal using Generalized Teager Kaiser Operator and Signal Improvement Ratio

In this section, the derivation of some of the equations described in the section 6.3 is given.

A. Cross Term Energy Operator (Ψ_c)

The cross term energy operator (Ψ_c) [equation 6.9] between the fault impulses and vibration interference signal is given as

$$\Psi_c = \Psi\left[I_f\, e^{-\beta n}\cos(\omega_n n + \varphi), V_i\cos(\omega_v n)\right]$$

$$= -[I_f e^{-\beta(n+M)}\cos(\omega_n(n+M)+\varphi)\ V_i\cos\omega_v - 2I_f\, e^{-\beta n}\cos(\omega_n n+\varphi)\, V_i\cos\omega_v n + I_f\, e^{-\beta(n-M)}\cos(\omega_n(n-M) + \varphi)\ V_i\cos\omega_n(n+M)]$$

$$= V_i I_f e^{-\beta(n+M)}\{\cos[\omega_n n + M\omega_n + \omega_v n - \omega_v M + \varphi] + \cos[\omega_n n + M\omega_n - \omega_v n + \omega_v M + \varphi]\} - 2V_i I_f\, e^{-\beta n}\{\cos[\omega_n n + \omega_v n + \varphi] + \cos[\omega_n n - \omega_v n + \varphi]\} + V_i I_f e^{-\beta(n-M)}\{\cos[\omega_n n - M\omega_n + \omega_v n + \omega_v M + \varphi] + \cos[\omega_n n - M\omega_n - \omega_v n - \omega_v M + \varphi]\}$$

$$\begin{aligned} = V_i I_f e^{-\beta(n+M)}\{&\cos[(\omega_n+\omega_v)n + (\omega_n-\omega_v)M + \varphi] \\ &+ \cos[(\omega_n-\omega_v)n + (\omega_n+\omega_v)M + \varphi]\} \\ &- 2V_i I_f\, e^{-\beta n}\{\cos[(\omega_n+\omega_v)n + \varphi] + \cos[(\omega_n-\omega_v)n + \varphi]\} \\ &+ V_i I_f e^{-\beta(n-M)}\{\cos[(\omega_n+\omega_v)n - (\omega_n-\omega_v)M + \varphi] \\ &+ \cos[(\omega_n-\omega_v)n - (\omega_n+\omega_v)M + \varphi]\} \end{aligned}$$

$$\begin{aligned} = V_i I_f e^{-\beta n}\{&e^{-\beta M}[\cos[(\omega_n+\omega_v)n + (\omega_n-\omega_v)M + \varphi] \\ &+ \cos[(\omega_n-\omega_v)n + (\omega_n+\omega_v)M + \varphi]] \\ &- 2(\cos[(\omega_n+\omega_v)n + \varphi] \\ &+ \cos[(\omega_n-\omega_v)n + \varphi]) + e^{\beta M}([\cos[(\omega_n+\omega_v)n - (\omega_n-\omega_v)M + \varphi] \\ &+ \cos[(\omega_n-\omega_v)n - (\omega_n+\omega_v)M + \varphi]])\} \end{aligned}$$

Finally, we get

$$\Psi_c = V_i I_f e^{-\beta n} L(n) \tag{A.1}$$

where,

$$L(n) = \{e^{-\beta M}[\cos[(\omega_n + \omega_v)n + (\omega_n - \omega_v)M + \varphi] + \cos[(\omega_n - \omega_v)n + (\omega_n + \omega_v)M + \varphi]] - 2(\cos[(\omega_n + \omega_v)n + \varphi] + \cos[(\omega_n - \omega_v)n + \varphi]) + e^{\beta M}([\cos[(\omega_n + \omega_v)n - (\omega_n - \omega_v)M + \varphi] + \cos[(\omega_n - \omega_v)n - (\omega_n + \omega_v)M + \varphi]])\}$$

B. GTKEO of fault impulses

GTKEO of fault impulses [equation 6.12] is given as

$$\Psi[I_f\, e^{-\beta n} \cos(\omega_n n + \varphi)] = (I_f \cos(\omega_n + \varphi))^2\, \Psi\left[e^{-\beta n}\right] + \left(e^{-\beta n}\right)^2 \Psi[I_f\, \cos(\omega_n + \varphi)]$$

$$= 0 + e^{-2\beta n} {I_f}^2 \sin^2(\omega_n M)$$

$$= {I_f}^2\, e^{-2\beta n} \sin^2(\omega_n M) \tag{B.1}$$

C. Signal to Interference ratio (SIR)

Signal to Interference ratio (SIR) [equation 6.17] is

$$\mathrm{SIR}[X(n)] = \frac{\frac{1}{N_f}\int_0^{N_f}\left(I_f\, e^{-\beta n}\ \cos(\omega_n n+\varphi)\right)^2 dn}{\frac{1}{N_v}\int_0^{N_v}(V_i \cos(\omega_v n))^2 dn + \sigma^4} \tag{C.1}$$

Assume $a = \frac{1}{N_f}\int_0^{N_f}\left(I_f\, e^{-\beta n}\ \cos(\omega_n n + \varphi)\right)^2 dn$ (C.2)

$$b = \frac{1}{N_v}\int_0^{N_v}(V_i \cos(\omega_v n))^2\, dn \tag{C.3}$$

Using Wolfram Math tool

$$a \approx \frac{\beta^2 \cos 2\varphi - \beta\omega_n \sin 2\varphi + \beta^2 + {\omega_n}^2}{4\beta(\beta^2 + {\omega_n}^2)} \quad \text{for } |\mathrm{Im}(\omega_n)| < Re(\beta) \tag{C.4}$$

$$\therefore\ a \approx \frac{{I_f}^2}{N_f}\left[\frac{\beta^2 + {\omega_n}^2}{4\beta(\beta^2 + {\omega_n}^2)} + \frac{\beta(\beta \cos 2\varphi - \omega_n \sin 2\varphi)}{4\beta(\beta^2 + {\omega_n}^2)}\right] \approx \frac{{I_f}^2}{N_f}\left[\frac{1}{4\beta} + \frac{(\beta \cos 2\varphi - \omega_n \sin 2\varphi)}{4(\beta^2 + {\omega_n}^2)}\right] \tag{C.5}$$

$$b = \frac{1}{N_v} V_i^2 \int_0^{N_v} (\cos(\omega_v n))^2 \, dn$$

$$= \frac{V_i^2}{N_v} \left[\frac{2N_v\omega_v + \sin(2N_v\omega_v)}{4\omega_v}\right] \quad (C.6)$$

In the above equation, we see that $2N_v\omega_v \gg \sin(2N_v\omega_v)$. Thus, $\sin(2N_v\omega_v)$ is neglected. Then, equation (C.6) becomes

$$b = \frac{V_i^2}{N_v} \left[\frac{2N_v\omega_v}{4\omega_v}\right] = \frac{V_i^2}{2} \quad (C.7)$$

Using equations (C.2, C.3, C.5, C.6), $SIR[X(n)]$ (equation C.1) becomes

$$SIR[X(n)] \approx \frac{\frac{I_f^2}{N_f}\left[\frac{1}{4\beta} + \frac{(\beta\cos 2\varphi - \omega_n \sin 2\varphi)}{4(\beta^2 + \omega_n^2)}\right]}{\frac{V_i^2}{2} + \sigma^4}$$

$$\approx \frac{I_f^2}{2N_f\beta(V_i^2 + 2\sigma^4)} + \frac{I_f^2(\beta\ \cos 2\varphi - \omega_n \sin 2\varphi)}{2N_f(V_i^2 + 2\sigma^4)(\beta^2 + \omega_n^2)}$$

$$\therefore\ SIR[X(n)] \approx \frac{I_f^2}{2N_f\beta(V_i^2 + 2\sigma^4)} + \frac{I_f^2(\beta\ \cos 2\varphi - 2\pi f_n \sin 2\varphi)}{2N_f(V_i^2 + 2\sigma^4)(\beta^2 + 4\pi^2 f_n^2)} \quad (C.8)$$

D. Calculation of SIR for $\beta \approx f_n$ and $\beta \ll f_n$

D.1 Case: $\beta \approx f_n$ (equation 6.18)

$$SIR[X(n)] \approx \frac{I_f^2}{2N_f\beta(V_i^2 + 2\sigma^4)} + \frac{I_f^2(\beta\ \cos 2\varphi - 2\pi f_n \sin 2\varphi)}{2N_f(V_i^2 + 2\sigma^4)(\beta^2 + 4\pi^2 f_n^2)} \quad \text{(from equation C.8)}$$

([φ is very low, $\therefore \sin 2\varphi \approx 0$ and $\cos 2\varphi \approx 1$)

$$\approx \frac{I_f^2}{2N_f\beta(V_i^2 + 2\sigma^4)} + \frac{I_f^2\beta}{2N_f(V_i^2 + 2\sigma^4)\beta^2(1 + 4\pi^2)}$$

$$\approx \frac{I_f^2}{2N_f\beta(V_i^2 + 2\sigma^4)} + \frac{I_f^2}{2N_f(V_i^2 + 2\sigma^4)\beta^2(1 + 4\pi^2)}$$

$$\approx \frac{I_f^2}{2N_f\beta(V_i^2 + 2\sigma^4)}\left[1 + \frac{1}{1 + 4\pi^2}\right]$$

$$\approx \frac{1.025 I_f^2}{2N_f\beta(V_i^2 + 2\sigma^4)}$$

Thus, $SIR[X(n)] \approx \frac{1.025 I_f^2}{2N_f f_n(V_i^2 + 2\sigma^4)}$ (D1.1)

D.2 Case: $\boldsymbol{\beta} \approx \mathbf{f_n}$ (equation 6.19)

$$\mathrm{SIR}[X(n)] \approx \frac{{I_f}^2}{2N_f\beta({V_i}^2+2\sigma^4)} + \frac{{I_f}^2(\beta\ \cos 2\varphi - 2\pi f_n \sin 2\varphi)}{2N_f({V_i}^2+2\sigma^4)(\beta^2+4\pi^2{f_n}^2)} \qquad \text{(from equation C.8)}$$

Based on the assumption of φ done for $\beta \approx f_n$, the second term in the above equation becomes negligible

Hence, $$\mathrm{SIR}[X(n)] \approx \frac{{I_f}^2}{2N_f\beta({V_i}^2+2\sigma^4)} \qquad \text{(D2.1)}$$

REFERENCES

Abbasion, S., Rafsanjani, A., Farshidianfar, A., & Irani, N. (2007). Rolling element bearings multi-fault classification based on the wavelet denoising and support vector machine. *Mechanical Systems and Signal Processing*, *21*(7), 2933-2945.

Ai, S., Li, H., & Zhang, Y. (2009, April). Condition Monitoring for Bearing Using Envelope Spectrum of EEMD. In Measuring *Technology and Mechatronics Automation, 2009. ICMTMA'09. International Conference on* (Vol. 1, pp. 190-193). IEEE.

Al Regib, E. and Ni, J. (2010). Chatter Detection in machining using non linear energy operator. Journal of Dynamic system, measurement and control, Vol. 132, issue 3, 034502-1–034502-4.

Albrecht, P. F., Appiarius, J. C., Cornell, E. P., Houghtaling, D. W., McCoy, R. M., Owen, E. L., & Sharma, D. K. (1987). Assessment of the reliability of motors in utility applications. Energy Conversion, IEEE Transactions on, (3), 396-406.

Alfredson, R. J., & Mathew, J. (1985a). Time domain methods for monitoring the condition of rolling element bearings. *Transactions of the Institution of Engineers, Australia. Mechanical engineering*, *10*(2), 102-107.

Alfredson, R. J., & Mathew, J. (1985b). Frequency domain methods for monitoring the condition of rolling element bearings. *Transactions of the Institution of Engineers, Australia. Mechanical engineering*, *10*(2), 108-112.

Alonso, F.J., & Salgado, D.R. (2008). Analysis of the structure of vibration signals for tool wear detection. Mechanical Systems and Signal Processing, 22(3),735–748.

Al-Raheem, K. F., Roy, A., Ramachandran, K. P., Harrison, D. K., & Grainger, S. (2008). Application of the Laplace-wavelet combined with ANN for rolling bearing fault diagnosis. *Journal of vibration and acoustics*, *130*(5).

Antoni, J. (2005). Blind separation of vibration components: Principles and demonstrations. *Mechanical Systems and Signal Processing*, *19*(6), 1166-1180.

Antoni, J. (2007). Fast computation of the kurtogram for the detection of transient faults. *Mechanical Systems and Signal Processing*, *21*(1), 108-124.

Antoni, J., & Randall, R. B. (2004a). Unsupervised noise cancellation for vibration signals: Part I—Evaluation of adaptive algorithms. *Mechanical Systems and Signal Processing*, *18*(1), 89-101.

Antoni, J., & Randall, R. B. (2004b). Unsupervised noise cancellation for vibration signals: part II—a novel frequency-domain algorithm. *Mechanical Systems and Signal Processing*, *18*(1), 103-117.

Antoni, J., & Randall, R. B. (2006). The spectral kurtosis: application to the vibratory surveillance and diagnostics of rotating machines. *Mechanical Systems and Signal Processing*, *20*(2), 308-331.

Baillie, D. C., & Mathew, J. (1996). A comparison of autoregressive modeling techniques for fault diagnosis of rolling element bearings. *Mechanical Systems and Signal Processing*, *10*(1), 1-17.

Balderston, H.L. (1969). The detection of incipient failure in bearings. *Mater Evaluation*, *27*(6), 121-128.

Bao, W., Zhou, R., Yang, J., Yu, D., & Li, N. (2009). Anti-aliasing lifting scheme for mechanical vibration fault feature extraction. *Mechanical Systems and Signal Processing*, *23*(5), 1458-1473

Bari, H. M., Deshpande, A. A., Jalkote, P. S., & Patil, S. S. (2012, May). Pump Coupling & Motor bearing damage detection using Condition Monitoring at DTPS. In Journal of Physics: Conference Series (Vol. 364, No. 1, p. 012022). IOP Publishing.

Barszcz, T., & JabŁoński, A. (2011). A novel method for the optimal band selection for vibration signal demodulation and comparison with the Kurtogram. *Mechanical Systems and Signal Processing*, *25*(1), 431-451.

Bearing data Centre, Case Western Reserve University Available : <http://csegroups.case.edu/bearingdatacenter/home>> [accessed May 2010]

Bell, R. N., McWilliams, D. W., O'Donnell, P., Singh, C., & Wells, S. J. (1985). Report of large motor reliability survey of industrial and commercial installations. I.IEEE Transactions on Industry Applications, 21(4), 853-864.

Bendat, J.S., & Piersol, A. G. (1971). *Random data: analysis of measurement procedures*, Wiley Interscience.

Berry, J.E. (1991). How to track rolling element bearing health with vibration signature analysis, Sound Vib. 25 (1991) 24–35.

Bouguerriou, N., Haritopoulos, M., Capdessus, C., & Allam, L. (2005). Novel cyclostationarity-based blind source separation algorithm using second order statistical properties: Theory and application to the bearing defect diagnosis. *Mechanical Systems and Signal Processing*, *19*(6), 1260-1281.

Boustany, R., & Antoni, J. (2005). A subspace method for the blind extraction of a cyclostationary source: Application to rolling element bearing diagnostics. *Mechanical Systems and Signal Processing*, *19*(6), 1245-1259.

Boutros, T., & Liang, M. (2011). Detection and diagnosis of bearing and cutting tool faults using hidden Markov models. *Mechanical systems and signal processing*, *25*(6), 2102-2124.

Bozchalooi, I. S., & Liang, M. (2007). A smoothness index-guided approach to wavelet parameter selection in signal de-noising and fault detection. *Journal of Sound and Vibration*, *308*(1), 246-267.

Bozchalooi, I. S., & Liang, M. (2008). A joint resonance frequency estimation and in-band noise reduction method for enhancing the detectability of bearing fault signals. *Mechanical Systems and Signal Processing*, *22*(4), 915-933.

Bozchalooi, I.S. & Liang, M. (2009). Parameter-free bearing fault detection based on maximum likelihood estimation and differentiation. Measurement Science and Technology, 20(6), 065102-1– 065102-14.

Bradshaw, P., & Randall, R. B. (1983, September). Early detection and diagnosis of machine faults on the Trans Alaska Pipeline. In *MSA session, ASME Conference, Dearborn, Mich.*

Brüel & Kjaer (1990). *Machine health monitoring using vibration analysis*. Proceedings of the workshop presented by J. Courrech and R.B. Randall, Monash university, September.

Caesarendra, W., Widodo, A., & Yang, B. S. (2010). Application of relevance vector machine and logistic regression for machine degradation assessment. *Mechanical Systems and Signal Processing*, *24*(4), 1161-1171.

Caesarendra, W., Widodo, A., & Yang, B. S. (2011). Combination of probability approach and support vector machine towards machine health prognostics. *Probabilistic Engineering Mechanics*, *26*(2), 165-173.

Carniel, R., Barazza, F., Tárraga, M., & Ortiz, R. (2006). On the singular values decoupling in the Singular Spectrum Analysis of volcanic tremor at Stromboli. *Natural Hazards and Earth System Science, 6*(6), 903-909.

Chaturvedi, G. K. (1982). Bearing fault detection using adaptive noise cancelling. *Trans. of the ASME Journal of Mechanical Design*, *104*, 280-289.

Chau, T., & Wong, A. K. (1999). Pattern discovery by residual analysis and recursive partitioning. *Knowledge and Data Engineering, IEEE Transactions on,11*(6), 833-852

Chen, J., Zi, Y., He, Z., & Yuan, J. (2012). Improved spectral kurtosis with adaptive redundant multiwavelet packet and its applications for rotating machinery fault detection. *Measurement Science and Technology*, *23*(4), 045608.

Chen, Q., Chen, Z., Sun, W., Yang, G., Palazoglu, A., & Ren, Z. (2013). A new structuring element for multi-scale morphology analysis and its application in rolling element bearing fault diagnosis. *Journal of Vibration and Control*.

Cheng, J., Yang, Y., & Yang, Y. (2012). A rotating machinery fault diagnosis method based on local mean decomposition. *Digital Signal Processing*, *22*(2), 356-366.

Christian, K., Mureithi, N., Lakis, A., & Thomas, M. (2007). On the use of time synchronous averaging, independent component analysis and support vector machines for bearing fault diagnosis. In *First international conference on industrial risk engineering*.

Coffin, T., & Jong, J. Y. (1986). *Signal detection techniques for diagnostic monitoring of space shuttle main engine turbomachinery*. National Aeronautics and Space Administration.

Cong, F., Chen, J., & Pan, Y. (2011). Kolmogorov-Smirnov test for rolling bearing performance degradation assessment and prognosis. *Journal of vibration and control*, *17*(9), 1337-1347

Da Silva Vicente, S. A., Fujimoto, R. Y., & Padovese, L. R. (2001, December). Rolling bearing fault diagnostic system using fuzzy logic. In *Fuzzy Systems, 2001. The 10th IEEE International Conference on* (Vol. 2, pp. 816-819

Darlow, M.S., Badgley, R.H. & Hogg G.W. (1974): Application of high frequency resonance techniques for bearing diagnostics in helicopter gearboxes, *Us Army Air Mobility Research and Development Laboratory*, Technical Report, pp. 74-77.

DD toolbox. Available: http: www-ict.ewi.tudelft.nl/_davidt/dd_tools.html. (July 2013).

Dong, G., & Chen, J. (2012). Noise resistant time frequency analysis and application in fault diagnosis of rolling element bearings. *Mechanical Systems and Signal Processing*, 33, 212-236

Dong, Y., Liao, M., Zhang, X., & Wang, F. (2011). Faults diagnosis of rolling element bearings based on modified morphological method. *Mechanical Systems and Signal Processing*, *25*(4), 1276-1286.

Dutoit, T., Kandia, V. and Stylianou, Y. (2009). How can marine biologists track sperm whales in the oceans. Applied signal Processing, Springer, Ch.6, 185-221.

Dyer, D., & Stewart, R. M. (1978). Detection of rolling element bearing damage by statistical vibration analysis. *Journal of Mechanical Design*, *100(2)*, 229-235.

Ebersbach, S., & Peng, Z. (2008). Expert system development for vibration analysis in machine condition monitoring. *Expert Systems with Applications*, *34*(1), 291-299

Engja, H., Rasmussen, M., & Lippe, J. (1977). Vibration analysis used for detection of rolling element bearing failures. Norwegian Maritime Research, 3, 23–33.

Eschmann P, Hasbargen L, Weigand K 1958 *Ball and roller bearings: Their theory, design, and application.*

FAG Bearing, (1979), antriebstechnik 18 (3), 71-74

FAG Bearings (1997). Rolling Bearing Damage Publ. No. WL 82 102/2 ED

Fatima, S., Dastidar, S. G., Mohanty, A. R., & Naikan, V. N. A. (2013). Technique for optimal placement of transducers for fault detection in rotating machines. *Proceedings of the Institution of Mechanical Engineers, Part O: Journal of Risk and Reliability*, *227*(2), 119-131.

Feng, Z., & Chu, F. (2008). Application of adaptive time–frequency analysis to fault diagnosis of machinery. *Chin. J. Sci. Instrum*, 29 (4), 604–608.

Garamani, Z. (2001). An Introduction to Hidden Markov Models and Bayesian Networks. *International Journal of Pattern Recognition and Artificial Intelligence.* 15(1), 9-42

Golyandina, N., Nekrutkin, V., & Zhigljavsky, A. A. (2010). *Analysis of time series structure: SSA and related techniques*. CRC Press.

Graney, B.P., & Starry, K. (2012) Rolling element bearing analysis, Materials Evaluation, 70 (1), 78-85.

Gupta, S., Singh, D., Srivastav, A., & Ray, A. (2009). Measurement Of Behavioral Uncertainties In Mechanical Vibration Systems: A Symbolic Dynamics Approach. *Mechanical Vibrations: Measurement, Effects and Control*, 1-29.

Hansen, H.K. (2002). Envelope analysis for diagnostics of local faults in rolling element bearing, Application Note 7773, Bruel & Kjaer. Available: http://www.bksv.com/doc/bo0501.pdf

Hao, R., & Chu, F. (2009). Morphological undecimated wavelet decomposition for fault diagnostics of rolling element bearings. *Journal of Sound and Vibration*, *320*(4), 1164-1177.

Heng, R.B.W., & Nor, M.J.M. (1998). Statistical analysis of sound and vibration signals for monitoring rolling element bearing condition. *Applied Acoustics*, *53*(1), 211-226.

Ho, D., & Randall, R. B. (2000). Optimisation of bearing diagnostic techniques using simulated and actual bearing fault signals. *Mechanical systems and signal processing*, *14*(5), 763-788.

Hoffman, A. J., & Van der Merwe, N. T. (2002). The application of neural networks to vibrational diagnostics for multiple fault conditions. *Computer Standards & Interfaces*, *24*(2), 139-149.

Honarvar, F., & Martin, H. R. (1997). New statistical moments for diagnostics of rolling element bearings. *Journal of manufacturing science and engineering*, *119*(3), 425-432.

Hou, Z., Yang, J., & Zhang, X. (2010). Bearing Defect Diagnosis Based on S-Transform and Singular Value Ratio Spectrum. *Journal of Computational Information Systems*, *6*(10), 3285-3292.

Howard, I. M. (1993). Signal Processing Techniques for Mechanical Diagnosis of Space Shuttle Main Engine Turbomachinery Using Vibration Analysis. *Technology Integration IncolJlOIllledReponR9301-002-RD. Arepon on data analysis performed under contract NAS8-38955, January*

Howard, I.M. (1994). *A Review of Rolling Element Bearing Vibration'Detection, Diagnosis and Prognosis'* (No. DSTO-RR-0013). Defence Science and Technology Organization Canberra (Australia)

Immovilli, F., Bellini, A., Rubini, R., & Tassoni, C. (2010). Diagnosis of bearing faults in induction machines by vibration or current signals: A critical comparison. *Industry Applications, IEEE Transactions on*, *46*(4), 1350-1359.

ISO 10816-3, Mechanical Vibration—Evaluation of Machine Vibration by Measurement on Non-Rotating Parts—Part 3, 1998.

ISO 281: 2007. *Rolling bearings - Dynamic load ratings and rating life.*

Jammu, N.S., & Kankar, P. K. (2011). A Review on Prognosis of Rolling Element Bearings. *International Journal of Engineering Science*, 3(10), 7497-7503.

Jardine, A.K.S., Lin, D.M., & Banjevic, D. (2006). A review on machinery diagnostics and prognostics implementing condition-based maintenance, *Mechanical Systems and Signal Processing*, 20 (7), 1483–1510.

Jiang, L., Liu, Y., Li, X., & Chen, A. (2011). Degradation assessment and fault diagnosis for roller bearing based on AR model and fuzzy cluster analysis. *Shock and Vibration*, *18*(1), 127-137.

Jiang, L., Xuan, J., & Shi, T. (2013). Feature extraction based on semi-supervised kernel Marginal Fisher analysis and its application in bearing fault diagnosis.*Mechanical Systems and Signal Processing.*

Junsheng, C., Dejie, Y., & Yu, Y. (2006). A fault diagnosis approach for roller bearings based on EMD method and AR model. *Mechanical Systems and Signal Processing*, *20*(2), 350-362.

Junsheng, C., Dejie, Y., & Yu, Y. (2007). The application of energy operator demodulation approach based on EMD in machinery fault diagnosis. *Mechanical Systems and Signal Processing*, *21*(2), 668-677.

Kaewkongka, T., Joe, Y. H., Rakowski, R. T., & Jones, B. E. (2003). A comparative study of short time Fourier transform and continuous wavelet transform for bearing condition monitoring. *International Journal of COMADEM*, *6*(1), 41-48.

Kaiser, J.F. (1990). On a simple algorithm to calculate the energy of a signal in Proc. IEEE Int. Conference on Acoustics, Speech, and Signal Processing (ICASSP-90), Albuquerque, New Mexico, Vol. 1, 381-384.

Kakizawa, Y., Shumway, R. H., & Taniguchi, M. (1998). Discrimination and clustering for multivariate time series. *Journal of the American Statistical Association*, *93*(441), 328-340.

Karimi, M. (2006). Rolling element bearing fault diagnostics using the blind deconvolution technique. PhD thesis.

Kennel, M. B., & Buhl, M. (2003). Estimating good discrete partitions from observed data: symbolic false nearest neighbors. *Physical Review Letters*, *91*(8), 084102

Kilundu, B., Chiementin, X., & Dehombreux, P. (2011). Singular Spectrum Analysis for Bearing defect Detection, Journal of Vibration and Acoustics, 133(5), 051007-1 – 051007-7.

Lee, J., Qiu, H., Yu, G., Lin, J. & Rexnord Technical Services (2007). 'Bearing Data Set', IMS, University of Cincinnati. NASA Ames Prognostics Data Repository, [http://ti.arc.nasa.gov/project/prognostic-data-repository] [accessed: April 2013]

Lei, Y., He, Z., & Zi, Y. (2009). Application of the EEMD method to rotor fault diagnosis of rotating machinery. *Mechanical Systems and Signal Processing*, *23*(4), 1327-1338.

Lei, Y., Lin, J., He, Z., & Zi, Y. (2011). Application of an improved kurtogram method for fault diagnosis of rolling element bearings. *Mechanical Systems and Signal Processing*, *25*(5), 1738-1749

Lei, Y., Lin, J., He, Z., & Zuo, M. J. (2013). A review on empirical mode decomposition in fault diagnosis of rotating machinery. *Mechanical Systems and Signal Processing*, 35(1-2), 108-126.

Li, B., & Zhang, Y. (2011). Supervised locally linear embedding projection (SLLEP) for machinery fault diagnosis. *Mechanical Systems and Signal Processing*, *25*(8), 3125-3134

Li, B., Chow, M. Y., Tipsuwan, Y., & Hung, J. C. (2000). Neural-network-based motor rolling bearing fault diagnosis. *Industrial Electronics, IEEE Transactions on*, *47*(5), 1060-1069.

Li, B., Zhang, P. L., Liu, D. S., Mi, S. S., Ren, G. Q., & Tian, H. (2011). Feature extraction for rolling element bearing fault diagnosis utilizing generalized S transform and two-dimensional non-negative matrix factorization. *Journal of Sound and Vibration*, *330*(10), 2388-2399.

Li, B., Zhang, P. L., Wang, Z. J., Mi, S. S., & Liu, D. S. (2011). A weighted multi-scale morphological gradient filter for rolling element bearing fault detection. *ISA transactions*, *50*(4), 599-608.

Li, C. Q., & Pickering, C. J. D. (1992). Robustness and sensitivity of non-dimensional amplitude parameters for diagnosis of fatigue spalling. *Cond Monit Diagn Technol*, *2*(3), 81-84.

Li, C., & Liang, M. (2012). Continuous-scale mathematical morphology-based optimal scale band demodulation of impulsive feature for bearing defect diagnosis. *Journal of Sound and Vibration*.

Li, C., Liang, M., Zhang, Y., & Hou, S. (2012). Multi-scale autocorrelation via morphological wavelet slices for rolling element bearing fault diagnosis. *Mechanical Systems and Signal Processing*, *31*, 428-446.

Li, F., Ye, L., Zhang, G. C., & Meng, G. (2007). Bearing Fault Detection Using Higher-Order Statistics Based ARMA Model. *Key Engineering Materials*, *347*, 271-276.

Li, H., Zhang, Y., & Zheng, H. (2009). Hilbert-Huang transform and marginal spectrum for detection and diagnosis of localized defects in roller bearings. *Journal of Mechanical Science and Technology*, *23*(2), 291-301.

Li, H., Zhang, Y., & Zheng, H. (2010). Bearing fault detection and diagnosis based on order tracking and Teager-Huang transform. *Journal of Mechanical Science and Technology*, *24*(3), 811-822.

Li, W., Huang, Z., Lin, H., & Ding, K. (2013, May). Envelope analysis by wavelet-filter based spectral kurtosis for bearing health monitoring. In *Instrumentation and Measurement Technology Conference (I2MTC), 2013 IEEE International* (pp. 1721-1724). IEEE.

Liang, M., & Soltani Bozchalooi, I. (2010). An energy operator approach to joint application of amplitude and frequency-demodulations for bearing fault detection. *Mechanical systems and signal processing*, *24*(5), 1473-1494.

Liao, L., & Lee, J. (2009). A novel method for machine performance degradation assessment based on fixed cycle features test. *Journal of Sound and Vibration*, *326*(3), 894-908.

Lin, W., Hamilton, C. and Chitrapu, P. (1995). A Generalization to the Teager- Kaiser Energy Function and application to resolving two closely spaced tones in Proc. IEEE Int. Conference on Acoustics, Speech, and Signal Processing (ICASSP-95), Vol. 3,1637-1640.

Lind, D. A. (1995). *An introduction to symbolic dynamics and coding*. Cambridge University Press.

Liu, B., Ling, S. F., & Gribonval, R. (2002). Bearing failure detection using matching pursuit. *NDT & E International*, *35*(4), 255-262.

Liu, T., Chen, J., & Dong, G. (2013). Zero crossing and coupled hidden Markov model for a rolling bearing performance degradation assessment. *Journal of Vibration and Control*.

Liu, T., Chen, J., Zhou, X. N., & Xiao, W. B. (2012, May). Bearing Performance Degradation Assessment Using Linear Discriminant Analysis and Coupled HMM. In *Journal of Physics: Conference Series* (Vol. 364, No. 1, p. 012028). IOP Publishing.

Logan, D.B., & Mathew, J. (1996a). Using the correlation dimension for vibration fault diagnosis of rolling element bearings—I. Basic concepts. *Mechanical Systems and Signal Processing*, *10*(3), 241-250.

Logan, D.B., & Mathew, J. (1996b). Using the correlation dimension for vibration fault diagnosis of rolling element bearings—II. Selection of experimental parameters. *Mechanical Systems and Signal Processing*, *10*(3), 251-264.

Loparo, K. A., Adams, M. L., Lin, W., Abdel-Magied, M. F., & Afshari, N. (2000). Fault detection and diagnosis of rotating machinery. *Industrial Electronics, IEEE Transactions on*, *47*(5), 1005-1014.

Lybeck, N., Marble, S., & Morton, B. (2007, March). Validating prognostic algorithms: a case study using comprehensive bearing fault data. In *Aerospace Conference, 2007 IEEE* (pp. 1-9). IEEE.

Ma, J., & Li, J. C. (1995). Detection of localised defects in rolling element bearings via composite hypothesis test. *Mechanical Systems and Signal Processing*, *9*(1), 63-75.

Makowski, R., & Zimroz, R. (2013). A procedure for weighted summation of the derivatives of reflection coefficients in adaptive Schur filter with application to fault detection in rolling element bearings. *Mechanical Systems and Signal Processing*, *38*(1), 65-77.

Malhi, A., & Gao, R. X. (2004). PCA-based feature selection scheme for machine defect classification. *Instrumentation and Measurement, IEEE Transactions on*, *53*(6), 1517-1525.

Maragos, P., Kaiser, J.F. and Quatieri, T.F. (1993). On amplitude and frequency demodulation using energy operators. Signal Processing, IEEE Transactions on. Vol. 41, issue 4, 532-1549.

Martin, H.R., Ismail, F., & Sakuta, A. (1992). Algorithms for statistical moment evaluation for machine health monitoring. *Mechanical Systems and Signal Processing*, *6*(4), 317-327.

Mathew, J., & Alfredson, R. J. (1984). The condition monitoring of rolling element bearings using vibration analysis. *Journal of Vibration Acoustics Stress and Reliability in Design*, *106*, 447.

Mathew, J., Nirbito, W., & Tan, A. (2001). Detection on Incipient Rolling Element Bearing Failure by Blind Deconvolution.

McCormick, A. C., & Nandi, A. K. (1999). Bispectral and trispectral features for machine condition diagnosis. *IEE Proceedings-Vision, Image and Signal Processing*, *146*(5), 229-234.

McDonald, G. L., Zhao, Q., & Zuo, M. J. (2012). Maximum correlated Kurtosis deconvolution and application on gear tooth chip fault detection. *Mechanical Systems and Signal Processing*, 33, 237-255.

McDonald, G.L, (2011). Vibration Signal-Based Fault Detection for Rotating Machines, MS thesis, University of Alberta.

McFadden, P. D., & Smith, J. D. (1985). The vibration produced by multiple point defects in a rolling element bearing. *Journal of Sound and Vibration*, *98*(2), 263-273.

McFadden, P. D., & Toozhy, M. M. (2000). Application of synchronous averaging to vibration monitoring of rolling element bearings. *Mechanical Systems and Signal Processing*, *14*(6), 891-906.

McFadden, P.D., & Smith, J.D. (1984a). Model for the Vibration produced by a Single Point Defect in a Rolling Element Bearing, *Journal of Sound and Vibration*, 96 (1), pp 69-82.

McFadden, P.D., & Smith, J.D. (1984b). Vibration monitoring of rolling element bearings by the high-frequency resonance technique—a review. *Tribology international*, *17*(1), 3-10.

Mechefske, C. K., & Mathew, J. (1991). Trending the gradual deterioration of low speed rolling element bearings using parametric spectra. In *Proceedings of the 3rd International Machinery Monitoring and Diagnostics Conference* (pp. 232-320).

Mechefske, C. K., & Mathew, J. (1992a). Fault detection and diagnosis in low speed rolling element bearings Part I: The use of parametric spectra. *Mechanical systems and signal processing*, *6*(4), 297-307

Mechefske, C. K., & Mathew, J. (1992b). Fault detection and diagnosis in low speed rolling element bearings part II: the use of nearest neighbour classification. *Mechanical Systems and Signal Processing*, *6*(4), 309-316

Meng, Q., & Qu, L. (1991). Rotating machinery fault diagnosis using Wigner distribution. *Mechanical Systems and Signal Processing*, *5*(3), 155-166.

MFPT. Society for Machinery failure Prevention Technology http://www.mfpt.org/FaultData/FaultData.htm [accessed: May 2013]

Miyachi, T., & Seki, K. (1986, September). An investigation of the early detection of defects in ball bearings using vibration monitoring—practical limit of detectability and growth speed of defects. In *Proceedings of the International Conference on Rotor dynamics, JSME-IftoMM, Tokyo, Japan* (pp. 403-408).

Mobius Institute, Detecting rolling element bearing faults with vibration analysis. Available:http://www.mobiusinstitute.com/articles.aspx?id=2088

NASA Ames Prognostics Data Repository . J. Lee, H. Qiu, G. Yu, J. Lin, and Rexnord Technical Services (2007). 'Bearing Data Set', IMS, University of Cincinnati. [http://ti.arc.nasa.gov/project/prognostic-data-repository] [Accessed: April 2013]

Nelwamondo, F. V., Marwala, T., & Mahola, U. (2006). Early classifications of bearing faults using hidden Markov models, Gaussian mixture models, mel-frequency cepstral coefficients and fractals. *International Journal of Innovative Computing, Information and Control*, *2*(6), 1281-1299

Nikolaou, N. G., & Antoniadis, I. A. (2003). Application of morphological operators as envelope extractors for impulsive-type periodic signals. *Mechanical Systems and Signal Processing*, *17*(6), 1147-1162.

Obuchowski, J, Wylomanska, A., Zimroz, R. & (2013). Stochastic Modeling of Time Series with Application to Local Damage Detection in Rotating Machinery. *Key Engineering Materials*, *569*, 441-448.

Ocak, H., & Loparo, K.A. (2004). Estimation of the running speed and bearing defect frequencies of an induction motor from vibration data, *Mechanical systems and signal processing*, 18, 515–533.

Ocak, H., Loparo, K. A., & Discenzo, F. M. (2007). Online tracking of bearing wear using wavelet packet decomposition and probabilistic modeling: A method for bearing prognostics. *Journal of sound and vibration*, *302*(4), 951-961.

Pan, Y., Chen, J., & Guo, L. (2009). Robust bearing performance degradation assessment method based on improved wavelet packet–support vector data description. *Mechanical Systems and Signal Processing*, *23*(3), 669-681.

Pan, Y., Chen, J., & Li, X. (2010). Bearing performance degradation assessment based on lifting wavelet packet decomposition and fuzzy c-means. *Mechanical Systems and Signal Processing*, *24*(2), 559-566.

Pan, Y.N., Chen, J., & Li, X. L. (2009). Spectral entropy: A complementary index for rolling element bearing performance degradation assessment. *Proceedings of the*

Institution of Mechanical Engineers, Part C: Journal of Mechanical Engineering Science, *223*(5), 1223-1231.

Patil, M. S., Mathew, J., & RajendraKumar, P. K. (2008). Bearing signature analysis as a medium for fault detection: A review. *Journal of Tribology*, *130*(1).

Peled, R., Braun, S., & Zacksenhouse, M. (2005). A blind deconvolution separation of multiple sources, with application to bearing diagnostics. *Mechanical Systems and Signal Processing*, *19*(6), 1181-1195

Peng, Z. K., Tse, P. W., & Chu, F. L. (2005). A comparison study of improved Hilbert–Huang transform and wavelet transform: application to fault diagnosis for rolling bearing. *Mechanical systems and signal processing*, *19*(5), 974-988.

Peter, W. T., Zhang, J. Y., & Wang, X. J. (2006). Blind source separation and blind equalization algorithms for mechanical signal separation and identification. *Journal of Vibration and Control*, *12*(4), 395-423.

Qian, Y., Hu, S., & Yan, R. (2013, May). Bearing performance degradation evaluation using recurrence quantification analysis and auto-regression (AR) model. In*Instrumentation and Measurement Technology Conference (I2MTC), 2013 IEEE International* (pp. 1713-1716). IEEE.

Qiu, H., Lee, J., Lin, J., & Yu, G. (2003). Robust performance degradation assessment methods for enhanced rolling element bearing prognostics. *Advanced Engineering Informatics*, *17*(3), 127-140.

Qiu, H., Lee, J., Lin, J., & Yu, G. (2006). Wavelet filter-based weak signature detection method and its application on rolling element bearing prognostics.*Journal of Sound and Vibration*, *289*(4), 1066-1090.

Rai, V. K., & Mohanty, A. R. (2007). Bearing fault diagnosis using FFT of intrinsic mode functions in Hilbert–Huang transform. *Mechanical Systems and Signal Processing*, *21*(6), 2607-2615.

Raj, A.S., & Murali, N. (2013). A novel application of Lucy-Richardson deconvolution: bearing fault diagnosis. *Journal of Vibration and Control*.

Raj, A.S., & Murali, N. (2013). Early classification of bearing faults using morphological operators and fuzzy inference. IEEE Transaction on Industrial Electronics, 60(2), 567-574.

Rajagopalan, V., & Ray, A. (2006). Symbolic time series analysis via wavelet-based partitioning. *Signal Processing*, *86*(11), 3309-3320

Rajagopalan, V., Ray, A., Samsi, R., & Mayer, J. (2007). Pattern identification in dynamical systems via symbolic time series analysis. *Pattern recognition*, *40*(11), 2897-2907

Randall, R. B. (2004). Detection and diagnosis of incipient bearing failure in helicopter gearboxes. Engineering Failure Analysis, 11(2), 177-190.

Randall, R.B. (1985). Computer aided vibration spectrum trend analysis for condition monitoring. *Maintenance Management International*, *5*, 161-167.

Randall, R.B. (1987): *Frequency analysis* (3rd Edition). Bruel & Kjaer, Denmark.

Randall, R.B. (2004). Detection and diagnosis of incipient bearing failure in helicopter gearboxes. *Engineering Failure Analysis*, *11*(2), 177-190.

Randall, R.B. (2011) Vibration based condition monitoring: industrial aerospace and automotive applications, Wiley.

Randall, R.B., & Antoni, J. (2011). Rolling element bearing diagnostics—A tutorial. *Mechanical Systems and Signal Processing*, *25*(2), 485-520.

Randall, R.B., Sawalhi, N., & Coats, M. (2011). A comparison of methods for separation of deterministic and random signals. *International Journal of Condition Monitoring*, *1*(1), 11-19.

Ray, A. (1980, September). Monitoring rolling contact bearings under adverse conditions. In *2nd International Conference of Vibrations in rotating Machinery, Institution of Mechanical Engineers, Cambridge* (pp. 1-4).

Remo, B., & Antonio, P. (1997). Complexity: Hierarchical structures and scaling in physics, Cambridge University Press.

Rolo-Naranjo, A., & Montesino-Otero, M. E. (2005). A method for the correlation dimension estimation for on-line condition monitoring of large rotating machinery. *Mechanical Systems and Signal Processing*, *19*(5), 939-954.

Rubini, R and Meneghetti, U. (2001). Application of the envelope and wavelet transform analyses for the diagnosis of incipient faults in ball bearings, Mechanical Systems and Signal Processing 15(2)(2001) 287–302.

Salami, M. J. E., Gani, A., & Pervez, T. (2001). Machine condition monitoring and fault diagnosis using spectral analysis techniques. In *Proceedings of the First International Conference on Mechatronics (ICOM'01)* (Vol. 2, pp. 690-700).

Samanta, B., Al-Balushi, K. R., & Al-Araimi, S. A. (2003). Artificial neural networks and support vector machines with genetic algorithm for bearing fault detection. *Engineering Applications of Artificial Intelligence*, *16*(7), 657-665.

Sawalhi, N., & Randall, R. B. (2008). Simulating gear and bearing interactions in the presence of faults: Part I. The combined gear bearing dynamic model and the simulation of localised bearing faults. Mechanical Systems and Signal Processing, 22(8), 1924-1951.

Sawalhi, N., Randall, R. B., & Endo, H. (2007). The enhancement of fault detection and diagnosis in rolling element bearings using minimum entropy deconvolution combined with spectral kurtosis. *Mechanical Systems and Signal Processing*,*21*(6), 2616-2633.

Serridge, M. (1991). What makes vibration condition monitoring reliable?. *Noise and Vibration Worldwide*, *22*(8), 17-24.

Shen, Y. J., & Yang, S. P. (2006). A new Blind-Source-Separation method and its application to fault diagnosis of rolling bearing. *International Journal of Nonlinear Sciences and Numerical Simulation*, *7*(3), 245-250.

Shiroishi, J. Y. S. T., Li, Y., Liang, S., Kurfess, T., & Danyluk, S. (1997). Bearing condition diagnostics via vibration and acoustic emission measurements. *Mechanical systems and signal processing*, *11*(5), 693-705.

Si, X. S., Wang, W., Hu, C. H., & Zhou, D. H. (2011). Remaining useful life estimation–A review on the statistical data driven approaches. *European Journal of Operational Research*, *213*(1), 1-14.

Siegel, D., Al-Atat, H., Shauche, V., Liao, L., Snyder, J., & Lee, J. (2012). Novel method for rolling element bearing health assessment—A tachometer-less synchronously averaged envelope feature extraction technique. *Mechanical Systems and Signal Processing*, *29*, 362-376.

Singh, D. S., Gupta, S., & Ray, A. (2009). In-situ fatigue damage monitoring using symbolic dynamic filtering of ultrasonic signals. *Proceedings of the Institution of Mechanical Engineers, Part G: Journal of Aerospace Engineering*, *223*(6), 643-653.

Sinha, B. K. (2002). Trend prediction from steam turbine responses of vibration and eccentricity. *Proceedings of the Institution of Mechanical Engineers, Part A: Journal of Power and Energy*, *216*(1), 97-103.

Smith, J. D. (1982). Vibration monitoring of bearings at low speeds. *Tribology International*, *15*(3), 139-144.

Sreejith, B., Verma, A. K., & Srividya, A. (2008, December). Fault diagnosis of rolling element bearing using time-domain features and neural networks. In *Industrial and Information Systems, 2008. ICIIS 2008. IEEE Region 10 and the Third international Conference on* (pp. 1-6). IEEE.

Starns, G.K. (2002). Bearing life. Available : http://www.public.iastate.edu/~gkstarns/ME325/lecture35.pdf

Su, Y. T., & Lin, S. J. (1992). On initial fault detection of a tapered roller bearing: frequency domain analysis. *Journal of Sound and Vibration*, *155*(1), 75-84.

Subbu, A., & Ray, A. (2008). Space partitioning via Hilbert transform for symbolic time series analysis. *Applied Physics Letters*, *92*(8), 084107-084107.

Sujatha, C., & Chandran, C. (2002). On various specialized vibration techniques for detection of bearing faults. In *SPIE proceedings series*. Society of Photo-Optical Instrumentation Engineers.

Sunnersjo, C.S. (1985). Rolling bearing vibrations—the effects of geometrical imperfections and wear, *Journal of Sound and Vibration*, 98(4), 455–474.

Swanson, D. C. (2001). A general prognostic tracking algorithm for predictive maintenance. In *Aerospace Conference, 2001, IEEE Proceedings.* (Vol. 6, pp. 2971-2977). IEEE

Tan, A.C., Karimi, M., & Mathew, J. (2006). Blind deconvolution using the eigenvector algorithm (EVA) method for the enhancement of bearing signal through the transmission channel. In *Engineering Asset Management* (pp. 198-205). Springer London.

Tandon, N. (1994). A comparison of some vibration parameters for the condition monitoring of rolling element bearings. *Measurement*, *12*(3), 285-289.

Tandon, N., & Choudhury, A. (1999). A review of vibration and acoustic measurement methods for the detection of defects in rolling element bearings.*Tribology International*, *32*(8), 469-480.

Tandon, N., & Kumar, K. S. (2003). Detection of defects at different locations in ball bearings by vibration and shock pulse monitoring. *Noise & Vibration Worldwide*, *34*(3), 9-16.

Tandon, N., & Nakra, B. C. (1993). Detection of defects in rolling element bearings by vibration monitoring. *Indian Journal of Mechanical Engineering Division*, *73*, 271-282.

Tao, B., Zhu, L., Ding, H., & Xiong, Y. (2007). An alternative time-domain index for condition monitoring of rolling element bearings—A comparison study. *Reliability Engineering & System Safety*, *92*(5), 660-670.

Tax, D. M., & Laskov, P. (2003, September). Online SVM learning: from classification to data description and back. In *Neural Networks for Signal Processing, 2003. NNSP'03. 2003 IEEE 13th Workshop on* (pp. 499-508). IEEE.

Tax, D.M., & Duin, R. P. (2004). Support vector data description. *Machine learning*, *54*(1), 45-66.

Teager, H.M. (1980). Some observations on oral air flow during phonation. Acoustics, Speech and Signal Processing, IEEE Transactions on. Vol. 28, issue 5, 599-601.

Thorsen, O. V., & Dalva, M. (1995). A survey of faults on induction motors in offshore oil industry, petrochemical industry, gas terminals, and oil refineries. Industry Applications, IEEE Transactions on, 31(5), 1186-1196.

Tiwari, D. (2002). *Symbolic dynamic models for highly varying power system loads* (Doctoral dissertation, Arizona State University)

Tranter, T., Rienstra, A., & Murphy, T. (2013) Vibration vs Ultrasound: Two Techniques to consider in Condition monitoring, Uptime, Feb/March, 56-57.

Tse, P. W., & Wang, D. (2013a). The design of a new sparsogram for fast bearing fault diagnosis: Part 1 of the two related manuscripts that have a joint title as "Two automatic vibration-based fault diagnostic methods using the novel sparsity measurement–Parts 1 and 2". *Mechanical Systems and Signal Processing*. (Online July 2013)

Tse, P. W., & Wang, D. (2013b). The automatic selection of an optimal wavelet filter and its enhancement by the new sparsogram for bearing fault detection: Part 2 of the two related manuscripts that have a joint title as "Two automatic vibration-based fault diagnostic methods using the novel sparsity measurement—Parts 1 and 2".*Mechanical Systems and Signal Processing*. (Online July 2013)

Tse, P., & Lai, W. X. (2003, August). Minimizing interference in bearing condition monitoring and diagnosis by using adaptive noise cancellation. In *Proceedings of* *the 16th International Congress and Exhibition on Condition Monitoring and Diagnostic Engineering Management* (pp. 739-748).

Van wyk, B. J., Van wyk, M. A., & Qi, G. (2009). Difference Histograms: A new tool for time series analysis applied to bearing fault diagnosis. *Pattern Recognition Letters*, *30*(6), 595-599.

Veenman, C. J., Reinders, M. J. T., & Backer, E. (2002). A maximum variance cluster algorithm. *Pattern Analysis and Machine Intelligence, IEEE Transactions on*, *24*(9), 1273-1280.

Wang, C. C., Kang, Y., Shen, P. C., Chang, Y. P., & Chung, Y. L. (2010). Applications of fault diagnosis in rotating machinery by using time series analysis with neural network. *Expert Systems with Applications*, *37*(2), 1696-1702.

Wang, D., Peter, W. T., & Yiu, L. T. (2012). A morphogram with the optimal selection of parameters used in morphological analysis for enhancing the ability in bearing fault diagnosis. *Measurement Science and Technology*, *23*(6), 065001.

Wang, D., Tse, P. W., & Tsui, K. L. (2013). An enhanced Kurtogram method for fault diagnosis of rolling element bearings. *Mechanical Systems and Signal Processing*, *35*, 176-199.

Wang, G. F., Li, Y. B., & Luo, Z. G. (2009). Fault classification of rolling bearing based on reconstructed phase space and Gaussian mixture model. *Journal of Sound and Vibration*, *323*(3), 1077-1089.

Wang, Y., & Liang, M. (2011). An adaptive SK technique and its application for fault detection of rolling element bearings. *Mechanical Systems and Signal Processing*, *25*(5), 1750-1764.

Wang, Y., & Liang, M. (2012). Identification of multiple transient faults based on the adaptive spectral kurtosis method. *Journal of Sound and Vibration*, *331*(2), 470-486.

Widner, R. L., and Littmann, W. E., "Bearing Damage Analysis," National Bureau of Standard special publication No. 423, April 1976

Widodo, A., & Yang, B. S. (2011). Application of relevance vector machine and survival probability to machine degradation assessment. *Expert Systems with Applications*, *38*(3), 2592-2599.

William, P. E., & Hoffman, M. W. (2011). Identification of bearing faults using time domain zero-crossings. *Mechanical systems and signal processing*, *25*(8), 3078-3088.

Williams, T., Ribadeneira, X., Billington, S. & Kurfess, T. (2001). Rolling element bearing diagnostics in run-to-failure lifetime testing, Mechanical Systems and Signal Processing 15 (5), 979–993

Wong, M. L. D., Jack, L. B., & Nandi, A. K. (2006). Modified self-organising map for automated novelty detection applied to vibration signal monitoring. *Mechanical Systems and Signal Processing*, *20*(3), 593-610

Woodward, R, "Single Amplitude BPFO or BPFI (Velocity in/s) with. 4 Stages of Bearing Wear, General Guideline for Overall Alarm Criteria", BPG Engineering, Ocean Township, New Jersey, 1995.

Xiang, X., Zhou, J., Li, C., Li, Q., & Luo, Z. (2009). Fault diagnosis based on Walsh transform and rough sets. *Mechanical Systems and Signal Processing*, *23*(4), 1313-1326.

Xiong, G. L., Zhang, L., Liu, H. S., Zou, H. J., & Guo, W. Z. (2010). A comparative study on ApEn, SampEn and their fuzzy counterparts in a multiscale framework for feature extraction. *Journal of Zhejiang University Science A*, *11*(4), 270-279.

XY Extract. http://zeus.df.ufcg.edu.br/labfit/index_xyExtract.htm

Yan, R., & Gao, R. X. (2006). Hilbert–Huang transform-based vibration signal analysis for machine health monitoring. *Instrumentation and measurement, IEEE Transactions on*, *55*(6), 2320-2329.

Yan, R., & Gao, R. X. (2007). Approximate entropy as a diagnostic tool for machine health monitoring. *Mechanical Systems and Signal Processing*, *21*(2), 824-839.

Yang, B. S., Han, T., & An, J. L. (2004). ART–KOHONEN neural network for fault diagnosis of rotating machinery. *Mechanical Systems and Signal Processing*, *18*(3), 645-657.

Yang, H., Mathew, J., & Ma, L. (2003). Vibration feature extraction techniques for fault diagnosis of rotating machinery: a literature survey.

Yang, H., Mathew, J., & Ma, L. (2005). Fault diagnosis of rolling element bearings using basis pursuit. *Mechanical Systems and Signal Processing*, *19*(2), 341-356

Yang, J., Zhang, Y., & Zhu, Y. (2007). Intelligent fault diagnosis of rolling element bearing based on SVMs and fractal dimension. *Mechanical Systems and Signal Processing*, *21*(5), 2012-2024.

Yang, Z., Cai, L., Gao, L., & Wang, H. (2012). Adaptive redundant lifting wavelet transform based on fitting for fault feature extraction of roller bearings. *Sensors*, *12*(4), 4381-4398.

Yu, J.B. (2011a). Bearing performance degradation assessment using locality preserving projections. *Expert Systems with Applications*, *38*(6), 7440-7450.

Yu, J.B. (2011b). Bearing performance degradation assessment using locality preserving projections and Gaussian mixture models. *Mechanical Systems and Signal Processing*, *25*(7), 2573-2588.

Yu, J.B. (2012). Local and nonlocal preserving projection for bearing defect classification and performance assessment. *Industrial Electronics, IEEE Transactions on*, *59*(5), 2363-2376

Yu, Y., Dejie, Y., & Junsheng, C. (2006). A roller bearing fault diagnosis method based on EMD energy entropy and BPNN. *Journal of Sound and Vibration*, 294 (1-2), 269–277.

Zhang, L., Xu, J., Yang, J., Yang, D., & Wang, D. (2008). Multiscale morphology analysis and its application to fault diagnosis. *Mechanical Systems and Signal Processing*, *22*(3), 597-610.

Zhao, F., Chen, J., Guo, L., & Li, X. (2009). Neuro-fuzzy based condition prediction of bearing health. *Journal of Vibration and Control*, *15*(7), 1079-1091.

Zhen, L., Zhengjia, H., Yanyang, Z., & Xuefeng, C. (2008). Bearing condition monitoring based on shock pulse method and improved redundant lifting scheme. *Mathematics and computers in simulation*, *79*(3), 318-338.

Zhou, W., Habetler, T. G., & Harley, R. G. (2007, September). Bearing condition monitoring methods for electric machines: A general review. In Diagnostics for Electric Machines, Power Electronics and Drives, 2007. SDEMPED 2007. IEEE International Symposium on (pp. 3-6). IEEE.